Research Repository UCD

Title	Tough Injectable Hydrogels by Combining Elastic and Energy Dissipation
Authors(s)	Song, Rijian
Publication date	2024
Publication information	Song, Rijian. “Tough Injectable Hydrogels by Combining Elastic and Energy Dissipation.” University College Dublin. School of Medicine, 2024.
Publisher	University College Dublin. School of Medicine
Item record/more information	http://hdl.handle.net/10197/30006

Downloaded 2026-04-30 18:55:46

The UCD community has made this article openly available. Please share how this access benefits you. Your story matters! (@ucd_oa)

© Some rights reserved. For more information



Tough Injectable Hydrogels by Combining Elastic and Energy Dissipation

Rijian Song

UCD student number: 20204866

The thesis is submitted to University College Dublin in fulfilment of the requirements for the degree of Doctor of Philosophy

Charles Institute of Dermatology

School of Medicine

Head of School: Professor Michael Keane

Principal Supervisor: Professor Wenxin Wang

June/2024

TABLE OF CONTENTS

TABLE OF CONTENTS ..... **ii**

LIST OF APPENDICES ..... **iv**

LIST OF FIGURES ..... **v**

LIST OF TABLES ..... **xviii**

ABBREVIATIONS ..... **xix**

ABSTRACT ..... **xxiv**

STATEMENT OF ORIGINAL AUTHORSHIP ..... **xxvi**

COLLABORATIONS ..... **xxvii**

ACKNOWLEDGEMENTS ..... **xxviii**

Chapter One: Introduction **1**

1.1 Tough Injectable Hydrogels Overview 2

1.2 Common Polymers for Injectable Hydrogels 5

1.3 Common Crosslink Methods for Injectable Hydrogels 23

1.4 Toughening Strategies for Injectable Hydrogels 44

1.5 Aims and Objectives 66

1.6 References 67

Chapter Two: Tough Injectable Hydrogels via Flexible Chains Linking Rigid Homogeneous Framework **117**

2.1 Introduction 118

2.2 Materials and Methods 122

2.3 Results and Discussion 126

2.4 Conclusion 148

2.5 References 150
Chapter Three: Tough Injectable Hydrogel Via Thermal Self-entangled Chains Linking Rigid Framework 157
3.1 Introduction 158
3.2 Materials and Methods 163
3.3 Results and discussion 169
3.4 Conclusion 184
3.5 References 185
Chapter Four: Double Network Injectable Hydrogel with Enhanced Toughness by Acid-Triggered Scond Homogeneous Network 191
4.1 Introduction 192
4.2 Materials and Methods 197
4.3 Results and Discussion 204
4.4 Conclusion 226
4.5 References 227
Chapter Five: Summary and Future Directions 233
5.1 Summary 234
5.2 Limitations 239
5.3 Future Directions 241
5.4 Conclusion 251
5.5 References 252
Appendices 257

LIST OF APPENDICES

Appendices 257

Work Output During PhD..... 258

Conference Proceedings..... 261

Accepted Representative Publication..... 262

LIST OF FIGURES

Figure 1.1 Illustrated overview of the *in situ* forming methods and toughening designs of tough injectable hydrogels, and their biomedical applications. [Created with BioRender]..... 5

Figure 1.2 Chemical structure and schematics of typical raw polymers for injectable hydrogels: (a) natural polymers; (b) synthetic polymers. [Created with BioRender] 6

Figure 1.3 Examples of injectable hydrogels prepared by Thiol-ene Michael addition reaction: (a) Thiol-ene Michael addition reaction; (b) HA-based hybrid hydrogel created by Thiol-ene Michael addition reaction.[49] [Cropped image. Copyright© 2018 Royal Society of Chemistry] 26

Figure 1.4 Examples of injectable hydrogels prepared by Schiff base reaction: (a) Schiff base reaction; (b) an *in situ* formed hydrogel created by Schiff base reaction.[215] [Cropped image. Copyright© 2015 Royal Society of Chemistry] 29

Figure 1.5 Examples of injectable hydrogels prepared by photo crosslinking: (a) photo crosslinking reaction example; (b) an injectable hydrogel created by photo crosslinking reaction.[222] [Cropped image. Copyright© 2018 American Chemical Society] 32

Figure 1.6 Examples of injectable hydrogels prepared by hydrogen bonding used for cell delivery in intervertebral disc degeneration treatment.[248] [Cropped, reorganised, and relabelled image. Copyright© 2024 John Wiley and Sons]....38
Figure 1.7 Examples of injectable hydrogels prepared by coordination bonding.[252] [Cropped and relabelled image. Copyright© 2017 American Chemical Society].....40
Figure 1.8 Examples of injectable hydrogels prepared by amphiphilic self-assembly.[263] [Cropped and relabelled image. Copyright© 2017 Elsevier].....43
Figure 1.9 Illustration of the stress-strain curve for hydrogels. The yellow line represents the compression curve of a regular hydrogel, while the red line indicates the compression curve of a tougher hydrogel. Tough hydrogels typically possess higher limit stress, higher limit strain, and a larger area under the stress-strain curve. 45
Figure 1.10 Example of the ideally homogeneous network tough hydrogel.[275] [Cropped and relabelled image. Open Access]..48
Figure 1.11 Example of the slide ring network tough hydrogel. The close-packed structure of PEG is formed and destroyed during stretching and releasing.[41] [Cropped and relabelled image.

Copyright© 2021 The American Association for the Advancement of Science] 52
Figure 1.12 Example of the highly entangled network tough hydrogel. A stretched polymer showing transmission of the tension to other chains.[36] [Cropped and relabelled image. Copyright© 2021 The American Association for the Advancement of Science] 54
Figure 1.13 Example of the tough hydrogel with the sacrificial bonding feature.[290] [Cropped and relabelled image. Copyright© 2017 The Society of Polymer Science, Japan (SPSJ)] 59
Figure 1.14 Example of the tough hydrogel with domain transformation feature.[38] [Cropped and relabelled image. Copyright© 2024 The American Association for the Advancement of Science] 62
Figure 1.15 Example of the tough hydrogel with fibre reinforce feature.[302] [Cropped, reorganised and relabelled image. Copyright© 2014 Elsevier] 65
Figure 2.1 Illustrates how incorporating flexible long chains improves the toughness of SN hydrogels: (a) chain fracture and stress distribution in a classical SN hydrogel; (b) chain fracture and stress distribution in a hydrogel framework linked with

flexible long chains. 121
Figure 2.2 Illustration of the preparation process of *in situ* formed FF injectable hydrogel. 128
Figure 2.3 Mechanical properties of A_{10}+B_{20}/P_{4k} hydrogels with different flexible-to-rigid chain ratios: (a) compressive stress-strain curves, (b) G', and (c) compressive toughness of A_{10}+B_{20}/P_{4k} hydrogels. (d) illustrates of the replacement of B_{20} by P_{4k}. The representative images presented are randomly selected from replicate samples (n=3), and data are presented as mean ± standard deviation (n=3). 130
Figure 2.4 Mechanical properties of A_{10}+B_{10}/P_{8k} hydrogels with different flexible-to-rigid chain ratios: (a) compressive stress-strain curves, (b) G', and (c) compressive toughness of A_{10}+B_{10}/P_{8k} hydrogels; (d) illustrates of the replacement of B_{10} by P_{8k}. The representative images presented are randomly selected from replicate samples (n=3), and data are presented as mean ± standard deviation (n=3). 135
Figure 2.5 Mechanical properties of A_{10}+B_4/P_{20k} hydrogels with different flexible-to-rigid chain ratios: (a) compressive stress-strain, (b) G', (c) compressive toughness of A_{10}+B_4/P_{20k} hydrogels; (d) illustrates of the replacement of B_4 by P_{20k}. The

representative images presented are randomly selected from replicate samples (n=3), and data are presented as mean ± standard deviation (n=3). 138
Figure 2.6 Anti-fatigue behaviour of SN hydrogel and FF hydrogel (80% limit strains for each hydrogel): 20 unspaced load-unload compression tests of (a) A_{10}+B_4/P_{20k}-10/0 SN hydrogel, (b) A_{10}+B_4/P_{20k}-0/10 SN hydrogel, and (c) A_{10}+B_4/P_{20k}-5/5 FF hydrogel; calculated results of the corresponding total and dissipative toughness of 20 unspaced load-unload compression tests of (d) A_{10}+B_4/P_{20k}-10/0 SN hydrogel, (e) A_{10}+B_4/P_{20k}-0/10 SN hydrogel, and (f) A_{10}+B_4/P_{20k}-5/5 FF hydrogel. The representative images presented are randomly selected from replicate samples (n=3). 140
Figure 2.7 Adjustable mechanical properties of FF hydrogel by changing of polymer concentration and Mw of flexible PEG chains: (a) compressive stress-strain curves. (b) G', and (c) compressive toughness of A_{10}+B_4/P_{20k} -5/5 FF hydrogels with different polymer concentrations; (d) compressive stress-strain curves, (e) G', and (f) compressive toughness of A_{10}+B_4/P_z -5/5 FF hydrogels with different Mw of flexible PEG long chains. The representative images presented are randomly selected

from replicate samples (n=3), and data are presented as mean ± standard deviation (n=3). 143
Figure 2.8 Mechanical properties of B_{20}+A_{10}/O_{8k} FF hydrogels with different flexible-to-rigid chain ratios: (a) compressive stress-strain curves, (b) G', and (c) compressive toughness of A_{10}+B_4/O_{8k} hydrogels. The representative strain-stress curves presented are randomly selected from replicate samples (n=3), and bar charts are presented as mean ± standard deviation (n=3). 146
Figure 2.9 Cytocompatibility assessment of A_{10}+B_4/P_{20k} hydrogels: (a) Live/dead staining images, showing overlay images where green represents live cells and red represents dead cells and (b) alamarBlue cell viability assessment of HaCaT cells cultured on the surface of TC-plate, A_{10}+B_4/P_{20k} - 10/0 and A_{10}+B_4/P_{20k} – 5/5 FF hydrogels at day 1 and 3. Scale bar: 200 μm. The representative images presented are randomly selected from replicate samples (n=3), and bar charts are presented as mean ± standard deviation (n=3). 148
Figure 3.1 Illustration of the preparation and features of ABF-37°C hydrogels. [Created with BioRender] 162
Figure 3.2 Characterisation of F127-DA hydrogel system. (a) GPC

traces of PEG, PEG-DA, F127, and F127DA polymers; (b) temperature sweep of PEG-DA and thermo-responsive F127-DA polymer solutions; (c) time sweep of F127 and F127-DA polymer solutions with UV-crosslinking for 30 seconds from 60 to 90 s; (d) 37℃ with more entanglement and (e) 20℃ with less entanglement of F127-DA hydrogel system; (f) swelling test; (g) G'; (h) compression stress-strain curve; and (i) compressive toughness of PEG-20℃, PEG-37℃, F127-20 and self-entangled F127-37℃ hydrogels. The representative images presented are randomly selected from replicate samples (n=3), and data are presented as mean ± standard deviation (n=3). 172

Figure 3.3 Characterisation of ABF hydrogel system. (a) gelation time assay of ABF hydrogel system at 20℃ and 37℃; (b) unreacted thiol groups with different reaction time at 20℃ and 37℃; (c) G' and G'', hydrogels swelling at (d) 20℃ and (e) 37℃; (f) strain sweep of ABF-20℃ and self-entangled ABF-37℃ hydrogels; (g) illustration of the swelling limitation of ABF-20℃ and self-entangled ABF-37℃ hydrogels. The representative images presented are randomly selected from replicate samples (n=3), and data are presented as mean ±

standard deviation (n=3). 177
Figure 3.4 Mechanical Properties of ABF hydrogel system: (a) illustration of the structure changing in deformation process of self-entangled ABF-37℃ hydrogel; (b) compression stress-strain curve and (c) compressive toughness of AB, ABP-37℃, ABF-20℃, and self-entangled ABF-37℃ hydrogels. The representative images presented are randomly selected from replicate samples (n=3), and data are presented as mean ± standard deviation (n=3). 179
Figure 3.5 Fatigue resistance properties of ABF hydrogel system: 20 unspaced loading-unloading compression stress-strain curve of (a) self-entangled ABF-37℃ hydrogel, (b) ABF-20℃ hydrogel, and (c) ABP-37℃ hydrogel; total and dissipated toughness of (d) self-entangled ABF-37℃ hydrogel, (e) ABF-20℃ hydrogel, and (f) ABP-37℃ hydrogel. The representative images presented are randomly selected from replicate samples (n=3), and data are presented as mean ± standard deviation (n=3). 181
Figure 3.6 Cytocompatibility assessment of ABF hydrogel system: (a) Live/dead staining images, showing overlay images where green represents live cells and red represents dead cells and (b)

alamarBlue cell viability assessment of HaCaT cells cultured on the surface of TC-plate, ABP-37℃ and self-entangled ABF-37℃ hydrogels at day 1 and 3. Scale bar: 200 μm. The representative images presented are randomly selected from replicate samples (n=3), and data are presented as mean ± standard deviation (n=3). 184

Figure 4.1 Illustration of the preparation and features of DN-ABSH injectable hydrogels. [Created with BioRender] 196

Figure 4.2 Characterisation of the acid-triggered SA/HAp hydrogel system: (a) particle distribution analysis of the HAp solution; (b) particle distribution analysis of the SA/HAp solution; (c) transmittance analysis of the SA/HAp hydrogel system under varying pH conditions; (d) illustration of the egg-box model of SA chains crosslinked by HAp-released Ca^{2+}.; (e) zeta potential of the SA/HAp hydrogel system under varying pH conditions; (f) G' and G'' of the SA/HAp hydrogel system with increasingly SA content; (g) G' and G'' of the SA/HAp hydrogel system with increasingly HAp content. The representative images presented are randomly selected from replicate samples (n=3), and data are presented as mean ± standard deviation (n=3). 206

Figure 4.3 Characterisation of the SN-ABSH hydrogel: (a) schematic representation of the Michael Addition reaction in the SN-ABSH hydrogel system; (b) assessment of the gelling time of the SN-ABSH hydrogel system through a time sweep test; (c) general observation of HA/HAp immediately after mixing and 20 minutes later; (d) injectable properties of the HA/HAp hydrogel. The representative images presented are randomly selected from replicate samples (n=3)..... 210
Figure 4.4 Characterisation of the DN-ABSH hydrogel: (a) general observation of DN-ABSH upon immersion in acidic PBS buffer; (b) the transmittance and G' of ABSH hydrogel systems with varying pH; (c) the G' and G'' of ABSH and TC-plate hydrogel systems; (d) strain sweep test of ABSH and TC-plate hydrogel systems; (e) illustration of the acid-trigged formation of second SA network and macroscopic observation of SN-ABSH and DN-ABSH hydrogels. The representative images presented are randomly selected from replicate samples (n=3), and data are presented as mean ± standard deviation (n=3).212
Figure 4.5 Mechanical properties of DN-ABSH hydrogel: (a) compression strain-Stress curve of SN and DN hydrogels; (b) compressive toughness of SN and DN hydrogels; (c) toughness

of repetitive compression test of DN-ABSH and DN-Blank hydrogels; (g) illustration of the inhomogeneous DN-Blank and homogeneous DN-ABSH hydrogel during deformation process; SEM images of freeze-dried (d) SN-ABSH, (e) DN-ABSH, and (f) DN-Blank, scale bar: 100 μm. The representative images presented are randomly selected from replicate samples (n=3), and data are presented as mean ± standard deviation (n=3).216

Figure 4.6 Anti-swelling, anti-degradation, and resistance to gastric acid properties of DN-ABSH hydrogel: (a) hydrogel mass in the DPBS swelling process in 24 hours; (b) hydrogel mass in the hyaluronidase with 100 U/mL enzyme activity in 8 days; (c) hydrogel mass in the SGF (pH≈1.2) in 63 days. The data are presented as mean ± standard deviation (n=3). 220

Figure 4.7 Acid-triggered customisable patterning strategy of DN-ABSH hydrogel: (a) Illustration of the patterning process on the DN-ABSH hydrogel system using acid stamping, scale bar: 1 cm; (b) schematic illustration of the moment the acid stamp touches the hydrogel, where the Ca^{2+} released in situ crosslinks the SA in the underlying SN-ABSH hydrogel; (c) a 3D colour mapping of the grayscale analysis of acid stamp treated ABSH hydrogel. The blue part indicates DN-ABSH regions with

lower grayscale, while the red part indicates SN-ABSH regions with higher grayscale; (d) swelling behaviour of acid stamp treated ABSH hydrogel system. The DN-ABSH part shows minimal swelling, while the SN-ABSH part exhibits significant swelling. 221

Figure 4.8 Cytocompatibility assessment of DN-ABSH hydrogel system: (a) Live/dead staining images, showing overlay images where green represents live cells and red represents dead cells. Scale bar: 200 μm. (b) alamarBlue cell viability assessment of HaCaT cells cultured on the surface of TC-plate, SN-AB and DN-ABSH at day 1 and 3; (c) cell dispersed growth on the TC-plate surface, and (d) aggregate growth on the hydrogel surface. The representative images presented are randomly selected from replicate samples (n=3), and data are presented as mean ± standard deviation (n=3). 225

Figure 5.1 Biomimetic *in situ* formed hydrogel mimicking the cartilage matrix: (a) structure of cartilage glycosaminoglycans and proteoglycans;[20] [Cropped image. Copyright© 2021 American Chemical Society] (b) illustration of thermo-responsive bottlebrush *in situ* formed hydrogel.[21] [Cropped and reorganised image. Open Access] 246

Figure 5.2 Structure of spider silk-like hydrogel and illustration of their tension process.[22] [Cropped and reorganised image. Copyright© 2021 American Chemical Society] 248
Figure 5.3 A promising strategy to design tough injectable hydrogels by collaborating multi-scale mechanisms. [Created with BioRender] 251

LIST OF TABLES

Table 5.1 A matrix provides design guides and publication references of *in situ* formed tough injectable hydrogels by combining mechanisms for elastic maintenance and energy dissipation structure. Notably, it reveals many promising yet unexplored combinations. [Created with BioRender] 244

ABBREVIATIONS

3D	Three-dimensional
Ad	Adamantaneamine
BDDE	1,4-Butanediol diglycidyl ether
BIS	N,N'-methylene-bis-acrylamide
BMSC	Bone marrow stromal cells
CaCl2	Calcium chloride
CDs	Cyclodextrins
CMC	Carboxymethyl cellulose
CS	Chondroitin sulfate
CTS	Chitosan
CTS-CHO	Oxidised chitosan
DE-ATRP	Deactivation enhanced atom transfer radical polymerization
DMEM	Dulbecco's Modified Eagle Medium
DN	Double network
DPBS	Dulbecco's phosphate-buffered saline

DTT	1,4-dithiothreitol
DVS	divinyl sulfone
ECH	Epichlorohydrin
ECM	Extracellular matrix
EGDGE	Ethylene glycol diglycidyl ether
FBS	Fetal Bovine Serum
F127-DA	Diacrylated F127
G’	Storage modulus
G”	Loss modulus
GA	Glutaraldehyde
GAG	Glycosaminoglycan
GelMA	Methacryloyl gelatin
HA	Hyaluronic acid
HAp	Hydroxyapatite
HA-A	Acrylated hyaluronic acid
HA-CHO	Aldehyde-functionalised hyaluronic acid

HA-MA	Methacrylated hyaluronic acid
HA-SH	Thiolated hyaluronic acid
HB-GMA-PEG	Hyperbranched methacrylate-copolymerised polyethylene glycol diacrylate
HB-PEG	Hyperbranched polyethylene glycol
HB-PEG-HDZ	Hyperbranched polyethylene glycol-based hydrazide
HBSS	Hank's balanced salt solution
HCl	Hydrochloric acid
HP	Hydrophobic peptide
HPC	Hydroxypropyl cellulose
H_3PO_4	Phosphoric acid
HPMC	Hydroxypropyl methylcellulose
HRP	Horseradish peroxidase
I2959	2-Hydroxy-4′-(2-hydroxyethoxy)-2-methylpropiophenone
LAP	Lithium phenyl-2,4,6-trimethylbenzoylphosphinate
LBL	Linear-bottlebrush-linear

LCST	Lower critical solution temperature
MMP	Matrix metalloproteinase
Mw	Molecular weights
NaCl	Sodium chloride
NaOH	Sodium hydroxide
NHS	N-hydroxysuccinimide
PAA	Polyacrylic acid
PAM	Polyacrylamide
PBS	Phosphate buffer solution
PEG	Polyethylene glycol
PEG-DA	Polyethylene glycol diacrylate
PEG-DE	Polyethylene glycol diglycidyl ether
PEG-DMA	Dimethacrylated polyethylene glycol
PEG-DSH	Dithiolated polyethylene glycol
PEG-MA	polyethylene glycol methacrylate
PEO	Polyethylene oxide

PNIPAAm	Poly(N-isopropylacrylamide)
PR	Polyrotaxane
PS	Penicillin/streptomycin
PVA	Polyvinyl alcohol
RAFT	Reversible addition fragmentation chain transfer
RGD	Arginylglycylaspartic acid
SA	Sodium alginate
SGF	Simulated gastric fluid
SN	Single network
TGases	Transglutaminase
TPO	Diphenyl(2,4,6-trimethylbenzoyl)phosphine oxide
UPy	Ureido-pyrimidinone
UV	Ultraviolet

ABSTRACT

Hydrogels closely resemble living tissues, featuring a classical three-dimensional (3D) network structure composed of a hydrophilic polymer network and surrounding water-based fillers. This bionic resemblance has led to the development of hydrogels for numerous biomedical applications. Among these, injectable hydrogel systems have attracted significant attention due to their ease of operation, efficient encapsulation viability, minimal invasiveness, and enhanced patient compliance. However, injectable hydrogels have long been considered mechanically weak and challenging to meet the requirements of biological applications under load-bearing conditions. The objective of this study is to develop tough injectable hydrogel systems without compromising their biocompatibility. **Chapter One** introduces the raw materials and *in situ* crosslinking methods for injectable hydrogels, and the universal hydrogel toughening design including elastic maintenance and mechanical energy dissipation. It also proposes combining mechanisms and guides the design of hydrogels with improved mechanical properties through biomimetic structuring and multi-scale collaboration, for diverse clinical applications. **Chapter Two** presents a single network (SN)

injectable hydrogel with enhanced toughness, featuring a rigid and homogeneous hyaluronic acid (HA) framework linked by polyethylene glycol (PEG) flexible long chains. This structure design increases compressive stress by 7 times and toughness by 4 times compared to conventional SN hydrogels. **Chapter Three** presents a thermo-entangled injectable hydrogel with high toughness, formed by self-assembly of diacrylated F127 (F127-DA) and crosslinked with HA framework via Thiol-ene Michael addition. It achieves a compressive strength of 9.08 MPa and toughness of 753 kJ/m³. **Chapter Four** investigates an acid-triggered double network (DN) injectable hydrogel. The first HA network forms via Thiol-ene Michael addition, while the second sodium alginate (SA) network is crosslinked by Ca^{2+} from acid-dissolvable hydroxyapatite (HAp) nanoparticles. This results in a 3-fold increase in compressive strength and 2.5-fold increase in toughness compared to normal DN hydrogels, with improved resistance to fatigue, swelling, and degradation. **Chapter Five** summarises the research findings and discusses future directions for the development of tough injectable hydrogels.

STATEMENT OF ORIGINAL AUTHORSHIP

I hereby certify that the submitted work is my own work, was completed while registered as a candidate for the degree stated on the Title Page, and I have not obtained a degree elsewhere on the basis of the research presented in this submitted work.

_____

Rijian Song

COLLABORATIONS

I sincerely acknowledge the contributions of the following individuals for their conduction or assistance in the experimental procedures of my dissertation:

Chapter 2: Altan Demircan assisted with the visualisation of the injectability and *in situ* gelation of hydrogels.

Chapter 3: Chunyu Zhao assisted with the swelling behaviour and rheological properties of the hydrogels.

Chapter 4: Altan Demircan assisted with particle size analysis, transmittance testing, surface potential measurement, rheological properties, and swelling behaviour assessments. Tianyu Guan conducted the SEM testing of the freeze-dried hydrogel samples. Xinhui Wang 3D-printed the moulds used for hydrogel stamping. Chunyu Zhao assisted in the visualisation of the hydrogels.

Their invaluable contributions have significantly enhanced the quality and depth of this research.

ACKNOWLEDGEMENTS

I do consider myself incredibly fortunate to have met so many wonderful people during my PhD journey. I am deeply grateful for your companionship, guidance, and support throughout these years.

First and foremost, I want to thank my supervisor, Prof. Wenxin Wang, for his guidance, support, and mentorship throughout my studies. His expertise and enthusiasm have significantly influenced my research, academic journey, and future career, and personal life. I am grateful to have been mentored by Prof. Wang, and I am confident that his influence will benefit my future career and personal life.

I would like to express my sincere appreciation to my doctoral studies panel, Prof. Amanda McCann and Dr. Stephen Lalor, for their insightful suggestions and input throughout my dissertation work. Their constructive guidance has helped me improve the quality of my research.

I am also grateful to my colleagues, Melissa Johnson, and Cameron Milne, for their invaluable assistance with English, experiments, thesis writing, and cultural understanding. Special

thanks go to Dr. Sigen A for his direction, suggestions, and support throughout my research. Additionally, I want to express my gratitude to my friends, Yinghao Li, Chunyu Zhao, Zhonglei He, Xi Wang, Altan Demircan, Zishan Li, Jing Lyu, Qiang Geng, and Runqi Zhu, for their friendship, support, and encouragement during my time in Dublin. Their camaraderie has greatly enriched my academic journey.

I would like to extend my appreciation to all the team members in our lab and to everyone who has supported me throughout my PhD journey: Hongyun Tai, Qian Xu, Hong Zhang, Xianqing Wang, Irene Lara Sáez, Jing Zhang, Jing Wu, Liang Yao, Hanqing Yu, Yi Cai, Francesca Santoro Ferrer, Hang Yin, Albina Bushmalyova, Darío Manzanares Sandoval, Bei Qiu, Mihai Negru, Josie Ward, Yi Situ, Irene Reuben, Ruth Foley, Tongfan Hao, Lizhu Yang, Xueyan Yun, Jasmine Cautley, Eoghain Murphy, Xiaoyu Wang, Zhiran Wang, Xinhui Wang, and Tianyu Guan for their professional advice and support. Their diverse perspectives and expertise have enriched my academic experience and made it possible for me to achieve my research goals.

Last but not least, my heartfelt thanks go to my family. I am profoundly thankful for their understanding and unwavering support, which have been essential as I have explored the boundaries of knowledge, cognition, and experience for nearly 30 years.

At the end, I am deeply aware that my limited knowledge restricted my exploration process, my restricted cognition slowed my understanding of first principles, and my language proficiency has hindered the true expression of my thoughts. However, I would like to thank myself for not being stopped by these difficulties; instead, they have gradually brought me towards the places I aspire to reach.

Rijian Song

May 2024

Chapter One

Introduction

Part of this chapter has been organised in the manuscript:

Song, R., Milne, C., Johnson, M., Zhao, C., A, S.*, Wang, W.* 'Advances in Toughness for *in situ* Formed Hydrogels'. In preparation.

1.1 Tough Injectable Hydrogels Overview

Hydrogels consist of a classic three-dimensional (3D) network structure comprising hydrophilic polymer frameworks and surrounding water fillers.[1,2] Hydrogels possess elastic solid properties due to the presence of a cross-linked network framework.[3,4] Moreover, owing to the abundant bound water surrounding the polymers as well as free water, hydrogels also exhibit liquid characteristics.[5,6] Most of the fundamental components of the human body, such as cells, extracellular matrix (ECM), tissues, and organs, are similarly constituted by a hydrogel-like structure infused with hydrophilic biopolymer networks.[5,7] These hydrogel components are soft and elastic, facilitating the thorough and orderly exchange of nutrients and waste, as well as the efficient transmission of bioelectric signals within organisms.[8,9] It is undeniable that throughout the natural evolutionary process, many biological functions in organisms have chosen to rely on the advantageous hydrogel structure.[10–12] Therefore, it is not surprising that artificial hydrogels have been widely applied in various biomedical fields such as tissue engineering and drug delivery systems.[4,12–15]

Among various hydrogel systems, injectable hydrogel systems

have garnered significant attention in the biomedical field due to their ease of application, efficient encapsulation capabilities, minimally invasive nature, and improved patient compliance.[13,16,17] Injectable hydrogels involve the injection of precursor solutions into the target site without the need for complicated surgical procedures.[18,19] Subsequently, through various *in situ* crosslinking mechanisms, the formed hydrogels perfectly conform to the shape of the treated tissue or organ defect, providing excellent tissue contact and integration capabilities.[20,21] This simple and flexible nature gives it unparalleled advantages in areas such as injectable tissue engineering scaffolds,[22,23] local minimally invasive drug and cell delivery,[24,25] tissue sealants,[26,27] and medical implants.[13,28,29]

The mechanical properties of hydrogels play a crucial role in their practical applications.[30,31] Over the past few decades, soft material scientists have devoted significant efforts to developing tough hydrogel systems, such as homogeneous hydrogels,[32,33] double network (DN) hydrogels,[34,35] highly entangled hydrogels,[36,37] pearl-necklace structure hydrogel,[38] weak and strong crosslink hydrogel,[39] nano clay hydrogel,[40] and slide ring hydrogel.[41] However, these toughening designs often cannot be achieved

through injectable methods. Additionally, the development of tough injectable hydrogels has predominantly relied on trial-and-error approaches, and their mechanical properties still fall short of meeting clinical application requirements. Therefore, thorough investigation of existing *in situ* forming methods and toughening designs for injectable hydrogels is essential to inspire universal strategies for mechanically strong injectable hydrogels.

As shown in **Figure 1.1**, we summarise the general constructions of injectable hydrogel systems, including raw materials and *in situ* crosslinking reactions in this chapter. Additionally, we discuss the network characteristics of general tough hydrogels, including structures for maintaining high elasticity and dissipating mechanical energy. By combination of the characteristic structure of tough hydrogels and *in situ* forming strategies, the tough injectable hydrogel can be designed and achieved. Based on the analysis above, we provide potential implementation strategies to enhance the toughness of *in situ* formed hydrogels, guiding the design of mechanically strong injectable hydrogels for various future applications.

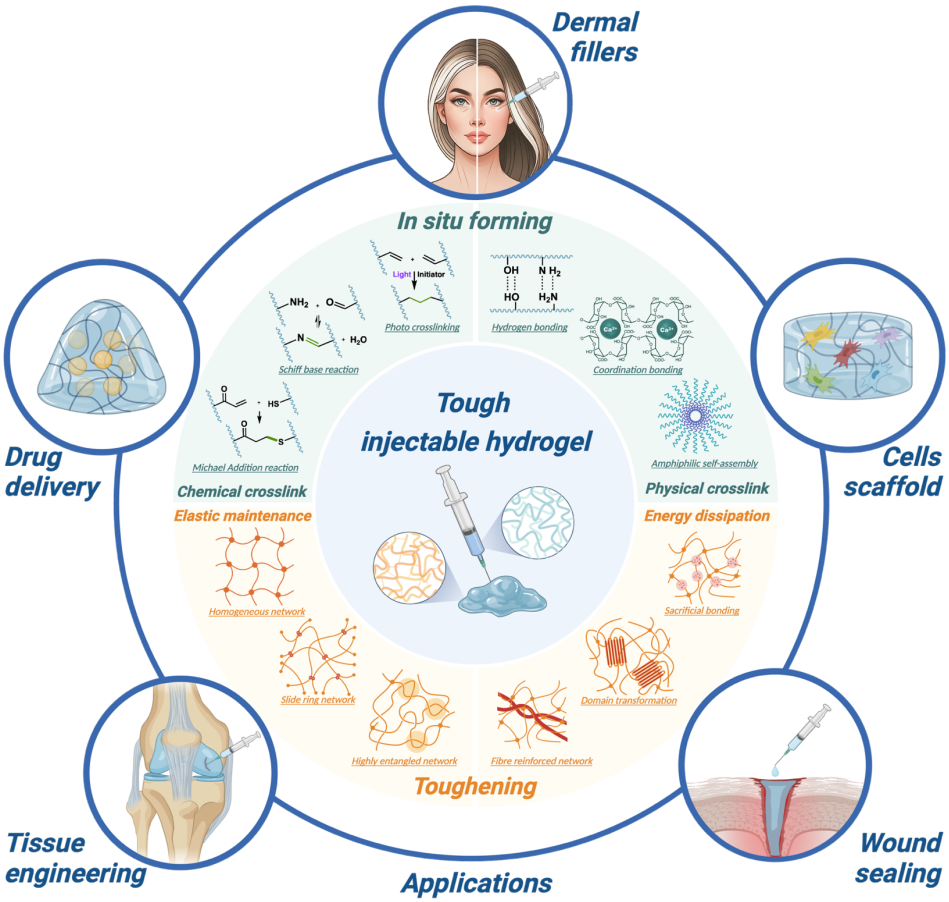


Figure 1.1 Illustrated overview of the *in situ* forming methods and toughening designs of tough injectable hydrogels, and their biomedical applications. [Created with BioRender]

1.2 Common Polymers for Injectable Hydrogels

After decades of development, polymer substrates for constructing hydrogels have a rich resource pool.[31,42,43] Researchers crosslink these polymers into network structures through physical or chemical methods, utilising their hydrophilicity to retain water and

form hydrogels with solid-like properties.[44] However, only a small fraction of these polymers is suitable for constructing injectable hydrogels, which can be categorised into natural polymers and synthetic polymers (**Figure 1.2**).[21] In this section, we will briefly discuss the natural and synthetic polymers that can be used for injectable hydrogels, while their specific *in situ* forming mechanisms will be discussed in the section 1.3.

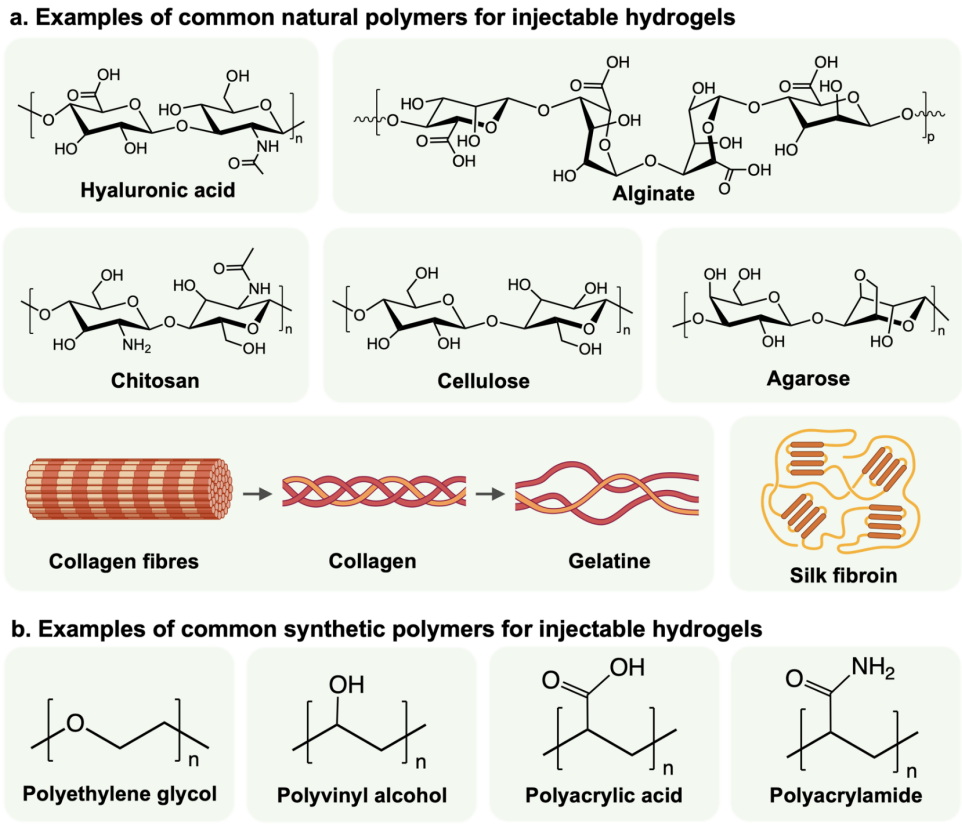


Figure 1.2 Chemical structure and schematics of typical raw polymers for injectable hydrogels: (a) natural polymers; (b) synthetic polymers. [Created with BioRender]

1.2.1 Natural Polymers for Injectable Hydrogels

Natural polymers, also known as biopolymers, are widely used in constructing biomedical hydrogel systems due to their component resemblance to biological tissues.[43,45] In many cases, hydrogels composed of natural biopolymers exhibit biodegradability and excellent biocompatibility.[46] Moreover, most natural polymers possess inherent biological activity, which can be inherited by the hydrogels and then provide advantages in applications.[47,48] Natural polymers typically have abundant chemical sites available for crosslinking or modification, allowing for functionalisation and imparting *in situ* crosslinking capabilities to these hydrogels.[43,49] Commonly, biopolymers are ionically charged polymer chains (polyelectrolytes) with strong affinity for water molecules.[50,51] This water absorption ability enables the formation of stable 3D hydrogel structures even at low polymer contents.[52] This section provides a brief introduction to the most common biopolymers.

1.2.1.1 Hyaluronic Acid

Hyaluronic Acid (HA) is a natural, linear polysaccharide. Its structure consists of repeating disaccharide units of N-acetyl-D-glucosamine and D-glucuronic acid linked alternately by β-(1→4)

and β-(1→3) glycosidic bonds.[53] HA is widely present in the epithelial, connective, and neural tissues of all mammals, serving as one of the most important constituents of the ECM.[54] Due to its large molecular size, remarkable hydrophilicity, and viscoelasticity, HA regulates tissue hydration, osmotic balance, and the physical properties of the ECM, establishing a hydrated and stable extracellular space to maintain an optimal cellular environment.[55] As a signalling molecule, HA interacts with proteins to promote or inhibit inflammation, cell migration, and cell division or differentiation, depending on its molecular weight, location, and specific cellular factors such as receptor expression, signalling pathways, and cell cycle.[56–58] Additionally, the abundant carboxyl and hydroxyl groups on HA provide numerous active sites for chemical modification and crosslinking, offering extensive possibilities for preparing HA-based hydrogels.[59–61] HA can be covalently crosslinked in alkaline solutions using small molecule crosslinkers such as 1,4-butanediol diglycidyl ether (BDDE),[62–64] polyethylene glycol diglycidyl ether (PEG-DE),[65–67] and divinyl sulfone (DVS) to form stable 3D hydrogel systems.[68] These hydrogels have been utilised in the field of medical aesthetics for nearly 20 years.[69] However, due to concerns about

residual crosslinkers, uncontrolled crosslinking structures, and limitations on pre-formed crosslinking methods, they have gradually become unsuitable for the latest biomedical demands.[67,70] Injectable HA hydrogels have made significant progress in recent years thanks to advances in chemical modification and processing technologies.[21,43] HA can be modified to obtain functional groups such as acrylic, thiol, aldehyde, and tyramine, and applied directly to target sites through different *in situ* crosslinking strategies.[71,72] These injectable HA hydrogels, characterised by endogenous sourcing, minimally invasive implementation, and non-toxic components, have been widely used as scaffolds for tissue engineering,[73] drug delivery,[24,74] stem cell therapy,[25] bioprinting,[75,76] cartilage repairing,[77] wound healing,[78] and cells transplantation.[79]

1.2.1.2 Sodium Alginate

Sodium alginate (SA) is a natural polysaccharide derived from brown algae.[80] SA is composed of alternating β-D-mannuronic acid (M-unit) and α-L-guluronic acid (G-unit) residues, linked via β-(1→4) glycosidic bonds.[81] These repeat units are arranged in the polymer chain in continuing (e.g., MMMMMM or GGGGGG) or alternating (e.g., GMGMGM) forms.[82] SA hydrogels can be

formed using a variety of covalent and physical crosslinking methods, with coordination bonding being a widely utilised technique. When metal ions, especially divalent cations (such as Ca^{2+}, Mg^{2+}, Ba^{2+}, and Sr^{2+}), are added to a SA, they interact with the G-units to form coordination bonding resembling the "egg-box" structure.[83] In this structure, each metal ion acts as a cavity in the egg-box, and carboxylate groups from multiple G-units cluster around the metal ions, forming a stable connection through coordination bonds, thus creating a hydrogel with a stable 3D network structure.[84] By adjusting various parameters such as molecular weight, polymer concentration, and G/M ratio, the mechanical properties of SA hydrogels can be tailored to match those of different biological tissues.[85] The coordination bonding technique in injectable SA hydrogel skills has been utilised in the preparation of hydrogel microsphere and sutures.[86] However, the excessively rapid crosslinking process and inhomogeneous network structure hinder their practical application.[87,88] Chemical modification of SA can further enhance the stability of injectable SA hydrogels, impart *in situ* chemical crosslinking capabilities, or improve cell recognition and adhesion.[89,90] Injectable SA hydrogels has been widely used in tissue engineering scaffolds,

wound dressings, intervertebral disc regeneration, and 3D bioprinting.[91–94] Despite its many advantages, injectable SA hydrogel still faces challenges in biomedical applications, such as insufficient mechanical strength.[95]

1.2.1.3 Agarose

Agarose is a polysaccharide extracted from red seaweed, comprising a linear biopolymer of D-galactose and 3,6-anhydro-l-galactopyranose units linked by β-(1→4) glycosidic bonds.[96] It is a thermo-responsive biopolymer that dissolves in hot water and forms intermolecular hydrogen bonds as the temperature decreases. During this process, the structure of agarose transitions from random coils to double helices, aggregating into a network structure.[97] By adjusting the concentration and molecular weight of agarose in hydrogels, both the gelation temperature and the mechanical properties can be fine-tuned. The biologically inert nature of agarose hydrogels imparts them with immune evasion properties.[98] Moreover, the thermally reversible gelling behaviour makes injectable agarose easily constructed.[99] These advantages have led to the widespread utilising of injectable agarose hydrogels in various biomedical applications, including tissue engineering, cell culture, *in situ* drug delivery, wound healing, and

skin regeneration.[100–104] Furthermore, chemical modification can grant agarose the capacity for *in situ* covalent crosslinking, thereby enhancing its mechanical stability.[105]

1.2.1.4 Chitosan

Chitosan (CTS) is a linear cationic polysaccharide obtained through the partial deacetylation of chitin, which is found in the exoskeletons of crustaceans like crabs and shrimp.[106] It is composed of β-(1→4)-linked D-glucosamine and N-acetyl-D-glucosamine. The physical, chemical, and biological properties of CTS are closely related to their degree of deacetylation and molecular weight.[107,108] CTS hydrogels can be prepared using various methods, including physical crosslinking, chemical crosslinking, photo-crosslinking, biological crosslinking, and combined methods.[109,110] Physical crosslinking methods are simple and environmentally friendly but produce gels with relatively weak mechanical properties that are significantly affected by pH and temperature.[111,112] Chemical crosslinking, using aldehydes or isocyanates as crosslinking agents, offers stronger mechanical properties and more stable network structures, but may involve toxic chemicals.[113] Additionally, CTS can be modified with acrylic acid or azide groups to form injectable

hydrogel systems that can be photo crosslinked.[114] Due to their excellent biocompatibility, biodegradability, and antibacterial properties, CTS hydrogels are ideal materials for various fields including biomedicine, drug delivery, and tissue engineering.[47,115,116]

1.2.1.5 Cellulose

Cellulose is one of the most abundant polysaccharides in nature, composed of β-(1→4) linked D-glucose units. Its high crystallinity and insolubility in water limit direct applications.[117] Chemical modifications produce derivatives like carboxymethyl cellulose (CMC) and hydroxypropyl cellulose (HPC), widely used in the medical and food industries due to their improved solubility and processability.[118] Cellulose and its derivatives can form stable 3D network structures through chemical crosslinking with agents such as epichlorohydrin (ECH), ethyleneglycol diglycidylether (EGDE), and succinic anhydride, creating covalent ester or ether bonds.[119–121] Electron beam and γ-irradiation offer alternative covalent crosslinking methods, avoiding toxic agents and allowing sterilisation of the resulting hydrogels.[122,123] Cellulose can also be chemically modified to incorporate functional groups such as aldehyde and amine, thereby gaining the ability to form *in situ* and

be injectable hydrogel.[124] Cellulose hydrogels, known for their excellent hydrophilicity, biocompatibility, and transparency, are extensively applied in drug delivery, tissue engineering, and blood purification.[125–127]

1.2.1.6 Collagen

Collagen is one of the primary components of the ECM, constituting over one-third of the protein content in human body.[128] To date, about 29 types of collagens have been identified, with types I, II, III, and IV being the most common. Type I collagen represents over 85% of human collagen.[129] The structure of collagens includes primary (amino acid triplets), secondary (α-helix), tertiary (triple helix), and quaternary (fibrous) levels.[130] Its primary structure features a tripeptide sequence of -(Gly-X-Y-)$_n$-, where Gly is glycine, and X and Y are other amino acids, typically proline and hydroxyproline.[131] Collagen hydrogels are commonly prepared by adjusting the pH of collagen solutions to neutral, causing molecules to aggregate, rearrange, and self-assemble via physical crosslinking.[132] UV and γ-irradiation can create new crosslinked network structures by breaking and recombining chemical bonds in collagen molecules.[133] Additionally, collagen hydrogels can be reinforced and stabilised through covalent

amine/imine bonds using agents like glutaraldehyde (GA), genipin, and N-hydroxysuccinimide (NHS).[134] Transglutaminases (TGases) and horseradish peroxidase (HRP) can *in situ* crosslink collagen networks enzymatically and create injectable hydrogels.[135] Additionally, by utilising the amino groups on collagen or through chemical modification, collagen hydrogels can be endowed with the ability for *in situ* crosslinking and injectability.[136] Compared to non-crosslinked collagen, crosslinked collagen hydrogels usually have better stability, mechanical properties, and slower degradation rates, although crosslinking can reduce biological activity.[137] Collagen hydrogels, characterised for low antigenicity, excellent biocompatibility, and natural cell growth and migration promotion, are widely used in tissue engineering, wound healing scaffolds, cartilage repair and regeneration, drug and protein delivery, and cosmetic and reconstructive surgery.[138–140]

1.2.1.7 Gelatine

Gelatine is a biopolymer obtained by breaking down the triple-helix structure of collagen into single-stranded molecules through hydrolysis and denaturation.[141] There are two types of gelatine produced from collagens: Type A, derived from acid-treated collagen, and Type B, derived from alkali-treated collagen.[142]

Although the preparation of gelatine destroys the triple-helix structure of collagen, the tripeptide sequence Gly-X-Y is preserved.[143] Additionally, gelatine contains the arginylglycylaspartic acid (RGD) sequence (Arg-Gly-Asp), serving as a cell adhesion site that enhances cell integration and tissue repair in tissue engineering applications.[144] Gelatine hydrogels can be physically crosslinked by lowering the temperature. However, these physical hydrogels are typically unstable under physiological conditions, posing a challenge for biomedical applications.[145] To achieve stable gelatine hydrogels, aldehyde crosslinkers, such as formaldehyde and GA, are used to react with the free amine and carboxyl groups on the gelatine molecules, facilitating covalent bonding.[146] *In situ* chemical crosslinking further offers injectability and enhanced stability, achieved by grafting functional groups on the gelatine chains. This method not only improves mechanical properties but also expands the application range of gelatine hydrogels.[147] Their ease of preparation, coupled with exceptional biocompatibility, biodegradability, biological activity, temperature sensitivity, and cell adhesion capability, makes gelatine hydrogels highly valued in biomedical applications such as drug delivery, tissue

engineering, and wound healing.[148–150]

1.2.1.8 Silk Fibroin

Silk protein, produced by the glands of various arthropods including silkworms and spiders, consists of multiple proteins.[151] It primarily comprises two proteins: fibroin and sericin. Fibroin, consisting of heavy and light chains linked by disulfide bonds, is characterised by highly repetitive sequences and hydrophobic regions that confer crystallinity. This structure contributes to the environmental stability of fibroin, providing significant strength and elasticity to silk fibres. Sericin, acting as a glue-like substance, envelops fibroin, binding the fibres together.[152] Hydrogels derived from silk fibroin closely mimic the ECM, offering mechanical support and physicochemical cues similar to the ECM.[153] The transition of β-sheet structures allows the hydrophobic amino acid groups in silk fibroin, such as glycine, serine, and alanine, to physically crosslink and form an injectable hydrogel.[154] Nonetheless, silk fibroin that is physically crosslinked often lacks stability under physiological conditions, presenting challenges for its biomedical use.[155] Chemically crosslinked silk fibroin demonstrates enhanced stability, fulfilling the requirements of biomedical applications, such as cartilage tissue engineering,

tissue repair, and regeneration.[156–158]

1.2.2 Synthetic Polymer for *in situ* Formed Hydrogels

It is widely acknowledged that synthetic polymers generally do not match biopolymers in terms of biocompatibility and biodegradability.[159] However, synthetic polymers normally offer controllability and processability that biopolymers cannot match.[160] Functionalisation, grafting, and modification of synthetic polymers can yield highly tuneable and ideal characteristics.[161] Moreover, synthetic polymers can achieve block copolymer features through copolymerisation, thereby endowing a single polymer chain with controllable physical properties or crosslinking potential.[162] Additionally, controlled polymerisation of polyvinyl monomers can produce polymers with unique topological structures such as hyperbranching or knots, leading to exceptional hydrogel properties.[163] The following section provides a brief overview of the most common synthetic polymers.

1.2.2.1 Polyethylene glycol

Polyethylene glycol (PEG) has long been regarded as the biocompatible gold standard among synthetic polymers, typically synthesised through the ring-opening polymerisation of ethylene

oxide.[164] When it has a relatively high molecular weight, PEG is also named polyethylene oxide (PEO). However, the naming can vary depending on the application field, so the distinction is not strictly enforced. The unique structure of PEG, where the spacing of oxygen atoms matches that of hydrogen in water molecules, grants it unparalleled water solubility among polyethers.[165] Attributed to the high hydrophilicity of PEG, it allows for the formation of a stable hydration layer in water.[166] This structure effectively 'camouflages' PEG molecules, making them less recognisable to immune cells and thus reducing immunogenicity.[167] Hydrogels constructed from PEG inherit its biologically inert characteristics, preventing adverse interactions with cells.[168] Although there are various methods to crosslink PEG polymers into hydrogels, most involve functionalising the ends of PEG chains with groups such as acrylates, thiols, maleimides, N-hydroxysuccinimide, adenine, and β-cyclodextrin.[169] These functional groups not only allow PEG hydrogels to form stable 3D structures in injectable methods but also enable the grafting of biologically active molecules.[170] Furthermore, due to the controllable chain length and multi-arm structures of PEG, it can be used to study the effects of network topology on hydrogel

properties. [171] Because of these advantages, PEG hydrogels are among the most widely used materials in injectable hydrogel design.[172]

1.2.2.2 Polyvinyl alcohol

Polyvinyl alcohol (PVA) is typically produced by the hydrolysis of polyvinyl acetate. It is observed that with an increase in the degree of hydrolysis and molecular weight, a more regular and dense arrangement of hydroxyl groups is formed along the PVA chain.[173] Due to the presence of both intermolecular and intramolecular hydrogen bonds, as well as a high degree of crystallinity, the dissolution of PVA in water above 80°C necessitates vigorous stirring.[174] Furthermore, the extensive interchain hydrogen bonding causes PVA with high concentration (greater than 15wt%) to become exceedingly viscous, posing challenges in processing.[175] The most straightforward approach for fabricating PVA hydrogels involves the use of repeated freeze-thaw cycles.[176] In addition, covalent crosslinking of PVA can be achieved using bifunctional crosslinkers, such as aldehydes or epoxides, or through gamma ray irradiation.[177] Moreover, by functionalising the hydroxyl groups on the PVA chains, including modifications with vinyl and amino groups, the material is

endowed with injectable and *in situ* forming capabilities.[178,179] The outstanding biocompatibility, mechanical strength, and permeability of PVA hydrogels account for their extensive application in the field of biomedical engineering, notably in joint cartilage replacement and drug delivery systems.[180–182]

1.2.2.3 Polyacrylic acid

Polyacrylic acid (PAA) is produced by synthesizing acrylic acid monomers through free radical polymerization, resulting in a linear polymer.[183] PAA is characterised by a high content of carboxylic groups that are ionizable, rendering it an effective artificial polyelectrolyte. It has the capacity to draw and hold water molecules from its environment.[184] The crosslinking of PAA into hydrogels, achievable through either chemical or physical means, is facilitated with ease.[185] Structurally stable 3D hydrogels are formed by incorporating various fillers like trivalent iron ions, MXene, and nano clay, utilising coordination bonds, hydrogen bonds, or electrostatic interactions.[186–188] Owing to its simple crosslinking techniques, economical production, and superior water absorption properties, PAA hydrogels find extensive applications in areas such as drug delivery, wound care, haemostatic products, and soft sensors.[189–191]

1.2.2.4 Polyacrylamide

Polyacrylamide (PAM) is synthesised through the free radical polymerisation of acrylamide monomers.[192] PAM is often considered to be an inert polymer due to the abundant amide bonds on its side chains, which make it extremely hydrophilic.[193] There are various methods for preparing PAM hydrogels, with common techniques involving the addition of crosslinkers such as N,N'-methylene-bis-acrylamide (BIS) or GA to achieve stable chemical bonding.[194,195] Over the past 20 years, PAM hydrogels have been widely used as polymer soft tissue fillers. However, in recent years, cases of inflammatory reactions caused by polyacrylamide hydrogels have gradually emerged.[196] In current research and practical applications, other polymers from the PAM family have emerged as crucial materials for hydrogel construction.[197,198] Through copolymerisation, it is possible to create side chains with positive charges, negative charges, hydrophilicity, or hydrophobicity, enabling PAM-related polymer hydrogels to be injectable and meet the application needs of various fields, including biomedicine. [199,200]

1.3 Common Crosslink Methods for Injectable Hydrogels

Considering the intended applications of injectable hydrogels, whether inside the body or on its surface, the gelation process and materials must not adversely affect the organism or the encapsulated drugs or cells.[201] This section focuses on the prevalent physical and chemical *in situ* crosslinking methods applicable to injectable hydrogels. It is critical to acknowledge that the mechanical properties of hydrogels are significantly determined by the bond energies involved. Typically, the energy associated with covalent bonds surpasses that of dynamic covalent bonds and physical interactions, although exceptions exist.[31] Furthermore, highly organised, and densely packed physical bonds can likewise ensure robust hydrogel performance.[202] However, the enhancement of toughness in injectable hydrogels is severely constrained by the limited availability of materials and *in situ* crosslinking methods.[203] The exploration of this subject will proceed in the section 1.4.

1.3.1 Chemical Crosslinking

The pursuit of scientific discovery, much like the alchemists'

search for gold, often leads to the unveiling of knowledge far more valuable than originally sought. This is particularly true in the realm of chemistry, whose advancements have consistently propelled the field of biomedical sciences forward. For example, the introduction of chemical covalent crosslinking techniques has facilitated the creation of highly stable hydrogels. Innovations in chemical dynamic covalent crosslinking have endowed hydrogels with properties such as stability, self-healing, and responsiveness to environment stimulation. Ideally, the chemical crosslinking approaches used to develop *in situ* formed injectable hydrogels should avoid any toxic monomers, initiators, or crosslinkers, aiming for minimal energy input and output.[204] This section will discuss several of the most widely accepted chemical crosslinking methods for achieving injectable hydrogels.

1.3.1.1 Thiol-ene Michael addition

The Michael addition reaction is a type of nucleophilic addition involving α, β-unsaturated ketones or esters with nucleophiles **(Figure 1.3a**).[205] Under alkaline conditions, the Thiol-ene Michael addition reaction combines thiol molecules (Michael donors, nucleophiles) with electron-deficient alkenes (Michael acceptors, α, β-unsaturated carbonyl compounds such as acrylate esters,

maleimide, vinyl sulfone, acrylamide, etc.), forming thioether bonds (C-S).[206] These electron-deficient alkenes typically feature a strong electron-withdrawing group adjacent to the alkene (carbonyl, sulfonyl, etc.), rendering the vinyl groups susceptible to attack by nucleophilic thiols. Biopolymers can be functionalised through either alkene or thiol groups to form a pair of Thiol-ene Michael addition materials, enabling *in situ* formation **(Figure 1.3b**).[49] Synthetic polymers can achieve similar functionalities through functionalisation of end groups, copolymerization, or polymerisation using monomers containing α, β-unsaturated carbonyl compounds. This reaction proceeds efficiently under mild conditions without the need for initiators and does not produce any toxic by-products. By adjusting the concentration and ratio of Michael Addition donor and acceptor groups, as well as the environmental pH, the gelling process can be controlled from a few seconds to several hours.[207]

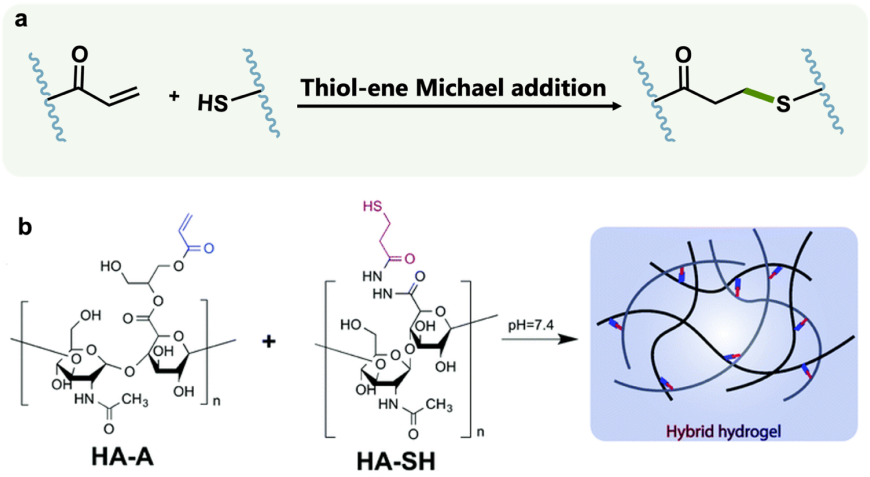


Figure 1.3 Examples of injectable hydrogels prepared by Thiol-ene Michael addition reaction: (a) Thiol-ene Michael addition reaction; (b) HA-based hybrid hydrogel created by Thiol-ene Michael addition reaction.[49] [Cropped image. Copyright© 2018 Royal Society of Chemistry]

To date, numerous studies have utilised the Thiol-ene Michael addition reaction to prepare advanced *in situ* formable injectable hydrogels.[208] Shu et al. conducted a detailed investigation into the gelation rates by reacting thiolated hyaluronic acid (HA-SH) with PEG of different reactivities as Michael acceptors.[209] *In vivo* and *in vitro* fibroblast culture tests also demonstrated its enormous potential in cell encapsulation applications. Liu et al. prepared an injectable stem cell hydrogel scaffold through the Thiol-ene Michael addition reaction between glycidyl methacrylate-modified poly(γ-glutamic acid) and 1,4-dithiothreitol (DTT).[210] Cells cultured *in vitro* on this scaffold showed good proliferation

and adhesion capabilities, and the hydrogel scaffold containing stem cells significantly accelerated the regeneration of rabbit ear cartilage. Jing et al. prepared an injectable hydrogel via the Thiol-ene Michael addition reaction between 4-arm thiolated PEG and maleimide-functionalised HA, extensively exploring the effects of polymer concentration and the degree of maleimide substitution on HA on the gelation time and modulus of the hydrogels.[211] Xu et al. synthesised multi-acrylate hyperbranched PEG (HB-PEG) using an *in situ* reversible addition fragmentation chain transfer (RAFT) polymerisation.[212] They developed an injectable hydrogel system for *in situ* delivery of stem cells using HB-PEG and HA-SH, demonstrating enhanced healing effects on chronic wounds. Furthermore, Chen et al. created a purely biopolymer-based *in situ* formed injectable hydrogel system using acrylated HA (HA-A) and HA-SH. After loading with dexamethasone, this hydrogel exhibited an ability to long-term alleviate sciatic nerve pain caused by lumbar disc herniation.[24]

1.3.1.2 Schiff base reaction

Schiff bases, named after Hugo Schiff, are dynamic covalent imines that result from the reaction between primary amines and carbonyl compounds, including aldehydes and ketones.[213] In this

reaction, the nitrogen atom from the primary amine nucleophilically attacks the carbon atom of the carbonyl, creating an unstable transition-state intermediate. This intermediate then rearranges, losing a water molecule and forming an imine bond (**Figure 1.4a**). This reversible process occurs rapidly under physiological conditions and produces only water as a by-product, showcasing outstanding biocompatibility.[214] Materials derived from Schiff bases are utilised to create self-healing injectable hydrogels (**Figure 1.4b**).[215] By modifying the ratio and concentration of the amine and carbonyl groups, both the gelation time and the mechanical strength of the hydrogel can be precisely adjusted.[216] Additionally, the degradation rate of Schiff bases hydrogel can be tailored by altering the pH level.[217] The residual carbonyl groups of hydrogels can interact with protein drugs or the amine groups of endogenous biomolecules, offering diverse functionalities.[218]

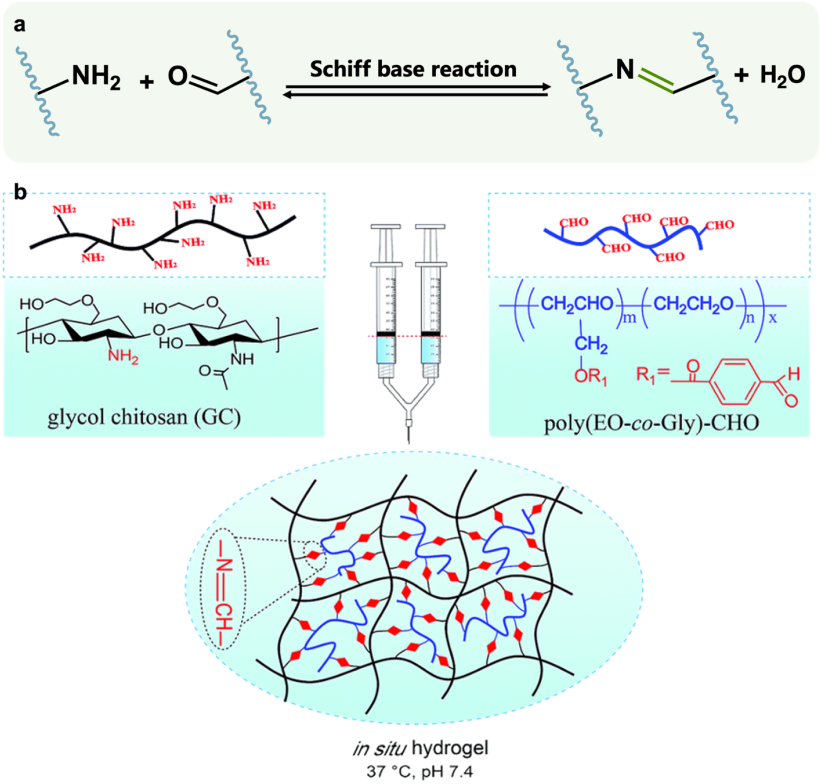


Figure 1.4 Examples of injectable hydrogels prepared by Schiff base reaction: (a) Schiff base reaction; (b) an *in situ* formed hydrogel created by Schiff base reaction.[215] [Cropped image. Copyright© 2015 Royal Society of Chemistry]

Research and practical applications have extensively explored hydrogels based on Schiff base reactions. For example, Wang et al. developed an injectable hydrogel wound dressing through dynamic Schiff base bonding between oxidised chitosan (CTS-CHO) and CTS, demonstrating self-healing properties, antibacterial effectiveness, and good biocompatibility.[47] Similarly, Wu and his team formulated an injectable drug carrier hydrogel by

using aldehyde-functionalised 4-arm polyethylene glycol and 4-arm polyethylene glycol-b-poly(L-lysine).[219] This hydrogel enables the pH-controlled release of metformin and 5-fluorouracil, showing promise for colon cancer therapy. When primary amines, attached to nitrogen or oxygen atoms, react with carbonyl groups, they form hydrazones and oximes, which are more stable than imines. Some researchers include hydrazones and oximes in the category of Schiff base linkages, as these are also condensation products of carbonyls, characterised by dynamic covalent bonding. Sigen A et al. developed a printable hydrogel using hyperbranched PEG-based hydrazide (HB-PEG-HDZ) combined with aldehyde-functionalised hyaluronic acid (HA-CHO).[220] This injectable system offers protection to cells from shear damage during printing, markedly improving the survival rates of transplanted cells.

1.3.1.3 Photo Crosslinking

Photo crosslinking is not a perfect method for injectable hydrogel preparation due to its dependence on photo-initiators and external energy inputs.[221] However, photo crosslinking technology enables the rapid and controllable *in situ* formation of hydrogels, significantly expanding their engineering applications (**Figure**

1.5a).[222] The essence of constructing photo-initiated hydrogels lies in the cleavage of photo-initiators, releasing free radicals to initiate the polymerisation and crosslinking of vinyl-containing monomers.[223] Common photo-initiators used in hydrogel construction include Lithium phenyl-2,4,6-trimethylbenzoylphosphinate (LAP), 2-Hydroxy-4′-(2-hydroxyethoxy)-2-methylpropiophenone (I2959), diphenyl(2,4,6-trimethylbenzoyl) phosphine oxide (TPO), among others.[224] These photo-initiators generally possess good water solubility and can generate free radicals under ultraviolet (UV) or visible light exposure. By adjusting the polymer concentration, initiator concentration, light intensity, and exposure time, the strength of the hydrogels can be controlled.[225] Since monomers and crosslinkers are usually toxic, they are not suitable for direct crosslinking in the human body.[226]

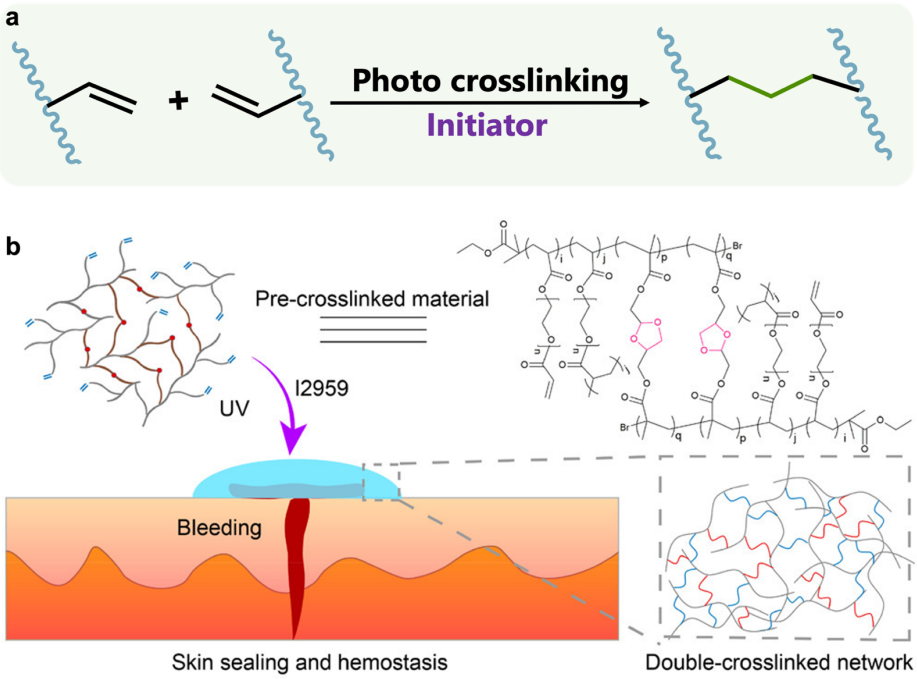


Figure 1.5 Examples of injectable hydrogels prepared by photo crosslinking: (a) photo crosslinking reaction example; (b) an injectable hydrogel created by photo crosslinking reaction.[222] [Cropped image. Copyright© 2018 American Chemical Society]

The most common photo crosslinking materials are usually macromolecular prepolymers or vinyl-modified polymers. Hwang et al. conducted photo crosslinking of mixtures of polyethylene glycol methacrylate (PEG-MA) and polyethylene glycol dimethacrylate (PEG-DMA).[227] They provided detailed research on the effects of the proportions of different photo-initiating groups, initiator concentrations on the rheological properties, swelling ratio, and mechanical strength of the hydrogels. As

shown in **Figure 1.5b**, Xu et al. synthesised hyperbranched methacrylate-copolymerised polyethylene glycol diacrylate polymers (HB-GMA-PEG) through *in situ* deactivation enhanced atom transfer radical polymerization (DE-ATRP).[222] This hydrogel constructs a pre-gel through the reaction of aldehydes with diols and forms a high-strength dual-crosslinked hydrogel via UV secondary crosslinking of reserved vinyl groups. This hydrogel also demonstrates good cell compatibility and strong water absorption capacity, making it an ideal material for wound sealing. Gelatin methacryloyl (GelMA) not only contains the RGD sequence that supports cell adhesion, expansion, and differentiation but also includes matrix metalloproteinase (MMP) sequences that support enzymatic degradation, making it one of the most popular photo crosslinking materials. Injectable hydrogels prepared using GelMA as 3D printing ink have been used in fields such as stem cell scaffolds, skin repair, bone regeneration, and corneal regeneration.[228–231]

1.3.1.4 Other Chemical Reactions

Under mild conditions, reactions with high chemical reaction rates in aqueous environments can be developed as a crosslinking method for *in situ* formed hydrogels. These materials often require

initiators or crosslinkers, along with the input or output of energy. Despite this, the associated disadvantages in constructing *in situ* formed injectable hydrogels have been significantly mitigated through the efforts of researchers.[208] By integrating various *in situ* forming mechanisms to construct interpenetrating or uniquely structured hydrogel networks, their mechanical properties have potentially been enhanced. These reactions include click chemistry, disulfide crosslinking, and catechol crosslinking.

Click Chemistry: As a typical example of click chemistry, the copper-catalysed azide-alkyne cycloaddition can be performed in water environments and is used to construct *in situ* formed hydrogels.[232] This reaction is characterised by high yield, strong regioselectivity, and highly controllable gel properties, offering significant advantages. However, considering its biomedical applications as an *in situ* formed hydrogel system, the toxicity of copper presents a concern. Agard et al. have utilised strain-promoted azide-alkyne cycloaddition by combining azides with strained cyclooctynes.[233] This click chemistry approach does not require traditional copper catalysis, thereby offering improved biocompatibility.

Disulfide Crosslinking: Disulfide bonds are crucial in biological processes such as protein folding and redox signalling. Commonly, hydrogels crosslinked through disulfide bonds are formed by the oxidation of thiols. However, the oxidation of thiols under physiological conditions (pH 7.4) is a very slow process. Consequently, many studies have resorted to increasing the pH or adding oxidizing agents like hydrogen peroxide (H_2O_2) to facilitate crosslinking.[234] Bian et al. conducted a detailed investigation into the gelation time and properties of disulfide crosslinked hydrogels at various thiol substitution degrees (SD) and concentrations.[235] Moreover, they explored the advantages of HA-SH hydrogels as intelligent degradable scaffolds for *in vitro* cell culture applications.

Catechol: Catechol, also known as pyrocatechol, is an ortho-isomer of benzenediol. It is capable of crosslinking through the formation of covalent bonds, metal coordination bonds, and hydrogen bonds.[236] A notable example in nature is how mussels firmly adhere to dynamic, moist surfaces; they secrete catechol groups to achieve this strong bond. When dopamine oxidizes, it forms a quinone structure. This structure then reacts with surrounding catechol to create covalent linkages. Zhou et al. have

developed a catechol-modified CTS injectable hydrogel, catalysed by horseradish peroxidase/H_2O_2.[237] This hydrogel enhances the proliferation and chondrogenic differentiation of bone marrow stromal cells (BMSC) *in vitro*. Furthermore, it has demonstrated the ability to promote cartilage repair *in vivo*.

1.3.2 Physical Crosslinks

As Leonardo da Vinci stated, "Nature is the best teacher," the discovery of the DNA double helix structure unveils a remarkable example of physical crosslinking in nature. The essence of physical crosslinking lies in utilising intermolecular attractions that do not involve electron pair sharing or transfer to form weak crosslinking points between polymers.[31,238] The inherent instability (or reversibility) of these physical crosslinks grants hydrogels shear-thinning and self-healing properties, facilitating the construction of injectable hydrogels.[239] However, the bond energy of individual physical bonds is generally low, often resulting in poor mechanical properties of the hydrogels.[31] The mechanical performance of physically crosslinked hydrogels depends on the concentration of polymers and crosslinking groups, the orderliness of their arrangement, and the affinity strength between groups.[240] This section discusses the physical

crosslinking mechanisms commonly employed in constructing injectable hydrogels, including hydrogen bonding, coordination bonding, and amphiphilic self-assembly. Despite the challenge of achieving robust mechanical properties through purely physical crosslinking, the self-healing nature of physical crosslinks is significantly meaningful for maintaining toughness under repeated loading of hydrogels.

1.3.2.1 Hydrogen Bonding

Hydrogen bonding is a type of dipole-dipole interaction that typically occurs between a hydrogen atom and a more electronegative atom, such as oxygen, nitrogen, or fluorine.[241] Although weaker than covalent bonds, hydrogen bonds play a crucial role in the structural stability and molecular recognition of many biological macromolecules.[242] Hydrogen bonds have been utilised in constructing injectable hydrogels such as CTS, polyethyleneimine, PVA, guar gum, and carboxybetaine thermoplastic polyurethane acrylate.[243–247] Hydrogels formed through hydrogen bonding are often self-healing. This self-healing property is due to the weaker hydrogen bonds breaking during injection, but reforming once the injection process is complete, as the polymer chains re-establish hydrogen bonds between them

(**Figure 1.6**).[248] Since the crosslinking process does not involve any crosslinking agents, it exhibits excellent biocompatibility.

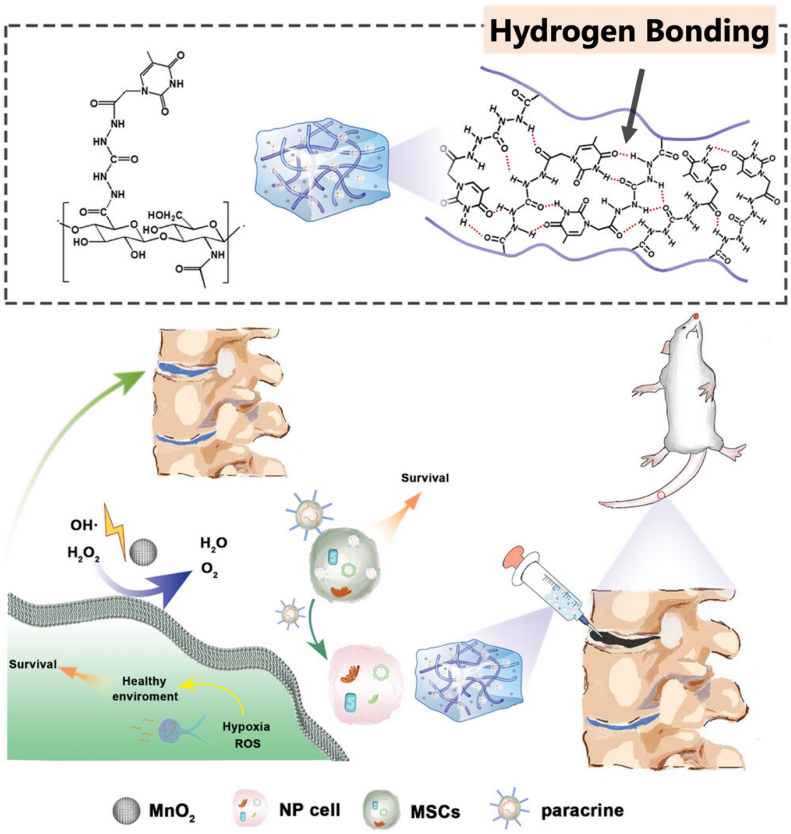


Figure 1.6 Examples of injectable hydrogels prepared by hydrogen bonding used for cell delivery in intervertebral disc degeneration treatment.[248] [Cropped, reorganised, and relabelled image. Copyright© 2024 John Wiley and Sons]

Dai et al. have regulated the strength of the hydrogen bonding network by adjusting the regularity and quantity of amide groups on the polymer side chains.[249] This hydrogel exhibits thermal processability, injectability, self-healing properties, and highly

tuneable mechanical performance. However, the high-water content of the extracellular matrix poses a challenge for the use of *in situ* formed injectable hydrogels that rely on hydrogen bonding. The water-rich dynamic environment within the body can weaken the inter-polymer hydrogen bonds through hydration, leading to a decrease in hydrogel stability. Hou et al. constructed a stronger physical crosslinking by grafting ureido-pyrimidinone (UPy), a quadruple hydrogen bonding unit, onto dextran.[250] Although this hydrogel is inevitably eroded over time through hydration, the degradation time can be adjusted by controlling the concentration of UPy. It is anticipated that the *in vivo* stability of injectable hydrogels crosslinked by hydrogen bonds could be further improved through interactions with hydrophobic groups.

1.3.2.2 Coordination Bonding

Coordination bonding is a type of physical bond characterised by relatively high bond energy.[251] Typically, coordination bonding consists of a central metal ion surrounded by ligands. Common ligands form coordination bonds by donating lone pairs of electrons to the metal ion, where the metal ion acts as the centre, and polymer molecules serve as ligands arranged around this metal centre (**Figure 1.7**).[252] The formation of such structures enhances

the system's stability. A common example is the formation of hydrogels through coordination bonds between SA and divalent cations.[81] Han et.al encapsulated calcium silicate, SA, and D-gluconic acid δ-lactone in the same solution system.[253] After the injection, the gradual release of Ca^{2+} led to the *in situ* crosslinking and formation of SA hydrogels. Sun et al. achieved extremely high mechanical performance by constructing a bilayer assembly hydrogel of Ca^{2+} crosslinked SA and PAM.[39] However, the complex preparation process prevents its realisation through *in situ* formed methods. Additionally, the coordination bond between SA and Ca^{2+} is typically irreversible due to the stable egg-box structure, which cannot spontaneously reassemble after breaking.

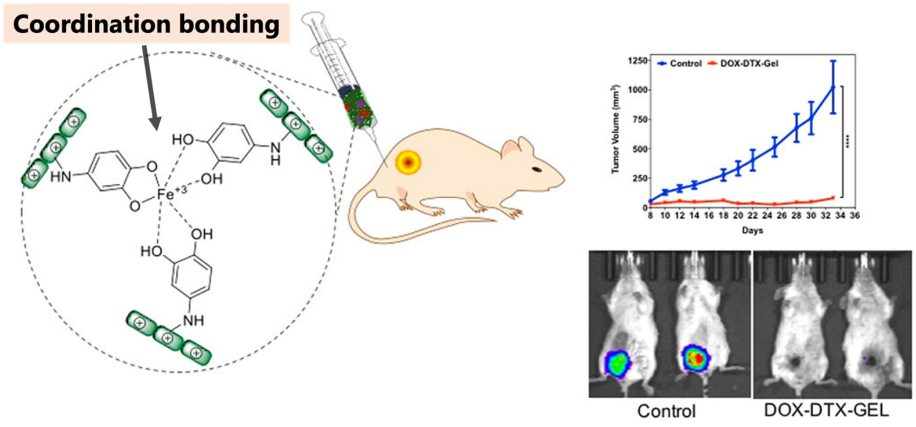


Figure 1.7 Examples of injectable hydrogels prepared by coordination bonding.[252] [Cropped and relabelled image. Copyright© 2017 American Chemical Society]

Another type of coordination bonding crosslinked hydrogel is constructed with catechol and metal ions (including Fe(III), Cu(II), and Al(III)). Yavvari et al. prepared a CTS-catechol based hydrogel assembled through catechol-Fe(III) synergistic interactions for localised combinatorial treatment in rodent models of lung and breast cancer.[252] This work presents a new injectable hydrogel drug delivery scaffold that significantly improved the median survival time in models of rodent lung and breast cancer.

1.3.2.3 Amphiphilic Self-Assembly

The hydrophilicity and hydrophobicity of polymers are influenced by the nature, distribution, and density of the functional groups in their main and side chains.[254] Amphiphilic polymers often exhibit self-assembly characteristics due to changes in the solvent. This phenomenon is prominently observed within biological organisms, especially in aspects such as the structure and function of cell membranes, protein folding, and the transport of biomacromolecules.[255] Some amphiphilic polymers undergo a transition from a dissolved state to a phase-separated state as the environmental temperature increases, with the transition temperature threshold known as the lower critical solution temperature (LCST).[256] Poly(N-isopropylacrylamide) (PNIPAAm)

serves as a classic example, possessing both hydrophilic amide groups and hydrophobic propyl groups.[200] At low temperatures, water molecules form a "hydration shell" around the hydrophobic propyl groups, increasing solubility. However, as the temperature rises (above 34°C), the entropy of the entire dissolution system tends to increase. The destabilisation of the hydration shell and the increase in molecular motion cause hydrophobic molecules to aggregate more easily, leading to microscopic phase separation. The phase-separated regions act as physical crosslinking points, transforming the entire solution system into a hydrogel.[257] PNIPAAm has been grafted onto many biopolymers to form thermo-responsive injectable hydrogels, including HA, SA, CTS, cellulose, and gelatin.[258–262]

Pluronic F127 (PEO100-PPO65-PEO100) triblock copolymer is one of the most commonly used thermo-responsive hydrogels in biomedicine (**Figure 1.8**).[263] Depending on the concentration, F127 can form a stable hydrogel when the temperature rises to approximately 25-30°C. Shriky et al. conducted a comprehensive study on the thermal, rheological, and structural properties of the F127 system.[264] Their work also proposed a set of empirical rules that can predict the rheological behaviour of F127 hydrogels at

concentrations above 20%, offering guidance for the development of F127 drug-loaded hydrogels. Ya et al. developed an injectable hydrogel scaffold composed of F127, carboxymethyl hexanoyl CTS, and GA.[265] During a 5-day incubation, the encapsulated cells in this hydrogel proliferated by over 400%. Park et al. grafted F127 onto CTS to prepare a thermo-responsive injectable hydrogel at 25°C.[266] The storage modulus (G') of this hydrogel was close to 10,000 Pa. *In vitro* cell culture tests showed that the proliferation of bovine chondrocytes and the synthesised amount of glycosaminoglycans increased over 28 days.

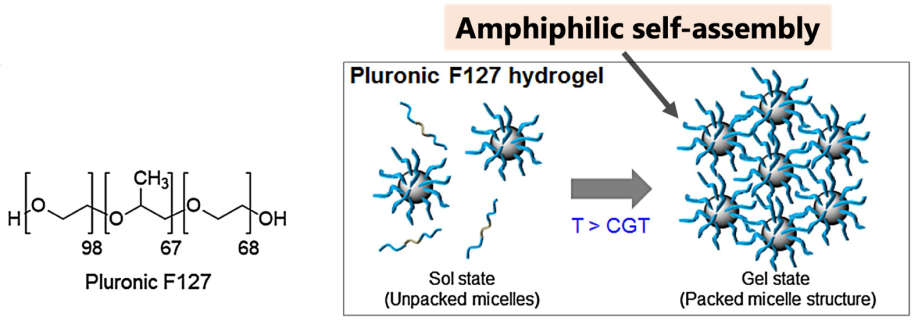


Figure 1.8 Examples of injectable hydrogels prepared by amphiphilic self-assembly.[263] [Cropped and relabelled image. Copyright© 2017 Elsevier]

Host-guest interactions typically involve the rapid formation of guest-host complexes between a "host" pocket with one or more

hydrophobic "guest" entities.[267] Cyclodextrins (CDs) are among the most common host molecules, consisting of 6 (α-CD), 7 (β-CD), or 8 (γ-CD) pyranoglucoside units, featuring a hydrophobic cavity. Adamantaneamine (Ad), as a hydrophobic guest, quickly forms shear-thinning, self-healing hydrogels upon mixing with the host.[268] Rasouli et al. conducted detailed studies on the capture behaviour between hosts and guests, finding β-cyclodextrin to be the optimal host for capturing the Ad guest.[269] By modifying materials with either CD or Ad, injectable hydrogels based on host-guest interactions can be constructed, including those made from HA, CTS, and cellulose.[270–272]

1.4 Toughening Strategies for Injectable Hydrogels

Tough hydrogel is defined as hydrogel that can dissipate a significant amount of mechanical energy while undergoing large deformations and can maintain their original configuration after deformation.[40] This is more intuitively reflected in the stress-strain curve, where tough hydrogels typically possess higher limit stress, limit strain, and a larger area under the stress-strain curve (**Figure 1.9**).

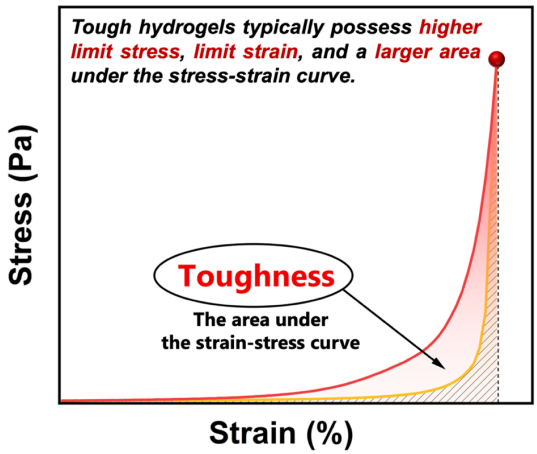


Figure 1.9 Illustration of the stress-strain curve for hydrogels. The yellow line represents the compression curve of a regular hydrogel, while the red line indicates the compression curve of a tougher hydrogel. Tough hydrogels typically possess higher limit stress, higher limit strain, and a larger area under the stress-strain curve.

Scientists have been exploring ways to enhance the toughness of hydrogels for decades.[30] Despite being limited by lower polymer concentrations (compared to other soft materials), novel crosslinking methods and structures have allowed hydrogels to break through the limits of mechanical performance. However, for injectable hydrogels, the limited options for crosslinking methods restrict improvements in toughness.[208] Moreover, considering their applications inside or on the surface of the body, the high requirements for biocompatibility limit the choice of building materials.[21] "Standing on the shoulders of giants," in this section,

we will refer to established mechanisms for toughening hydrogels, analyse, and design universal strategies that could be utilised to improve the mechanical performance of injectable hydrogels.

1.4.1 Elastic Maintenance Structure

Elastic maintenance property, characterised by high limit elasticity and extensibility, is crucial for tough hydrogels.[273] When hydrogels deform under mechanical force, higher limit stress and strain enable them to maintain integrity and the ability to recover elasticity even under extreme stress conditions. The limit extensibility of hydrogels is fundamentally influenced by the chain length between crosslink points. Longer chain lengths afford hydrogels higher extensibility (limit strain).[31] However, simply increasing the chain length by reducing the crosslinking density is less meaningful.[274] This is because the distribution of chain lengths between crosslink points in hydrogel networks is not monodisperse, and simply adjusting the crosslinking density cannot eliminate the heterogeneity of short chain defects. A notable example is that many hydrogels with high extensibility fail to return to their original shape after the external force is removed, or their stress capacity significantly decreases. Therefore, to construct hydrogels that possess both high limit elasticity and

extensibility, it is necessary not only to increase the chain length between crosslinks but also to reduce the heterogeneity of short chain defects in the crosslinking network. When defects in the hydrogel network are reduced, more long chains can stiffen simultaneously before breaking, enhancing the elastic limit. Thus, achieving a structure for hydrogels that supports elastic maintenance typically requires balancing longer polymer chains with a uniform polymer network structure. This section introduces several toughening designs that have been validated in non-injectable hydrogels and are expected to be applicable in the development of tough injectable hydrogels.

1.4.1.1 Ideally Homogeneous Network

The chain length between crosslink points is typically polydisperse in hydrogel network. When hydrogels undergo deformation, shorter chains usually experience stress concentration first and break. This structural drawback reduces the load-bearing capacity of hydrogel networks. Therefore, enhancing the homogeneity of the hydrogel network to construct hydrogels capable of maintaining elasticity is highly effective (**Figure 1.10**).[275]

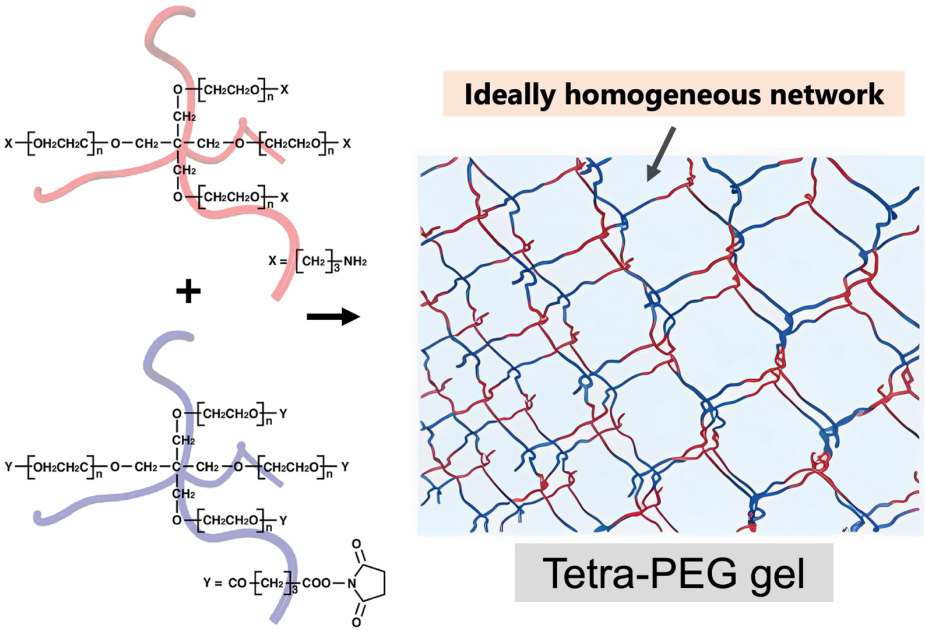


Figure 1.10 Example of the ideally homogeneous network tough hydrogel.[275] [Cropped and relabelled image. Open Access]

Sakai et al. created hydrogels with an ideally homogeneous network structure by covalently crosslinking two types of tetrahedral-shaped PEG monomers of the same size and with distinct symmetries.[33] Their work thoroughly discusses the relationship between the mechanical properties of the network structure and its heterogeneity. The compressive strength of the hydrogels formed by this *in situ* formed method is in the MPa range, significantly surpassing single network (SN) agarose hydrogels or PAM hydrogels with the same polymer concentration. However, tetra-NHS-glutarate-terminated PEG readily reacts with

amines in tissues, disrupting the design of its homogeneous network structure. Moreover, this reaction also can induce protein denaturation, making it unsuitable for the design of injectable hydrogels for biomedical applications. Following the goal of an ideally homogeneous network design, Wang et al. constructed injectable hydrogels using guest-host interactions with tetra-arm PEG to create a homogeneous structured network.[276] This design significantly enhances the biocompatibility of the homogeneous hydrogel system. However, the relatively weak host-guest bonds limit improvements in mechanical performance. Fujiyabu et al. have shown that branched polymer hydrogels with the lowest branching factor, namely tri-arm polymers, exhibit greater ultimate elastic deformation.[277] This enhancement is due to reversible strain-induced crystallisation observed in hydrogel networks composed of tri-arm monomers, which is not seen in networks of tetra-arm monomers. This study offers a highly promising design for optimising the toughness of injectable hydrogels with homogeneous network structures. Notably, while an ideally homogeneous network can provide excellent elasticity and extensibility to hydrogels, the lack of energy dissipative structures means that the hysteresis loop in their stress-strain

curves is almost negligible. This disadvantage implies that these hydrogels lack the capacity to absorb deformation energy, failing to meet the needs of biomedical applications requiring cushioning or protection.

1.4.1.2 Slide Ring Network

In covalently crosslinked hydrogel networks, the distance between two crosslink points is typically fixed. However, Liu et al. reported a high-elasticity hydrogel with a slide ring structure, achieving mechanical performance that significantly surpasses that of ideal homogeneous networks by an order of magnitude.[41] This enhancement was achieved by using DVS to crosslink polyrotaxane (PR), creating a polymer network capable of dynamic sliding. Unlike the fixed covalent crosslinks found in traditional chemical hydrogels, the crosslinking regions within slide ring hydrogels can slide along PEG chains, reducing stress concentration within the network. As the hydrogel is stretched, the polymer chains slide and move closer together. Concurrently, the length of polymer chains between crosslinks increases, resulting in a uniform extension in the direction of stretching.

As shown in **Figure 1.11**, under significant strain, highly oriented

PEG molecules align closely, forming clusters that resemble crystalline domains. Moreover, the study also carefully examined how the concentration of PEG and the number of CDs on PEG chains affect strain-induced crystallisation and the mechanical properties of the hydrogel. Building on this concept, Wang et al. developed a water-soluble PR with enhanced solubility (hydroxypropyl-modified α-cyclodextrin and acrylamide-PEG-acrylamide).[278] They crosslinked CDs using BDDE in a sodium hydroxide solution, creating a highly elastic sliding ring supramolecular hydrogel. However, neither of the above systems is suitable for the implementation of *in situ* formed injectable hydrogels. Tang et al. designed a PEG double helix γ-cyclodextrin-based precursor sliding ring crosslinker.[279] Utilising this crosslinker, they produced injectable slide ring hydrogels with exceptional elasticity and extensibility. However, due to the lack of end-capping for the slip rings, it is difficult to involve enough chains in co-stiffening, thus limiting the increase in strength and toughness.

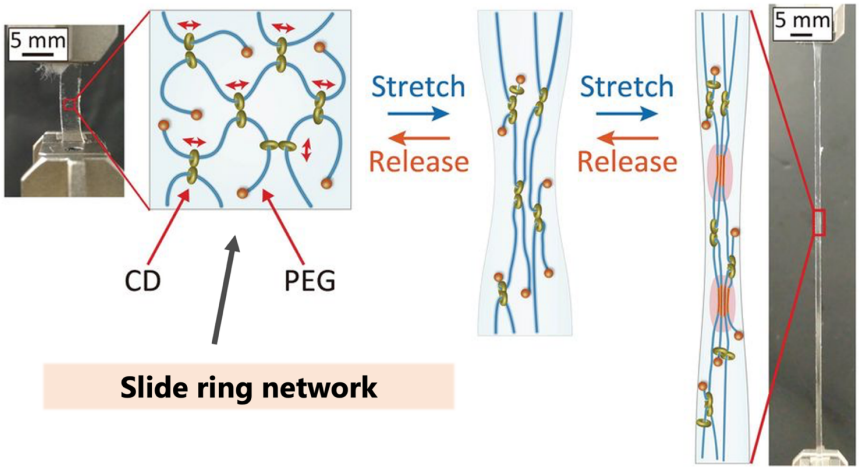


Figure 1.11 Example of the slide ring network tough hydrogel. The close-packed structure of PEG is formed and destroyed during stretching and releasing.[41] [Cropped and relabelled image. Copyright© 2021 The American Association for the Advancement of Science]

Notably, since sliding ring structures rely on PR or its analogues crosslinkers, this structure is considered broadly applicable. Functionalising ring molecules can endow them with the capability to generate slide ring crosslinkers *in situ*. It is anticipated that such crosslinkers can be used to produce highly elastic injectable hydrogels with a slide ring network structure. Additionally, for DN hydrogels, when the rigid first network fractures, the fragments of this broken network interact with the flexible second network to form structures similar to SR. This mechanism explains the exceptional ability of DN hydrogels to

maintain elasticity.[35]

1.4.1.3 Highly Entangled Network

Common hydrogels have a network-like topological structure. In such structures, dense crosslinking shortens the chain length between crosslink points, making the hydrogel harder yet more brittle. Kim et al. adjusted the proportions of crosslinker, initiator, and monomer, constructing highly entangled hydrogels through swelling methods.[36]

As shown in **Figure 1.12**, these hydrogels feature a low degree of crosslinking and an abundance of long, entangled chains. The entanglement sites easily slide, allowing stress to be transferred along the length to other chains. Moreover, the process of stress transmission among the chains is accompanied by a dynamic adjustment of chain length between entanglement points. Compared to ordinary network hydrogels, entangled hydrogels more readily achieve simultaneous stiffening of more chains before the breaking point, enhancing the elastic limit. Fu et al. enhanced the toughness of hydrogels by incorporating folded globular proteins to increase the entanglement within the hydrogel network.[280] This entanglement enhances the stiffness of the

hydrogel without making the network brittle. The stretching of the globular proteins effectively dissipates energy, while their refolding contributes to a rapid recovery of toughness.

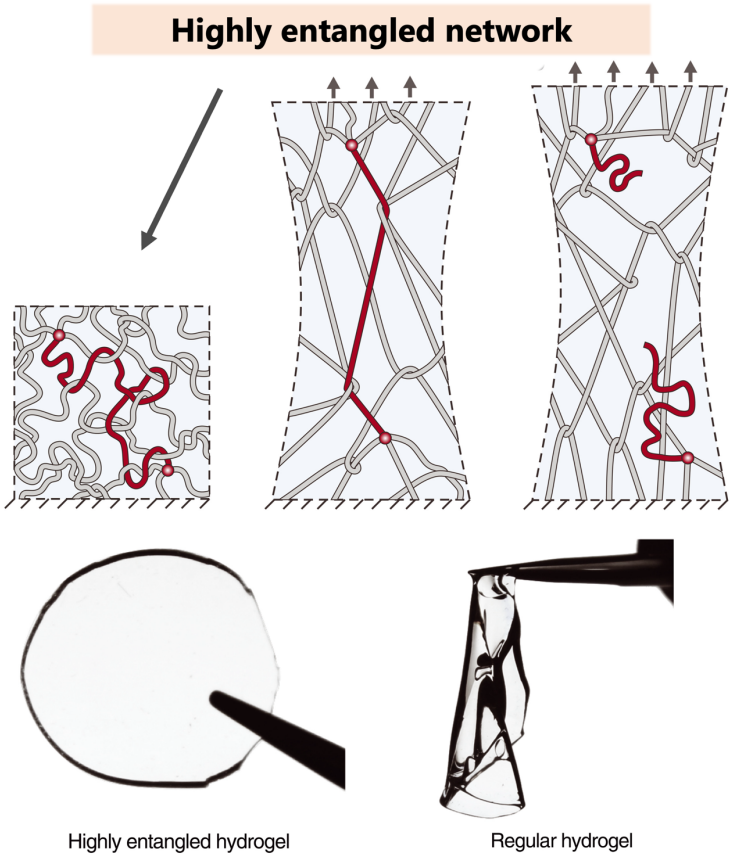


Figure 1.12 Example of the highly entangled network tough hydrogel. A stretched polymer showing transmission of the tension to other chains. [36] [Cropped and relabelled image. Copyright© 2021 The American Association for the Advancement of Science]

Wang et al. developed an *in situ* formed injectable hydrogel based on the principle of chain entanglement.[281] By exploring the power-

law relationship between the viscosity of PEG solutions and molecular weight, they successfully identified the critical entanglement molecular weight. Based on this critical molecular weight and specific concentration design, they prepared an entangled injectable hydrogel dressing with good elasticity, demonstrating its ability to promote skin wound healing. However, the construction of highly entangled networks follows the principle of entropy increase and critical entanglement theory. This means that achieving the higher chain entangled network relies on very higher polymer concentrations and longer polymer chains.

Although, to date, there have been no reports of an adjustable and one-step process to achieve *in situ* formed injectable hydrogels with a highly entangled network structure. It can be foreseen that, with the advancement of supramolecular chemistry, utilising self-assembly behaviours, including protein folding, holds promise for obtaining highly entangled injectable tough hydrogels at lower polymer concentrations and middle molecular weights.

1.4.1.4 Other Elastic Maintenance Network Design

Beyond the above-mentioned hydrogel design, enhancing the

extensibility of hydrogel networks can also be achieved by allowing the breakage of short chains while preserving the presence of long chains. Wang et al. reported a hydrogel prepared with a mechanically sensitive crosslinker based on cyclobutane, which exhibited toughness up to nine times higher than that of traditional analogues.[282] These mechanically sensitive crosslink points are more susceptible to mechanical disruption than the typical carbon-carbon bonds in polymer chains. During deformation, the mechanically sensitive crosslink points act as sacrificial bonds, allowing the bridging chains to elongate rather than break. For the injectable hydrogel system, this structure can be readily achieved through multiple *in situ* crosslinking methods with different bond energies, thereby increasing the strain limit. Bao et al. built a tough injectable hydrogel through photo crosslinking, characterised by clear phase separation and robust interfacial bonding.[283] Upon deformation, the homogeneous PEG network in the hydrogel demonstrates high extensibility, while the strong crosslinked interface supports efficient load transfer between phases. Adjusting the hard methacrylated hyaluronic acid (HA-MA) particles within the hydrogel further controls its extensibility and elasticity. The study found that when HA

particles are relatively small, they cannot withstand stress internally. This occurs because the strong interfacial interactions cause the forces transferred from PEG chains to first disrupt the internal network of HA particles, while the unbroken long-chain PEG provides the hydrogel with better extensibility. In contrast, when HA particles are reinforced to resist the load transferred from PEG chains, the highly crosslinked HA particles cannot be internally disrupted, and simultaneous stiffening significantly increases the fracture strength. However, due to the absence of short chain sacrifice to preserve long chains, the fracture strain of this significantly decreases. Additionally, there are many examples of highly extensible hydrogels that maintain elasticity by protecting long chains through the detachment of short chains from high functionality crosslinkers.[284–288]

In reality, the breaking of chains within hydrogels typically starts with the shorter chains in the plastic region. The strategy of breaking some short chains to preserve the integrity of longer chains is commonly observed across most hydrogel systems. This fact raises the question: why do some heterogeneous hydrogel systems exhibit excellent toughness, while others are notably brittle?

1.4.2 Energy Dissipation Structure

The ability to dissipate mechanical energy is essential for enhancing the toughness of hydrogels.[289] When hydrogels are subjected to force up to their deformation limit, stress tends to concentrate first on the shorter chains between crosslink points, leading to their breaking. Subsequently, stress concentrates on other short chains (in the plastic zone) near the fracture tips, promoting the continuation of crack propagation. Therefore, increasing the cost of crack propagation (mechanical energy dissipation capability) can dramatically improve the toughness of hydrogels. Given that the energy required to break individual chemical bonds in a hydrogel network is relatively low, improving mechanical energy dissipation is typically achieved by enlarging the plastic zone or increasing crosslink density near the crack tips. This section introduces several mechanical energy dissipation structures that have been utilised in non-injectable hydrogels and are expected to be applied to improve the toughness of injectable hydrogels.

1.4.2.1 Sacrificial Bonding

Incorporating a large number of densely crosslinked short chains

into hydrogels is the most straightforward method to achieve energy dissipation structure (**Figure 1.13**).[290] When hydrogels deform, the breaking of short chains dissipates mechanical energy, while long chains maintain the overall elasticity of the hydrogel.

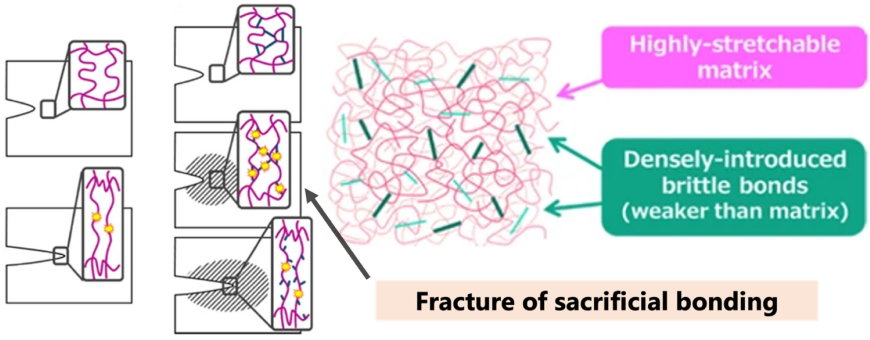


Figure 1.13 Example of the tough hydrogel with the sacrificial bonding feature.[290] [Cropped and relabelled image. Copyright© 2017 The Society of Polymer Science, Japan (SPSJ)]

Since Gong et al. pioneered DN hydrogel design, the concept of using a DN design to accommodate both energy-dissipating structures and elastic structures has been widely accepted.[35] DN hydrogels typically consist of a rigid network at a low polymer concentration interpenetrating with a flexible network at a high polymer concentration. In this arrangement, the rigid network acts as sacrificial bonding, dissipating energy during fracture. Despite extensive research on DN hydrogels, developing tough *in situ*

formed injectable DN hydrogels remains a challenge. Additionally, it should be noted that the breaking of sacrificial bonds often causes irreversible damage to the hydrogel network. Therefore, in tough hydrogels using covalent sacrificial bonds, the stress-strain hysteresis loop typically diminishes with repeated deformation, leading to hydrogel fatigue.[291] Introducing reversible physical or dynamic chemical crosslinks is an effective strategy to improve sacrificial bond hydrogels.[292] Chen et al. conducted detailed studies on the fracture of the physically crosslinked first network in hybrid DN hydrogels.[293] This hybrid DN hydrogel consists of an agarose network connected by hydrogen bonds and a covalently crosslinked PAM network interpenetrating each other. The agarose network can reform physical crosslink through a process of heating followed by cooling, thereby restoring the hydrogel toughness. Zhang et al. constructed a DN hydrogel with excellent fatigue resistance purely utilising physical crosslinked network.[294] The first network was formed by the self-assembly of amphiphilic triblock copolymers. Loosely crosslinked PAM was used as the second network. Amide groups on PAM could form hydrogen bonds with carboxylic acid groups on the hydrophilic middle block. Hydrogen bonds between the first and second networks act as

sacrificial bonds for energy dissipation.

Due to the relatively complicated preparation process, DN injectable hydrogels were not commonly seen in the past. However, in recent years, with the development of new *in situ* crosslinking systems, an increasing number of injectable DN hydrogels have emerged. Rodell et al. developed a DN injectable hydrogel composed of guest-host networks and covalent crosslinking networks.[295] The rapid self-healing capability of the guest-host interactions endows the hydrogel with excellent fatigue resistance and injectability. It is noteworthy that during large deformations, the breaking of linkage bonds is inevitable. The presence of sacrificial bonds only becomes meaningful when the integrity of the hydrogel network is maintained.

1.4.2.2 Domain Transformation

Polymers or crosslinkers may contain folded or orderly arranged structural domains, that undergo conformational transitions under mechanical load (**Figure 1.14**).[38] Typically, the process of domain transformation can dissipate mechanical energy. The result of domain transformation may endow the polymer network with new properties. Transformable structural domains are abundantly

present in the human body and function in various forms.[296] The contraction and relaxation of muscles involve domain transformation between myosin and actin. Domain transformation in tendon tissues can effectively absorb energy shocks during movement. In cancellous bone, trabeculae are arranged in specific directions, forming a structural domain that enhances the toughness of bones by withstanding pressure and impact.

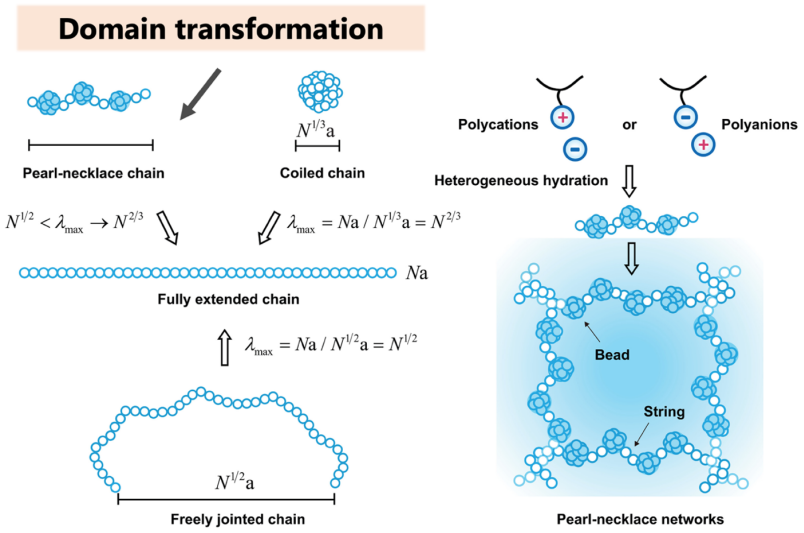


Figure 1.14 Example of the tough hydrogel with domain transformation feature.[38] [Cropped and relabelled image. Copyright© 2024 The American Association for the Advancement of Science]

Inspired by tendons, Hua et al. prepared a tough hydrogel with multi-level and anisotropic structures through the synergistic action of freeze-casting and salting out, where crystalline zones

act as the structural domains.[297] When a crack extends to the crystalline domains, more energy is required for structure transforming, thereby enhancing the toughness of the hydrogel. Fang et al. reported a chemically crosslinked, highly elastic, and tough protein hydrogel.[298] The ferredoxin-like fold structure domains in the hydrogel are forced to unfold under stress for energy dissipation and refold upon relaxation. This reversible protein folding domain grants the hydrogel excellent energy dissipation and fatigue resistance capabilities.

Domain transformation design can also be implemented in injectable hydrogels through appropriate *in situ* crosslinking methods, achieving high mechanical energy dissipation capabilities. Wang et al. integrated acylhydrazone bonds and micelle crosslinking as two dynamic crosslinking mechanisms to construct a self-healing, tough hydrogel.[299] Aldehyde-terminated F127 in water forms self-assembled micelle domains. Due to the hydrophobic affinity and physical rearrangement within the structural domains, this hydrogel exhibits outstanding energy dissipation and fatigue recovery abilities. Considering the rich variety of structural domain in nature, enhancing toughness of hydrogels through domain transformation holds significant

potential.

1.4.2.3 Fibre Reinforced Network

Utilising strong fibres to enhance the strength and toughness of materials is a common approach across various fields, such as reinforced concrete or carbon fibre-reinforced car bodies.[300] The primary principle of fibre reinforcement involves transferring and dispersing the applied force through the bridging action of tough fibres (expanding the plastic zone), thereby increasing the cost of crack propagation. Similarly, bundles of collagen fibres in cartilage, tendons, and ligaments also play a role akin to fibre reinforcement.[301] Illeperuma et al. demonstrated that incorporating stainless steel fibres into hydrogels significantly enhances their capacity for energy dissipation during deformation, which in turn improves the toughness of the hydrogels (**Figure 1.15**).[302] Ma et al. utilised a synergistic approach of freeze-drying and annealing to uniformly disperse flexible SiO_2 nano-fibres within a PVA hydrogel.[303] The strong and flexible nano-fibres and their intermolecular interactions with the hydrogel matrix effectively dispersed the load, minimising damage to the substrate. Kong et al. created a GelMA hydrogel reinforced with a lattice of poly(ε-caprolactone)-PEG micro-fibre scaffolds.[228] Besides transferring

and dispersing the load, this micro-fibre scaffold could also adjust the strength of the hydrogel by altering the fibre diameter. As the result, this hydrogel exhibited tensile strength comparable to natural cornea (3-5 MPa) and outstanding ability to induce corneal regeneration. Qiu et al. used peptide-modified polyacrylonitrile fibres to enhance a Schiff base crosslinked carboxymethyl chitosan and poly(dextran-g-4-formylbenzoic acid) injectable hydrogel.[304] The addition of nanofibers significantly improved the stability and mechanical strength of these hydrogels, also endowing them with haemostatic properties and a strong ability to kill bacterial biofilms.

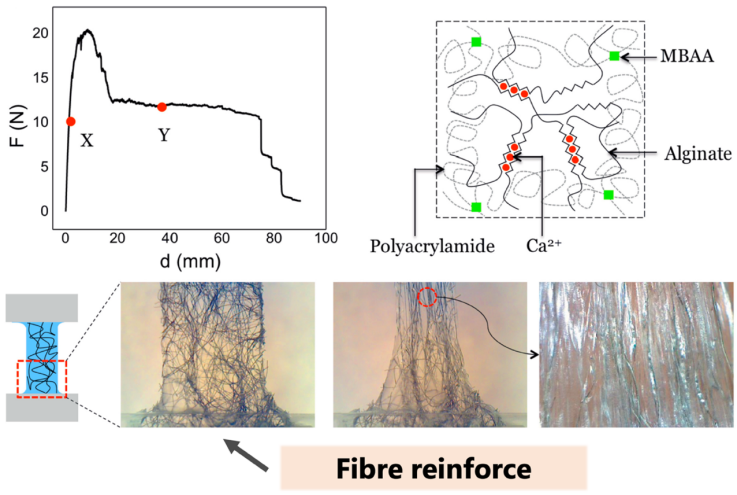


Figure 1.15 Example of the tough hydrogel with fibre reinforce feature.[302] [Cropped, reorganised and relabelled image. Copyright© 2014 Elsevier]

Although there are currently few reports on enhancing the mechanical energy dissipation capacity of injectable hydrogels through fibre reinforcement. Given that the micro or nano fibres do not interfere with the injection process, the fibre reinforced approach shows great potential to universally enhance the toughness of *in situ* formed injectable hydrogels.

1.5 Aims and Objectives

Injectable hydrogels have attracted widespread attention from biomedical researchers, yet their application is severely limited by their low mechanical performance. The primary aim of this thesis is to develop tough injectable hydrogel systems that exhibit high mechanical performance while maintaining their ease of administration, efficient encapsulation of drugs or cells, and minimal invasiveness. This overarching aim encompasses several specific goals. Firstly, these include conceptualising and creating universal structures for tough injectable hydrogels by leveraging underlying toughening mechanisms and *in situ* crosslinking methods. Secondly, it involves improving the mechanical toughness of injectable hydrogels by overcoming limitations associated with current crosslinking methods and material choices. Finally, the goal is to ensure that the gelation process and the

hydrogel components are safe for biological systems and do not potentially adversely affect encapsulated drugs or cells. To achieve these aims, the thesis is structured around the three objectives for each experimental chapter. 1. Develop tough injectable hydrogels via flexible chains linking rigid homogeneous framework in **Chapter Two**. 2. Develop tough injectable hydrogel via thermal self-entangled chains linking rigid framework in **Chapter Three**. 3. Double network injectable hydrogel with enhanced toughness by acid-triggered second homogeneous network in **Chapter Four**. These three chapters present distinct and potentially generalisable design strategies for tough injectable hydrogels. Each structure design enhances hydrogel toughness while maintaining injectability and good cell compatibility.

1.6 References

(1) Kopeček, J. Hydrogel Biomaterials: A Smart Future? *Biomaterials*. 2007, *28* (34), 5185–5192.

(2) Oyen, M. L. Mechanical Characterisation of Hydrogel Materials. *International Materials Reviews*. 2014, *59* (1), 44–59.

(3) Deligkaris, K.; Tadele, T. S.; Olthuis, W.; van den Berg, A. Hydrogel-Based Devices for Biomedical Applications. *Sensors and Actuators B: Chemical*. 2010, *147* (2), 765–

774.

(4) Ahmed, E. M. Hydrogel: Preparation, Characterization, and Applications: A Review. *Journal of Advanced Research*. 2015, *6* (2), 105–121.

(5) Liu, X.; Liu, J.; Lin, S.; Zhao, X. Hydrogel Machines. *Materials Today*. 2020, *36*, 102–124.

(6) Ho, T.-C.; Chang, C.-C.; Chan, H.-P.; Chung, T.-W.; Shu, C.-W.; Chuang, K.-P.; Duh, T.-H.; Yang, M.-H.; Tyan, Y.-C. Hydrogels: Properties and Applications in Biomedicine. *Molecules*. 2022, *27* (9), 2902.

(7) Zhang, Y.; Xu, Y.; Gao, J. The Engineering and Application of Extracellular Matrix Hydrogels: A Review. *Biomaterials. Science.* 2023, *11* (11), 3784–3799.

(8) Means, A. K.; Grunlan, M. A. Modern Strategies To Achieve Tissue-Mimetic, Mechanically Robust Hydrogels. *ACS Macro Letters.* 2019, *8* (6), 705–713.

(9) Wang, L.; Chen, D.; Jiang, K.; Shen, G. New Insights and Perspectives into Biological Materials for Flexible Electronics. *Chemical Society Reviews*. 2017, *46* (22), 6764–6815.

(10) Ionov, L. Biomimetic Hydrogel-Based Actuating Systems. *Advanced Functional Materials*. 2013, *23* (36), 4555–4570.

(11) Chai, Q.; Jiao, Y.; Yu, X. Hydrogels for Biomedical Applications: Their Characteristics and the Mechanisms behind Them. *Gels*. 2017, *3* (1), 6.

(12) Zhang, Y. S.; Khademhosseini, A. Advances in Engineering Hydrogels. *Science*. 2017, *356* (6337), eaaf3627.

(13) Correa, S.; Grosskopf, A. K.; Lopez Hernandez, H.; Chan, D.; Yu, A. C.; Stapleton, L. M.; Appel, E. A. Translational Applications of Hydrogels. *Chemical Reviews.* 2021, *121* (18), 11385–11457.

(14) Nele, V.; Wojciechowski, J. P.; Armstrong, J. P. K.; Stevens, M. M. Tailoring Gelation Mechanisms for Advanced Hydrogel Applications. *Advanced Functional Materials*. 2020, *30* (42), 2002759.

(15) Ullah, F.; Othman, M. B. H.; Javed, F.; Ahmad, Z.; Akil, H. Md. Classification, Processing and Application of Hydrogels: A Review. *Materials Science and Engineering: C*. 2015, *57*, 414–433.

(16) Yu, L.; Ding, J. Injectable Hydrogels as Unique Biomedical Materials. *Chemical Society Reviews*. 2008, *37* (8), 1473–1481.

(17) Overstreet, D. J.; Dutta, D.; Stabenfeldt, S. E.; Vernon, B. L. Injectable Hydrogels. *Journal of Polymer Science Part B: Polymer Physics*. 2012, *50* (13), 881–903.

(18) Li, Y.; Rodrigues, J.; Tomás, H. Injectable and Biodegradable Hydrogels: Gelation , Biodegradation and Biomedical Applications. *Chemical Society Reviews*. 2012, *41* (6), 2193–2221.

(19) Vashahi, F.; Martinez, M. R.; Dashtimoghadam, E.; Fahimipour, F.; Keith, A. N.; Bersenev, E. A.; Ivanov, D. A.;

Zhulina, E. B.; Popryadukhin, P.; Matyjaszewski, K.; Vatankhah-Varnosfaderani, M.; Sheiko, S. S. Injectable Bottlebrush Hydrogels with Tissue-Mimetic Mechanical Properties. *Science Advances*. 2022, *8* (3), eabm2469.

(20) Geisler, I. M.; Schneider, J. P. Evolution-Based Design of an Injectable Hydrogel. *Advanced Functional Materials*. 2012, *22* (3), 529–537.

(21) Ko, D. Y.; Shinde, U. P.; Yeon, B.; Jeong, B. Recent Progress of *in situ* Formed Gels for Biomedical Applications. *Progress in Polymer Science*. 2013, *38* (3), 672–701.

(22) Zhang, K.; Shi, Z.; Zhou, J.; Xing, Q.; Ma, S.; Li, Q.; Zhang, Y.; Yao, M.; Wang, X.; Li, Q.; Li, J.; Guan, F. Potential Application of an Injectable Hydrogel Scaffold Loaded with Mesenchymal Stem Cells for Treating Traumatic Brain Injury. *Journal of Materials Chemistry B*. 2018, *6* (19), 2982–2992.

(23) Portnov, T.; Shulimzon, T. R.; Zilberman, M. Injectable Hydrogel-Based Scaffolds for Tissue Engineering Applications. *Reviews in Chemical Engineering*. 2017, *33* (1), 91–107.

(24) Chen, L.; Jiang, C.; Xu, Q.; Jin, J.; A, S.; Wang, X.; Li, X.; Hu, Y.; Sun, H.; Lu, X.; Duan, S.; Gao, Z.; Wang, W.; Wang, Y. Biphasic Release of Betamethasone from an Injectable HA Hydrogel Implant for Alleviating Lumbar Disc Herniation Induced Sciatica. *Acta Biomaterialia*. 2024,

176, 173–189.

(25) Dong, Y.; Rodrigues, M.; Kwon, S. H.; Li, X.; A, S.; Brett, E. A.; Elvassore, N.; Wang, W.; Gurtner, G. C. Acceleration of Diabetic Wound Regeneration Using an *In situ*–Formed Stem-Cell-Based Skin Substitute. *Advanced Healthcare Materials*. 2018, *7* (17), 1800432.

(26) A, S.; Xu, Q.; Johnson, M.; Creagh-Flynn, J.; Venet, M.; Zhou, D.; Lara-Sáez, I.; Tai, H.; Wang, W. An Injectable Multi-Responsive Hydrogel as Self-Healable and on-Demand Dissolution Tissue Adhesive. *Applied Materials Today*. 2021, *22*, 100967.

(27) Milne, C.; Song, R.; Johnson, M.; Zhao, C.; Santoro Ferrer, F.; A, S.; Lyu, J.; Wang, W. Dual-Modified Hyaluronic Acid for Tunable Double Cross-Linked Hydrogel Adhesives. *Biomacromolecules*. 2024, *25* (4), 2645–2655.

(28) Dimatteo, R.; Darling, N. J.; Segura, T. *In situ* Forming Injectable Hydrogels for Drug Delivery and Wound Repair. *Advanced Drug Delivery Reviews*. 2018, *127*, 167–184.

(29) Li, Y.; Yang, H. Y.; Lee, D. S. Advances in Biodegradable and Injectable Hydrogels for Biomedical Applications. *Journal of Controlled Release*. 2021, *330*, 151–160.

(30) Zhao, X. Multi-Scale Multi-Mechanism Design of Tough Hydrogels: Building Dissipation into Stretchy Networks. *Soft Matter*. 2014, *10* (5), 672–687.

(31) Zhao, X.; Chen, X.; Yuk, H.; Lin, S.; Liu, X.; Parada, G. Soft Materials by Design: Unconventional Polymer

Networks Give Extreme Properties. *Chemical Reviews.* 2021, *121* (8), 4309–4372.

(32) Wang, Y.; Wu, J.; Cao, Z.; Ma, C.; Tong, Q.; Li, J.; Liu, H.; Zheng, J.; Huang, G. Mechanically Robust, Notch-Insensitive, Fatigue Resistant and Self-Recoverable Hydrogels with Homogeneous and Viscoelastic Network Constructed by a Novel Multifunctional Cross-Linker. *Polymer*. 2019, *179*, 121661.

(33) Sakai, T.; Matsunaga, T.; Yamamoto, Y.; Ito, C.; Yoshida, R.; Suzuki, S.; Sasaki, N.; Shibayama, M.; Chung, U. Design and Fabrication of a High-Strength Hydrogel with Ideally Homogeneous Network Structure from Tetrahedron-like Macromonomers. *Macromolecules*. 2008, *41* (14), 5379–5384.

(34) Aldana, A. A.; Houben, S.; Moroni, L.; Baker, M. B.; Pitet, L. M. Trends in Double Networks as Bioprintable and Injectable Hydrogel Scaffolds for Tissue Regeneration. *ACS Biomaterials Science & Engineering.* 2021, *7* (9), 4077–4101.

(35) Ping Gong, J. Why Are Double Network Hydrogels so Tough? *Soft Matter*. 2010, *6* (12), 2583–2590.

(36) Kim, J.; Zhang, G.; Shi, M.; Suo, Z. Fracture, Fatigue, and Friction of Polymers in Which Entanglements Greatly Outnumber Cross-Links. *Science*. 2021, *374* (6564), 212–216.

(37) Shi, M.; Kim, J.; Nian, G.; Suo, Z. Highly Entangled

Hydrogels with Degradable Crosslinks. *Extreme Mechanics Letters*. 2023, *59*, 101953.

(38) Chen, L.; Jin, Z.; Feng, W.; Sun, L.; Xu, H.; Wang, C. A Hyperelastic Hydrogel with an Ultralarge Reversible Biaxial Strain. *Science*. 2024, *383* (6690), 1455–1461.

(39) Sun, J.-Y.; Zhao, X.; Illeperuma, W. R. K.; Chaudhuri, O.; Oh, K. H.; Mooney, D. J.; Vlassak, J. J.; Suo, Z. Highly Stretchable and Tough Hydrogels. *Nature*. 2012, *489* (7414), 133–136.

(40) Han, L.; Lu, X.; Liu, K.; Wang, K.; Fang, L.; Weng, L. T.; Zhang, H.; Tang, Y.; Ren, F.; Zhao, C.; Sun, G.; Liang, R.; Li, Z. (2017). Mussel-inspired adhesive and tough hydrogel based on nanoclay confined dopamine polymerization. *ACS nano*, 2017, 11(3), 2561-2574.

(41) Liu, C.; Morimoto, N.; Jiang, L.; Kawahara, S.; Noritomi, T.; Yokoyama, H.; Mayumi, K.; Ito, K. Tough Hydrogels with Rapid Self-Reinforcement. *Science*. 2021, *372* (6546), 1078–1081.

(42) Laftah, W. A.; Hashim, S.; Ibrahim, A. N. Polymer Hydrogels: A Review. *Polymer-Plastics Technology and Engineering*. 2011, *50* (14), 1475–1486.

(43) Muir, V. G.; Burdick, J. A. Chemically Modified Biopolymers for the Formation of Biomedical Hydrogels. *Chemical Reviews.* 2021, *121* (18), 10908–10949.

(44) Fan, H.; Gong, J. Fabrication of Bioinspired Hydrogels: Challenges and Opportunities. *Macromolecules*. 2020, *53*

(8), 2769–2782.

(45) Van Vlierberghe, S.; Dubruel, P.; Schacht, E. Biopolymer-Based Hydrogels as Scaffolds for Tissue Engineering Applications: A Review. *Biomacromolecules*. 2011, *12* (5), 1387–1408.

(46) Mahmood, A.; Patel, D.; Hickson, B.; DesRochers, J.; Hu, X. Recent Progress in Biopolymer-Based Hydrogel Materials for Biomedical Applications. *International Journal of Molecular Sciences*. 2022, *23* (3), 1415.

(47) Wang, X.; Song, R.; Johnson, M.; A, S.; He, Z.; Milne, C.; Wang, X.; Lara-Sáez, I.; Xu, Q.; Wang, W. An Injectable Chitosan-Based Self-Healable Hydrogel System as an Antibacterial Wound Dressing. *Materials*. 2021, *14* (20), 5956.

(48) Levett, P. A.; Melchels, F. P. W.; Schrobback, K.; Hutmacher, D. W.; Malda, J.; Klein, T. J. A Biomimetic Extracellular Matrix for Cartilage Tissue Engineering Centered on Photocurable Gelatin, Hyaluronic Acid and Chondroitin Sulfate. *Acta Biomaterialia*. 2014, *10* (1), 214–223.

(49) A, S.; Xu, Q.; McMichael, P.; Gao, Y.; Li, X.; Wang, X.; Greiser, U.; Zhou, D.; Wang, W. A Facile One-Pot Synthesis of Acrylated Hyaluronic Acid. *Chemical Communications.* 2018, *54* (9), 1081–1084.

(50) Shang, J.; Shao, Z.; Chen, X. Electrical Behavior of a Natural Polyelectrolyte Hydrogel:

Chitosan/Carboxymethylcellulose Hydrogel. *Biomacromolecules*. 2008, *9* (4), 1208–1213.

(51) Wang, C.-G.; Surat'man, N. E. B.; Chang, J. J.; Ong, Z. L.; Li, B.; Fan, X.; Loh, X. J.; Li, Z. Polyelectrolyte Hydrogels for Tissue Engineering and Regenerative Medicine. *Chemistry – An Asian Journal*. 2022, *17* (18), e202200604.

(52) Lv, X.; Zhang, W.; Liu, Y.; Zhao, Y.; Zhang, J.; Hou, M. Hygroscopicity Modulation of Hydrogels Based on Carboxymethyl Chitosan/Alginate Polyelectrolyte Complexes and Its Application as pH-Sensitive Delivery System. *Carbohydrate Polymers*. 2018, *198*, 86–93.

(53) Fallacara, A.; Baldini, E.; Manfredini, S.; Vertuani, S. Hyaluronic Acid in the Third Millennium. *Polymers*. 2018, *10* (7), 701.

(54) Hemshekhar, M.; Thushara, R. M.; Chandranayaka, S.; Sherman, L. S.; Kemparaju, K.; Girish, K. S. Emerging Roles of Hyaluronic Acid Bioscaffolds in Tissue Engineering and Regenerative Medicine. *International Journal of Biological Macromolecules*. 2016, *86*, 917–928.

(55) Dicker, K. T.; Gurski, L. A.; Pradhan-Bhatt, S.; Witt, R. L.; Farach-Carson, M. C.; Jia, X. Hyaluronan: A Simple Polysaccharide with Diverse Biological Functions. *Acta Biomaterialia*. 2014, *10* (4), 1558–1570.

(56) Abatangelo, G.; Vindigni, V.; Avruscio, G.; Pandis, L.; Brun, P. Hyaluronic Acid: Redefining Its Role. *Cells*. 2020, *9* (7), 1743.

(57) Jiang, D.; Liang, J.; Noble, P. W. Hyaluronan as an Immune Regulator in Human Diseases. *Physiological Reviews*. 2011, *91* (1), 221–264.

(58) Cyphert, J. M.; Trempus, C. S.; Garantziotis, S. Size Matters: Molecular Weight Specificity of Hyaluronan Effects in Cell Biology. *International Journal of Cell Biology*. 2015, *2015*, e563818.

(59) Pérez, L. A.; Hernández, R.; Alonso, J. M.; Pérez-González, R.; Sáez-Martínez, V. Hyaluronic Acid Hydrogels Crosslinked in Physiological Conditions: Synthesis and Biomedical Applications. *Biomedicines*. 2021, *9* (9), 1113.

(60) Luo, Y.; Tan, J.; Zhou, Y.; Guo, Y.; Liao, X.; He, L.; Li, D.; Li, X.; Liu, Y. From Crosslinking Strategies to Biomedical Applications of Hyaluronic Acid-Based Hydrogels: A Review. *International Journal of Biological Macromolecules*. 2023, *231*, 123308.

(61) Burdick, J. A.; Prestwich, G. D. Hyaluronic Acid Hydrogels for Biomedical Applications. *Advanced Materials*. 2011, *23* (12), H41–H56.

(62) Xue, Y.; Chen, H.; Xu, C.; Yu, D.; Xu, H.; Hu, Y. Synthesis of Hyaluronic Acid Hydrogels by Crosslinking the Mixture of High-Molecular-Weight Hyaluronic Acid and Low-Molecular-Weight Hyaluronic Acid with 1,4-Butanediol Diglycidyl Ether. *RSC Advances*. 2020, *10* (12), 7206–7213.

(63) Faivre, J.; Pigweh, A. I.; Iehl, J.; Maffert, P.; Goekjian, P.;

Bourdon, F. Crosslinking Hyaluronic Acid Soft-Tissue Fillers: Current Status and Perspectives from an Industrial Point of View. *Expert Review of Medical Devices*. 2021, *18* (12), 1175–1187.

(64) Zhang, J. N.; Chen, B. Z.; Ashfaq, M.; Zhang, X. P.; Guo, X. D. Development of a BDDE-Crosslinked Hyaluronic Acid Based Microneedles Patch as a Dermal Filler for Anti-Ageing Treatment. *Journal of Industrial and Engineering Chemistry*. 2018, *65*, 363–369.

(65) Øvrebø, Ø.; Giorgi, Z.; De Lauretis, A.; Vanoli, V.; Castiglione, F.; Briatico-Vangosa, F.; Ma, Q.; Perale, G.; Haugen, H. J.; Rossi, F. Characterisation and Biocompatibility of Crosslinked Hyaluronic Acid with BDDE and PEGDE for Clinical Applications. *Reactive and Functional Polymers*. 2024, *200*, 105920.

(66) Zerbinati, N.; Esposito, C.; Cipolla, G.; Calligaro, A.; Monticelli, D.; Martina, V.; Golubovic, M.; Binic, I.; Sigova, J.; Gallo, A. L.; D'Este, E.; Jafferany, M.; Pratosoni, M.; Tirant, M.; Van Thuong, N.; Sangalli, F.; Rauso, R.; Lotti, T. Chemical and Mechanical Characterization of Hyaluronic Acid Hydrogel Cross-Linked with Polyethylen Glycol and Its Use in Dermatology. *Dermatologic Therapy*. 2020, *33* (4), e13747.

(67) Zerbinati, N.; Sommatis, S.; Maccario, C.; Capillo, M. C.; Grimaldi, G.; Alonci, G.; Protasoni, M.; Rauso, R.; Mocchi, R. Toward Physicochemical and Rheological

Characterization of Different Injectable Hyaluronic Acid Dermal Fillers Cross-Linked with Polyethylene Glycol Diglycidyl Ether. *Polymers*. 2021, *13* (6), 948.

(68) Perera, G. G. G.; Argenta, D. F.; Caon, T. The Rheology of Injectable Hyaluronic Acid Hydrogels Used as Facial Fillers: A Review. *International Journal of Biological Macromolecules*. 2024, *268*, 131880.

(69) Kontis, T. C.; Rivkin, A. The History of Injectable Facial Fillers. *Facial Plastic Surgery*. 2009, *25* (02), 067–072.

(70) Cassuto, D.; Bellia, G.; Schiraldi, C. An Overview of Soft Tissue Fillers for Cosmetic Dermatology: From Filling to Regenerative Medicine. *Clinical, Cosmetic and Investigational Dermatology*. 2021, *14*, 1857–1866.

(71) Segura, T.; Anderson, B. C.; Chung, P. H.; Webber, R. E.; Shull, K. R.; Shea, L. D. Crosslinked Hyaluronic Acid Hydrogels: A Strategy to Functionalize and Pattern. *Biomaterials*. 2005, *26* (4), 359–371.

(72) Highley, C. B.; Prestwich, G. D.; Burdick, J. A. Recent Advances in Hyaluronic Acid Hydrogels for Biomedical Applications. *Current Opinion in Biotechnology*. 2016, *40*, 35–40.

(73) Sekar, M. P.; Suresh, S.; Zennifer, A.; Sethuraman, S.; Sundaramurthi, D. Hyaluronic Acid as Bioink and Hydrogel Scaffolds for Tissue Engineering Applications. *ACS Biomaterials Science & Engineering.* 2023, *9* (6), 3134–3159.

(74) Zhang, W.; Jin, X.; Li, H.; Zhang, R.; Wu, C. Injectable and Body Temperature Sensitive Hydrogels Based on Chitosan and Hyaluronic Acid for pH Sensitive Drug Release. *Carbohydrate Polymers*. 2018, *186*, 82–90.

(75) Noh, I.; Kim, N.; Tran, H. N.; Lee, J.; Lee, C. 3D Printable Hyaluronic Acid-Based Hydrogel for Its Potential Application as a Bioink in Tissue Engineering. *Biomaterials Research*. 2019, *23* (1), 3.

(76) Antich, C.; de Vicente, J.; Jiménez, G.; Chocarro, C.; Carrillo, E.; Montañez, E.; Gálvez-Martín, P.; Marchal, J. A. Bio-Inspired Hydrogel Composed of Hyaluronic Acid and Alginate as a Potential Bioink for 3D Bioprinting of Articular Cartilage Engineering Constructs. *Acta Biomaterialia*. 2020, *106*, 114–123.

(77) Tan, H.; Chu, C. R.; Payne, K. A.; Marra, K. G. Injectable *in situ* Forming Biodegradable Chitosan–Hyaluronic Acid Based Hydrogels for Cartilage Tissue Engineering. *Biomaterials*. 2009, *30* (13), 2499–2506.

(78) Xu, Q.; Guo, L.; A, S.; Gao, Y.; Zhou, D.; Greiser, U.; Creagh-Flynn, J.; Zhang, H.; Dong, Y.; Cutlar, L.; Wang, F.; Liu, W.; Wang, W.; Wang, W. Injectable Hyperbranched Poly(β-Amino Ester) Hydrogels with on-Demand Degradation Profiles to Match Wound Healing Processes. *Chemical Science.* 2018, *9* (8), 2179–2187.

(79) Liang, Y.; Walczak, P.; Bulte, J. W. M. The Survival of Engrafted Neural Stem Cells within Hyaluronic Acid

Hydrogels. *Biomaterials*. 2013, *34* (22), 5521–5529.

(80) Sahoo, D. R.; Biswal, T. Alginate and Its Application to Tissue Engineering. *SN Applied Sciences.* 2021, *3* (1), 30.

(81) Lee, K. Y.; Mooney, D. J. Alginate: Properties and Biomedical Applications. *Progress in Polymer Science*. 2012, *37* (1), 106–126.

(82) Hernández-González, A. C.; Téllez-Jurado, L.; Rodríguez-Lorenzo, L. M. Alginate Hydrogels for Bone Tissue Engineering, from Injectables to Bioprinting: A Review. *Carbohydrate Polymers*. 2020, *229*, 115514.

(83) Makarova, A. O.; Derkach, S. R.; Khair, T.; Kazantseva, M. A.; Zuev, Y. F.; Zueva, O. S. Ion-Induced Polysaccharide Gelation: Peculiarities of Alginate Egg-Box Association with Different Divalent Cations. *Polymers*. 2023, *15* (5), 1243.

(84) Wang, Y.; Zhao, Y.; He, J.; Sun, C.; Lu, W.; Zhang, Y.; Fang, Y. Doubling Growth of Egg-Box Structure during Calcium-Mediated Molecular Assembly of Alginate. *Journal of Colloid and Interface Science*. 2023, *634*, 747–756.

(85) Hu, C.; Lu, W.; Mata, A.; Nishinari, K.; Fang, Y. Ions-Induced Gelation of Alginate: Mechanisms and Applications. *International Journal of Biological Macromolecules*. 2021, *177*, 578–588.

(86) Vicini, S.; Castellano, M.; Mauri, M.; Marsano, E. Gelling Process for Sodium Alginate: New Technical Approach by Using Calcium Rich Micro-Spheres. *Carbohydrate*

Polymers. 2015, *134*, 767–774.

(87) Li, Z.; Lin, Z. Recent Advances in Polysaccharide-Based Hydrogels for Synthesis and Applications. *Aggregate*. 2021, *2* (2), e21.

(88) Jejurikar, A.; Lawrie, G.; Martin, D.; Grøndahl, L. A Novel Strategy for Preparing Mechanically Robust Ionically Cross-Linked Alginate Hydrogels. *Biomedical Materials.* 2011, *6* (2), 025010.

(89) Yang, J.-S.; Xie, Y.-J.; He, W. Research Progress on Chemical Modification of Alginate: A Review. *Carbohydrate Polymers*. 2011, *84* (1), 33–39.

(90) Wei, Q.; Zhou, J.; An, Y.; Li, M.; Zhang, J.; Yang, S. Modification, 3D Printing Process and Application of Sodium Alginate Based Hydrogels in Soft Tissue Engineering: A Review. *International Journal of Biological Macromolecules*. 2023, *232*, 123450.

(91) Song, S.-J.; Choi, J.; Park, Y.-D.; Hong, S.; Lee, J. J.; Ahn, C. B.; Choi, H.; Sun, K. Sodium Alginate Hydrogel-Based Bioprinting Using a Novel Multinozzle Bioprinting System. *Artificial Organs*. 2011, *35* (11), 1132–1136.

(92) Krishna, D. V.; Sankar, M. R. Extrusion Based Bioprinting of Alginate Based Multicomponent Hydrogels for Tissue Regeneration Applications: State of the Art. *Materials Today Communications*. 2023, *35*, 105696.

(93) Ahmad Raus, R.; Wan Nawawi, W. M. F.; Nasaruddin, R. R. Alginate and Alginate Composites for Biomedical

Applications. *Asian Journal of Pharmaceutical Sciences*. 2021, *16* (3), 280–306.

(94) Tsujimoto, T.; Sudo, H.; Todoh, M.; Yamada, K.; Iwasaki, K.; Ohnishi, T.; Hirohama, N.; Nonoyama, T.; Ukeba, D.; Ura, K.; Ito, Y. M.; Iwasaki, N. An Acellular Bioresorbable Ultra-Purified Alginate Gel Promotes Intervertebral Disc Repair: A Preclinical Proof-of-Concept Study. *eBioMedicine*. 2018, *37*, 521–534.

(95) Wang, L.; Zhang, H. J.; Liu, X.; Liu, Y.; Zhu, X.; Liu, X.; You, X. A Physically Cross-Linked Sodium Alginate–Gelatin Hydrogel with High Mechanical Strength. *ACS Applied Polymer Materials.* 2021, *3* (6), 3197–3205.

(96) Jiang, F.; Xu, X.-W.; Chen, F.-Q.; Weng, H.-F.; Chen, J.; Ru, Y.; Xiao, Q.; Xiao, A.-F. Extraction, Modification and Biomedical Application of Agarose Hydrogels: A Review. *Marine Drugs*. 2023, *21* (5), 299.

(97) Salati, M. A.; Khazai, J.; Tahmuri, A. M.; Samadi, A.; Taghizadeh, A.; Taghizadeh, M.; Zarrintaj, P.; Ramsey, J. D.; Habibzadeh, S.; Seidi, F.; Saeb, M. R.; Mozafari, M. Agarose-Based Biomaterials: Opportunities and Challenges in Cartilage Tissue Engineering. *Polymers*. 2020, *12* (5), 1150.

(98) Lewis, J. S.; Roy, K.; Keselowsky, B. G. Materials That Harness and Modulate the Immune System. *MRS Bulletin*. 2014, *39* (1), 25–34.

(99) Nordqvist, D.; Vilgis, T. A. Rheological Study of the

Gelation Process of Agarose-Based Solutions. *Food Biophysics*. 2011, *6* (4), 450–460.

(100) Khodadadi Yazdi, M.; Taghizadeh, A.; Taghizadeh, M.; Stadler, F. J.; Farokhi, M.; Mottaghitalab, F.; Zarrintaj, P.; Ramsey, J. D.; Seidi, F.; Saeb, M. R.; Mozafari, M. Agarose-Based Biomaterials for Advanced Drug Delivery. *Journal of Controlled Release*. 2020, *326*, 523–543.

(101) Zarrintaj, P.; Manouchehri, S.; Ahmadi, Z.; Saeb, M. R.; Urbanska, A. M.; Kaplan, D. L.; Mozafari, M. Agarose-Based Biomaterials for Tissue Engineering. *Carbohydrate Polymers*. 2018, *187*, 66–84.

(102) Priya, M. V.; Kumar, R. A.; Sivashanmugam, A.; Nair, S. V.; Jayakumar, R. Injectable Amorphous Chitin-Agarose Composite Hydrogels for Biomedical Applications. *Journal of Functional Biomaterials*. 2015, *6* (3), 849–862.

(103) López-Marcial, G. R.; Zeng, A. Y.; Osuna, C.; Dennis, J.; García, J. M.; O'Connell, G. D. Agarose-Based Hydrogels as Suitable Bioprinting Materials for Tissue Engineering. *ACS Biomaterials Science & Engineering.* 2018, *4* (10), 3610–3616.

(104) Beaumont, M.; Tran, R.; Vera, G.; Niedrist, D.; Rousset, A.; Pierre, R.; Shastri, V. P.; Forget, A. Hydrogel-Forming Algae Polysaccharides: From Seaweed to Biomedical Applications. *Biomacromolecules*. 2021, *22* (3), 1027–1052.

(105) Hou, M.; Yang, R.; Zhang, L.; Zhang, L.; Liu, G.; Xu, Z.;

Kang, Y.; Xue, P. Injectable and Natural Humic Acid/Agarose Hybrid Hydrogel for Localized Light-Driven Photothermal Ablation and Chemotherapy of Cancer. *ACS Biomaterials Science & Engineering*. 2018, *4* (12), 4266–4277.

(106) Kaur, S.; Dhillon, G. S. The Versatile Biopolymer Chitosan: Potential Sources, Evaluation of Extraction Methods and Applications. *Critical Reviews in Microbiology*. 2014, *40* (2), 155–175.

(107) Aranaz, I.; Alcántara, A. R.; Civera, M. C.; Arias, C.; Elorza, B.; Heras Caballero, A.; Acosta, N. Chitosan: An Overview of Its Properties and Applications. *Polymers*. 2021, *13* (19), 3256.

(108) Shukla, S. K.; Mishra, A. K.; Arotiba, O. A.; Mamba, B. B. Chitosan-Based Nanomaterials: A State-of-the-Art Review. *International Journal of Biological Macromolecules*. 2013, *59*, 46–58.

(109) Wang, W.; Xue, C.; Mao, X. Chitosan: Structural Modification, Biological Activity and Application. *International Journal of Biological Macromolecules*. 2020, *164*, 4532–4546.

(110) Chen, Q.; Qi, Y.; Jiang, Y.; Quan, W.; Luo, H.; Wu, K.; Li, S.; Ouyang, Q. Progress in Research of Chitosan Chemical Modification Technologies and Their Applications. *Marine Drugs*. 2022, *20* (8), 536.

(111) Fletes-Vargas, G.; Espinosa-Andrews, H.; Cervantes-Uc, J.

M.; Limón-Rocha, I.; Luna-Bárcenas, G.; Vázquez-Lepe, M.; Morales-Hernández, N.; Jiménez-Ávalos, J. A.; Mejía-Torres, D. G.; Ramos-Martínez, P.; Rodríguez-Rodríguez, R. Porous Chitosan Hydrogels Produced by Physical Crosslinking: Physicochemical, Structural, and Cytotoxic Properties. *Polymers*. 2023, *15* (9), 2203.

(112) Physically Cross-Linked Chitosan-Based Hydrogels for Tissue Engineering Applications: A State-of-the-Art Review. *European Polymer Journal*. 2021, *145*, 110176.

(113) Goycoolea, F. M.; Heras, A.; Aranaz, I.; Galed, G.; Fernández-Valle, M. E.; Argüelles-Monal, W. Effect of Chemical Crosslinking on the Swelling and Shrinking Properties of Thermal and pH-Responsive Chitosan Hydrogels. *Macromolecular Bioscience*. 2003, *3* (10), 612–619.

(114) Osi, A. R.; Zhang, H.; Chen, J.; Zhou, Y.; Wang, R.; Fu, J.; Müller-Buschbaum, P.; Zhong, Q. Three-Dimensional-Printable Thermo/Photo-Cross-Linked Methacrylated Chitosan–Gelatin Hydrogel Composites for Tissue Engineering. *ACS Applied Materials & Interfaces*. 2021, *13* (19), 22902–22913.

(115) Bhattarai, N.; Gunn, J.; Zhang, M. Chitosan-Based Hydrogels for Controlled, Localized Drug Delivery. *Advanced Drug Delivery Reviews*. 2010, *62* (1), 83–99.

(116) Ribeiro, M. P.; Espiga, A.; Silva, D.; Baptista, P.; Henriques, J.; Ferreira, C.; Silva, J. C.; Borges, J. P.; Pires, E.; Chaves,

P.; Correia, I. J. Development of a New Chitosan Hydrogel for Wound Dressing. *Wound Repair and Regeneration*. 2009, *17* (6), 817–824.

(117) Seddiqi, H.; Oliaei, E.; Honarkar, H.; Jin, J.; Geonzon, L. C.; Bacabac, R. G.; Klein-Nulend, J. Cellulose and Its Derivatives: Towards Biomedical Applications. *Cellulose*. 2021, *28* (4), 1893–1931.

(118) Aziz, T.; Farid, A.; Haq, F.; Kiran, M.; Ullah, A.; Zhang, K.; Li, C.; Ghazanfar, S.; Sun, H.; Ullah, R.; Ali, A.; Muzammal, M.; Shah, M.; Akhtar, N.; Selim, S.; Hagagy, N.; Samy, M.; Al Jaouni, S. K. A Review on the Modification of Cellulose and Its Applications. *Polymers*. 2022, *14* (15), 3206.

(119) Kang, H.; Liu, R.; Huang, Y. Cellulose-Based Gels. *Macromolecular Chemistry and Physics*. 2016, *217* (12), 1322–1334.

(120) Westman, L.; Lindström, T. Swelling and Mechanical Properties of Cellulose Hydrogels. I. Preparation, Characterization, and Swelling Behavior. *Journal of Applied Polymer Science*. 1981, *26* (8), 2519–2532.

(121) Chang, C.; Duan, B.; Cai, J.; Zhang, L. Superabsorbent Hydrogels Based on Cellulose for Smart Swelling and Controllable Delivery. *European Polymer Journal*. 2010, *46* (1), 92–100.

(122) Liu, P.; Zhai, M.; Li, J.; Peng, J.; Wu, J. Radiation Preparation and Swelling Behavior of Sodium

Carboxymethyl Cellulose Hydrogels. *Radiation Physics and Chemistry*. 2002, *63* (3), 525–528.

(123) Fekete, T.; Borsa, J.; Takács, E.; Wojnárovits, L. Synthesis of Cellulose Derivative Based Superabsorbent Hydrogels by Radiation Induced Crosslinking. *Cellulose*. 2014, *21* (6), 4157–4165.

(124) Jiang, X.; Yang, X.; Yang, B.; Zhang, L.; Lu, A. Highly Self-Healable and Injectable Cellulose Hydrogels via Rapid Hydrazone Linkage for Drug Delivery and 3D Cell Culture. *Carbohydrate Polymers*. 2021, *273*, 118547.

(125) Kabir, S. M. F.; Sikdar, P. P.; Haque, B.; Bhuiyan, M. A. R.; Ali, A.; Islam, M. N. Cellulose-Based Hydrogel Materials: Chemistry, Properties and Their Prospective Applications. *Progress in Biomaterials*. 2018, *7* (3), 153–174.

(126) Dutta, S. D.; Patel, D. K.; Lim, K.-T. Functional Cellulose-Based Hydrogels as Extracellular Matrices for Tissue Engineering. *Journal of Biological Engineering*. 2019, *13* (1), 55.

(127) Fu, L.-H.; Qi, C.; Ma, M.-G.; Wan, P. Multifunctional Cellulose-Based Hydrogels for Biomedical Applications. *Journal of Materials Chemistry B*. 2019, *7* (10), 1541–1562.

(128) Geanaliu-Nicolae, R.-E.; Andronescu, E. Blended Natural Support Materials—Collagen Based Hydrogels Used in Biomedicine. *Materials*. 2020, *13* (24), 5641.

(129) Balasubramanian, P.; Prabhakaran, M. P.; Sireesha, M.; Ramakrishna, S. Collagen in Human Tissues: Structure,

Function, and Biomedical Implications from a Tissue Engineering Perspective. In *Polymer Composites – Polyolefin Fractionation – Polymeric Peptidomimetics – Collagens*; Abe, A., Kausch, H.-H., Möller, M., Pasch, H., Eds.; Springer: Berlin, Heidelberg, 2013; pp 173–206.

(130) Liu, X.; Zheng, C.; Luo, X.; Wang, X.; Jiang, H. Recent Advances of Collagen-Based Biomaterials: Multi-Hierarchical Structure, Modification and Biomedical Applications. *Materials Science and Engineering: C*. 2019, *99*, 1509–1522.

(131) Brodsky, B.; Persikov, A. V. Molecular Structure of the Collagen Triple Helix. In *Advances in Protein Chemistry.*70, 301-339

(132) Zhu, S.; Yuan, Q.; Yin, T.; You, J.; Gu, Z.; Xiong, S.; Hu, Y. Self-Assembly of Collagen-Based Biomaterials: Preparation, Characterizations and Biomedical Applications. *Journal of Materials Chemistry B*. 2018, *6* (18), 2650–2676.

(133) Wu, N.; Yu, H.; Sun, M.; Li, Z.; Zhao, F.; Ao, Y.; Chen, H. Investigation on the Structure and Mechanical Properties of Highly Tunable Elastomeric Silk Fibroin Hydrogels Cross-Linked by γ-Ray Radiation. *ACS Applied Bio Materials.* 2020, *3* (1), 721–734.

(134) Rýglová, Š.; Braun, M.; Suchý, T. Collagen and Its Modifications—Crucial Aspects with Concern to Its Processing and Analysis. *Macromolecular Materials and*

Engineering. 2017, *302* (6), 1600460.

(135) Le Thi, P.; Lee, Y.; Tran, D. L.; Hoang Thi, T. T.; Park, K. D. Horseradish Peroxidase-Catalyzed Hydrogelation of Fish Gelatin with Tunable Mechanical Properties and Biocompatibility. *Journal of Biomaterials Applications*. 2020, *34* (9), 1216–1226.

(136) Huang, X.; Zhang, Y.; Zheng, X.; Yu, G.; Dan, N.; Dan, W.; Li, Z.; Chen, Y.; Liu, X. Origin of Critical Nature and Stability Enhancement in Collagen Matrix Based Biomaterials: Comprehensive Modification Technologies. *International Journal of Biological Macromolecules*. 2022, *216*, 741–756.

(137) Kong, W.; Lyu, C.; Liao, H.; Du, Y. Collagen Crosslinking: Effect on Structure, Mechanics and Fibrosis Progression. *Biomedical Materials.* 2021, *16* (6), 062005.

(138) Deng, C.; Li, F.; Hackett, J. M.; Chaudhry, S. H.; Toll, F. N.; Toye, B.; Hodge, W.; Griffith, M. Collagen and Glycopolymer Based Hydrogel for Potential Corneal Application. *Acta Biomaterialia*. 2010, *6* (1), 187–194.

(139) Perez-Puyana, V.; Jiménez-Rosado, M.; Romero, A.; Guerrero, A. Fabrication and Characterization of Hydrogels Based on Gelatinised Collagen with Potential Application in Tissue Engineering. *Polymers*. 2020, *12* (5), 1146.

(140) Xu, Q.; Torres, J. E.; Hakim, M.; Babiak, P. M.; Pal, P.; Battistoni, C. M.; Nguyen, M.; Panitch, A.; Solorio, L.; Liu, J. C. Collagen- and Hyaluronic Acid-Based Hydrogels and

Their Biomedical Applications. *Materials Science and Engineering: R: Reports*. 2021, *146*, 100641.

(141) C. Echave, M.; S. Burgo, L.; L. Pedraz, J.; Orive, G. Gelatin as Biomaterial for Tissue Engineering. *Current Pharmaceutical Design*. 2017, *23* (24), 3567–3584.

(142) Ahmady, A.; Abu Samah, N. H. A Review: Gelatine as a Bioadhesive Material for Medical and Pharmaceutical Applications. *International Journal of Pharmaceutics*. 2021, *608*, 121037.

(143) Daneault, A.; Prawitt, J.; Fabien Soulé, V.; Coxam, V.; Wittrant, Y. Biological Effect of Hydrolyzed Collagen on Bone Metabolism. *Critical Reviews in Food Science and Nutrition*. 2017, *57* (9), 1922–1937.

(144) Xia, D.; Chen, J.; Zhang, Z.; Dong, M. Emerging Polymeric Biomaterials and Manufacturing Techniques in Regenerative Medicine. *Aggregate*. 2022, *3* (5), e176.

(145) Andreazza, R.; Morales, A.; Pieniz, S.; Labidi, J. Gelatin-Based Hydrogels: Potential Biomaterials for Remediation. *Polymers*. 2023, *15* (4), 1026.

(146) Ozeki, M.; Tabata, Y. *In vivo* Degradability of Hydrogels Prepared from Different Gelatins by Various Cross-Linking Methods. *Journal of Biomaterials Science, Polymer Edition*. 2005, *16* (5), 549–561.

(147) Mohanto, S.; Narayana, S.; Merai, K. P.; Kumar, J. A.; Bhunia, A.; Hani, U.; Al Fatease, A.; Gowda, B. H. J.; Nag, S.; Ahmed, M. G.; Paul, K.; Vora, L. K. Advancements in

Gelatin-Based Hydrogel Systems for Biomedical Applications: A State-of-the-Art Review. *International Journal of Biological Macromolecules*. 2023, *253*, 127143.

(148) Yue, K.; Trujillo-de Santiago, G.; Alvarez, M. M.; Tamayol, A.; Annabi, N.; Khademhosseini, A. Synthesis, Properties, and Biomedical Applications of Gelatin Methacryloyl (GelMA) Hydrogels. *Biomaterials*. 2015, *73*, 254–271.

(149) Lukin, I.; Erezuma, I.; Maeso, L.; Zarate, J.; Desimone, M. F.; Al-Tel, T. H.; Dolatshahi-Pirouz, A.; Orive, G. Progress in Gelatin as Biomaterial for Tissue Engineering. *Pharmaceutics*. 2022, *14* (6), 1177.

(150) Foox, M.; Zilberman, M. Drug Delivery from Gelatin-Based Systems. *Expert Opinion on Drug Delivery*. 2015, *12* (9), 1547–1563.

(151) Bini, E.; Knight, D. P.; Kaplan, D. L. Mapping Domain Structures in Silks from Insects and Spiders Related to Protein Assembly. *Journal of Molecular Biology*. 2004, *335* (1), 27–40.

(152) Zhang, Y.-Q. Applications of Natural Silk Protein Sericin in Biomaterials. *Biotechnology Advances*. 2002, *20* (2), 91–100.

(153) Kapoor, S.; Kundu, S. C. Silk Protein-Based Hydrogels: Promising Advanced Materials for Biomedical Applications. *Acta Biomaterialia*. 2016, *31*, 17–32.

(154) Li, G.; Sun, S. Silk Fibroin-Based Biomaterials for Tissue Engineering Applications. *Molecules*. 2022, *27* (9), 2757.

(155) Grabska-Zielińska, S.; Sionkowska, A. How to Improve Physico-Chemical Properties of Silk Fibroin Materials for Biomedical Applications? - Blending and Cross-Linking of Silk Fibroin - A Review. *Materials*. 2021, *14* (6), 1510.

(156) Zhang, H.; Xu, D.; Zhang, Y.; Li, M.; Chai, R. Silk Fibroin Hydrogels for Biomedical Applications. *Smart Medicine*. 2022, *1* (1), e20220011.

(157) Lyu, Y.; Liu, Y.; He, H.; Wang, H. Application of Silk-Fibroin-Based Hydrogels in Tissue Engineering. *Gels*. 2023, *9* (5), 431.

(158) Farokhi, M.; Aleemardani, M.; Solouk, A.; Mirzadeh, H.; Teuschl, A. H.; Redl, H. Crosslinking Strategies for Silk Fibroin Hydrogels: Promising Biomedical Materials. *Biomedical Materials*. 2021, *16* (2), 022004.

(159) Mtibe, A.; Motloung, M. P.; Bandyopadhyay, J.; Ray, S. S. Synthetic Biopolymers and Their Composites: Advantages and Limitations—An Overview. *Macromolecular Rapid Communications*. 2021, *42* (15), 2100130.

(160) Loo, S.-L.; Vásquez, L.; Athanassiou, A.; Fragouli, D. Polymeric Hydrogels—A Promising Platform in Enhancing Water Security for a Sustainable Future. *Advanced Materials Interfaces*. 2021, *8* (24), 2100580.

(161) S. Place, E.; H. George, J.; K. Williams, C.; M. Stevens, M. Synthetic Polymer Scaffolds for Tissue Engineering. *Chemical Society Reviews*. 2009, *38* (4), 1139–1151.

(162) Huynh, C. T.; Nguyen, M. K.; Lee, D. S. Injectable Block

Copolymer Hydrogels: Achievements and Future Challenges for Biomedical Applications. *Macromolecules*. 2011, *44* (17), 6629–6636.

(163) Gao, Y.; Zhou, D.; Lyu, J.; A, S.; Xu, Q.; Newland, B.; Matyjaszewski, K.; Tai, H.; Wang, W. Complex Polymer Architectures through Free-Radical Polymerization of Multivinyl Monomers. *Nature Reviews Chemistry*. 2020, *4* (4), 194–212.

(164) D'souza, A. A.; Shegokar, R. Polyethylene Glycol (PEG): A Versatile Polymer for Pharmaceutical Applications. *Expert Opinion on Drug Delivery*. 2016, *13* (9), 1257–1275.

(165) Ensing, B.; Tiwari, A.; Tros, M.; Hunger, J.; Domingos, S. R.; Pérez, C.; Smits, G.; Bonn, M.; Bonn, D.; Woutersen, S. On the Origin of the Extremely Different Solubilities of Polyethers in Water. *Nature Communications*. 2019, *10* (1), 2893.

(166) Li, K.; Qi, Y.; Zhou, Y.; Sun, X.; Zhang, Z. Microstructure and Properties of Poly(Ethylene Glycol)-Segmented Polyurethane Antifouling Coatings after Immersion in Seawater. *Polymers*. 2021, *13* (4), 573.

(167) d'Avanzo, N.; Celia, C.; Barone, A.; Carafa, M.; Di Marzio, L.; Santos, H. A.; Fresta, M. Immunogenicity of Polyethylene Glycol Based Nanomedicines: Mechanisms, Clinical Implications and Systematic Approach. *Advanced Therapeutics*. 2020, *3* (3), 1900170.

(168) Zhu, J. Bioactive Modification of Poly(Ethylene Glycol)

Hydrogels for Tissue Engineering. *Biomaterials*. 2010, *31* (17), 4639–4656.

(169) Wang, Z.; Ye, Q.; Yu, S.; Akhavan, B. Poly Ethylene Glycol (PEG)-Based Hydrogels for Drug Delivery in Cancer Therapy: A Comprehensive Review. *Advanced Healthcare Materials*. 2023, *12* (18), 2300105.

(170) Bakaic, E.; Smeets, N. M. B.; Hoare, T. Injectable Hydrogels Based on Poly(Ethylene Glycol) and Derivatives as Functional Biomaterials. *RSC Advances.* 2015, *5* (45), 35469–35486.

(171) Lin, C.-C. Recent Advances in Crosslinking Chemistry of Biomimetic Poly(Ethylene Glycol) Hydrogels. *RSC Advances*. 2015, *5* (50), 39844–39853.

(172) Liang, K.; Hyun Bae, K.; Kurisawa, M. Recent Advances in the Design of Injectable Hydrogels for Stem Cell-Based Therapy. *Journal of Materials Chemistry B*. 2019, *7* (24), 3775–3791.

(173) Aruldass, S.; Mathivanan, V.; Mohamed, A. R.; Tye, C. T. Factors Affecting Hydrolysis of Polyvinyl Acetate to Polyvinyl Alcohol. *Journal of Environmental Chemical Engineering*. 2019, *7* (5), 103238.

(174) Teodorescu, M.; Bercea, M.; Morariu, S. Biomaterials of Poly(Vinyl Alcohol) and Natural Polymers. *Polymer Reviews*. 2018, *58* (2), 247–287.

(175) Briscoe, B.; Luckham, P.; Zhu, S. The Effects of Hydrogen Bonding upon the Viscosity of Aqueous Poly(Vinyl

Alcohol) Solutions. *Polymer*. 2000, *41* (10), 3851–3860.

(176) Adelnia, H.; Ensandoost, R.; Shebbrin Moonshi, S.; Gavgani, J. N.; Vasafi, E. I.; Ta, H. T. Freeze/Thawed Polyvinyl Alcohol Hydrogels: Present, Past and Future. *European Polymer Journal*. 2022, *164*, 110974.

(177) Kumar, A.; Han, S. S. PVA-Based Hydrogels for Tissue Engineering: A Review. *International Journal of Polymeric Materials and Polymeric Biomaterials*. 2017, *66* (4), 159–182.

(178) Martens, P.; Anseth, K. S. Characterization of Hydrogels Formed from Acrylate Modified Poly(Vinyl Alcohol) Macromers. *Polymer*. 2000, *41* (21), 7715–7722.

(179) Ossipov, D. A.; Piskounova, S.; Hilborn, J. Poly(Vinyl Alcohol) Cross-Linkers for *in vivo* Injectable Hydrogels. *Macromolecules*. 2008, *41* (11), 3971–3982.

(180) Alves, M.-H.; Jensen, B. E. B.; Smith, A. A. A.; Zelikin, A. N. Poly(Vinyl Alcohol) Physical Hydrogels: New Vista on a Long Serving Biomaterial. *Macromolecular Bioscience*. 2011, *11* (10), 1293–1313.

(181) Jiang, S.; Liu, S.; Feng, W. PVA Hydrogel Properties for Biomedical Application. *Journal of the Mechanical Behavior of Biomedical Materials*. 2011, *4* (7), 1228–1233.

(182) Baker, M. I.; Walsh, S. P.; Schwartz, Z.; Boyan, B. D. A Review of Polyvinyl Alcohol and Its Uses in Cartilage and Orthopedic Applications. *Journal of Biomedical Materials Research Part B: Applied Biomaterials*. 2012, *100B* (5),

1451–1457.

(183) Kausar, A. Poly(Acrylic Acid) Nanocomposites: Design of Advanced Materials. *Journal of Plastic Film & Sheeting*. 2021, *37* (4), 409–428.

(184) Arkaban, H.; Barani, M.; Akbarizadeh, M. R.; Pal Singh Chauhan, N.; Jadoun, S.; Dehghani Soltani, M.; Zarrintaj, P. Polyacrylic Acid Nanoplatforms: Antimicrobial, Tissue Engineering, and Cancer Theranostic Applications. *Polymers*. 2022, *14* (6), 1259.

(185) Sennakesavan, G.; Mostakhdemin, M.; Dkhar, L. K.; Seyfoddin, A.; Fatihhi, S. J. Acrylic Acid/Acrylamide Based Hydrogels and Its Properties - A Review. *Polymer Degradation and Stability*. 2020, *180*, 109308.

(186) Swain, S. K.; Prusty, K. Biomedical Applications of Acrylic-Based Nanohydrogels. *Journal of Materials Science*. 2018, *53* (4), 2303–2325.

(187) Kang, M.; Cheng, Y.; Hu, Y.; Ding, H.; Yang, H.; Wei, Y.; Huang, D. Self-Healing Poly(Acrylic Acid) Hydrogels Fabricated by Hydrogen Bonding and Fe3+ Ion Cross-Linking for Cartilage Tissue Engineering. *Frontiers Materials Science.* 2023, *17* (3), 230655.

(188) Zhu, Y.; Liu, J.; Guo, T.; Wang, J. J.; Tang, X.; Nicolosi, V. Multifunctional Ti3C2Tx MXene Composite Hydrogels with Strain Sensitivity toward Absorption-Dominated Electromagnetic-Interference Shielding. *ACS Nano*. 2021, *15* (1), 1465–1474.

(189) Jiao, Y.; Lu, K.; Lu, Y.; Yue, Y.; Xu, X.; Xiao, H.; Li, J.; Han, J. Highly Viscoelastic, Stretchable, Conductive, and Self-Healing Strain Sensors Based on Cellulose Nanofiber-Reinforced Polyacrylic Acid Hydrogel. *Cellulose*. 2021, *28* (7), 4295–4311.

(190) Dalei, G.; Das, S. Polyacrylic Acid-Based Drug Delivery Systems: A Comprehensive Review on the State-of-Art. *Journal of Drug Delivery Science and Technology*. 2022, *78*, 103988.

(191) Wang, L.; Duan, L.; Liu, G.; Sun, J.; Shahbazi, M.-A.; Kundu, S. C.; Reis, R. L.; Xiao, B.; Yang, X. Bioinspired Polyacrylic Acid-Based Dressing: Wet Adhesive, Self-Healing, and Multi-Biofunctional Coacervate Hydrogel Accelerates Wound Healing. *Advanced Science*. 2023, *10* (16), 2207352.

(192) Rabiee, A.; Ershad-Langroudi, A.; Jamshidi, H. Polyacrylamide-Based Polyampholytes and Their Applications. *Reviews in Chemical Engineering*. 2014, *30* (5), 501–519.

(193) Li, C.; Zheng, H.; Zhang, X.; Pu, Z.; Li, D.; Zwitterionic Hydrogels and Their Biomedical Applications: A Review. *Chemical Synthesis*. 2024, *4* (1), 17.

(194) Dmitriev, I.; Kuryndin, I.; Bobrova, N.; Smirnov, M. Swelling Behavior and Network Characterization of Hydrogels from Linear Polyacrylamide Crosslinked with Glutaraldehyde. *Materials Today Communications*. 2015,

4, 93–100.

(195) Shen, J.; Yan, B.; Li, T.; Long, Y.; Li, N.; Ye, M. Study on Graphene-Oxide-Based Polyacrylamide Composite Hydrogels. *Composites Part A: Applied Science and Manufacturing*. 2012, *43* (9), 1476–1481.

(196) Manafi, A.; Emami, A.-H.; Pooli, A. H.; Habibi, M.; Saidian, L. Unacceptable Results with an Accepted Soft Tissue Filler: Polyacrylamide Hydrogel. *Aesth Plast Surg*. 2010, *34* (4), 413–422.

(197) Haq, M. A.; Su, Y.; Wang, D. Mechanical Properties of PNIPAM Based Hydrogels: A Review. *Materials Science and Engineering: C*. 2017, *70*, 842–855.

(198) Tang, L.; Wang, L.; Yang, X.; Feng, Y.; Li, Y.; Feng, W. Poly(*N*-Isopropylacrylamide)-Based Smart Hydrogels: Design, Properties and Applications. *Progress in Materials Science*. 2021, *115*, 100702.

(199) Alexander, A.; Ajazuddin; Khan, J.; Saraf, S.; Saraf, S. Polyethylene Glycol (PEG)–Poly(N-Isopropylacrylamide) (PNIPAAm) Based Thermosensitive Injectable Hydrogels for Biomedical Applications. *European Journal of Pharmaceutics and Biopharmaceutics*. 2014, *88* (3), 575–585.

(200) Lanzalaco, S.; Armelin, E. Poly(N-Isopropylacrylamide) and Copolymers: A Review on Recent Progresses in Biomedical Applications. *Gels*. 2017, *3* (4), 36.

(201) Mathew, A. P.; Uthaman, S.; Cho, K.-H.; Cho, C.-S.; Park,

I.-K. Injectable Hydrogels for Delivering Biotherapeutic Molecules. *International Journal of Biological Macromolecules*. 2018, *110*, 17–29.

(202) Ji, D.; Kim, J. Recent Strategies for Strengthening and Stiffening Tough Hydrogels. *Advanced NanoBiomed Research*. 2021, *1* (8), 2100026.

(203) Almawash, S.; Osman, S. K.; Mustafa, G.; El Hamd, M. A. Current and Future Prospective of Injectable Hydrogels—Design Challenges and Limitations. *Pharmaceuticals*. 2022, *15* (3), 371.

(204) El-Husseiny, H. M.; Mady, E. A.; Hamabe, L.; Abugomaa, A.; Shimada, K.; Yoshida, T.; Tanaka, T.; Yokoi, A.; Elbadawy, M.; Tanaka, R. Smart/Stimuli-Responsive Hydrogels: Cutting-Edge Platforms for Tissue Engineering and Other Biomedical Applications. *Materials Today Bio*. 2022, *13*, 100186.

(205) Nair, D. P.; Podgórski, M.; Chatani, S.; Gong, T.; Xi, W.; Fenoli, C. R.; Bowman, C. N. The Thiol-Michael Addition Click Reaction: A Powerful and Widely Used Tool in Materials Chemistry. *Chemistry of Materiasl.* 2014, *26* (1), 724–744.

(206) Mather, B. D.; Viswanathan, K.; Miller, K. M.; Long, T. E. Michael Addition Reactions in Macromolecular Design for Emerging Technologies. *Progress in Polymer Science*. 2006, *31* (5), 487–531.

(207) Chan, J. W.; Hoyle, C. E.; Lowe, A. B.; Bowman, M.

Nucleophile-Initiated Thiol-Michael Reactions: Effect of Organocatalyst, Thiol, and Ene. *Macromolecules*. 2010, *43* (15), 6381–6388.

(208) Yang, J.-A.; Yeom, J.; Hwang, B. W.; Hoffman, A. S.; Hahn, S. K. *In situ*-Forming Injectable Hydrogels for Regenerative Medicine. *Progress in Polymer Science*. 2014, *39* (12), 1973–1986.

(209) Zheng Shu, X.; Liu, Y.; Palumbo, F. S.; Luo, Y.; Prestwich, G. D. *In situ* Crosslinkable Hyaluronan Hydrogels for Tissue Engineering. *Biomaterials*. 2004, *25* (7), 1339–1348.

(210) Liu, S.; Pu, Y.; Yang, R.; Liu, X.; Wang, P.; Wang, X.; Ren, Y.; Tan, X.; Ye, Z.; Chi, B. Boron-Assisted Dual-Crosslinked Poly (γ-Glutamic Acid) Hydrogels with High Toughness for Cartilage Regeneration. *International Journal of Biological Macromolecules*. 2020, *153*, 158–168.

(211) Jin, R.; Dijkstra, P. J.; Feijen, J. Rapid Gelation of Injectable Hydrogels Based on Hyaluronic Acid and Poly(Ethylene Glycol) via Michael-Type Addition. *Journal of Controlled Release*. 2010, *148* (1), e41–e43.

(212) Xu, Q.; A, S.; Gao, Y.; Guo, L.; Creagh-Flynn, J.; Zhou, D.; Greiser, U.; Dong, Y.; Wang, F.; Tai, H.; Liu, W.; Wang, W.; Wang, W. A Hybrid Injectable Hydrogel from Hyperbranched PEG Macromer as a Stem Cell Delivery and Retention Platform for Diabetic Wound Healing. *Acta*

Biomaterialia. 2018, *75*, 63–74.

(213) Fabbrizzi, L. Beauty in Chemistry: Making Artistic Molecules with Schiff Bases. *Journal of Organic Chemistry.* 2020, *85* (19), 12212–12226.

(214) Jia, Y.; Li, J. Molecular Assembly of Schiff Base Interactions: Construction and Application. *Chemical Reviews.* 2015, *115* (3), 1597–1621.

(215) Cao, L.; Cao, B.; Lu, C.; Wang, G.; Yu, L.; Ding, J. An Injectable Hydrogel Formed by *in situ* Cross-Linking of Glycol Chitosan and Multi-Benzaldehyde Functionalized PEG Analogues for Cartilage Tissue Engineering. *Journal of Materials Chemistry B*. 2015, *3* (7), 1268–1280.

(216) Ding, X.; Li, G.; Xiao, C.; Chen, X. Enhancing the Stability of Hydrogels by Doubling the Schiff Base Linkages. *Macromolecular Chemistry and Physics*. 2019, *220* (3), 1800484.

(217) Su, H.; Zheng, R.; Jiang, L.; Zeng, N.; Yu, K.; Zhi, Y.; Shan, S. Dextran Hydrogels via Disulfide-Containing Schiff Base Formation: Synthesis, Stimuli-Sensitive Degradation and Release Behaviors. *Carbohydrate Polymers*. 2021, *265*, 118085.

(218) Mo, C.; Xiang, L.; Chen, Y. Advances in Injectable and Self-Healing Polysaccharide Hydrogel Based on the Schiff Base Reaction. *Macromolecular Rapid Communications*. 2021, *42* (10), 2100025.

(219) Wu, X.; He, C.; Wu, Y.; Chen, X. Synergistic Therapeutic

Effects of Schiff's Base Cross-Linked Injectable Hydrogels for Local Co-Delivery of Metformin and 5-Fluorouracil in a Mouse Colon Carcinoma Model. *Biomaterials*. 2016, *75*, 148–162.

(220) A, S.; Lyu, J.; Johnson, M.; Creagh-Flynn, J.; Zhou, D.; Lara-Sáez, I.; Xu, Q.; Tai, H.; Wang, W. Instant Gelation System as Self-Healable and Printable 3D Cell Culture Bioink Based on Dynamic Covalent Chemistry. *ACS Applied Materials & Interfaces*. 2020, *12* (35), 38918–38924.

(221) Lindberg, G. C. J.; Lim, K. S.; Soliman, B. G.; Nguyen, A.; Hooper, G. J.; Narayan, R. J.; Woodfield, T. B. F. Biological Function Following Radical Photo-Polymerization of Biomedical Polymers and Surrounding Tissues: Design Considerations and Cellular Risk Factors. *Applied Physics Reviews*. 2021, *8* (1), 011301.

(222) Xu, Q.; A, S.; McMichael, P.; Creagh-Flynn, J.; Zhou, D.; Gao, Y.; Li, X.; Wang, X.; Wang, W. Double-Cross-Linked Hydrogel Strengthened by UV Irradiation from a Hyperbranched PEG-Based Trifunctional Polymer. *ACS Macro Lett.* 2018, *7* (5), 509–513.

(223) Yao, H.; Wang, J.; Mi, S. Photo Processing for Biomedical Hydrogels Design and Functionality: A Review. *Polymers*. 2018, *10* (1), 11.

(224) Wang, Y.; Zhang, S.; Wang, J. Photo-Crosslinkable Hydrogel and Its Biological Applications. *Chinese*

Chemical Letters. 2021, *32* (5), 1603–1614.

(225) Chen, G.; Kawazoe, N.; Ito, Y. Photo-Crosslinkable Hydrogels for Tissue Engineering Applications. *Photochemistry for Biomedical Applications: From Device Fabrication to Diagnosis and Therapy*. 2018, 277–300.

(226) Mironi-Harpaz, I.; Wang, D. Y.; Venkatraman, S.; Seliktar, D. Photopolymerization of Cell-Encapsulating Hydrogels: Crosslinking Efficiency versus Cytotoxicity. *Acta Biomaterialia*. 2012, *8* (5), 1838–1848.

(227) Hwang, J. W.; Noh, S. M.; Kim, B.; Jung, H. W. Gelation and Crosslinking Characteristics of Photopolymerized Poly(Ethylene Glycol) Hydrogels. *Journal of Applied Polymer Science*. 2015, *132* (22).

(228) Kong, B.; Chen, Y.; Liu, R.; Liu, X.; Liu, C.; Shao, Z.; Xiong, L.; Liu, X.; Sun, W.; Mi, S. Fiber Reinforced GelMA Hydrogel to Induce the Regeneration of Corneal Stroma. *Nature Communications*. 2020, *11* (1), 1435.

(229) Chen, X.; Zhang, D.; Wang, X.; Liu, Z.; Kang, H.; Liu, C.; Chen, F. Preparation of Porous GelMA Microcarriers by Microfluidic Technology for Stem-Cell Culture. *Chemical Engineering Journal*. 2023, *477*, 146444.

(230) Yan, L.; Han, K.; Pang, B.; Jin, H.; Zhao, X.; Xu, X.; Jiang, C.; Cui, N.; Lu, T.; Shi, J. Surfactin-Reinforced Gelatin Methacrylate Hydrogel Accelerates Diabetic Wound Healing by Regulating the Macrophage Polarization and Promoting Angiogenesis. *Chemical Engineering Journal*.

2021, *414*, 128836.

(231) Mahmoud, A. H.; Han, Y.; Dal-Fabbro, R.; Daghrery, A.; Xu, J.; Kaigler, D.; Bhaduri, S. B.; Malda, J.; Bottino, M. C. Nanoscale β-TCP-Laden GelMA/PCL Composite Membrane for Guided Bone Regeneration. *ACS Applied Materials & Interfaces*. 2023, *15* (27), 32121–32135.

(232) Devaraj, N. K.; Finn, M. G. Introduction: Click Chemistry. *Chemical Reviews.* 2021, *121* (12), 6697–6698.

(233) Agard, N. J.; Prescher, J. A.; Bertozzi, C. R. A Strain-Promoted [3+2] Azide−Alkyne Cycloaddition for Covalent Modification of Biomolecules in Living Systems. *Journal of the American Chemical Society.* 2004, *126* (46), 15046–15047.

(234) Laurano, R.; Boffito, M.; Cassino, C.; Liberti, F.; Ciardelli, G.; Chiono, V. Design of Injectable Bioartificial Hydrogels by Green Chemistry for Mini-Invasive Applications in the Biomedical or Aesthetic Medicine Fields. *Gels*. 2023, *9* (1), 59.

(235) Bian, S.; He, M.; Sui, J.; Cai, H.; Sun, Y.; Liang, J.; Fan, Y.; Zhang, X. The Self-Crosslinking Smart Hyaluronic Acid Hydrogels as Injectable Three-Dimensional Scaffolds for Cells Culture. *Colloids and Surfaces B: Biointerfaces*. 2016, *140*, 392–402.

(236) Zhang, W.; Wang, R.; Sun, Z.; Zhu, X.; Zhao, Q.; Zhang, T.; Cholewinski, A.; Fut (Kuo) Yang; Zhao, B.; Pinnaratip, R.; Kord Forooshani, P.; P. Lee, B. Catechol-Functionalized

Hydrogels: Biomimetic Design, Adhesion Mechanism, and Biomedical Applications. *Chemical Society Reviews*. 2020, *49* (2), 433–464.

(237) Zhou, S.; Bei, Z.; Wei, J.; Yan, X.; Wen, H.; Cao, Y.; Li, H. Mussel-Inspired Injectable Chitosan Hydrogel Modified with Catechol for Cell Adhesion and Cartilage Defect Repair. *Journal of Materials Chemistry B*. 2022, *10* (7), 1019–1030.

(238) Hennink, W. E.; van Nostrum, C. F. Novel Crosslinking Methods to Design Hydrogels. *Advanced Drug Delivery Reviews*. 2012, *64*, 223–236.

(239) Tu, Y.; Chen, N.; Li, C.; Liu, H.; Zhu, R.; Chen, S.; Xiao, Q.; Liu, J.; Ramakrishna, S.; He, L. Advances in Injectable Self-Healing Biomedical Hydrogels. *Acta Biomaterialia*. 2019, *90*, 1–20.

(240) Bertsch, P.; Diba, M.; Mooney, D. J.; Leeuwenburgh, S. C. G. Self-Healing Injectable Hydrogels for Tissue Regeneration. *Chemical Reviews.* 2023, *123* (2), 834–873.

(241) Rizzo, F.; Kehr, N. S. Recent Advances in Injectable Hydrogels for Controlled and Local Drug Delivery. *Advanced Healthcare Materials*. 2021, *10* (1), 2001341.

(242) Huang, X.; Nakagawa, S.; Houjou, H.; Yoshie, N. Insights into the Role of Hydrogen Bonds on the Mechanical Properties of Polymer Networks. *Macromolecules*. 2021, *54* (9), 4070–4080.

(243) Pang, Y.; Wang, H.; Yao, Y.; Chen, D.; Yang, R.; Wang, Z.;

Yang, J.; Li, Y.; Liu, W. An Injectable Self-Crosslinked Wholly Supramolecular Polyzwitterionic Hydrogel for Regulating Microenvironment to Boost Infected Diabetic Wound Healing. *Advanced Functional Materials*. 2023, *33* (36), 2303095.

(244) Gao, L. T.; Chen, Y. M.; Aziz, Y.; Wei, W.; Zhao, X. Y.; He, Y.; Li, J.; Li, H.; Miyatake, H.; Ito, Y. Tough, Self-Healing and Injectable Dynamic Nanocomposite Hydrogel Based on Gelatin and Sodium Alginate. *Carbohydrate Polymers*. 2024, *330*, 121812.

(245) Fang, Z.; Lin, T.; Fan, S.; Qiu, X.; Zhong, Z.; Yang, G.; Yang, J.; Zhang, G.; Feng, Y.; Ai, F.; Shi, Q.; Wan, W. Antibacterial, Injectable, and Adhesive Hydrogel Promotes Skin Healing. *Frontiers in Bioengineering and Biotechnology.* 2023, *11*.

(246) Azadikhah, F.; Karimi, A. R. Injectable Photosensitizing Supramolecular Hydrogels: A Robust Physically Cross-Linked System Based on Polyvinyl Alcohol/Chitosan/Tannic Acid with Self-Healing and Antioxidant Properties. *Reactive and Functional Polymers*. 2022, *173*, 105212.

(247) Wang, Y.; Yang, M.; Zhao, Z. Facile Fabrication of Self-Healing, Injectable and Antimicrobial Cationic Guar Gum Hydrogel Dressings Driven by Hydrogen Bonds. *Carbohydrate Polymers*. 2023, *310*, 120723.

(248) Yang, R.; Wang, B.; Zhang, X.; Sun, Y.; Zhang, Y.; Xu, Z.;

Yang, Q.; Liu, W. A Nucleobase-Driven Self-Gelled Hyaluronic Acid-Based Injectable Adhesive Hydrogel Enhances Intervertebral Disc Repair. *Advanced Functional Materials*. 2024, 2401232.

(249) Dai, X.; Zhang, Y.; Gao, L.; Bai, T.; Wang, W.; Cui, Y.; Liu, W. A Mechanically Strong, Highly Stable, Thermoplastic, and Self-Healable Supramolecular Polymer Hydrogel. *Advanced Materials*. 2015, *27* (23), 3566–3571.

(250) Hou, S.; Wang, X.; Park, S.; Jin, X.; Ma, P. X. Rapid Self-Integrating, Injectable Hydrogel for Tissue Complex Regeneration. *Advanced Healthcare Materials*. 2015, *4* (10), 1491–1495.

(251) Shi, L.; Ding, P.; Wang, Y.; Zhang, Y.; Ossipov, D.; Hilborn, J. Self-Healing Polymeric Hydrogel Formed by Metal–Ligand Coordination Assembly: Design, Fabrication, and Biomedical Applications. *Macromolecular Rapid Communications*. 2019, *40* (7), 1800837.

(252) Yavvari, P. S.; Pal, S.; Kumar, S.; Kar, A.; Awasthi, A. K.; Naaz, A.; Srivastava, A.; Bajaj, A. Injectable, Self-Healing Chimeric Catechol-Fe(III) Hydrogel for Localized Combination Cancer Therapy. *ACS Biomaterials Science & Engineering*. 2017, *3* (12), 3404–3413.

(253) Han, Y.; Zeng, Q.; Li, H.; Chang, J. The Calcium Silicate/Alginate Composite: Preparation and Evaluation of Its Behavior as Bioactive Injectable Hydrogels. *Acta Biomaterialia*. 2013, *9* (11), 9107–9117.

(254) Chang, H.; Li, C.; Huang, R.; Su, R.; Qi, W.; He, Z. Amphiphilic Hydrogels for Biomedical Applications. *Journal of Materials Chemistry B*. 2019, *7* (18), 2899–2910.

(255) Wang, C.; Wang, Z.; Zhang, X. Amphiphilic Building Blocks for Self-Assembly: From Amphiphiles to Supra-Amphiphiles. *Accounts of Chemical Research.* 2012, *45* (4), 608–618.

(256) Yuan, Y.; Raheja, K.; B. Milbrandt, N.; Beilharz, S.; Tene, S.; Oshabaheebwa, S.; A. Gurkan, U.; S. Samia, A. C.; Karayilan, M. Thermoresponsive Polymers with LCST Transition: Synthesis, Characterization, and Their Impact on Biomedical Frontiers. *RSC Applied Polymers*. 2023, *1* (2), 158–189.

(257) Pardeshi, S.; Damiri, F.; Zehravi, M.; Joshi, R.; Kapare, H.; Prajapati, M. K.; Munot, N.; Berrada, M.; Giram, P. S.; Rojekar, S.; Ali, F.; Rahman, M. H.; Barai, H. R. Functional Thermoresponsive Hydrogel Molecule to Material Design for Biomedical Applications. *Polymers*. 2022, *14* (15), 3126.

(258) Wang, L.; Li, A.; Zhang, D.; Zhang, M.; Ma, L.; Li, Y.; Wang, W.; Nan, K.; Chen, H.; Li, L. Injectable Double-Network Hydrogel for Corneal Repair. *Chemical Engineering Journal*. 2023, *455*, 140698.

(259) Tan, H.; Ramirez, C. M.; Miljkovic, N.; Li, H.; Rubin, J. P.; Marra, K. G. Thermosensitive Injectable Hyaluronic Acid Hydrogel for Adipose Tissue Engineering. *Biomaterials*.

2009, *30* (36), 6844–6853.

(260) Leal, D.; De Borggraeve, W.; Encinas, M. V.; Matsuhiro, B.; Müller, R. Preparation and Characterization of Hydrogels Based on Homopolymeric Fractions of Sodium Alginate and PNIPAAm. *Carbohydrate Polymers*. 2013, *92* (1), 157–166.

(261) Lin, T.-H.; Wang, H.-C.; Wu, M.-C.; Hsu, H.-C.; Yeh, M.-L. A Bilineage Thermosensitive Hydrogel System for Stimulation of Mesenchymal Stem Cell Differentiation and Enhancement of Osteochondral Regeneration. *Composites Part B: Engineering*. 2022, *233*, 109614.

(262) Lü, S.; Liu, M.; Ni, B. Degradable, Injectable Poly(*N*-Isopropylacrylamide)-Based Hydrogels with Low Gelation Concentrations for Protein Delivery Application. *Chemical Engineering Journal*. 2011, *173* (1), 241–250.

(263) Jung, Y.; Park, W.; Park, H.; Lee, D.-K.; Na, K. Thermo-Sensitive Injectable Hydrogel Based on the Physical Mixing of Hyaluronic Acid and Pluronic F-127 for Sustained NSAID Delivery. *Carbohydrate Polymers*. 2017, *156*, 403–408.

(264) Shriky, B.; Kelly, A.; Isreb, M.; Babenko, M.; Mahmoudi, N.; Rogers, S.; Shebanova, O.; Snow, T.; Gough, T. Pluronic F127 Thermosensitive Injectable Smart Hydrogels for Controlled Drug Delivery System Development. *Journal of Colloid and Interface Science*. 2020, *565*, 119–130.

(265) Yap, L.-S.; Yang, M.-C. Thermo-Reversible Injectable

Hydrogel Composing of Pluronic F127 and Carboxymethyl Hexanoyl Chitosan for Cell-Encapsulation. *Colloids and Surfaces B: Biointerfaces*. 2020, *185*, 110606.

(266) Park, K. M.; Lee, S. Y.; Joung, Y. K.; Na, J. S.; Lee, M. C.; Park, K. D. Thermosensitive Chitosan–Pluronic Hydrogel as an Injectable Cell Delivery Carrier for Cartilage Regeneration. *Acta Biomaterialia*. 2009, *5* (6), 1956–1965.

(267) Liu, G.; Yuan, Q.; Hollett, G.; Zhao, W.; Kang, Y.; Wu, J. Cyclodextrin-Based Host–Guest Supramolecular Hydrogel and Its Application in Biomedical Fields. *Polymer Chemistry*. 2018, *9* (25), 3436–3449.

(268) Wang, S.; Ong, P. J.; Liu, S.; Thitsartarn, W.; Tan, M. J. B. H.; Suwardi, A.; Zhu, Q.; Loh, X. J. Recent Advances in Host-Guest Supramolecular Hydrogels for Biomedical Applications. *Chemistry - An Asian Journal*. 2022, *17* (18), e202200608.

(269) Rasouli, S.; Hashemianzadeh, S. M. Thermal Behavior of Cyclodextrin/Adamantane Host/Guest Inclusion Complex in an Aqueous Media. *Journal of Molecular Liquids*. 2023, *390*, 123096.

(270) Jiang, X.; Zeng, F.; Yang, X.; Jian, C.; Zhang, L.; Yu, A.; Lu, A. Injectable Self-Healing Cellulose Hydrogel Based on Host-Guest Interactions and Acylhydrazone Bonds for Sustained Cancer Therapy. *Acta Biomaterialia*. 2022, *141*, 102–113.

(271) Bezold, M. G.; Hanna, A. R.; Dollinger, B. R.; Patil, P.; Yu,

F.; Duvall, C. L.; Gupta, M. K. Hybrid Shear-Thinning Hydrogel Integrating Hyaluronic Acid with ROS-Responsive Nanoparticles. *Advanced Functional Materials*. 2023, *33* (31), 2213368.

(272) Zhang, B.; He, J.; Shi, M.; Liang, Y.; Guo, B. Injectable Self-Healing Supramolecular Hydrogels with Conductivity and Photo-Thermal Antibacterial Activity to Enhance Complete Skin Regeneration. *Chemical Engineering Journal*. 2020, *400*, 125994.

(273) Li, X.; Gong, J. Design Principles for Strong and Tough Hydrogels. *Nature Reviews Materials*. 2024, 1–19.

(274) Puza, F.; Zheng, Y.; Han, L.; Xue, L.; Cui, J. Physical Entanglement Hydrogels: Ultrahigh Water Content but Good Toughness and Stretchability. *Polymer Chemistry*. 2020, *11* (13), 2339–2345.

(275) Fujiyabu, T.; Yoshikawa, Y.; Chung, U.; Sakai, T. Structure-Property Relationship of a Model Network Containing Solvent. *Science and Technology of Advanced Materials*. 2019, *20* (1), 608–621.

(276) Wang, Y.; Xu, Q.; Chen, T.; Zuo, Y.; Wang, J. A Supramolecular Hydrogel with an Ideally Homogeneous 3D Network Structure Based on a (Cucurbit [8] Uril) Host-(Tetrahedron-like) Guest Interaction. *Materials Research Express*. 2019, *6* (8), 085419.

(277) Fujiyabu, T.; Sakumichi, N.; Katashima, T.; Liu, C.; Mayumi, K.; Chung, U.; Sakai, T. Tri-Branched Gels:

Rubbery Materials with the Lowest Branching Factor Approach the Ideal Elastic Limit. *Science Advances*. 2022, *8* (14), eabk0010.

(278) Wang, S.; Chen, Y.; Sun, Y.; Qin, Y.; Zhang, H.; Yu, X.; Liu, Y. Stretchable Slide-Ring Supramolecular Hydrogel for Flexible Electronic Devices. *Communications Materials*. 2022, *3* (1), 1–9.

(279) Tang, M.; Zheng, D.; Samanta, J.; Tsai, E. H. R.; Qiu, H.; Read, J. A.; Ke, C. Reinforced Double-Threaded Slide-Ring Networks for Accelerated Hydrogel Discovery and 3D Printing. *Chem*. 2023, *9* (12), 3515–3531.

(280) Fu, L.; Li, L.; Bian, Q.; Xue, B.; Jin, J.; Li, J.; Cao, Y.; Jiang, Q.; Li, H. Cartilage-like Protein Hydrogels Engineered via Entanglement. *Nature*. 2023, *618* (7966), 740–747.

(281) Wang, K.; Zhang, Y.; Chen, T.; Bai, L.; Li, H.; Tan, H.; Liu, C.; Qu, X. Chain Entanglement-Driven Tough, Fatigue-Resistant PEG-Based Injectable Hydrogel Adhesive for Joint Skin Wound Healing. *Composites Part B: Engineering*. 2023, *266*, 110991.

(282) Wang, S.; Hu, Y.; Kouznetsova, T. B.; Sapir, L.; Chen, D.; Herzog-Arbeitman, A.; Johnson, J. A.; Rubinstein, M.; Craig, S. L. Facile Mechanochemical Cycloreversion of Polymer Cross-Linkers Enhances Tear Resistance. *Science*. 2023, *380* (6651), 1248–1252.

(283) Bao, B.; Zeng, Q.; Li, K.; Wen, J.; Zhang, Y.; Zheng, Y.; Zhou, R.; Shi, C.; Chen, T.; Xiao, C.; Chen, B.; Wang, T.;

Yu, K.; Sun, Y.; Lin, Q.; He, Y.; Tu, S.; Zhu, L. Rapid Fabrication of Physically Robust Hydrogels. *Nature Materials*. 2023, *22* (10), 1253–1260.

(284) Liu, R.; Liang, S.; Tang, X.-Z.; Yan, D.; Li, X.; Yu, Z.-Z. Tough and Highly Stretchable Graphene Oxide/Polyacrylamide Nanocomposite Hydrogels. *J. Mater. Chem.* 2012, *22* (28), 14160–14167.

(285) Huang, T.; Xu, H. G.; Jiao, K. X.; Zhu, L. P.; Brown, H. R.; Wang, H. L. A Novel Hydrogel with High Mechanical Strength: A Macromolecular Microsphere Composite Hydrogel. *Advanced Materials*. 2007, *19* (12), 1622–1626.

(286) Haraguchi, K.; Takehisa, T. Nanocomposite Hydrogels: A Unique Organic–Inorganic Network Structure with Extraordinary Mechanical, Optical, and Swelling/De-Swelling Properties. *Advanced Materials*. 2002, *14* (16), 1120–1124.

(287) Wang, Q.; Mynar, J. L.; Yoshida, M.; Lee, E.; Lee, M.; Okuro, K.; Kinbara, K.; Aida, T. High-Water-Content Mouldable Hydrogels by Mixing Clay and a Dendritic Molecular Binder. *Nature*. 2010, *463* (7279), 339–343.

(288) Liu, J.; Chen, C.; He, C.; Zhao, J.; Yang, X.; Wang, H. Synthesis of Graphene Peroxide and Its Application in Fabricating Super Extensible and Highly Resilient Nanocomposite Hydrogels. *ACS Nano*. 2012, *6* (9), 8194–8202.

(289) Moghadam, M. N.; Pioletti, D. P. Improving Hydrogels′

Toughness by Increasing the Dissipative Properties of Their Network. *Journal of the Mechanical Behavior of Biomedical Materials*. 2015, *41*, 161–167.

(290) Nakajima, T. Generalization of the Sacrificial Bond Principle for Gel and Elastomer Toughening. *Polymer Journal*. 2017, *49* (6), 477–485.

(291) Gong, J.; Katsuyama, Y.; Kurokawa, T.; Osada, Y. Double-Network Hydrogels with Extremely High Mechanical Strength. *Advanced Materials*. 2003, *15* (14), 1155–1158.

(292) Chen, Q.; Chen, H.; Zhu, L.; Zheng, J. Engineering of Tough Double Network Hydrogels. *Macromolecular Chemistry and Physics*. 2016, *217* (9), 1022–1036.

(293) Chen, Q.; Zhu, L.; Huang, L.; Chen, H.; Xu, K.; Tan, Y.; Wang, P.; Zheng, J. Fracture of the Physically Cross-Linked First Network in Hybrid Double Network Hydrogels. *Macromolecules*. 2014, *47* (6), 2140–2148.

(294) Zhang, H. J.; Sun, T. L.; Zhang, A. K.; Ikura, Y.; Nakajima, T.; Nonoyama, T.; Kurokawa, T.; Ito, O.; Ishitobi, H.; Gong, J. Tough Physical Double-Network Hydrogels Based on Amphiphilic Triblock Copolymers. *Advanced Materials*. 2016, *28* (24), 4884–4890.

(295) Rodell, C. B.; Dusaj, N. N.; Highley, C. B.; Burdick, J. A. Injectable and Cytocompatible Tough Double-Network Hydrogels through Tandem Supramolecular and Covalent Crosslinking. *Advanced Materials*. 2016, *28* (38), 8419–8424.

(296) Miserez, A.; Guerette, P. A. Phase Transition-Induced Elasticity of α-Helical Bioelastomeric Fibres and Networks. *Chemical Society Reviews.* 2013, *42* (5), 1973–1995.

(297) Hua, M.; Wu, S.; Ma, Y.; Zhao, Y.; Chen, Z.; Frenkel, I.; Strzalka, J.; Zhou, H.; Zhu, X.; He, X. Strong Tough Hydrogels via the Synergy of Freeze-Casting and Salting Out. *Nature*. 2021, *590* (7847), 594–599.

(298) Fang, J.; Mehlich, A.; Koga, N.; Huang, J.; Koga, R.; Gao, X.; Hu, C.; Jin, C.; Rief, M.; Kast, J.; Baker, D.; Li, H. Forced Protein Unfolding Leads to Highly Elastic and Tough Protein Hydrogels. *Nature Communications*. 2013, *4* (1), 2974.

(299) Wang, P.; Deng, G.; Zhou, L.; Li, Z.; Chen, Y. Ultrastretchable, Self-Healable Hydrogels Based on Dynamic Covalent Bonding and Triblock Copolymer Micellization. *ACS Macro Lett.* 2017, *6* (8), 881–886.

(300) Zhang, J.; Lin, G.; Vaidya, U.; Wang, H. Past, Present and Future Prospective of Global Carbon Fibre Composite Developments and Applications. *Composites Part B: Engineering*. 2023, *250*, 110463.

(301) Tang, Y.; Wang, Z.; Xiang, L.; Zhao, Z.; Cui, W. Functional Biomaterials for Tendon/Ligament Repair and Regeneration. *Regenerative Biomaterials*. 2022, *9*, rbac062.

(302) Illeperuma, W. R. K.; Sun, J.-Y.; Suo, Z.; Vlassak, J. J. Fiber-Reinforced Tough Hydrogels. *Extreme Mechanics*

Letters. 2014, *1*, 90–96.

(303) Ma, Y.; Gong, J.; Li, Q.; Liu, X.; Qiao, C.; Zhang, J.; Zhang, S.; Li, Z. Triple-Mechanism Enhanced Flexible SiO2 Nanofiber Composite Hydrogel with High Stiffness and Toughness for Cartilaginous Ligaments. *Small*. 2024, *n/a* (n/a), 2310046.

(304) Qiu, W.; Han, H.; Li, M.; Li, N.; Wang, Q.; Qin, X.; Wang, X.; Yu, J.; zhou, Y.; Li, Y.; Li, F.; Wu, D. Nanofibers Reinforced Injectable Hydrogel with Self-Healing, Antibacterial, and Hemostatic Properties for Chronic Wound Healing. *Journal of Colloid and Interface Science*. 2021, *596*, 312–323.

Chapter Two

Tough Injectable Hydrogels via Flexible Chains Linking Rigid Homogeneous Framework

Part of this chapter has been organised in the manuscript:

Song, R., Milne, C., Johnson, M., Li, Y., Zhao, C., Geng, Q., A, S.*, Wang, W.* 'Tough Injectable Hydrogels via Flexible Chains Linking Rigid Homogeneous Framework', Submitted.

2.1 Introduction

The injectable hydrogel is in a solution state before injection, and it undergoes *in situ* crosslinking at the target site.[1,2] Benefiting from this feature, injectable hydrogels can be administered through minimally invasive injections and adapt to irregular defects by forming the required shape.[3–5] Moreover, injectable hydrogels can easily be combined with drugs and biological agents for therapeutic purposes.[6–9] These advantages make injectable hydrogels highly promising for clinical practices such as wound healing,[10] tissue scaffolds,[11] and localised delivery of drugs and cells.[12–14] However, injectable hydrogels have long been considered 'weak and fragile'.[15–17] The mechanical disadvantage dramatically restricts their biomedical applications in load-bearing situations, which are crucial for tissue engineering scaffolds.[18] Currently, the reports on tough injectable hydrogels are relatively rare, and their development primarily relies on trial-and-error methods.[19,20] Moreover, the toughening techniques employed in these hydrogels are not universally applicable to other injectable hydrogel systems.[18,21] To date, there is no clear, universal strategy to guide the design of tough injectable hydrogels. Therefore, developing a general toughening strategy remains a significant

challenge.

To enhance the toughness of injectable hydrogels, it is effective to introduce the elastic maintenance structure and mechanical energy dissipation structure into the same injectable hydrogel system.[20,22] Currently, the widely accepted toughening design approach involves multiple interpenetrated networks within the same hydrogel system, such as double network (DN) hydrogel.[23] The crosslinking densities of these independent networks are controlled separately to reconcile the energy dissipation and high elasticity advantages.[24] However, the preparation of these tough hydrogels typically require complicated multi-step preparation, and involve toxic molecules such as monomers, crosslinkers, and initiators.[25–27] This makes it challenging to be implemented through in injectable methods and to be applied in clinical practice.[28,29] However, the preparation steps for single network (SN) injectable hydrogels are generally simpler and easier to be implemented. This actual prompts us to consider whether it is possible to synergistically achieve the elastic maintenance structure and mechanical energy dissipation structure in SN injectable hydrogels.

Previous research has shown that higher crosslink densities typically result in shorter chain lengths between crosslink points.[30–32] These rigid, short chains are prone to stress concentration and quickly dissipate mechanical energy during significant deformations.[33] In contrast, hydrogel networks with lower crosslink densities feature longer chain lengths between crosslink points and have higher strain limits.[34,35] As shown in **Figure 2.1**, we propose incorporating flexible long chains into the rigid hydrogel network framework to reduce stress concentration and increase the energy cost of crack propagation. This structural design is also potentially to enhance both the elasticity and mechanical energy dissipation capacity of the hydrogel, thereby improving its toughness.

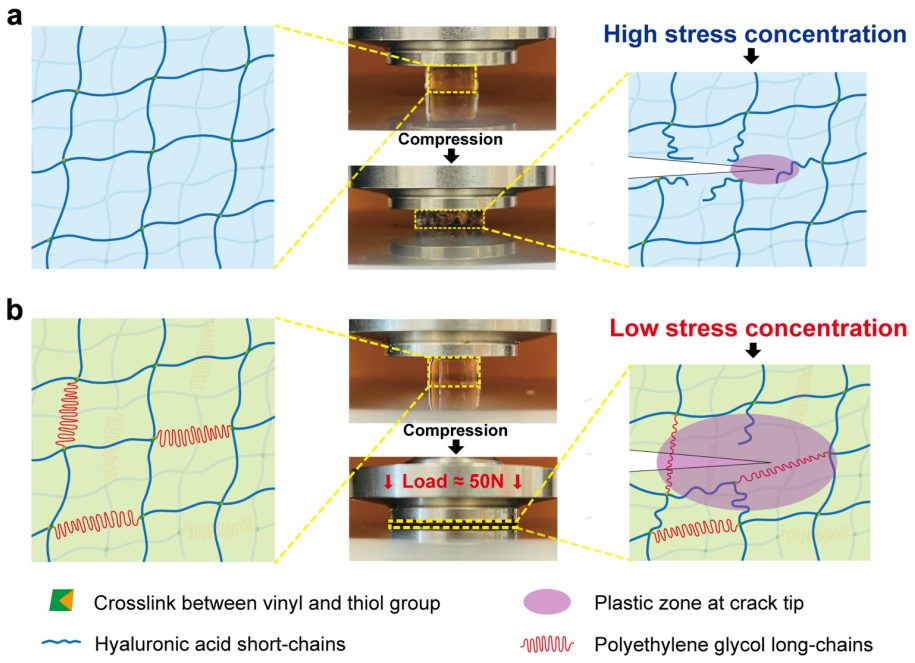


Figure 2.1 Illustrates how incorporating flexible long chains improves the toughness of SN hydrogels: (a) chain fracture and stress distribution in a classical SN hydrogel; (b) chain fracture and stress distribution in a hydrogel framework linked with flexible long chains.

In this study, acrylated hyaluronic acid (HA-A) and thiolated hyaluronic acid (HA-SH) were crosslinked by Thiol-ene Michael addition reaction and work as rigid framework. Acrylated polyethylene glycol (PEG-DA) and thiolated polyethylene glycol (PEG-DSH) were chosen as flexible long chains linked with the framework (**Figure 2.2**). Further research has shown that when these flexible long chains are linked with a homogeneous rigid framework, the toughness of the injectable hydrogel is optimised.

This resulting hydrogel, which incorporates both flexible long chains and a rigid homogeneous framework, is referred to as the FF hydrogel. Compared to the normal SN injectable hydrogel, the FF injectable hydrogels exhibit an almost 7-fold increase in compressive strength and a 4-fold improvement in toughness.

The aim of this chapter is to enhance the toughness of injectable single-network (SN) hydrogels by integrating flexible long chains into a homogeneous rigid framework. The objectives include incorporating flexible long chains into the hydrogel framework and evaluating the resulting mechanical properties, developing an AB-type injectable SN hydrogel through Michael Addition reaction, using acrylated hyaluronic acid (HA-A) and thiolated hyaluronic acid (HA-SH) combined with polyethylene glycol (PEG), and achieving significant improvements in compressive strength and toughness while maintaining high water content and good cytocompatibility.

2.2 Materials and Methods

2.2.1 Materials

HA-A (220 kDa, purity>98%; 10%SD) and HA-SH (220 kDa, purity>98%; 4%SD, 10%SD, and 20%SD) were purchased from

Blafar Ltd. PEG-DA (8kDa, purity≥95%) and PEG-DSH (4, 8, and 20 kDa, purity≥95%) were brought from Biopharma PEG Scientific Inc. Sodium phosphate (567547), Dulbecco's modified eagle medium (DMEM-high glucose, D6429), Hank's balanced salt solution (HBSS, H4641) were purchased from Sigma-Aldrich. Pepsin, Penicillin/streptomycin (PS, 15140122), Dulbecco's phosphate-buffered saline (DPBS, 14190094), alamarBlue Cell Viability Reagent (DAL1100) and Live/Dead Cell Viability Assay Kit (L3224) were purchased from Thermo Fisher Scientific. Human epidermal keratinocyte (HaCaT, CLS300493) cell line was obtained from CLS Cell Lines Service GmbH. Trypsin-EDTA (0.25%, 25200056) and Fetal Bovine Serum (FBS, 10270106) was purchased from Gibco. All the chemicals were used without purification and all aqueous solutions were prepared with deionised water.

2.2.2 Preparation and Characterisation of Hydrogels

HA-A, HA-SH, PEG-DA, and PEG-DSH were fully dissolved in 0.1M sodium phosphate buffer to prepare sample stock solutions at the designated concentrations. Subsequently, the sample solutions were mixed according to the predetermined ratios and then injected into moulds for crosslinking at 25°C for 24 hours.

The rheological properties of the hydrogels were evaluated using a rheometer (HR-2, TA) with an 8 mm diameter steel parallel-plate geometry, following an established protocol. Specifically, cylindrical hydrogels with 4 mm in height and 8 mm in diameter were subjected to time sweep tests. These tests were conducted at 1% strain and 1 Hz frequency, maintained at a temperature of 37°C.

The test on the hydrogels was performed at an axial velocity of 40 μm/s using a rheometer (HR-2, TA) at 37°C. The toughness was determined by calculating the area under the stress-strain curve.

The anti-fatigue properties of the hydrogels were evaluated using the repeated method. Specifically, the hydrogels were compressed to 80% of their limit strain and then allowed to return to their original height. The load-unload cycles were repeated 20 times at a speed of 40 μm/s and a temperature of 37°C. The dissipated energy was calculated by determining the difference between the areas under the loading and unloading stress-strain curves.

2.2.3 Cytocompatibility Assessment

HaCaT cells were used to assess the cell compatibility of FF hydrogels. The HaCaT cell line was cultured in DMEM supplemented with 10% FBS and 1% PS at 37°C in a humidified

atmosphere containing 5% CO_2. Cells were passaged at a ratio of 1:3 every 3-4 days. During passage, cells were detached using 0.25% trypsin-EDTA, counted with a hemocytometer, and reseeded in new culture flasks at the specified dilution ratio. For the compatibility test, 300 μL of both A_{10}+B_4/P_{20k}-10/0 and A_{10}+B_4/P_{20k}-5/5 FF hydrogels were initially placed at the bottom of a 24-well plate and crosslinked at 25°C for 24 hours crosslink. Subsequently, HaCaT cells were seeded onto the top surface of the hydrogels at a concentration of 10,000 cells per well and then cultured in a standard cell incubator at 37°C and 5% CO_2. HaCaT cells cultured on TC-plates under the same medium and environmental conditions served as the control group. alamarBlue assays were used to evaluate cell viability on days 1 and 3 using fluorescence as the readout method. Specifically, fluorescence was measured using a microplate reader (SpectraMax M3) with an excitation wavelength of 560 nm and an emission wavelength of 590 nm. Cell viability was calculated using the formula*: Cell Viability (%) = (Vt/Vb) × 100%*, where *Vt* represents the fluorescence intensity at a given time point and *Vb* the fluorescence intensity of the TC-plate group. A Live/Dead staining kit was employed to assess cell viability and adhesion status.

Similarly, cells were treated with staining reagents for 25 minutes on days 1 and 3. Subsequently, the hydrogels and TC-plate groups were washed three times with DPBS. Images were captured using a fluorescence microscope (IX81, Olympus Life Science) equipped with a camera (QImaging QiClick Mono) and software (cellSens Dimension 1.12). The images were taken using a 10× objective lens, with a 50 ms exposure time, and a 1× gain.

2.2.4 Statistical Analysis

All cytocompatibility values are expressed as mean ± standard deviation (SD). Statistical differences among the three groups were determined using one-way analysis of variance (ANOVA) followed by Turkey's Honest Significant Difference (HSD) post-hoc test for multiple comparisons in SPSS v29. A P value of less than 0.05 was considered statistically significant.

2.3 Results and Discussion

2.3.1 Configuration of Hydrogels

HA and PEG were chosen as the building blocks for FF hydrogels not only because of their inherently excellent biocompatibility but also, they can meet the FF hydrogel design requirement: rigid homogeneous framework, and flexible long chains. For the

structure of the polymer chains, HA is composed of repeating cyclic disaccharide units, whereas PEG is a simple linear structure.[36–38] Thus, with a consistent density of functional groups, PEG has a longer chain length between substituents on average. From the perspective of the SN hydrogel network structure, due to the longer PEG chains between adjacent crosslinking points compared to HA chains, they can serve as flexible long chains within the hydrogel network, while the HA component can be considered as a rigid framework.

As shown in **Figure 2.2**, HA-A solution was stored in the left chamber of the dual barrel syringe, while the mixture of HA-SH and PEG-DSH was stored in the right chamber. Subsequently, during the injection step, the two solutions were brought into contact, fully mixed, and then triggered a Thiol-ene Michael addition reaction between the thiol group and the vinyl group of functionalised HA and PEG. Of which, the rigid framework is formed through crosslinking between functionalised HA-A and HA-SH, while the flexible long PEG chains are connected within the HA framework. Under the condition of an equal number of thiol and vinyl groups, the mass ratio between PEG-DSH and HA-SH also determines the ratio of flexible long chains to rigid

frameworks within their respective hydrogel systems.

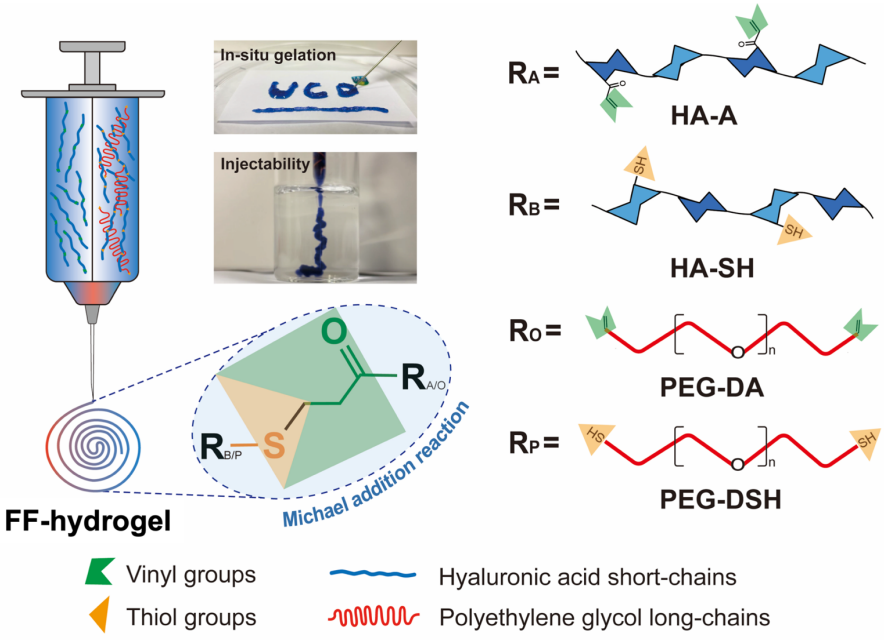


Figure 2.2 Illustration of the preparation process of *in situ* formed FF injectable hydrogel.

To evaluate the mechanical enhancement of SN hydrogels by FF design, the HA-SH with varying substitution degrees (SD) and PEG-DSH with different molecular weights (Mw) were utilised. To facilitate further discussion, it is noted that HA-A (SD=x %) + HA-SH (SD = y %) / PEG-DSH (Mw = z Da) hydrogels are abbreviated as A_x+B_y/P_z, where x and y represents SD of HA-A and HA-SH respectively, and z represents the Mw of PEG-DSH. The study of different SN hydrogel network configurations and their corresponding mechanical properties in the following three

experimental designs provides important data support for understanding the construction of highly tough FF hydrogels: A_{10}+B_{20}/P_{4k}, A_{10}+B_{10}/P_{8k}, and A_{10}+B_4/P_{20k}.

2.3.2 Characterisation of Hydrogels

Although all the hydrogels have similar high water content (98.5%), their mechanical properties varied significantly, as shown in **Figure 2.3**, **Figure 2.4**, and **Figure 2.5**. When comparing the stress-strain behaviours of different hydrogel groups, it can be observed that the trend of changes in mechanical properties induced by the substitution of flexible PEG long chains for rigid frameworks is not monotonic. Numerous studies have already demonstrated that hydrogels with a homogeneous network structure exhibit better mechanical strength. Therefore, we initially achieve a more homogeneous hydrogel network by replacing HA short chains with flexible PEG long chains. For ease of description, the A_x+B_y/P_z was followed by - m/n, where m/n represented the mass ratio of HA-SH/PEG-DSH.

As shown in **Figure 2.3**, the network structure of the A_{10}+B_{20}/P_{4k}–10/0 hydrogel can be understood in a simplified way as consisting of a number of rectangles with different long and short sides. In

this inhomogeneous SN structure, the short chains of B_{20} can be regarded as hydrogel defects, often breaking first during deformation to dissipate energy. However, there are no flexible long chains in the A_{10}+B_{20}/P_{4k}–10/0 hydrogel network to impede the propagation of cracks and maintain integrity under high deformation. Therefore, the limit stress, limit strain and compressive toughness are as low as 0.065 MPa, 57.64%, and 5.422 kJ/m^3 respectively (**Figure 2.3a and c**).

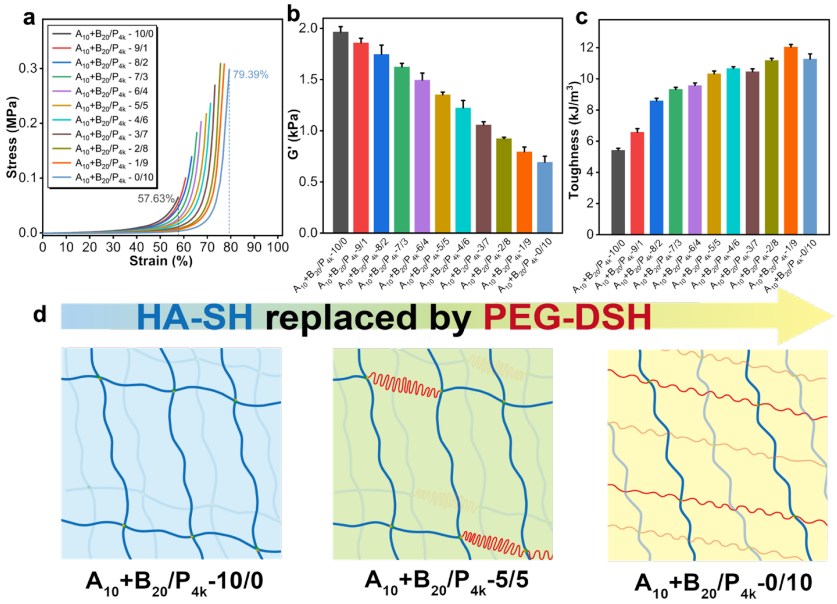


Figure 2.3 Mechanical properties of A_{10}+B_{20}/P_{4k} hydrogels with different flexible-to-rigid chain ratios: (a) compressive stress-strain curves, (b) G', and (c) compressive toughness of A_{10}+B_{20}/P_{4k} hydrogels. (d) illustrates of the replacement of B_{20} by P_{4k}. The representative images presented are randomly selected from replicate samples (n=3), and data are presented as mean ± standard deviation (n=3).

As more B_{20} is replaced by P_{4k}, the difference in chain lengths between adjacent crosslinking points in the hydrogel network also decreases. At the same time, a higher amount of flexible long chains can maintain the integrity of the hydrogel even if a small number of short chains have broken. As the replacement process continues of A_{10}+B_{20}/P_{4k} hydrogels from 9/1 to 3/7, the shorter B_{20} chains in the hydrogel were gradually replaced by longer P4k chains, thereby forming a relatively more homogeneous hydrogel network (**Figure 2.3d**). This more homogeneous network structure reduces the mechanical defects within the SN hydrogel, thereby enhancing its toughness by increasing the limit stress and strain. The highest compressive strength around 0.3 MPa was achieved at the final stage of the replacement process from A_{10}+B_{20}/P_{4k}–2/8 to 0/10. In this case, nearly all of the rigid B_{20} short chains were replaced by flexible long chains of P_{4k}, resulting in a more homogeneous network. However, the absence of rigid B_{20} short chains in the hydrogels also led to a reduced energy dissipation capability. The toughness of A_{10}+B_{20}/P_{4k}-0/10 hydrogel slightly decreased from 12.05 kJ/m^3 to 11.28 kJ/m^3 compared to A_{10}+B_{20}/P_{4k}-1/9. The gap size in rheological testing of hydrogels involves trade-offs between achieving higher shear rates and

minimising edge effects. Smaller gaps are advantageous for high shear rate studies and require less sample volume but are more prone to edge effects. Larger gaps minimise edge effects but limit the achievable shear rates and require more sample volume. Balancing these factors is crucial for optimising the rheological testing protocol to obtain accurate and reliable data for hydrogel materials. Given that this work focuses on the macroscopic mechanical properties of hydrogels at low shear rates and aims to minimise the influence of edge effects, cylindrical hydrogel samples with the same dimensions as those used in compression tests (4 mm in diameter and 8 mm in height) were also selected for the rheological viscoelasticity tests. With the increase content ratio of the PEG flexible long chain, the network undergoes a progressive relaxation, resulting in a gradual decline of storage modulus (G') from 1.966 kPa to 0.694 kPa (**Figure 2.3b**).

We were curious to see what would happen if this process of gradual homogenisation of the hydrogel network was reversed. The A_{10}+B_{10}/P_{8k} hydrogel group was therefore design to implement this change in network structure, and the changing trends observed in it exhibits a striking disparity compared to the A_{10}+B_{20}/P_{4k} group.

For the A_{10}+B_{10}/P_{8k}–10/0 hydrogel, which had a relatively homogeneous HA framework, the limit stress is approximately 0.24 MPa and the limit strain is 67.76%, both of which are higher than A_{10}+B_{20}/P_{4k}-10/0. However, when only a small amount of B_{10} was replaced with P_{8k} (A_{10}+B_{10}/P_{8k}-9/1), its limit stress significantly increased to 0.39 MPa (**Figure 2.4a**). This is because the presence of a small number of flexible long chains in a homogeneous SN framework increases the plastic zone area at the crack tip. This hydrogel network structure allows more chains to simultaneously resist deformation, thereby enhancing the values of limit stress and strain. However, as more rigid B_{10} chains were replaced by flexible P_{8k} long chains, the limit stress of the A_{10}+B_{10}/P_{8k} hydrogel did not increase further. It is speculated that in a SN hydrogel system, the variation in limit stress is jointly influenced by the homogeneous degree of framework and the quantity of co-tensioned chains in the plastic zone near the crack tip. For the A_{10}+B_{10}/P_{8k} group, the gradual replacement of B_{10} with P_{8k} disrupts the uniformity of the rigid framework chains in the SN hydrogel, further generating network defects and resulting in a decrease in the macroscopic limit stress of the hydrogel. However, with the increasing proportion of flexible P_{8k} chains, the plastic

zone area at the crack tip is gradually expanding, which reduces the sensitivity of network defects during the deformation process. As more chains are included in the plastic zone, they collectively resist deformation and dissipate deformation energy. These two opposing influences force the limit stress of the A_{10}+B_{10}/P_{8k}-9/1 to 4/6 SN hydrogel group to stabilise within a narrow range of 0.38 - 0.35 MPa. However, as more P_{8k} flexible long chains were replaced into the hydrogel network, its initially uniform structure becomes increasingly inhomogeneous. This change inevitably leads to a decrease in limit stress (**Figure 2.4a**). Simultaneously, as the overall average chain length in the network increases, the hydrogel network gradually relaxes. This leads to a reduction in the G' of A_{10}+B_{10}/P_{8k} hydrogels from 1.258 kPa to 0.465 kPa (**Figure 2.4b**). At the end of the replacement process, the non-uniform chain length in the A_{10}+B_{10}/P_{8k}-0/10 hydrogel network results in a compressive strength of only 0.16 MPa, which is even lower than the 0.24 MPa of the A_{10}+B_{10}/P_{8k}-10/0 group. Moreover, the toughness outcomes for this experimental group align with the trend of the stress-strain experiments, displaying a similar pattern of initial increase, followed by a plateau, and ultimately a decrease. (**Figure 2.4c**). As HA-SH is replaced by PEG-DSH, the changes

in the overall hydrogel network structure are illustrated in **Figure 2.4d**.

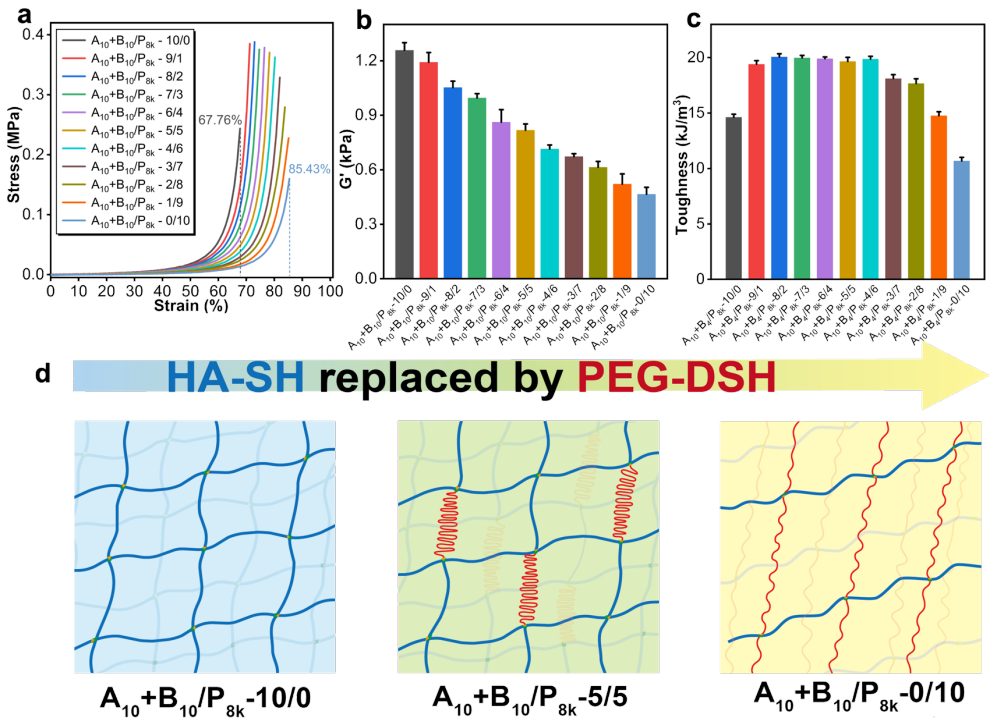


Figure 2.4 Mechanical properties of A_{10}+B_{10}/P_{8k} hydrogels with different flexible-to-rigid chain ratios: (a) compressive stress-strain curves, (b) G', and (c) compressive toughness of A_{10}+B_{10}/P_{8k} hydrogels; (d) illustrates of the replacement of B_{10} by P_{8k}. The representative images presented are randomly selected from replicate samples (n=3), and data are presented as mean ± standard deviation (n=3).

The above results reveal several important insights: (i) a homogeneous network framework has a positive effect on enhancing the toughness of SN hydrogels; (ii) the addition of flexible long chains within a relatively homogeneous rigid

network framework further enhances the toughness of SN hydrogels; (iii) improving either the uniformity of the framework or the quantity of flexible long chains while causing a decrease in the other is detrimental to the enhancement of toughness in SN hydrogels. Therefore, we infer that in SN hydrogel systems, simultaneously achieving a homogeneous rigid framework and flexible chains in the network while striking a balance between the two is crucial for achieving optimal toughness.

As shown in **Figure 2.5**, the design of the A_{10}+B_4/P_{20k} SN hydrogel system has found a delicate balance that allows for the formation of a relatively homogeneous rigid HA framework while also accommodating a certain number of flexible long chains connected to this framework. In this balanced FF structure, the homogeneous and rigid HA framework reduces defects in the SN hydrogel network, enabling more chains to undergo simultaneous stiffening before fracture and increasing the limit stress. Moreover, a quantity of flexible long chains extends the plastic zone at the crack tip, allowing more short chains to resist deformation simultaneously and provide energy dissipation upon fracture. Initially, in the A_{10}+B_4/P_{20k}-10/0 SN hydrogel, there exists a relatively inhomogeneous network structure. However, as the B_4

components within the network are gradually replaced by the flexible long chains of P_{20k}, the originally rigid framework composed of A_{10} and B_4 tends toward homogeneity. Furthermore, the increasing presence of flexible P_{20k} long chains within the SN further enhances the area of plastic zone at the fracture tip. As illustrated in **Figure 2.5d**, the A_{10}+B_4/P_{20k}-5/5 FF hydrogel configuration exhibits a distinctive arrangement in which half of the vinyl groups from A_{10} are connected to thiol groups from B_4 chains, while the remaining half are linked with P_{20k} flexible long chains. In that case, the A_{10}+B_4/P_{20k}-5/5 FF hydrogel network achieves a delicate equilibrium by striking a balance between a homogeneous rigid framework and suitable configuration of flexible long chains, forming the FF structure. It is primarily attributed to this optimised structure of the FF hydrogel that the A_{10}+B_4/P_{20k}-5/5 configuration attains a remarkable compressive strength of around 1 MPa, accompanied by a corresponding toughness value of 31.77 kJ/m^3, as depicted in **Figure 2.5a and c**. However, with the further replacement of B_4 with P_{20k} in A_{10}+B_4/P_{20k}-4/6 to 0/10 hydrogels, more than 60% of the vinyl groups on A_{10} were linked to P_{20k} rather than to B_4. Consequently, the optimal network structure of the FF hydrogel gradually

undergoes degradation. This structural alteration precipitates a rapid decline in both the compressive strength and toughness. Additionally, as more rigid B_4 chains were replaced by flexible P_{20k} chains, the G' gradually decreased, consistent with findings from previous research groups (**Figure 2.5b**).

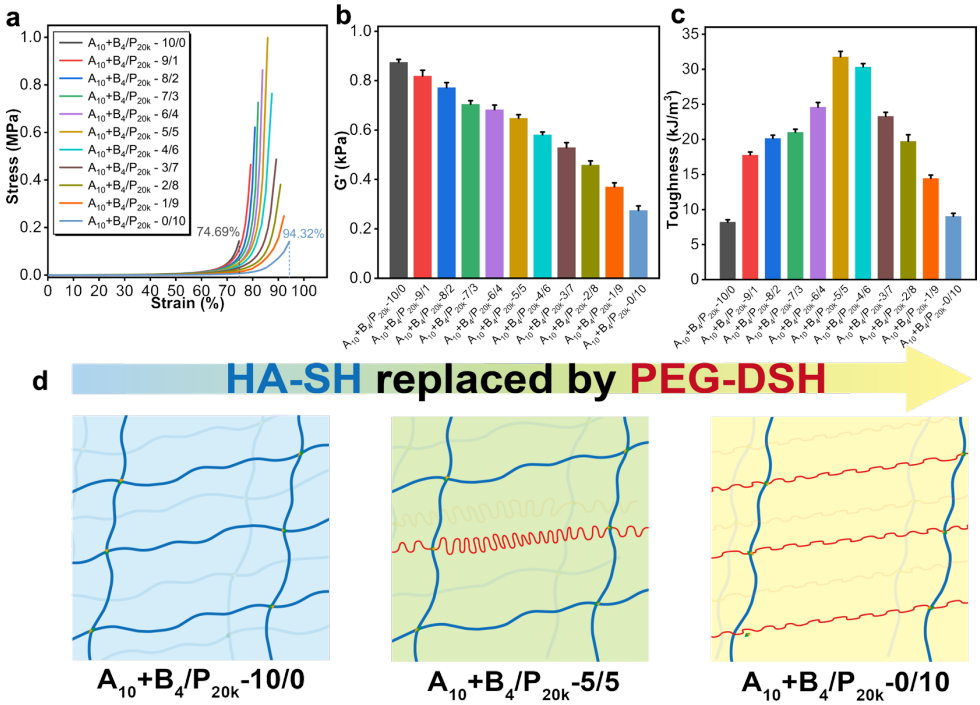


Figure 2.5 Mechanical properties of A_{10}+B_4/P_{20k} hydrogels with different flexible-to-rigid chain ratios: (a) compressive stress-strain, (b) G', (c) compressive toughness of A_{10}+B_4/P_{20k} hydrogels; (d) illustrates of the replacement of B_4 by P_{20k}. The representative images presented are randomly selected from replicate samples (n=3), and data are presented as mean ± standard deviation (n=3).

These findings demonstrate that by adjusting the uniformity of the

SN hydrogel rigid framework and the proportion of flexible long chains, the mechanical properties of SN hydrogels can be precisely tuned. Furthermore, through the appropriate replacement of rigid short chains with flexible long chains, the ability to withstand and dissipate the deformation force by a homogeneous rigid framework and the ability to maintain high elasticity by flexible long chains are synergistically achieved. Considering the widespread applicability of FF structures, there is the potential for enhancing the mechanical properties of numerous SN hydrogels. Another feature of A+B/P FF hydrogel that cannot be ignored is that the polymer contents of samples are only 1.5%.

2.3.3 Anti-fatigue Properties of Hydrogels

Hydrogels with loosely crosslinked SN structures can achieve superior elastic recovery capabilities under higher deformations through flexible adjustment of chain arrangements.[39–41] Nevertheless, due to the absence of energy dissipation structures, they are unable to achieve the toughness and load-unloading capability similar to human soft tissues such as cartilage during multiple mechanical cycles.[21] In addition, while rigid network structures do indeed achieve improved energy dissipation by sacrificing chains during the loading process, they struggle to

maintain their initial mechanical performance through repeated load-unloading cycles.[40] Therefore, obtaining hydrogels that combine high strength, toughness, and fatigue resistance remains a challenge.

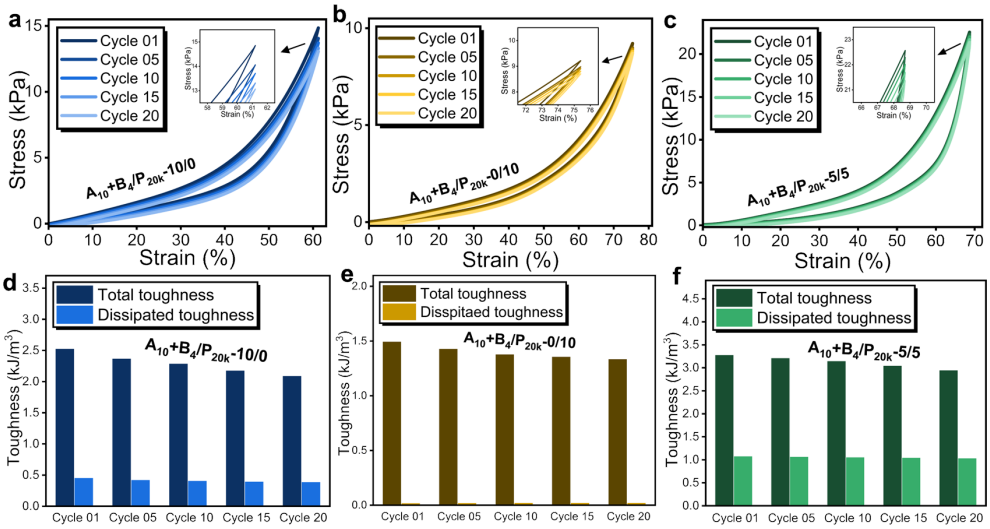


Figure 2.6 Anti-fatigue behaviour of SN hydrogel and FF hydrogel (80% limit strains for each hydrogel): 20 unspaced load-unload compression tests of (a) A_{10}+B_4/P_{20k}-10/0 SN hydrogel, (b) A_{10}+B_4/P_{20k}-0/10 SN hydrogel, and (c) A_{10}+B_4/P_{20k}-5/5 FF hydrogel; calculated results of the corresponding total and dissipative toughness of 20 unspaced load-unload compression tests of (d) A_{10}+B_4/P_{20k}-10/0 SN hydrogel, (e) A_{10}+B_4/P_{20k}-0/10 SN hydrogel, and (f) A_{10}+B_4/P_{20k}-5/5 FF hydrogel. The representative images presented are randomly selected from replicate samples (n=3).

As shown in **Figure 2.6**, the FF hydrogel also exhibits excellent anti-fatigue performance caused by the simultaneous integration

of a homogeneous rigid framework and flexible long chains within an SN structure. When the hydrogel is loaded with continuous load-unload cycles, the effective energy dissipation will show a clear hysteresis loop in the stress-strain curve. In general, the area of the hysteresis loop is used to measure the dissipated energy per unit volume, and the area is expanded by an efficient energy dissipation mechanism. After the repeat loading-unloading cycles of different SN hydrogel, the hysteresis loops show a completely different shape and changing trend (**Figure 2.6 a, b, and c**). After 20 cycles of repeated compression to 80% limit strain, the A_{10}+B_4/P_{20k}-10/0 hydrogel exhibited a clear hysteresis loop, while the A_{10}+B_4/P_{20k}-0/10 hydrogels showed a negligible one. Conversely, the A_{10}+B_4/P_{20k}-5/5 FF hydrogel displayed a larger hysteresis loop, indicating substantial energy dissipation ability (**Figure 2.6c**). Specifically, 1.073 kJ/m^3 (33% of the total compression energy) was dissipated of the A_{10}+B_4/P_{20k}-5/5 FF hydrogel in the first compression circle (**Figure 2.6f**). However, the A_{10}+B_4/P_{20k}-10/0 and A_{10}+B_4/P_{20k}-0/10 hydrogel showed smaller hysteresis loops, and only 0.451 kJ/m^3 (18% of the total compression energy), as well as 0.018 kJ/m^3 (1% of the total compression energy), were dissipated in the first compression

circle (**Figure 2.6d and e**). These findings indicate that the FF structure confers upon SN hydrogels not only enhanced energy dissipation but also superior anti-fatigue capabilities. These remarkable properties hold promising potential for the utilisation of FF hydrogels in various biomedical applications, including scenarios involving in frequently load-bearing situation.

2.3.4 Adjustable Mechanical Properties of Hydrogels

Based on the results obtained, it is apparent that the mechanical properties of FF hydrogels with the same crosslinking density undergo significant changes in response to variations in the proportion of flexible long chains to rigid framework. However, in a conventional SN hydrogel, both crosslinking density and polymer concentration play key roles in determining the 3D structure of the hydrogel network, thereby affecting its mechanical properties. Consequently, we propose that both the polymer concentration and the length of flexible long chains also further affect the mechanical properties of FF hydrogel. To verify this hypothesis, two distinct experiments were conducted. Firstly, the A_{10}+B_4/P_{20k}-5/5 FF hydrogels were prepared using five different polymer concentrations and subsequently subjected to testing. Secondly, the A_{10}+B_{10}/P_x-5/5 FF hydrogels were prepared with

three different lengths of flexible PEG long chains and subjected to testing.

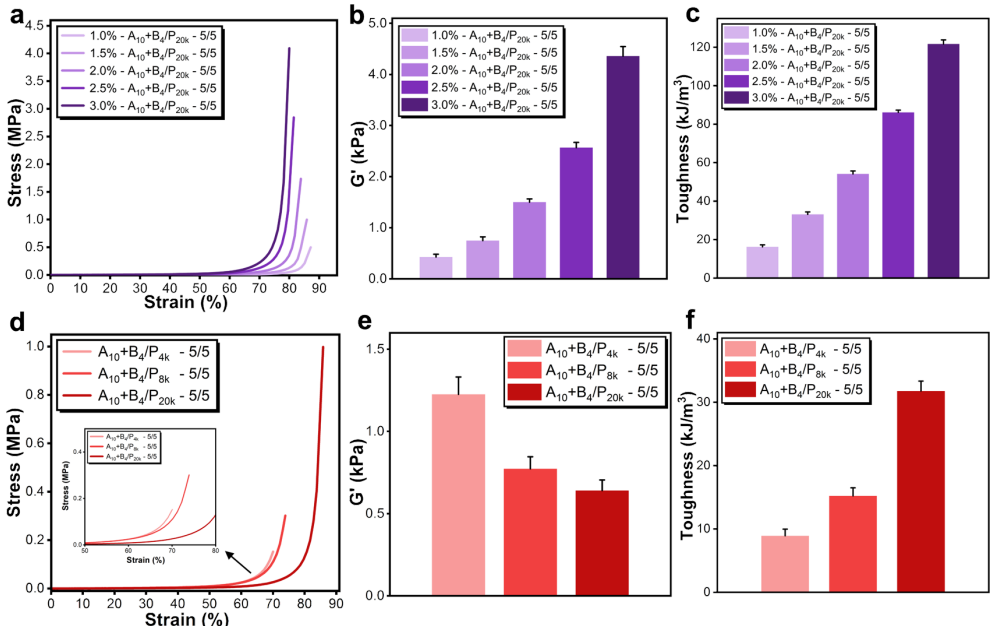


Figure 2.7 Adjustable mechanical properties of FF hydrogel by changing of polymer concentration and Mw of flexible PEG chains: (a) compressive stress-strain curves. (b) G', and (c) compressive toughness of A_{10}+B_4/P_{20k} -5/5 FF hydrogels with different polymer concentrations; (d) compressive stress-strain curves, (e) G', and (f) compressive toughness of A_{10}+B_4/P_z -5/5 FF hydrogels with different Mw of flexible PEG long chains. The representative images presented are randomly selected from replicate samples (n=3), and data are presented as mean ± standard deviation (n=3).

As shown in **Figure 2.7**, the increase in biopolymer concentration led to the elevation of both compressive strength and toughness in A_{10}+B_4/P_{20k}-5/5 FF hydrogels. Furthermore, the 3% concentration

of the A_{10}+B_4/P_{20k}-5/5 FF hydrogel has resulted in an 8.2-fold increase in limit stress, 7.5-fold increase in toughness and a 10-fold increase in G' compared with the 1% concentration group, respectively (**Figure 2.7a, b, and c).** However, it must be noted that the increase in the concentration of FF hydrogels inevitably enhances the stiffness of the hydrogel system, which also resulted in a slight decrease in the limit strain of the A_{10}+B_4/P_{20k}-5/5 FF hydrogel from 87.14% at 1.0% concentration to 79.98% at 3.0% concentration (**Figure 2.7a**). Furthermore, the aforementioned results have confirmed the crucial role of flexible long chains in the FF hydrogel network in determining the macroscale mechanical properties at a specific polymer concentration.

For the A_{10}+B_4/P_x–5/5 FF hydrogels, 50% of the vinyl groups of A_{10} were linked with B_4, while the remaining 50% were connected to PEG-DSH chains with molecular weights of 4 kDa, 8 kDa, and 20 kDa. Apparently, when compared to the A_{10}+B_4/P_{8k}–5/5 FF hydrogel, the A_{10}+B_4/P_{20k}–5/5 FF hydrogel with a longer flexible PEG chains (20 kDa) exhibits enhanced limit stress and strain, increasing from 0.30 MPa to 1 MPa and 73.90% to 85.86%, respectively (**Figure 2.7d**). In contrast, the hydrogel composed of shorter PEG chains (4 kDa) linked HA frameworks exhibits a

lower limit stress of 0.15 MPa and a strain of 70%. Moreover，with the increase in the flexibility of PEG chains, the FF hydrogel exhibits improved toughness. As shown in **Figure 2.7f**, the compression toughness of A_{10}+B_{10}/P_{20}k–5/5 FF hydrogel is 31.77 kJ/m³, A_{10}+B_{10}/P_{8k}–5/5 FF hydrogel is 15.22 kJ/m³, and the A_{10}+B_{10}/P_{4k}–5/5 FF hydrogel is 8.92 kJ/m³. As shown in **Figure 2.7e**, in terms of changes in G', A_{10}+B_{10}/P_{4k}–5/5 FF hydrogel with shorter PEG chains exhibits higher values, whereas A_{10}+B_{10}/P_{20k}–5/5 FF hydrogel with longer and more relaxed PEG chains has lower G'. This is attributed to the tightening of the HA framework and an increase in network rigidity caused by the shorter PEG connecting chains within the hydrogel.

2.3.5 A universal FF design for toughening SN hydrogels

Based on the toughening mechanism observed in FF hydrogels, we speculated that the flexible long chains linked rigid and uniform framework structure design is a universal criterion to enhance the classical SN hydrogels. To validate this hypothesis, a similar B_{20}+A_{10}/O_{8k} FF hydrogel system was constructed, wherein the A_{10} (HA-A, 10%SD) component was progressively replaced by O_{8k} (PEG-DA, 8kDa). As anticipated, the observed trend

exhibited similarities to that of the A_{10}+B_4/P_{20k} FF hydrogels (**Figure 2.8a**). As the replacement of A_{10} with O_8 progresses in the B_{20}+A_{10}/O_{8k} hydrogel, the limit stress and toughness initially increase, followed by a subsequent decrease at higher proportions of O_{8k}.

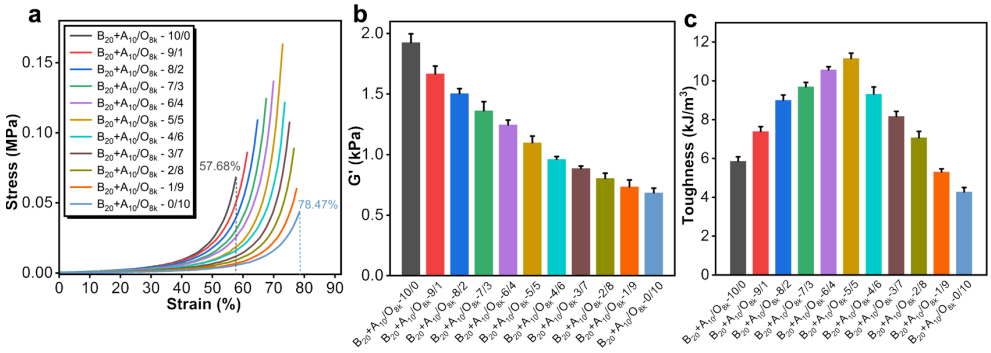


Figure 2.8 Mechanical properties of B_{20}+A_{10}/O_{8k} FF hydrogels with different flexible-to-rigid chain ratios: (a) compressive stress-strain curves, (b) G', and (c) compressive toughness of A_{10}+B_4/O_{8k} hydrogels. The representative strain-stress curves presented are randomly selected from replicate samples (n=3), and bar charts are presented as mean ± standard deviation (n=3).

The B_{20}+A_{10}/O_{8k}-5/5 FF hydrogel achieves a delicate equilibrium between the homogeneous framework and an optimal configuration for the dissipation of connected flexible long chains. In comparison to the B_{20}+A_{10}/O_{8k}-10/0 SN hydrogel, the B_{20}+A_{10}/O_{8k}-5/5 FF hydrogel exhibited notable enhancements in both compressive strengths, increasing from 0.06 to 0.16 MPa, and

toughness, lifting from 5.86 to 11.16 kJ/m^3, respectively (**Figure 2.8a and c**). Despite the relatively low molecular weight of the PEG-DA at 8 kDa, the B_{20}+A_{10}/O_{8k}-5/5 FF hydrogel demonstrated a remarkable more than 2-fold increase in toughness. Therefore, the mechanical properties also increased with the FF network structure forming, which was in good agreement with the previous conclusion drawn from the A+B/P FF hydrogel series.

2.3.6 Cytocompatibility of Hydrogels

The preparation process for all injectable hydrogels avoids the use of toxic monomers, crosslinkers, or initiators, thereby ensuring excellent cytocompatibility. As shown in **Figure 2.9a**, HaCaT cells in all experiment groups displayed a good state of growth. In the TC-plate group, HaCaT cells exhibited characteristic polygonal or spindle shapes, whereas cells on the hydrogel surface tended to grow in clusters. Moreover, the green fluorescence intensity was higher in the PEG-free A_{10}+B_4/P_{20k} - 10/0 group than in the A_{10}+B_4/P_{20k}-10/0 group, indicating a faster cell proliferation rate. This result was also shown in the alamarBlue assay (**Figure 2.9b**). Due to the inherent excellent hydrophilicity and cell adhesion resistance of PEG, it is speculated that the inclusion of PEG components made it more difficult for cells to adhere to the

surface of the A_{10}+B_4/P_{20k}-5/5 hydrogel, thereby reducing cell proliferation activity in day 1 and 3. However, since no significant red dead cells were observed, all injectable hydrogel groups demonstrated good cell compatibility.

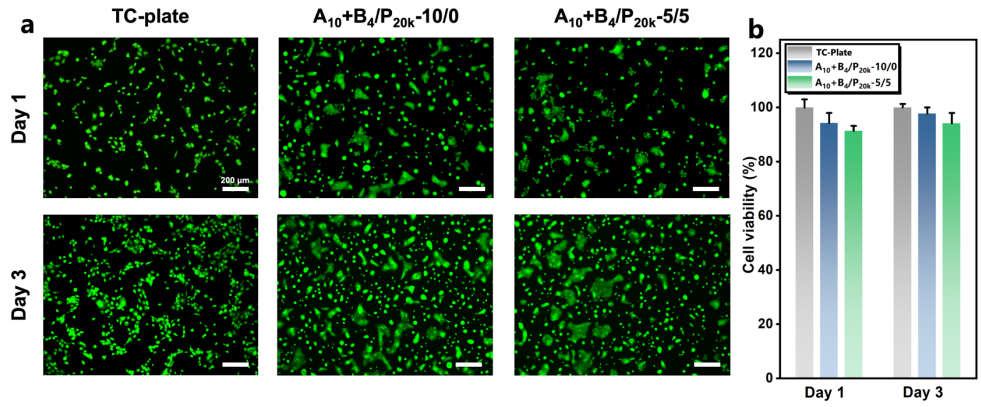


Figure 2.9 Cytocompatibility assessment of A_{10}+B_4/P_{20k} hydrogels: (a) Live/dead staining images, showing overlay images where green represents live cells and red represents dead cells and (b) alamarBlue cell viability assessment of HaCaT cells cultured on the surface of TC-plate, A_{10}+B_4/P_{20k} - 10/0 and A_{10}+B_4/P_{20k} – 5/5 FF hydrogels at day 1 and 3. Scale bar: 200 µm. The representative images presented are randomly selected from replicate samples (n=3), and bar charts are presented as mean ± standard deviation (n=3).

2.4 Conclusion

In conclusion, this study focuses on developing a universal strategy to enhance the mechanical properties of conventional SN injectable hydrogel while retaining their advantages of simplicity

in preparation, *in situ* formation, and biocompatibility. Through further investigation of toughening mechanisms, we have discovered that it is possible to efficiently modulate and enhance the toughness of hydrogels by adjusting the relaxation of certain polymer chains and the framework architecture within the hydrogel network. Moreover, increasing the proportion of flexible long chains can provide the hydrogel network with greater flexibility at the microscopic scale, allowing it to have a larger crack tip plasticity zone when subjected to stress. Additionally, a certain quantity of rigid and homogeneous framework structures can simultaneously reduce structural defects within the hydrogel network and enhance the energy dissipation capacity of the plasticity zone. Following this design, by substituting a specific quantity of PEG long chains into the HA-dominant SN network, FF hydrogels with flexible long chains linked rigid and homogeneous framework structures were prepared. This *in situ* formed FF injectable hydrogel achieved a compressive strength of nearly 1 MPa, a compressive toughness of 31.77 kJ/m^3, and excellent fatigue resistance at a polymer concentration of only 1.5%. As can be anticipated, the integration of the FF network design strategy with various SN hydrogels possessing exceptional

biological activity can assist in overcoming application bottlenecks caused by low mechanical strength and toughness. This, in turn, paves the way for the development of more clinically valuable advanced hydrogel systems.

2.5 References

(1) Pertici, V.; Pin-Barre, C.; Rivera, C.; Pellegrino, C.; Laurin, J.; Gigmes, D.; Trimaille, T. Degradable and Injectable Hydrogel for Drug Delivery in Soft Tissues. *Biomacromolecules*. 2019, 20 (1), 149–163.

(2) Ko, D. Y.; Shinde, U. P.; Yeon, B.; Jeong, B. Recent Progress of *in situ* Formed Gels for Biomedical Applications. *Progress in Polymer Science*. 2013, 38 (3), 672–701.

(3) Xu, Q.; A, S.; Gao, Y.; Guo, L.; Creagh-Flynn, J.; Zhou, D.; Greiser, U.; Dong, Y.; Wang, F.; Tai, H.; Liu, W.; Wang, W.; Wang, W. A Hybrid Injectable Hydrogel from Hyperbranched PEG Macromer as a Stem Cell Delivery and Retention Platform for Diabetic Wound Healing. *Acta Biomaterialia*. 2018, 75, 63–74.

(4) Correa, S.; Grosskopf, A. K.; Lopez Hernandez, H.; Chan, D.; Yu, A. C.; Stapleton, L. M.; Appel, E. A. Translational Applications of Hydrogels. *Chemical Reviews*. 2021, 121 (18), 11385–11457.

(5) Yang, J.-A.; Yeom, J.; Hwang, B. W.; Hoffman, A. S.; Hahn,

S. K. *In situ*-Forming Injectable Hydrogels for Regenerative Medicine. *Progress in Polymer Science*. 2014, 39 (12), 1973–1986.

(6) A. Young, S.; Riahinezhad, H.; G. Amsden, B. *In situ* - Forming, Mechanically Resilient Hydrogels for Cell Delivery. *Journal of Materials Chemistry B*. 2019, 7 (38), 5742–5761.

(7) Rizzo, F.; Kehr, N. S. Recent Advances in Injectable Hydrogels for Controlled and Local Drug Delivery. *Advanced Healthcare Materials*. 2021, 10 (1), 2001341.

(8) Yu, S.; He, C.; Chen, X. Injectable Hydrogels as Unique Platforms for Local Chemotherapeutics-Based Combination Antitumor Therapy. *Macromolecular Bioscience*. 2018, 18 (12), 1800240.

(9) Yu, L.; Ding, J. Injectable Hydrogels as Unique Biomedical Materials. *Chemical Society Reviews*. 2008, 37 (8), 1473–1481.

(10) Dimatteo, R.; Darling, N. J.; Segura, T. *In situ* Forming Injectable Hydrogels for Drug Delivery and Wound Repair. *Advanced Drug Delivery Reviews*. 2018, 127, 167–184.

(11) Olov, N.; Bagheri-Khoulenjani, S.; Mirzadeh, H. Injectable Hydrogels for Bone and Cartilage Tissue Engineering: A Review. *Progress in Biomaterials*. 2022, 11 (2), 113–135.

(12) Wang, K.; Han, Z. Injectable Hydrogels for Ophthalmic Applications. *Journal of Controlled Release*. 2017, 268, 212–224.

(13) Mathew, A. P.; Uthaman, S.; Cho, K. H.; Cho, C. S.; Park, I. K. Injectable Hydrogels for Delivering Biotherapeutic Molecules. International Journal of Biological *Macromolecules*. 2018, 110, 17–29.

(14) Liang, K.; Hyun Bae, K.; Kurisawa, M. Recent Advances in the Design of Injectable Hydrogels for Stem Cell-Based Therapy. *Journal of Materials Chemistry B*. 2019, 7 (24), 3775–3791.

(15) Ouyang, C.; Yu, H.; Wang, L.; Ni, Z.; Liu, X.; Shen, D.; Yang, J.; Shi, K.; Wang, H. Tough Adhesion Enhancing Strategies for Injectable Hydrogel Adhesives in Biomedical Applications. *Advances in Colloid and Interface Science*. 2023, 319, 102982.

(16) Overstreet, D. J.; Dutta, D.; Stabenfeldt, S. E.; Vernon, B. L. Injectable Hydrogels. *Journal of Polymer Science Part B: Polymer Physics*. 2012, 50 (13), 881–903.

(17) Vashahi, F.; Martinez, M. R.; Dashtimoghadam, E.; Fahimipour, F.; Keith, A. N.; Bersenev, E. A.; Ivanov, D. A.; Zhulina, E. B.; Popryadukhin, P.; Matyjaszewski, K.; Vatankhah-Varnosfaderani, M.; Sheiko, S. S. Injectable Bottlebrush Hydrogels with Tissue-Mimetic Mechanical Properties. *Science Advances*. 2022, 8 (3), eabm2469.

(18) Zhao, X.; Chen, X.; Yuk, H.; Lin, S.; Liu, X.; Parada, G. Soft Materials by Design: Unconventional Polymer Networks Give Extreme Properties. *Chemical Reviews*. 2021, 121 (8), 4309–4372.

(19) Fuchs, S.; Shariati, K.; Ma, M. Specialty Tough Hydrogels and Their Biomedical Applications. *Advanced Healthcare Materials*. 2020, 9 (2), 1901396.

(20) Zhao, X. Multi-Scale Multi-Mechanism Design of Tough Hydrogels: Building Dissipation into Stretchy Networks. *Soft Matter*. 2014, 10 (5), 672–687.

(21) Zhao, X. Designing Toughness and Strength for Soft Materials. *Proceedings of the National Academy of Sciences*. 2017, 114 (31), 8138–8140.

(22) Li, X.; Gong, J. Design Principles for Strong and Tough Hydrogels. *Nature Reviews Materials*. 2024, 1–19.

(23) Ping Gong, J. Why Are Double Network Hydrogels so Tough? *Soft Matter*. 2010, 6 (12), 2583–2590.

(24) Gong, J.; Katsuyama, Y.; Kurokawa, T.; Osada, Y. Double-Network Hydrogels with Extremely High Mechanical Strength. *Advanced Materials.* 2003, 15 (14), 1155–1158.

(25) Zhang, W.; Zhang, Y.; Zhang, Y.; Dai, Y.; Xia, F.; Zhang, X. Adhesive and Tough Hydrogels: From Structural Design to Applications. *Journal of Materials Chemistry B*. 2021, 9 (30), 5954–5966.

(26) Ahmed, E. M. Hydrogel: Preparation, Characterization, and Applications: A Review. *Journal of Advanced Research*. 2015, 6 (2), 105–121.

(27) Illeperuma, W. R. K.; Sun, J.-Y.; Suo, Z.; Vlassak, J. J. Fiber-Reinforced Tough Hydrogels. *Extreme Mechanics*

Letters. 2014, 1, 90–96.

(28) Hoeeg, C.; Dolatshahi-Pirouz, A.; Follin, B. Injectable Hydrogels for Improving Cardiac Cell Therapy-*In vivo* Evidence and Translational Challenges. *Gels*. 2021, 7(1), 7.

(29) Øvrebø, Ø.; Perale, G.; Wojciechowski, J. P.; Echalier, C.; Jeffers, J. R. T.; Stevens, M. M.; Haugen, H. J.; Rossi, F. Design and Clinical Application of Injectable Hydrogels for Musculoskeletal Therapy. *Bioengineering & Translational Medicine*. 2022, 7 (2), e10295.

(30) Jang, J.; Seol, Y.-J.; Kim, H. J.; Kundu, J.; Kim, S. W.; Cho, D.-W. Effects of Alginate Hydrogel Cross-Linking Density on Mechanical and Biological Behaviors for Tissue Engineering. *Journal of the Mechanical Behavior of Biomedical Materials*. 2014, 37, 69–77.

(31) Nielsen, L. E. Cross-Linking–Effect on Physical Properties of Polymers. *Journal of Macromolecular Science, Part C.* 1969, 3 (1), 69–103.

(32) Fumio, U.; Hiroshi, Y.; Kumiko, N.; Sachihiko, N.; Kenji, S.; Yasunori, M. Swelling and Mechanical Properties of Poly(Vinyl Alcohol) Hydrogels. *International Journal of Pharmaceutics*. 1990, 58 (2), 135–142.

(33) Nakajima, T. Generalization of the Sacrificial Bond Principle for Gel and Elastomer Toughening. *Polymer Journal*. 2017, 49 (6), 477–485.

(34) Kim, J.; Zhang, G.; Shi, M.; Suo, Z. Fracture, Fatigue, and Friction of Polymers in Which Entanglements Greatly

Outnumber Cross-Links. *Science*. 2021, 374 (6564), 212–216.

(35) Depalle, B.; Qin, Z.; Shefelbine, S. J.; Buehler, M. J. Influence of Cross-Link Structure, Density and Mechanical Properties in the Mesoscale Deformation Mechanisms of Collagen Fibrils. *Journal of the Mechanical Behavior of Biomedical Materials*. 2015, 52, 1–13.

(36) Kaufmann, J.; Möhle, K.; Hofmann, H.-J.; Arnold, K. Molecular Dynamics Study of Hyaluronic Acid in Water. *Journal of Molecular Structure: THEOCHEM*. 1998, 422 (1), 109–121.

(37) Fallacara, A.; Baldini, E.; Manfredini, S.; Vertuani, S. Hyaluronic Acid in the Third Millennium. *Polymers*. 2018, 10 (7), 701.

(38) D'souza, A. A.; Shegokar, R. Polyethylene Glycol (PEG): A Versatile Polymer for Pharmaceutical Applications. *Expert Opinion on Drug Delivery*. 2016, 13 (9), 1257–1275.

(39) Zhang, T.; Zuo, T.; Hu, D.; Chang, C. Dual Physically Cross-Linked Nanocomposite Hydrogels Reinforced by Tunicate Cellulose Nanocrystals with High Toughness and Good Self-Recoverability. *ACS Applied Materials & Interfaces.* 2017, 9 (28), 24230–24237.

(40) Bai, R.; Yang, J.; Suo, Z. Fatigue of Hydrogels. *European Journal of Mechanics - A/Solids*. 2019, 74, 337–370.

(41) Xue, B.; Bashir, Z.; Guo, Y.; Yu, W.; Sun, W.; Li, Y.; Zhang, Y.; Qin, M.; Wang, W.; Cao, Y. Strong, Tough, Rapid-

Recovery, and Fatigue-Resistant Hydrogels Made of Picot Peptide Fibres. *Nature Communications*. 2023, 14 (1), 2583.

Chapter Three

Tough Injectable Hydrogel via Thermal Self-entangled Chains Linking Rigid Framework

Part of this chapter has been organised in the manuscript:

Song, R., Milne, C., Zhao, C., Li, Y., Johnson, M., Geng, Q., Li, Z., Lyu, J., A, S.*, Wang, W.* 'Tough Injectable Hydrogel via Thermal Self-entangled Chains Linking Rigid Framework', submitted.

3.1 Introduction

Hydrogels are materials composed of crosslinked hydrophilic polymers surrounded by water.[1,2] This characteristic structure, resembling a framework filled with a solution, is commonly found in nature, constituting the extracellular matrix (ECM), tissues, and organs.[3–5] Benefiting from their similarity to natural structures, hydrogels show wide applications in the biomedical field, such as tissue scaffolds, skin wound dressings, artificial organs, and carriers for drugs or cells.[6–10] Hydrogels can be constructed in various ways, among which *in situ* formed injectable hydrogels are particularly advantageous.[11–13] They allow for implementation through minimally invasive procedures and can be shaped according to defects or specific designs.[14,15] These features make injectable hydrogels more clinically advantageous compared to traditional hydrogels.[16,17] However, the crosslinking mechanism of *in situ* crosslink renders many conventional hydrogels toughening structure designs inapplicable, resulting in difficulties in improving the mechanical properties of injectable hydrogels.[18–20] This drawback significantly limits the practical applications of injectable hydrogels.

The mechanical strength of hydrogels is strongly influenced by the

crosslinking density and the chain length between crosslinking points. As the crosslinking density increases, the chain length between crosslinking points decreases, resulting in a stiffer polymer network.[21,22] During deformation, the stiff short chains are more prone to isolated fracture, leading to crack propagation under concentrated stress and making the hydrogel brittle.[23] When the crosslinking density is too low, the polymer chains between crosslinking points are excessively long and loosely arranged.[24] During deformation, the flexible long chains cannot provide sufficient stress to maintain the shape, resulting in the hydrogel being excessively weak. The design of double network (DN) hydrogels combines the advantages of high and low crosslinking densities by interpenetrating two networks in the same hydrogel system.[25] The fracture of the rigid network provides the hydrogel with high energy dissipation capability, while the flexible crosslinked network gives the hydrogel high elasticity maintenance capability.[26] However, the construction of DN hydrogels often involves a complicated multi-step preparation process and the use of toxic reagents.[27–29] This makes it difficult to achieve through injectable methods and also raises concerns about safety for organisms.

Recent research has found that when highly entangled polymer networks are stretched, stress propagates along the polymer chains, leading to dynamic adjustments of the chain length between entanglement points.[30–32] Prior to network fracture, this adjustment can achieve uniform stress distribution within the polymer network and simultaneous stiffening of chains, resulting in outstanding limit strength.[33–35] However, the enhancement of toughness in such entangled hydrogels is limited due to the lack of mechanical energy dissipation structures.[36–38] Additionally, achieving entangled hydrogels through *in situ* formed methods is challenging. The existing preparation method for entangled hydrogels involves utilising the random thermal motion of high-concentration monomers and low-concentration crosslinkers during reaction processes for entanglement.[31] Subsequently, the polymers are immersed in water and allowed to swell to equilibrium, resulting in the formation of highly entangled hydrogels.

Here, we firstly explored the feasibility of constructing highly self-entangled injectable hydrogels using temperature-responsive amphiphilic diacrylated Pluronic F127 (F127-DA) polymers. Utilising the self-assembly behaviour of F127-DA at 37°C above

the lower critical solution temperature (LCST), the temporary entangled polymer chains were formed.[39] Subsequently, the vinyl groups at both ends of F127-DA chains are linked through UV initiation to form irreversible covalent bonds. The hydrogel network formed by covalent crosslinking prevents the untangling of the entangled structure within the F127 chains during deformation, thereby establishing a permanently preserved polymer entanglement structure. The compressive strength and toughness of this self-entangled hydrogel were increased by 4.1 and 4.3 times, respectively, compared to low entangled conventional network hydrogels. Subsequently, we combined this entangled structure with a rigid hyaluronic acid (HA) hydrogel framework to create a tough injectable single network (SN) hydrogel (**Figure 3.1**). Acrylated HA (HA-A) and thiolated HA (HA-SH) formed a homogeneous rigid hydrogel framework through a Michael Addition reaction. F127-DA served as self-entangled flexible long chains linked on the HA framework. This hydrogel exhibited a 1.7-fold increase in compressive strength and a 2-fold increase in toughness compared to its low entanglement counterpart. The significant enhancement in toughness is attributed to the synergistic effect of high elasticity and energy

dissipation structures. The self-assembled flexible chains provide high elasticity maintenance capability through knotting-sliding processes. Stretching of the self-assembled region and sacrifice of the rigid hydrogel framework contribute to high mechanical energy dissipation capability.

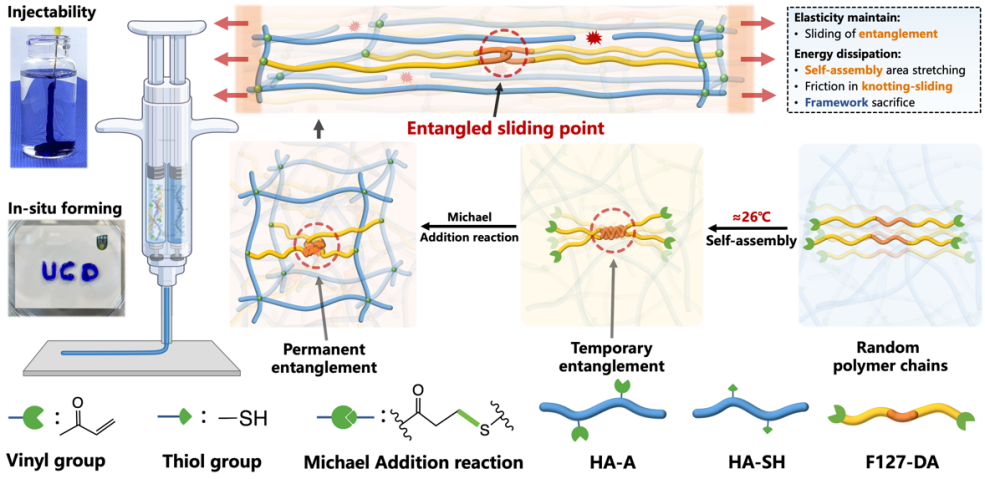


Figure 3.1 Illustration of the preparation and features of ABF-37℃ hydrogels. [Created with BioRender]

The aim of this chapter is to utilise the self-assembly behaviour of thermo-responsive polymer chains for the one-step construction of self-entangled tough injectable hydrogels. The objectives include investigating the use of self-assembly behaviour to create self-entangled regions, introducing the self-entangled structures into the hydrogel framework via Michael Addition reaction, and assessing the resulting mechanical performance enhancements

while maintaining cytocompatibility.

3.2 Materials and Methods

3.2.1 Materials

HA-A (110 kDa, purity >98%, 7% SD) and HA-SH (110kDa, purity >98%, 14% SD) were purchased from Blafar Ltd. PEG-DA (12 kDa, purity ≥ 95%) was purchased from Biopharma PEG scientific Inc. F127 (12.6 kDa, P2443), F127-DA (12.5 kDa, 901701), PEG (12 kDa), Chloroform (650498), Lithium phenyl-2,4,6-trimethylbenzoylphosphinate (LAP, 900889), Trypan Blue (T6146), sodium phosphate (342483), ethylenediaminetetraacetic acid (EDTA, E9884), L-cysteine hydrochloride (C1276), 5,5-dithio-bis-(2-nitrobenzoic acid) (Ellman's reagent, D218200), Dulbecco's modified eagle medium (DMEM-high glucose, D6429), Hank's balanced salt solution (HBSS, H4641) were purchased from Sigma-Aldrich. Penicillin/streptomycin (PS, 15140122), Dulbecco's phosphate-buffered saline (DPBS, 14190094), alamarBlue Cell Viability Reagent (DAL1100), Pepsin, and Live/Dead Cell Viability Assay Kit (L3224) were purchased from Thermo Fisher Scientific. Human epidermal keratinocyte (HaCaT, CLS300493) cell line was obtained from

CLS Cell Lines Service GmbH. Trypsin-EDTA (0.25%, 25200056), Fetal Bovine Serum (FBS, 10270106) was purchased from Gibco. All the chemicals were used without purification and all aqueous solutions were prepared with deionised water.

3.2.2 Preparation and Characterisation of F127-DA and PEG-DA hydrogel systems

The molecular of PEG, PEG-DA, F127, and F127-DA were tested by gel permeation chromatography (GPC, 1260 Infinity, Agilent Technologies). Specifically, 5 mg polymers were dissolved in 1 mL of chloroform, then filtered through a 0.2 μm filter, and then measured by GPC. The self-assembled F127 and F127-DA hydrogels were prepared through the aggregation of hydrophobic groups within their amphiphilic polymer chains, induced by thermal initiation. Specifically, F127 and F127-DA are fully dissolved in DPBS at 20% (unless otherwise specified, all ratios are by mass/volume) at 4°C. Subsequently, the solution is placed between the parallel plates of a rheometer (HR-2, TA) and subjected to temperature sweep tests from 10°C to 40°C at 1% strain and 1Hz frequency. PEG and PEG-DA of equivalent concentrations and under identical test conditions are employed as control groups.

The covalent crosslinked F127-DA and PEG-DA hydrogels were prepared by crosslinking vinyl groups via UV-induced photoinitiator LAP releasing free radicals. Specifically, LAP is dissolved in DPBS at a concentration of 0.5%. Then, this solution was used to fully dissolve PEG-DA and F127-DA at a concentration of 5%. Subsequently, time sweep tests are conducted on a rheometer, and at 60 seconds, the solution was exposed to 365nm UV light (Series 1000, OmniCure) for 30 seconds to completely crosslink the hydrogel. F127 and PEG raw materials of equivalent concentrations and under identical test conditions are employed as control groups. F127-37°C and PEG-37°C hydrogels are obtained by UV curing at 37°C, while F127-20°C and PEG-20°C hydrogels are obtained by UV curing at 20°C.

Swelling tests were conducted by placing hydrogel samples in DPBS solution at 25 times their volume, under conditions of either 20°C or 37°C. The following formula was used to calculate the mass of hydrogels after tests: $Hydrogel\ mass\ (\%) = Wt/Wi \times 100\%$, Where Wt represents the weight of hydrogels at the designed time point, and Wi is the weight of hydrogels before tests.

Rheological time sweep tests were conducted using a rheometer at

1% strain and 1Hz frequency. Compression tests were performed at an axial velocity of 40μm/s. Compressive toughness was determined by calculating the area under the compression stress-strain curve.

3.2.3 Preparation and characterisation of ABF and ABP hydrogel

For ABF (HA-A/HA-SH/F127-DA) hydrogel, HA-A and F127-DA were fully dissolved together at concentrations of 2.5% each in phosphate buffer solution to form Solution 1. HA-SH is fully dissolved at a concentration of 5% in phosphate buffer solution to form Solution 2. Solutions 1 and 2 are uniformly mixed at a volume ratio of 2:1 and placed in cylindrical moulds made of polytetrafluoroethylene for crosslinking. ABP (HA-A/HA-SH/PEG-DA) hydrogels were prepared similarly to ABF hydrogels, with the substitution of F127-DA by PEG-DA. AB (HA-A/HA-SH) hydrogel was prepared using a mixture of 5% HA-A and 5% HA-SH at a ratio of 2:1. Self-entangled ABF-37°C hydrogels were obtained after 12 hours of crosslinking at 37°C, while ABF-20°C hydrogels were obtained after 12 hours of crosslinking at 20°C. Similar procedures were used to prepare ABP-37°C and ABP-20°C hydrogels. The assessment of gelation

time is conducted by monitoring the modulus change using the time sweep mode of a rheometer. Strain sweep tests are performed at frequencies of 1Hz with shear strains ranging from 0.1% to 1000%. The unreacted thiol groups were tested by degrading the hydrogels at different reaction time points using hyaluronidase and then measuring it using Ellman's assay. Specifically, samples were prepared in Ellman reaction buffer at 1 mg/mL (0.1 M sodium phosphate, 1 mM EDTA, pH 8.0) and a standard curve of L-cysteine hydrochloride (0 - 30 mM) was prepared and mixed with Ellman solution (4 mg/mL) for 30 mins. Absorbance was determined at 412 nm. The concentration of the sample solution was determined by comparison with the standard curve of L-cysteine hydrochloride.

Swelling evaluation methods for ABF and ABP hydrogels are similar to those for PEG-DA and F127-DA hydrogels.

Compression and fatigue resistance tests involved placing hydrogel samples between the plates of a rheometer and conducting load and unload compression tests at a speed of 40 μm/s at 37°C. Three replicate tests were conducted for each measurement. Total toughness was determined by calculating the

area under the compression load stress-strain curve, while dissipative toughness was determined by calculating the area of the hysteresis loop.

3.2.4 Cytocompatibility Assessment of ABF and ABP hydrogel

HaCaT cells were used to assess the cell compatibility of ABF-37°C hydrogels. The HaCaT cell line was cultured in DMEM supplemented with 10% FBS and 1% PS at 37°C in a humidified atmosphere containing 5% CO_2. Cells were passaged at a ratio of 1:3 every 3-4 days. During passage, cells were detached using 0.25% trypsin-EDTA, counted with a hemocytometer, and reseeded in new culture flasks at the specified dilution ratio. For the cell compatibility test, 300 μL of ABF-37°C and ABP-37°C hydrogels were initially seeded at the bottom of a 24-well plate and incubated at 25°C for 24 hours crosslink. Subsequently, HaCaT cells were seeded onto the surface of the hydrogels at a concentration of 30,000 cells/well and cultured under conditions of 37°C and 5% CO_2. HaCaT cells cultured on TC-plates under the same medium and environmental conditions served as the control group. alamarBlue assays were performed on days 1 and 3 to assess cell viability using fluorescence as the readout method. Specifically,

fluorescence was measured using a microplate reader (SpectraMax M3) with an excitation wavelength of 560 nm and an emission wavelength of 590 nm. Cell viability was calculated using the formula: *Cell Viability (%) = Vt/Vb × 100%*, where *Vt* represents the fluorescence intensity at a given time point, and *Vb* represents the fluorescence intensity of the TC-plate group. A Live/Dead staining kit was used to confirm cell viability and adhesion status. Similarly, cells were treated with staining reagents for 25 minutes on days 1 and 3. Subsequently, hydrogels and TC-plate groups were washed with 3 times with DPBS. Images were captured using a fluorescence microscope (IX81, Olympus Life Science) equipped with a camera (QImaging QiClick Mono) and software (cellSens Dimension 1.12). The images were taken using a 10× objective lens, with a 50 ms exposure time, and a 1× gain.

3.2.5 Statistical Analysis

All cytocompatibility values are expressed as mean ± standard deviation (SD). Statistical differences among the three groups were determined using one-way analysis of variance (ANOVA) followed by Turkey's Honest Significant Difference (HSD) post-hoc test for multiple comparisons in SPSS v29. A P value of less than 0.05 was considered statistically significant.

3.3 Results and discussion

3.3.1 Characterisation of entangled F127-DA hydrogel system

F127-DA can form 3D hydrogel structures through two methods. The first method utilises the amphiphilic feature of the F127 chains to construct self-assembled physical hydrogels. When the F127-DA solution is heated above its LCST, the hydrophobic portions of the polymer assemble, leading to micro-scale phase separation. These phase-separated points act as physical crosslinking points to form the 3D network of the hydrogel. However, due to the low strength of this physical crosslinking, the resulting physical hydrogel essentially lacks elasticity. The second method involves the formation of chemically crosslinked hydrogels using acrylate groups that can be initiated by UV-induced free radicals. These two crosslinking methods do not interfere with each other and can act simultaneously.

As shown in **Figure 3.2a**, PEG-DA, which has a molecular weight similar to that of F127-DA, was used as the control group. In comparison to PEG-DA, F127-DA demonstrated thermo-responsive gelation capability. As shown in **Figure 3.2b**, F127-DA

exhibited a solution-to-hydrogel rheological transition at approximately 26°C. The presence of vinyl group at the chain ends of F127-DA also endowed it with the ability for UV crosslinking. As shown in **Figure 3.2c**, within 30 seconds of UV irradiation, F127-DA rapidly crosslinked and formed mechanically stable hydrogel. However, normal F127 lacked this capability.

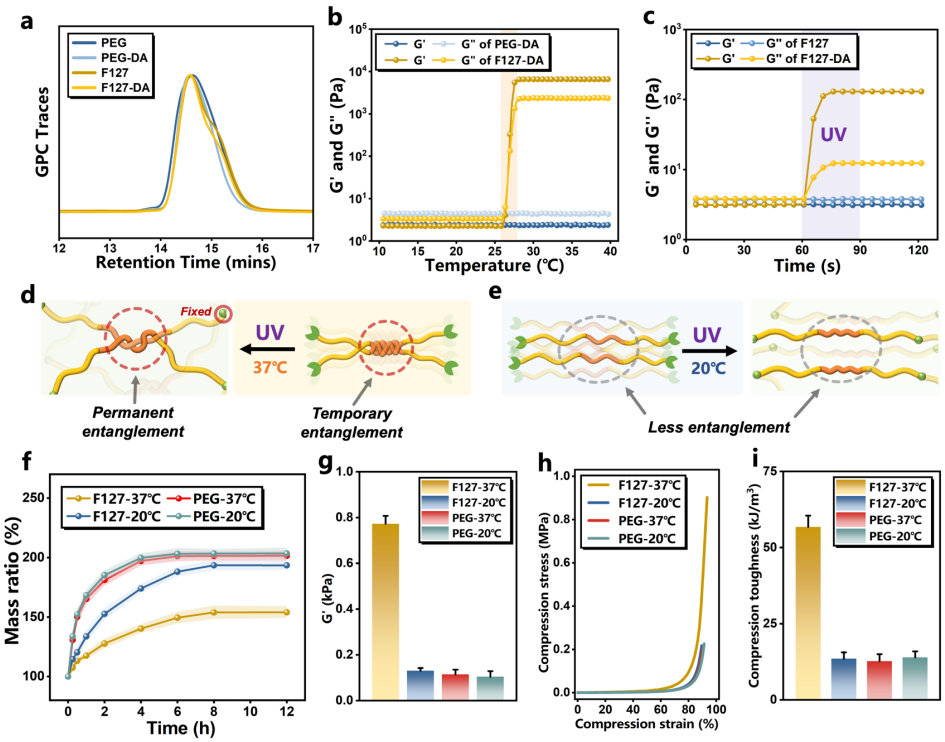


Figure 3.2 Characterisation of F127-DA hydrogel system. (a) GPC traces of PEG, PEG-DA, F127, and F127DA polymers; (b) temperature sweep of PEG-DA and thermo-responsive F127-DA polymer solutions; (c) time sweep of F127 and F127-DA polymer solutions with UV-crosslinking for 30 seconds from 60 to 90 s; (d) 37°C with more entanglement and (e) 20°C with less entanglement of F127-DA hydrogel system; (f) swelling test; (g) G'; (h) compression stress-strain curve; and (i) compressive toughness of PEG-20°C, PEG-37°C, F127-20 and self-entangled F127-37°C hydrogels. The representative images presented are randomly selected from replicate samples (n=3), and data are presented as mean ± standard deviation (n=3).

As shown in **Figure 3.2d**, the self-assembled F127-DA chains create a high polymer concentration around the hydrophobic areas

at 37°C, leading to significant chain entanglements. The subsequent UV crosslinking at 37°C makes these entanglements permanent, preventing them from being undone under deformation. However, as illustrated in **Figure 3.2e**, when F127-DA is UV crosslinked at 20°C, the uniformly dispersed F127-DA in the solution results in network-like topological features. The UV crosslinking locks these topological features, preventing additional entanglements. When the system temperature rises to 37°C, the resulting tentative entanglements cannot form knots or provide mechanical load-bearing capability.

The self-entangled F127-DA hydrogel (F127-37°C) was obtained through UV crosslinking at 37°C. At this temperature, the F127 chains are in a self-assembled entangled state. In addition, the low-entanglement F127-DA hydrogel (F127-20°C, HA-A, HA-SH, and F127-DA hydrogel crosslinked at 20°C) was obtained through UV crosslinking at 20°C, where the F127 chains are in a non-assembled, non-entangled state. The equilibrium swelling ratio of self-entangled F127-37°C group at 20°C was significantly lower than that of the F127-20°C group (**Figure 3.2f**). This was attributed to the greater number of physical entanglements in the F127-37°C hydrogel constraining the diffusion ability of polymer

network. Additionally, this high entanglement structure provides improvement in the mechanical properties of the hydrogel. As shown in **Figure 3.2g**, despite similar chemical crosslinking densities, the storage modulus (G') of F127-37°C was approximately 6 times that of F127-20°C due to more physical entanglements. Furthermore, the compressive strength and toughness of F127-37°C were respectively 4.1 and 4.3 times higher than those of F127-20°C (**Figure 3.2h and i**). This enhancement in mechanical performance was attributed to the role of entanglements as knotting-sliding. When the polymer network within the hydrogel is stretched, stress is transmitted along the chains and dispersed. Additionally, the process of stress transmission along the chains involves dynamic adjustment of chain lengths between entanglement points. This adjustment of chain lengths allows more chains in the hydrogel to undergo simultaneous stiffening before fracture, resulting in enhanced limit strain. We speculate that the self-entanglement behaviour of amphiphilic temperature-responsive materials can serve as a universal toughening strategy to enhance the mechanical performance of soft materials, including *in situ* formed injectable hydrogels.

3.3.2 Preparation of entangled ABF-37℃ hydrogel

Self-entangled F127-DA chains were linked to the HA hydrogel framework by Michael Addition reaction, thus constructing a biocompatible and tough *in situ* formed injectable hydrogel. As shown in **Figure 3.1**, HA-A was placed in the left chamber of the dual-chamber syringe together with PEG-DA, while HA-SH was placed in the right chamber. The subsequent injection process involved the mixing of the solutions. The vinyl groups on HA-A and F127-DA chains reacted with thiol groups on HA-SH through Michael Addition reaction to form a crosslinked hydrogel network. As shown in **Figure 3.3a**, the gelation process occurred more rapidly at 37°C. Around 11 minutes, the rheological properties of the ABF-37°C hydrogel system shifted from viscosity-dominated to elasticity-dominated, indicating rapid formation of the elastic network. Moreover, the solution-to-hydrogel transition of the ABF-20°C occurred at approximately 15 minutes. The progress of the Michael Addition reaction was assessed by monitoring the content of thiol groups in the hydrogel using Ellman's assay. As shown in **Figure 3.3b**, thiol groups in the ABF-37°C hydrogel were completely consumed within 6 hours, indicating completion of crosslinking. Moreover, thiol groups in the ABF-20°C hydrogel

were completely reacted in approximately 8 hours. To ensure complete crosslinking, all evaluation of hydrogel samples were conducted after 12 hours culturing. As shown in **Figure 3.3c**, both the G' and loss modulus (G") of self-entangled ABF-37°C hydrogel was higher than those of other experimental groups at 20°C. However, no significant differences were observed in G' and G" among ABF-20°C, ABP-37°C (HA-A, HA-SH, and PEG-DA hydrogel crosslinked at 37°C), and ABP-20°C (HA-A, HA-SH, and PEG-DA hydrogel crosslinked at 20°C). The results of the swelling test, as shown in **Figure 3.3d**, provided a more intuitive assessment of the entanglement degree of ABF hydrogels. Similar to F127-37°C hydrogel, ABF-37°C hydrogel exhibited a lower equilibrium swelling ratio at 20°C due to the constraining effect of entanglements of polymer chains (**Figure 3.3d**). At 37°C, the presence of hydrophobic self-assembled regions in F127 resulted in a significantly lower equilibrium swelling ratio of ABF hydrogels (**Figure 3.3e**). Strain sweep results demonstrated that self-entangled ABF-37°C hydrogel had a larger linear viscoelastic region (**Figure 3.3f**). This was attributed to the additional elastic capability provided by more polymer entanglement structures at shorter time scales. The rheological characteristics and swelling

behaviour of ABP-20°C and ABP-37°C hydrogels are remarkably similar. Therefore, only ABP-37°C hydrogel was selected as the control for subsequent mechanical performance evaluation.

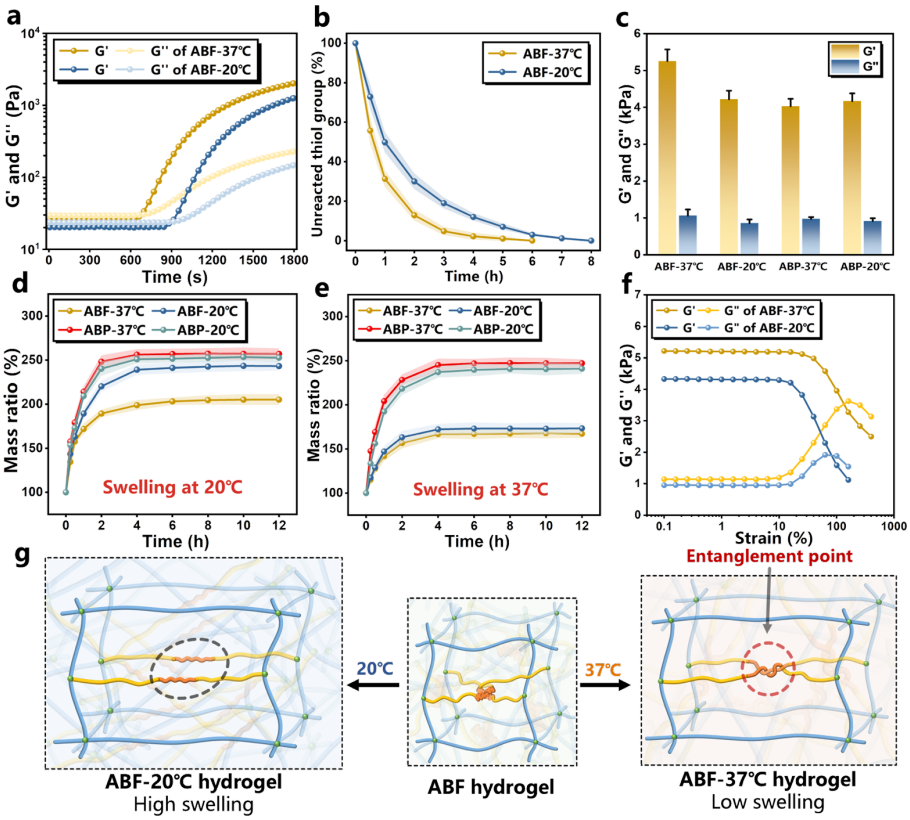


Figure 3.3 Characterisation of ABF hydrogel system. (a) gelation time assay of ABF hydrogel system at 20℃ and 37℃; (b) unreacted thiol groups with different reaction time at 20℃ and 37℃; (c) G' and G", hydrogels swelling at (d) 20℃ and (e) 37℃; (f) strain sweep of ABF-20℃ and self-entangled ABF-37℃ hydrogels; (g) illustration of the swelling limitation of ABF-20℃ and self-entangled ABF-37℃ hydrogels. The representative images presented are randomly selected from replicate samples (n=3), and data are presented as mean ± standard deviation (n=3).

3.3.3 Mechanical properties of self-entangled ABF-37°C hydrogel system

The presence of self-entangled polymer structures confers mechanical advantages to hydrogels, particularly in terms of strength, toughness, and fatigue resistance. As shown in **Figure 3.4a**, the stretching of self-assembled regions in the ABF-37°C hydrogel serves to dissipate energy during the initial deformation phase. As these self-assembled regions unfold, entanglement points act as physical sliding points within the hydrogel network. The distance between these sliding points adjusts automatically during deformation, reducing stress concentration on individual chains. Under high strain, stress is distributed evenly through the knotting-sliding process of polymer chains. This process facilitates simultaneous stiffening of more polymer chains in the hydrogel network before fracture, thus enhancing the elastic limit. Furthermore, the homogeneous and rigid framework structure of HA takes precedence in sacrificing, effectively dissipating mechanical energy. By combining high elasticity and energy dissipation structures, the ABF-37°C hydrogel demonstrates enhanced toughness.

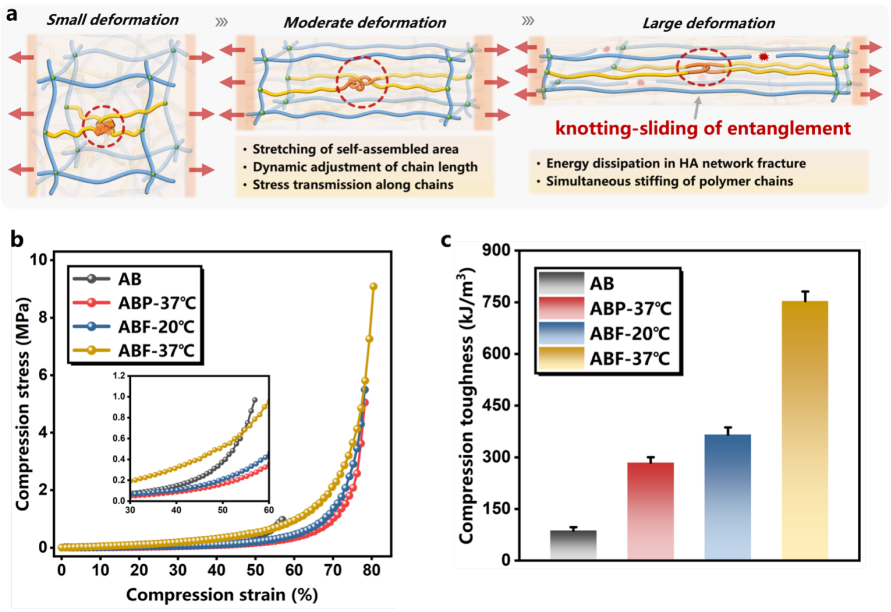


Figure 3.4 Mechanical Properties of ABF hydrogel system: (a) illustration of the structure changing in deformation process of self-entangled ABF-37℃ hydrogel; (b) compression stress-strain curve and (c) compressive toughness of AB, ABP-37℃, ABF-20℃, and self-entangled ABF-37℃ hydrogels. The representative images presented are randomly selected from replicate samples (n=3), and data are presented as mean ± standard deviation (n=3).

As shown in **Figure 3.4b**, both ABP and ABF hydrogels exhibit higher compressive strength compared to the AB hydrogel (HA-A and HA-SH hydrogel crosslinked at 37°C). The compressive strength increased from 0.97 MPa for AB to 5.04 MPa for ABP-37°C, 5.50 MPa for ABF-20°C, and 9.08 MPa for ABF-37°C. Moreover, when comparing the two groups of ABF hydrogels, the ABF-37°C hydrogel with more entanglements exhibits

approximately 1.65 times the compressive strength of the ABF-20°C hydrogel with fewer entanglements. In addition, ABF-37°C hydrogel also show a higher compression strain capability (80.48%). By calculating the area under the stress-strain curve, the toughness of the ABF-37°C hydrogel is 753 kJ/m^3, approximately 2.06 times higher than that of the ABF-20°C hydrogel, 2.65 times higher than that of the ABP-37°C hydrogel, and 8.67 times higher than that of the AB hydrogel (**Figure 3.4c**).

The results of the repeat compression tests confirmed the fatigue resistance of the self-entangled ABF-37°C hydrogel. The cyclic fatigue of hydrogels is caused by irreversible changes in the mechanical structure during the cyclic process. The compressive strength, total toughness, and dissipated toughness of the first compression cycle of all hydrogel groups were significantly higher than those in subsequent cycles. This is due to the irreversible sacrifice of polymer chains during the strain process in hydrogels. However, the self-entangled ABF-37°C exhibited larger hysteresis loops, total toughness, and dissipated toughness (**Figure 3.5a and d**). After 20 compression cycles at 37°C, the strength of ABF-37°C hydrogel only decreased by 4.5%, the total toughness decreased by 20.2%, and the dissipated toughness remained at 74.1%. In

contrast, after 20 compression cycles, the strength of ABF-20°C hydrogel decreased by 13.2%, the total toughness decreased by 28.1%, and the dissipated toughness only remained at 61% (**Figure 3.5b and e**).

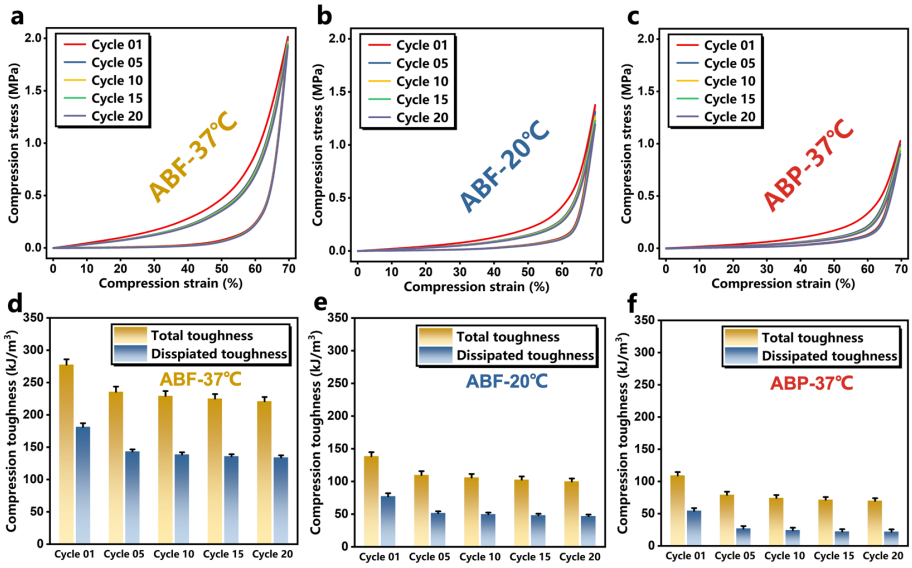


Figure 3.5 Fatigue resistance properties of ABF hydrogel system: 20 unspaced loading-unloading compression stress-strain curve of (a) self-entangled ABF-37°C hydrogel, (b) ABF-20°C hydrogel, and (c) ABP-37°C hydrogel; total and dissipated toughness of (d) self-entangled ABF-37°C hydrogel, (e) ABF-20°C hydrogel, and (f) ABP-37°C hydrogel. The representative images presented are randomly selected from replicate samples (n=3), and data are presented as mean ± standard deviation (n=3).

The fatigue resistance advantage of ABF-37°C hydrogel is attributed to the knotting-sliding process, which protects the

network structure by relieving stress concentration. For ABP-37°C hydrogel, its total toughness and dissipated toughness are significantly lower than those of ABF-20°C hydrogel due to the lack of self-assembly regions and chain entanglement structures. However, due to the presence of flexible PEG long chains, ABF-20°C hydrogel still maintained 87.5% of its strength after undergoing 20 compression cycles, a value similar to that of ABF-20°C hydrogel (**Figure 3.5c and f**).

3.3.4 Cytocompatibility evaluation of entangled ABF-37°C hydrogel system

The preparation process of *in situ* formed ABP and ABF injectable hydrogels do not involve toxic monomers, reagents, or side products, ensuring their excellent cell compatibility. As shown in **Figure 3.6a**, the growth of HaCaT cells on the surface of the hydrogels was evaluated by live-dead cell staining on day 1 and 3. For the TC-plate group, cells exhibited good proliferation trends on the TC culture plate surface on both day 1 and day 3, with polygonal or spindle-shaped normal cell morphology. However, for ABP-37°C and ABF-37°C, due to the presence of polyethylene glycol structures resistant to bacterial adhesion, cell attachment on the hydrogel surface was slightly lower than that of the TC-plate

group, which may affect cell proliferation activity. Additionally, ABF-37°C, with a higher G', demonstrated advantages in cell attachment and proliferation. Unlike cells in the TC-plate group, cells adhered to the surfaces of ABF-37°C and ABP-37°C hydrogels showed clustered growth morphology, more similar to the cell proliferation pattern in the ECM. This may be related to the class 3D environment presented by the hydrogel. As cells proliferate on the hydrogel surface, they migrate into the interior of the hydrogel and grow in clusters. The cell viability was assessed using the alamarBlue assay. As shown in **Figure 3.6b**, cells on the surfaces of ABP-37°C and ABF-37°C hydrogels exhibited excellent cell viability. Although slightly lower than the TC-plate group, on the 1st day, cell viability of ABP-37°C and ABF-37°C hydrogel groups were 88% and 91%, respectively. The clustered growth pattern of HaCaT cells on the hydrogel surfaces improved their cell viability on the 3rd day, reaching 94% (ABP-37°C) and 98% (ABF-37°C), respectively. These results indicate that this self-entangling toughening strategy can be achieved with cell compatibility. This biocompatible toughening strategy for injectable hydrogels is a significant advantage for their clinical application.

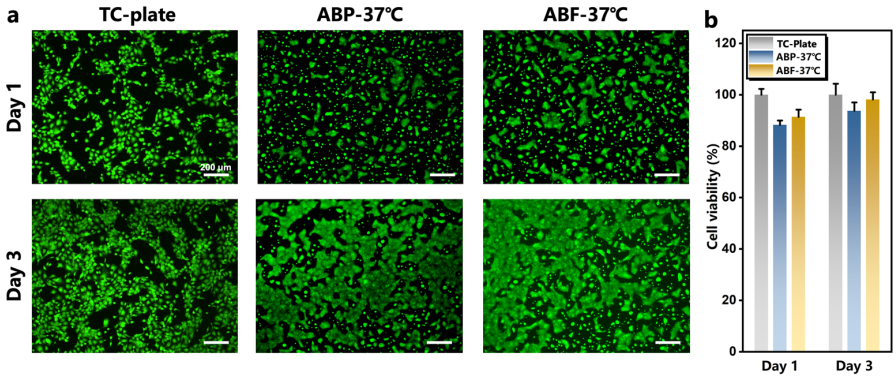


Figure 3.6 Cytocompatibility assessment of ABF hydrogel system: (a) Live/dead staining images, showing overlay images where green represents live cells and red represents dead cells and (b) alamarBlue cell viability assessment of HaCaT cells cultured on the surface of TC-plate, ABP-37℃ and self-entangled ABF-37℃ hydrogels at day 1 and 3. Scale bar: 200 μm. The representative images presented are randomly selected from replicate samples (n=3), and data are presented as mean ± standard deviation (n=3).

3.4 Conclusion

In summary, we have developed a novel toughening strategy for constructing injectable hydrogels with strong mechanical properties. Self-entangled F127-37°C tough hydrogels can be one-step achieved at a low polymer concentration by covalently crosslinking self-entangled F127-DA chains above the LCST temperature. Compared to netlike topology hydrogel, self-entangled F127-37°C hydrogel exhibits a 4.1-fold increase in compressive strength and a 4.3-fold increase in toughness.

Furthermore, this self-entangling strategy can also be combined with SN injectable hydrogel systems to enhance their mechanical performance. The compressive strength and toughness of the self-entangled ABF-37°C hydrogels are increased by 1.7 times and 2 times, respectively, compared to the lowly entangled ABF-20°C hydrogels, which feature a network-like topology. Additionally, self-entangled ABF-37°C hydrogels demonstrate resistance to swelling, fatigue, and good cell compatibility. We anticipate that this universal toughening strategy can guide the construction of a new generation of soft materials with tough mechanical properties, including *in situ* formed hydrogels.

3.5 References

(1) Ahmed, E. M. Hydrogel: Preparation, Characterization, and Applications: A Review. *Journal of Advanced Research*. 2015, 6 (2), 105–121.

(2) Liu, X.; Liu, J.; Lin, S.; Zhao, X. Hydrogel Machines. *Materials Today*. 2020, 36, 102–124.

(3) Yu, L.; Ding, J. Injectable Hydrogels as Unique Biomedical Materials. *Chemical Society Reviews*. 2008, 37 (8), 1473–1481.

(4) Hussey, G. S.; Dziki, J. L.; Badylak, S. F. Extracellular Matrix-Based Materials for Regenerative Medicine. *Nature*

Reviews Materials. 2018, 3 (7), 159–173.

(5) Zhang, Y.; Xu, Y.; Gao, J. The Engineering and Application of Extracellular Matrix Hydrogels: A Review. *Biomaterials Science*. 2023, 11 (11), 3784–3799.

(6) Chen, L.; Jiang, C.; Xu, Q.; Jin, J.; A, S.; Wang, X.; Li, X.; Hu, Y.; Sun, H.; Lu, X.; Duan, S.; Gao, Z.; Wang, W.; Wang, Y. Biphasic Release of Betamethasone from an Injectable HA Hydrogel Implant for Alleviating Lumbar Disc Herniation Induced Sciatica. *Acta Biomaterialia*. 2024, 176, 173–189.

(7) Zhu, J.; Marchant, R. E. Design Properties of Hydrogel Tissue-Engineering Scaffolds. *Expert Review of Medical Devices*. 2011, 8 (5), 607–626.

(8) Park, N.; Kim, J. Hydrogel-Based Artificial Muscles: Overview and Recent Progress. *Advanced Intelligent Systems*. 2020, 2 (4), 1900135.

(9) Verhulsel, M.; Vignes, M.; Descroix, S.; Malaquin, L.; Vignjevic, D. M.; Viovy, J.-L. A Review of Microfabrication and Hydrogel Engineering for Micro-Organs on Chips. *Biomaterials*. 2014, 35 (6), 1816–1832.

(10) Mathew, A. P.; Uthaman, S.; Cho, K.-H.; Cho, C.-S.; Park, I.-K. Injectable Hydrogels for Delivering Biotherapeutic Molecules. *International Journal of Biological Macromolecules*. 2018, 110, 17–29.

(11) Xu, Q.; A, S.; Gao, Y.; Guo, L.; Creagh-Flynn, J.; Zhou, D.; Greiser, U.; Dong, Y.; Wang, F.; Tai, H.; Liu, W.; Wang, W.;

Wang, W. A Hybrid Injectable Hydrogel from Hyperbranched PEG Macromer as a Stem Cell Delivery and Retention Platform for Diabetic Wound Healing. *Acta Biomaterialia*. 2018, 75, 63–74.

(12) Overstreet, D. J.; Dutta, D.; Stabenfeldt, S. E.; Vernon, B. L. Injectable Hydrogels. *Journal of Polymer Science Part B: Polymer Physics*. 2012, 50 (13), 881–903.

(13) Yang, J.-A.; Yeom, J.; Hwang, B. W.; Hoffman, A. S.; Hahn, S. K. *In situ*-Forming Injectable Hydrogels for Regenerative Medicine. *Progress in Polymer Science*. 2014, 39 (12), 1973–1986.

(14) Dong, Y.; A, S.; Rodrigues, M.; Li, X.; Kwon, S. H.; Kosaric, N.; Khong, S.; Gao, Y.; Wang, W.; Gurtner, G. C. Injectable and Tunable Gelatin Hydrogels Enhance Stem Cell Retention and Improve Cutaneous Wound Healing. *Advanced Functional Materials*. 2017, 27 (24), 1606619.

(15) Dimatteo, R.; Darling, N. J.; Segura, T. *In situ* Forming Injectable Hydrogels for Drug Delivery and Wound Repair. *Advanced Drug Delivery Reviews*. 2018, 127, 167–184.

(16) Rizzo, F.; Kehr, N. S. Recent Advances in Injectable Hydrogels for Controlled and Local Drug Delivery. *Advanced Healthcare Materials*. 2021, 10 (1), 2001341.

(17) Ko, D. Y.; Shinde, U. P.; Yeon, B.; Jeong, B. Recent Progress of *in situ* Formed Gels for Biomedical Applications. *Progress in Polymer Science*. 2013, 38 (3), 672–701.

(18) Fuchs, S.; Shariati, K.; Ma, M. Specialty Tough Hydrogels and Their Biomedical Applications. *Advanced Healthcare Materials*. 2020, 9 (2), 1901396.

(19) Correa, S.; Grosskopf, A. K.; Lopez Hernandez, H.; Chan, D.; Yu, A. C.; Stapleton, L. M.; Appel, E. A. Translational Applications of Hydrogels. *Chemical Reviews*. 2021, 121 (18), 11385–11457.

(20) Young, S. A.; Riahinezhad, H.; Amsden, B. G. *In situ*-Forming, Mechanically Resilient Hydrogels for Cell Delivery. *Journal of Materials Chemistry B*. 2019, 7 (38), 5742–5761.

(21) Nielsen, L. E. Cross-Linking–Effect on Physical Properties of Polymers. *Journal of Macromolecular Science, Part C*. 1969, 3 (1), 69–103.

(22) Jang, J.; Seol, Y.-J.; Kim, H. J.; Kundu, J.; Kim, S. W.; Cho, D.-W. Effects of Alginate Hydrogel Cross-Linking Density on Mechanical and Biological Behaviors for Tissue Engineering. *Journal of the Mechanical Behavior of Biomedical Materials*. 2014, 37, 69–77.

(23) Nakajima, T. Generalization of the Sacrificial Bond Principle for Gel and Elastomer Toughening. *Polymer Journal*. 2017, 49 (6), 477–485.

(24) Fumio, U.; Hiroshi, Y.; Kumiko, N.; Sachihiko, N.; Kenji, S.; Yasunori, M. Swelling and Mechanical Properties of Poly(Vinyl Alcohol) Hydrogels. *International Journal of Pharmaceutics*. 1990, 58 (2), 135–142.

(25) Gong, J. Why Are Double Network Hydrogels so Tough? *Soft Matter*. 2010, 6 (12), 2583–2590.

(26) Gong, J.; Katsuyama, Y.; Kurokawa, T.; Osada, Y. Double-Network Hydrogels with Extremely High Mechanical Strength. *Advanced Materials*. 2003, 15 (14), 1155–1158.

(27) Xin, H. Double-Network Tough Hydrogels: A Brief Review on Achievements and Challenges. *Gels*. 2022, 8 (4), 247.

(28) Bashir, S.; Hina, M.; Iqbal, J.; Rajpar, A. H.; Mujtaba, M. A.; Alghamdi, N. A.; Wageh, S.; Ramesh, K.; Ramesh, S. Fundamental Concepts of Hydrogels: Synthesis, Properties, and Their Applications. *Polymers*. 2020, 12 (11), 2702.

(29) Sun, J.-Y.; Zhao, X.; Illeperuma, W. R. K.; Chaudhuri, O.; Oh, K. H.; Mooney, D. J.; Vlassak, J. J.; Suo, Z. Highly Stretchable and Tough Hydrogels. *Nature*. 2012, 489 (7414), 133–136.

(30) Puza, F.; Zheng, Y.; Han, L.; Xue, L.; Cui, J. Physical Entanglement Hydrogels: Ultrahigh Water Content but Good Toughness and Stretchability. *Polymer Chemistry*. 2020, 11 (13), 2339–2345.

(31) Kim, J.; Zhang, G.; Shi, M.; Suo, Z. Fracture, Fatigue, and Friction of Polymers in Which Entanglements Greatly Outnumber Cross-Links. *Science*. 2021, 374 (6564), 212–216.

(32) Nian, G.; Kim, J.; Bao, X.; Suo, Z. Making Highly Elastic and Tough Hydrogels from Doughs. *Advanced Materials*. 2022, 34 (50), 2206577.

(33) Zhao, X. Multi-Scale Multi-Mechanism Design of Tough Hydrogels: Building Dissipation into Stretchy Networks. *Soft Matter*. 2014, 10 (5), 672–687.

(34) Shi, M.; Kim, J.; Nian, G.; Suo, Z. Highly Entangled Hydrogels with Degradable Crosslinks. *Extreme Mechanics Letters*. 2023, 59, 101953.

(35) Liu, P.; Zhang, Y.; Guan, Y.; Zhang, Y. Peptide-Crosslinked, Highly Entangled Hydrogels with Excellent Mechanical Properties but Ultra-Low Solid Content. *Advanced Materials*. 2023, 35 (13), 2210021.

(36) Zhao, X.; Chen, X.; Yuk, H.; Lin, S.; Liu, X.; Parada, G. Soft Materials by Design: Unconventional Polymer Networks Give Extreme Properties. *Chemical Reviews*. 2021, 121 (8), 4309–4372.

(37) Zhu, R.; Zhu, D.; Zheng, Z.; Wang, X. Tough Double Network Hydrogels with Rapid Self-Reinforcement and Low Hysteresis Based on Highly Entangled Networks. *Nature Communications*. 2024, 15 (1), 1344.

(38) Li, X.; Gong, J. Design Principles for Strong and Tough Hydrogels. *Nature Reviews Materials*. 2024, 1–19.

(39) Wang, P.; Deng, G.; Zhou, L.; Li, Z.; Chen, Y. Ultrastretchable, Self-Healable Hydrogels Based on Dynamic Covalent Bonding and Triblock Copolymer Micellization. *ACS Macro Letters*. 2017, 6 (8), 881–886.

Chapter Four

Double Network Injectable Hydrogel with Enhanced Toughness by Acid-Triggered Second Homogeneous Network

Part of this chapter has been organised in the manuscript:

Song, R., Demircan, A., Milne, C., Guan, T., Zhao, C., Wang, X., Johnson, M., Li, Y., Lyu, J., Zhang, N., A, S.*, Wang, W.* 'Double Network Injectable Hydrogel with Enhanced Toughness by Acid-Triggered Second Homogeneous Network', submitted.

4.1 Introduction

Hydrogels consist of hydrophilic polymers that are chemically or physically crosslinked and saturated with water.[1,2] Their structural characteristics closely resemble those of the extracellular matrix (ECM), tissues, and organs.[3,4] Hence, hydrogels find extensive applications in biomedical fields, including drug delivery, tissue engineering scaffolds, and wound dressings.[5–10] Among various hydrogel systems, injectable hydrogel systems are highly valued in the biomedical field for their easy application, efficient encapsulation, minimal invasiveness, and better patient compliance.[11,12] However, unlike natural hydrogels such as cartilage, tendons, or myocardium, which possess multi-scale assembly structures, injectable hydrogels face challenges in achieving similar mechanical properties due to inherent structural limitations.[13,14] This constraint significantly reduces their practicality in load-bearing applications.

In recent years, a series of mechanically strong hydrogels have been developed.[15,16] These systems include double network (DN) hydrogels, slide ring hydrogels, high functionality crosslinker hydrogels, and nanocomposite hydrogels. [17–19] Among these, DN hydrogels achieve exceptional toughness by combining the

structure advantages of energy dissipation and high elasticity through two independently interpenetrating rigid and flexible networks. [20–22] However, commonly preparation methods for DN hydrogels are rather complex.[23–25] They involve encapsulating the monomers required for building the second network within an existing first network. Subsequently, the second network is established through processes such as UV or heat-induced polymerisation.[26] During the preparing process, biologically incompatible monomers, initiators, or crosslinkers inevitably remain within the hydrogels, posing hazards for subsequent biomedical applications.[27,28] In addition, the complicated preparation processes of DN hydrogel systems are challenging to administer via injection method, thereby greatly limiting their clinical application.[29]

Constructing DN injectable hydrogels exclusively from functionalised biopolymers can combine the advantages of good mechanical properties, biocompatibility, injectability.[30] However, achieving a homogeneous structure in the second network using biopolymers has long been recognised as a challenge.[31] Firstly, unlike synthetic polymers, biopolymer networks cannot be formed through chemical methods of monomer polymerisation.[32]

Secondly, natural polymer networks constructed through weak physical crosslinking methods, such as hydrogen bonding or self-assembly, do not meet the necessary mechanical requirements.[4] Many hydrogel systems utilise the ability of L-guluronate (G-unit) in sodium alginate (SA) to be crosslinked by calcium ions (Ca^{2+}) in order to establish the second hydrogel network.[33,34] Initially, SA chains are included in the precursor solution. After completing the crosslinking of the first network, single network (SN) hydrogels are immersed in a calcium chloride ($CaCl_2$) solution to create the second SA network.[31,35] However, the uncontrollable and rapid gelation induced by $CaCl_2$ results in an inhomogeneous second SA network.[36] This defective SA network limits the enhancement of the toughness of DN hydrogels.[37]

Here, we have developed a homogeneous DN hydrogel system using pure biopolymers that can be formed and toughened *in situ*. As shown in **Figure 4.1**, we utilised a combination of acrylated hyaluronic acid (HA-A) and thiolated hyaluronic acid (HA-SH), which were crosslinked *in situ* through Thiol-ene Michael addition reactions, as the first network. This injectable hydrogel can conform to irregular defects, taking on any desired shape. The second SA network is homogeneously crosslinked by Ca^{2+}, which

are generated through the acid-triggered dissolution of encapsulated hydroxyapatite (HAp) nanoparticles. When compared to the counterpart inhomogeneous DN hydrogel, this homogeneous DN hydrogel exhibits an approximately 3-fold increase in compressive strength and a 2.5-fold improvement in compressive toughness. Additionally, this DN hydrogel demonstrates resistance to fatigue, swelling, degradation, and excellent biocompatibility. We further demonstrate an acid-triggered customisable patterning strategy for DN hydrogels. This strategy enables the creation of visually distinct high and low toughness zones within the same hydrogel, providing an innovative approach for manufacturing high-performance hydrogel scaffolds and mechanically customisable hydrogel devices.

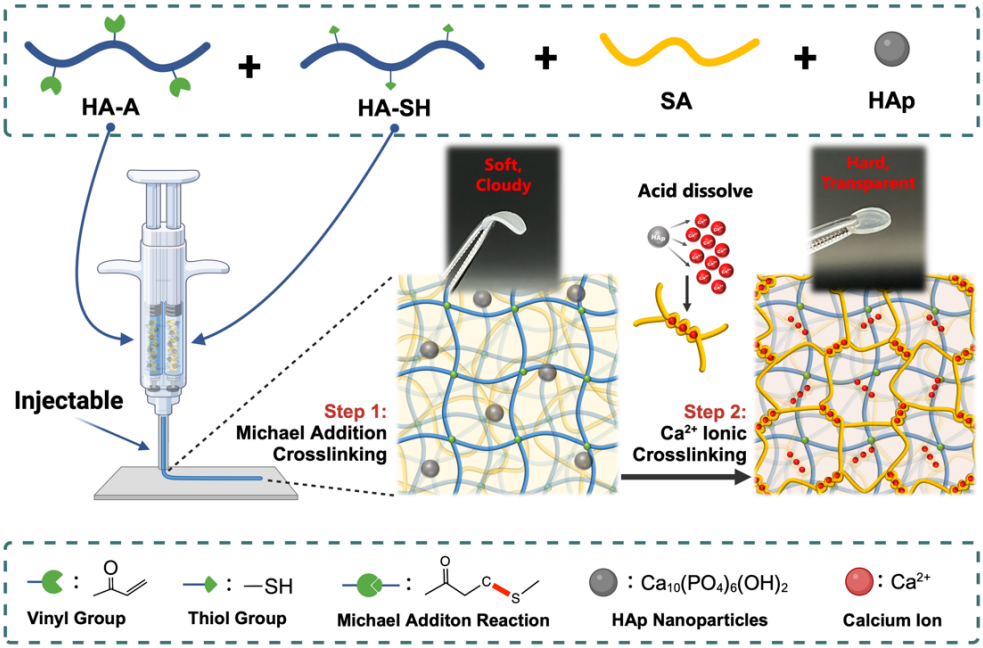


Figure 4.1 Illustration of the preparation and features of DN-ABSH injectable hydrogels. [Created with BioRender]

The aim of this chapter is to develop a double-network injectable hydrogel that combines high mechanical toughness with excellent biocompatibility by using an acid-triggered second homogeneous network. The objectives include investigating the utilisation of Ca^{2+} released by acid-triggered hydroxyapatite (HAp) nanoparticles to uniformly crosslink a sodium alginate (SA) network *in situ*, combining this network with the first injectable HA network to create an interpenetrating double-network structure, evaluating the mechanical enhancements and the preservation of

good cell compatibility, and demonstrating the potential practical applications of hydrogels.

4.2 Materials and Methods

4.2.1 Materials

HA-A (110 kDa, purity > 98%, 4% SD), HA-SH (110kDa, purity > 98%, 4% SD) were purchased from Blafar Ltd. SA (12 - 40 kDa, M/G ≈ 1.56), HAp (nanoparticles, < 200 nm, 677418), $CaCl_2$ (1.02378), sodium chloride (NaCl, S9888), hydrochloric acid (HCl, 258148), phosphoric acid (H_3PO_4, W290017), Pepsin (P6887), hyaluronidase (H3506), sodium hydroxide (NaOH, S5881), Dulbecco's modified eagle medium (DMEM-high glucose, D6429), Hank's balanced salt solution (HBSS, H4641) were purchased from Sigma-Aldrich. Penicillin/streptomycin (PS, 15140122), Dulbecco's phosphate-buffered saline (DPBS, 14190094), alamarBlue Cell Viability Reagent (DAL1100) and Live/Dead Cell Viability Assay Kit (L3224) were purchased from Thermo Fisher Scientific. Human epidermal keratinocyte (HaCaT, CLS300493) cell line was obtained from CLS Cell Lines Service GmbH. Trypsin-EDTA (0.25%. 25200056) and Fetal Bovine Serum (FBS, 10270106) was purchased from Gibco. Resin Aqua

Clear (SC-801) was purchased from Phrozen. All the chemicals were used without purification and all aqueous solutions were prepared with deionised water.

4.2.2 Preparation and Characterization of SA/HAp Hydrogels

SA and HAp solutions were each prepared independently before being combined. To start, SA was fully dissolved in 0.1M DPBS at a predetermined concentration. Likewise, HAp was introduced into DPBS at the designated concentration and exposed to 20 mins of ultrasonication to ensure thorough dispersion. Following this, the two liquids were combined in a 1:1 ratio and vortexed for 10 mins.

The particle size and zeta potential of the SA/HAp hydrogel system were measured using a Zetasizer Pro (Malvern Panalytical, Malvern, UK). The final concentration of SA and HAp in the test solutions was 0.01% (mass/volume ratio). The pH of the SA/HAp solution system was adjusted using 0.1M HCl and NaOH and monitored with a pH meter (Mettler Toledo). The transmittance of both hydrogels and solutions was monitored using a microplate reader (SpectraMax M3). Specifically, 100 μL of SA/HAp solution

at various pH levels were placed in a 96-well plate, with three replicates for each sample. The absorbance was measured between wavelengths of 400-800nm, and transmittance was calculated using the formula: $Transmittance\ (\%) = 10^{2\text{-}Absorbance\ (400\text{-}800nm)}$. The rheological properties of the SA/HAp hydrogel system were assessed using a rheometer (HR-2, TA) at a frequency of 1Hz, a strain of 1%, and a temperature of 37°C. The space between 8mm diameter plates was fully filled with the SA/HAp mixture at the designated concentration, with a gap distance of 1000 μm. Crosslinking triggered by acid was initiated by adding 1mL of 0.1M HCl to the hydrogel at the 60th second of the time sweep. Each test was replicated three times.

4.2.3 Preparation and Characterisation of DN-ABSH Injectable Hydrogels

The preparation of DN-ABSH hydrogel involves two steps. Firstly, a homogeneous solution containing 1% SA and 0.625% HAp nanoparticles was prepared. This solution was then used to fully dissolve HA-A and HA-SH, each at a 5% concentration. Subsequently, the completely dissolved solutions of HA-A and HA-SH were mixed in a 1:1 ratio and pipetted into corresponding moulds. They were allowed to culture at 37°C for 24 hours,

resulting in the formation of SN-ABSH hydrogel. In the second step, the hydrogels were removed from the moulds and immersed in acidic phosphate buffer solutions with varying pH levels for 30 minutes to produce DN-ABSH hydrogel.

The gelling time of the SN-ABSH hydrogel was assessed through the time sweep test. Similar to the previous rheological test, the SN-ABSH test was conducted at 37°C with a 1Hz frequency and a 1% strain. A humidity chamber was used during the test to prevent moisture loss from the hydrogel. The strain sweep tests for both SN and DN hydrogels encompassed a range from 0.1% to 50%, with the other test conditions mirroring those of the time sweep.

The transmittance test for the DN-ABSH hydrogel followed a method similar to previous tests. Specifically, 100 μL of SN-ABSH hydrogel was placed in a 96-well plate and immersed in phosphate buffer solutions with varying pH levels for 30 mins prior to measurement.

Compression and fatigue resistance tests entailed positioning the hydrogel samples between the plates of a rheometer and subjecting them to loading and unloading cycles at a speed of 40 μm/s at 37°C.

Each test was replicated three times.

The structure of the freeze-dried hydrogels was examined using scanning electron microscopy (SEM; Hitachi Topdesk 4000). The hydrogel samples were rapidly frozen in liquid nitrogen and subsequently freeze-dried. The freeze-dried samples were fixed on copper plates and coated with a thin layer of gold for observation.

In the swelling test, the immersion liquid utilised was 1×DPBS. For the enzyme degradation test, the immersion liquid comprised 100 U/mL hyaluronidase dissolved in 1×DPBS. Simulated gastric fluid (SGF) was prepared by dissolving 0.2g NaCl, 0.81mL HCl, and 1g pepsin in 100mL of distilled water, and the pH was adjusted to 1.2 using HCl or NaOH. In the swelling, enzyme degradation, and gastric acid resistance tests, 200 mg of hydrogels were immersed in sealed vials containing 20 mL of the respective solution, with three sets of replicates. These vials were placed in a 37°C incubator and gently shaking at 100 rpm. At specific time points, hydrogels were extracted from the solution, excess liquid was removed using filter paper, and the samples were weighed. The following formula was used to calculate the mass of hydrogels after tests: $Hydrogel\ mass\ (\%) = (Wt/Wi) \times 100\%$. Where *Wt*

represents the weight of hydrogels at a given time point, and *Wi* is the weight of hydrogels before tests.

4.2.4 Customisable Patterning of DN-ABSH Injectable Hydrogel

The surface of SN-ABSH hydrogel was contacted with an acidic mould, resulting in the formation of a DN-ABSH region characterised by high transmittance and excellent toughness. Petal-shaped mould was created using a self-constructed stereolithography 3D printing process. Following a 5-minute immersion in concentrated phosphoric acid solution, excess acid was removed using filter paper. The acid-treated petal-shaped mould was placed in contact with SN-ABSH hydrogel for 3 seconds, then immediately submerged in 500mL of distilled water and gently shaken to ensure the complete removal of residual phosphoric acid. Patterned DN-ABSH hydrogels were captured using the iBright CL750 Imaging System and analysed using Image J 1.53k.

4.2.5 Cytocompatibility Assessment of DN-ABSH Injectable Hydrogel

HaCaT cells were employed to assess the cell compatibility of

hydrogels. The HaCaT cell line was cultured in DMEM supplemented with 10% FBS and 1% PS at 37°C in a humidified atmosphere containing 5% CO_2. Cells were passaged at a ratio of 1:3 every 3-4 days. During passage, cells were detached using 0.25% trypsin-EDTA, counted with a hemocytometer, and reseeded in new culture flasks at the specified dilution ratio. For the cell compatibility test, 300μL of hydrogels were initially placed at the bottom of 24-well plates and incubated at 25℃ for 24 hours crosslink. For SN-ABSH hydrogel, it underwent a 10 mins immersion in 1 mL of 0.1 M HCl to convert it fully into DN-ABSH hydrogel. Following this, the pH of DN-ABSH hydrogel was adjusted to neutral using DPBS. HaCaT cells were then seeded on the hydrogel surface or TC-plate at a concentration of 20,000 cells/well. The TC-plate surface served as the control group. Incubation was carried out at 37℃ with 5% CO_2. On the 1st and 3rd days, alamarBlue assays were performed to assess cell viability using fluorescence as the readout method. Specifically, fluorescence was measured using a microplate reader with an excitation wavelength of 560 nm and an emission wavelength of 590 nm. Cell viability was calculated using the formula: $Cell\ viability\ (\%) = (Vt/Vb) \times 100\%$. Where Vt represents the

fluorescence intensity at a given time point, and *Vb* is the fluorescence intensity of the TC-plate group. A live/dead cell staining kit was utilised to confirm cell viability and adhesion status, calcein AM staining for live cells (green colour) and ethidium homodimer-1 for dead cells (red colour). Cells were treated with staining reagents for 25 mins at room temperature on the day 1 and day 3. Subsequently, the hydrogel and TC-plate groups were gently washed three times with DPBS. Images were captured using a fluorescence microscope (IX81, Olympus Life Science) equipped with a camera (QImaging QiClick Mono) and software (cellSens Dimension 1.12). The images were taken using a 10× objective lens, with a 50 ms exposure time, and a 1× gain.

4.2.6 Statistical Analysis

All cytocompatibility values are expressed as mean ± standard deviation (SD). Statistical differences among the three groups were determined using one-way analysis of variance (ANOVA) followed by Turkey's Honest Significant Difference (HSD) post-hoc test for multiple comparisons in SPSS v29. A P value of less than 0.05 was considered statistically significant.

4.3 Results and Discussion

4.3.1 Characterisation of SA/HAp Hydrogels

As the second network triggered by low pH, before its formation, SA and HAp exist separately in a semi-interpenetrating and dispersed state within the SN hydrogel. After formation, they transform into an independent and interpenetrating SA network along with the first HA network. Here, the SA/HAp hydrogel system was individually evaluated and discussed. Generally, nanoparticles in solutions without stabilisers tend to undergo self-aggregation, making it challenging to disperse them uniformly in the hydrogel system.[38,39] However, as an anionic and water-soluble polysaccharide, SA can prevent the self-aggregation of negatively charged HAp by intercalating between the nanoparticles and exerting charge repulsion, thereby maintaining their stable monodispersity.[40] As shown in **Figure 4.2a**, the particle distribution peak gradually shifts to the right and widens, indicating that pure HAp progressively self-aggregate in the suspension as time progresses. It starts with highly monodisperse particles of an average size of 100 nm aggregating to approximately 600 nm after 5 mins and to approximately 1100 nm after 10 mins. However, the SA solution effectively stabilised the dispersion. Over a wide period of 75 mins, the particle size in the

SA/HAp solution remained below 200 nm (**Figure 4.2b**).

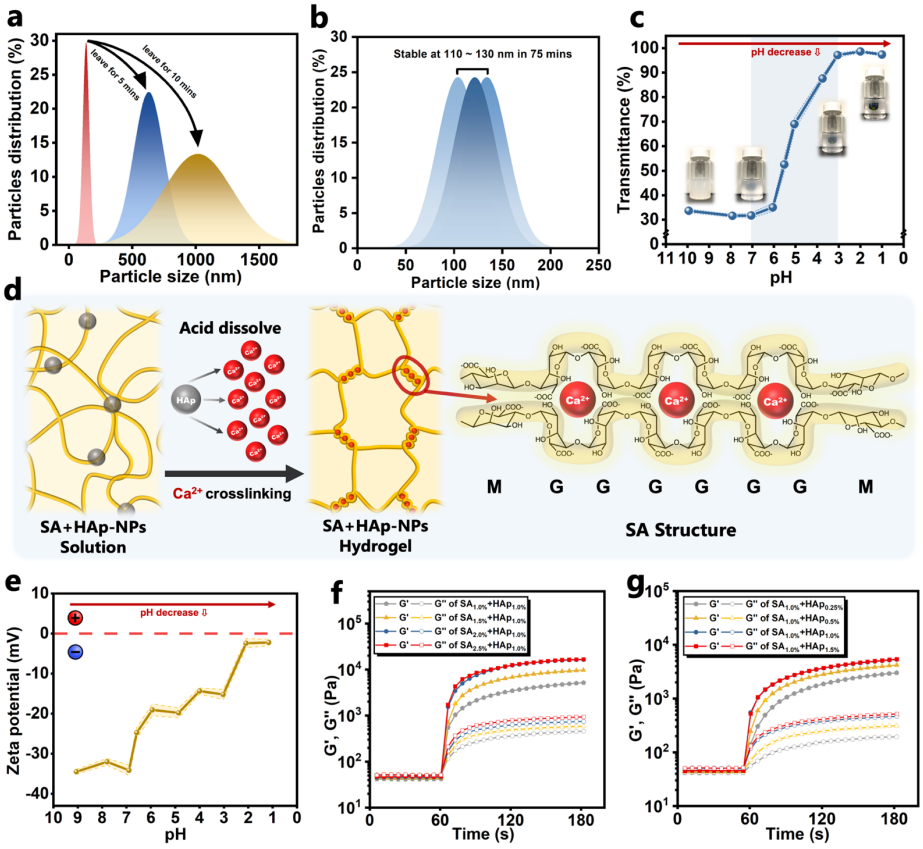


Figure 4.2 Characterisation of the acid-triggered SA/HAp hydrogel system: (a) particle distribution analysis of the HAp solution; (b) particle distribution analysis of the SA/HAp solution; (c) transmittance analysis of the SA/HAp hydrogel system under varying pH conditions; (d) illustration of the egg-box model of SA chains crosslinked by HAp-released Ca^{2+}.; (e) zeta potential of the SA/HAp hydrogel system under varying pH conditions; (f) G' and G" of the SA/HAp hydrogel system with increasingly SA content; (g) G' and G" of the SA/HAp hydrogel system with increasingly HAp content. The representative images presented are randomly selected from replicate samples (n=3), and data are presented as mean ± standard deviation (n=3).

The influence of particles on the transmittance of a suspension system is well-established. Previous research has shown that HAp remains highly stable in high-pH environments but gradually dissolve, releasing Ca^{2+}, in low-pH environments.[41] As the dissolution process occurs, the overall transmittance of the solution steadily increases. To validate the crosslinking of SA by the released Ca^{2+}, the transmittance and particle surface charge of the solution under varying pH conditions were characterised. As shown in **Figure 4.2c**, the transmittance of the SA/HAp solution increased gradually (from 33.68% to 98.6%) as the pH decreased from 7 to 3, indicating a significant reduction in insoluble particles. Furthermore, as the pH decreased, the zeta potential of particles in the SA/HAp solution shifted gradually from -34.49mV to nearly neutral, signifying the dissolution of HAp (**Figure 4.2e**). Additionally, numerous gel particles appeared within the SA/HAp system as the pH decreased. Even after adjusting the pH of the SA/HAp system back to alkaline or altering the system's temperature, these gel particles remained. These findings confirm that the Ca^{2+} released from the dissolution of HAp crosslinks the SA chains, resulting in a hydrogel that is both pH and thermally irreversible.

Additional calculations were conducted to confirm the relationship between the Ca^{2+} ion content in HAp and the ratio of G-unit receptors in SA. This hypothesis was then validated through changes in the rheological properties of the crosslinked hydrogels. As shown in **Figure 4.2d**, according to the egg-box model of Ca^{2+} crosslinked SA, every four G-units form a dimer with one Ca^{2+} and further aggregate into a network. Calculations based on the content of G-units in the SA used in this work and the molecular structure of HAp show that 1.6 times the mass of SA can be crosslinked if all the Ca^{2+} in 1 unit mass of HAp is released. Therefore, two separate sets of experiments were designed to verify the changes in rheological properties before and after the excess of SA or HAp in the gel system. It is often assumed that the G' of a hydrogel is a direct response to its crosslinking density. As shown in **Figure 4.2f**, when the Ca^{2+}contained in HAp1.0% is more than that required for cross-linking in SA1.0% and SA1.5%, the increase of SA content has a significant effect on the G' of hydrogel which increased from 5.18 kPa to 9.69 kPa. However, in the case of the insufficient Ca^{2+} provided by HAp, the further increase of the SA content (SA2.0% and SA2.5%) was not effective in enhancing the energy G' of the SA/HAp hydrogel

(stabilised at around 16 kPa). In order to exclude the effect on the G' due to the enhancement of the biopolymer SA content, the rheological properties of SA/HAp hydrogels with different contents of HAp were examined, and the results showed consistency (**Figure 4.2g**). In the case where the G-unit binding of SA is not saturated, the elevated HAp content significantly increases the G' of SA/HAp hydrogels. However, when the G-unit binding capacity was saturated, further enhancement of HAp content could not further increase the G' of the hydrogel system. This approach to SA hydrogel construction by acid initiation with controlled crosslinking degree well solves the problem of inhomogeneous crosslinking caused by the $CaCl_2$ immersion method and potentially reduces the structural defects of the SA hydrogel.

4.3.2 Configuration of DN-ABSH Hydrogels

As depicted in **Figure 4.1**, the preparation of the DN hydrogel system based on HA-A/HA-SH/SA/HAp (ABSH) involves a two-step technique. In the first step, SA and HAp are completely dissolved or dispersed in a phosphate buffer solution (PBS). Subsequently, this solution is used for the separate dissolution of HA-A and HA-SH. The fully dissolved HA-A and HA-SH are then

placed in the two chambers of a dual-barrel syringe. The subsequent injection process is accompanied by mixing.

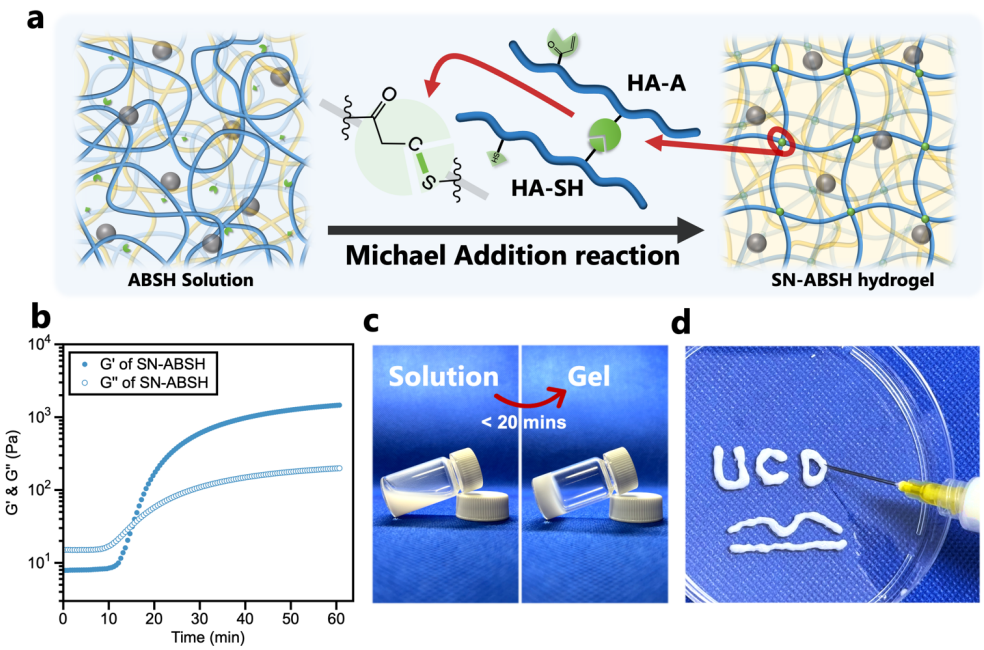


Figure 4.3 Characterisation of the SN-ABSH hydrogel: (a) schematic representation of the Michael Addition reaction in the SN-ABSH hydrogel system; (b) assessment of the gelling time of the SN-ABSH hydrogel system through a time sweep test; (c) general observation of HA/HAp immediately after mixing and 20 minutes later; (d) injectable properties of the HA/HAp hydrogel. The representative images presented are randomly selected from replicate samples (n=3).

After injection, the vinyl groups on HA-A crosslink with the thiol groups on HA-SH through a Michael Addition reaction, resulting in the *in situ* crosslinking of the SN-ABSH hydrogel (**Figure 4.3a**). As shown in **Figure 4.3b**, the gelation process of the SN-ABSH

injectable hydrogel was monitored through a time sweep test. At around 16 mins, G' surpasses G", indicating a transition from viscosity-dominated to elasticity-dominated rheological behaviour. As shown in **Figure 4.3c**, the crosslinking process of the SN-ABSH injectable hydrogel occurs rapidly within 40 minutes, ultimately forming a stable 3D structure. **Figure 4.3d** demonstrates that the SN-ABSH hydrogel can be injected through a needle and shaped into the desired shape.

In the second step, the SN-ABSH hydrogels were placed in an acidic PBS environment to initiate the formation of the second SA network. As shown in **Figure 4.4a**, the formation of the second network within the ABSH hydrogel was accompanied by changes in transmittance. This change resulted from an exchange of fluids between the interior of the hydrogel and the external acidic solution, leading to the gradual dissolution of HAp within SN-ABSH. The Ca^{2+} released during this dissolution was subsequently captured by the G units within the surrounding SA chains, thus constructing the second network. Similar to the behaviour observed in the SA/HAp hydrogel, immersing the SN-ABSH hydrogel in PBS solutions with varying pH levels resulted in a gradient of transmittance within the DN-ABSH hydrogel (**Figure**

4.4b).

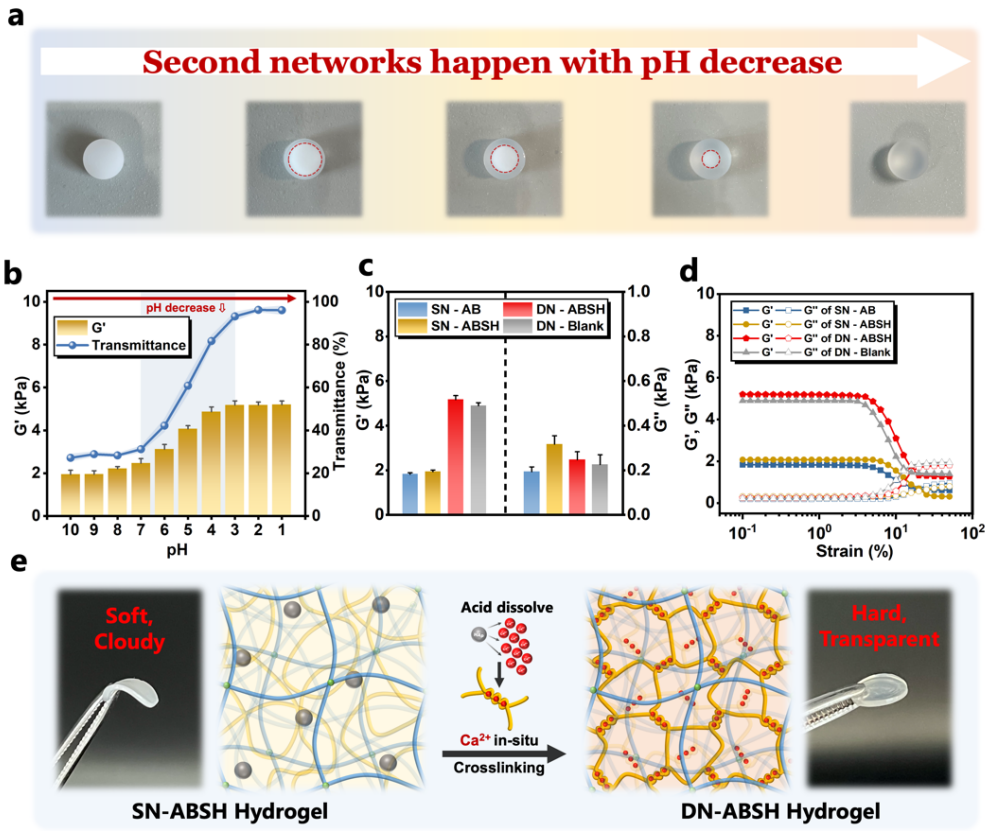


Figure 4.4 Characterisation of the DN-ABSH hydrogel: (a) general observation of DN-ABSH upon immersion in acidic PBS buffer; (b) the transmittance and G' of ABSH hydrogel systems with varying pH; (c) the G' and G" of ABSH and Blank hydrogel systems; (d) strain sweep test of ABSH and Blank hydrogel systems; (e) illustration of the acid-trigged formation of second SA network and macroscopic observation of SN-ABSH and DN-ABSH hydrogels. The representative images presented are randomly selected from replicate samples (n=3), and data are presented as mean ± standard deviation (n=3).

The analysis of its rheological properties indicates a positive

correlation between the G' of DN-ABSH hydrogel and its transmittance. These findings demonstrate the remarkable tuneable mechanical performance of DN-ABSH hydrogel. As shown in **Figure 4.4c**, the G' of the DN hydrogel exhibited significant differences compared to the SN hydrogel. Despite having the same polymer concentration, the G' of DN-ABSH hydrogel was approximately 2.8 times greater than SN-ABSH hydrogel. This disparity can be attributed to the notably higher crosslinking density of the second SA network, which contributed more to G' than the lower crosslinking density of the first HA network. Moreover, the G' of DN-Blank hydrogel, obtained through the traditional $CaCl_2$ immersion method, was also comparable to that of DN-ABSH hydrogel. Additionally, the uncrosslinked flexible SA chains within the soft material significantly influenced G". SN-ABSH hydrogel, owing to its semi-interpenetrating SA component, exhibited the highest G". As shown in **Figure 4.4d**, the results of strain sweep tests confirm that all hydrogels possess stable elastic structures. However, the higher crosslinking density of the second SA network slightly reduces the linear viscoelastic region of the DN-ABSH hydrogel. As shown in **Figure 4.4e**, in comparison to the SN-ABSH hydrogel, this DN-

ABSH hydrogel displays increased macroscopic hardness and transmittance.

4.3.3 Mechanical Properties of DN-ABSH Hydrogels

The *in situ* reinforced DN-ABSH hydrogel demonstrates notable advantages in terms of mechanical properties, particularly in compressive strength and toughness. This mechanical enhancement can be attributed to the more homogeneous DN structure within the DN-ABSH hydrogel. As shown in **Figure 4.5a**, when compared to the stress-strain curve of the SN-AB hydrogel, both DN-ABSH and DN-Blank hydrogels exhibit higher compressive strength. The compressive strength increased from 0.78 MPa for SN-AB to 7.77 MPa for DN-ABSH and 2.49 MPa for DN-Blank. Furthermore, when comparing the two sets of DN hydrogels, the DN-ABSH hydrogel demonstrates approximately three times the compressive strength of DN-Blank and a higher compression strain (86.42%). Calculations based on the integration of the area under the stress-strain curves reveal that the toughness of DN-ABSH is approximately 0.6 MJ/m^3, which is approximately 2.5 times that of DN-Blank and 14.2 times that of SN-AB (**Figure 4.5b**). This mechanical enhancement arises from DN hydrogels dissipating deformation energy through the

sacrificial fracture of the SA network while maintaining network integrity through the flexible crosslinked HA network. Furthermore, under high deformation, the fragmented SA network and flexible HA chains form a structure similar to a "slip-network" (**Figure 4.5d**).

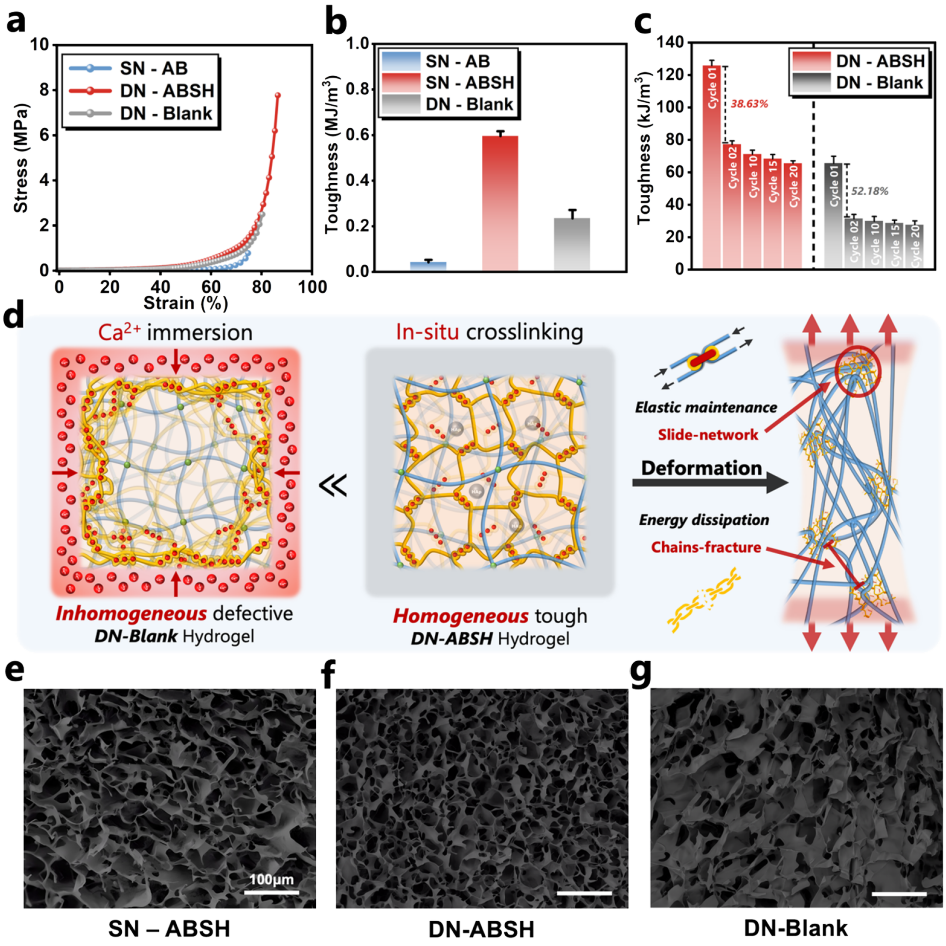


Figure 4.5 Mechanical properties of DN-ABSH hydrogel: (a) compression strain-Stress curve of SN and DN hydrogels; (b) compressive toughness of SN and DN hydrogels; (c) toughness of repetitive compression test of DN-ABSH and DN-Blank hydrogels; (g) illustration of the inhomogeneous DN-Blank and homogeneous DN-ABSH hydrogel during deformation process; SEM images of freeze-dried (d) SN-ABSH, (e) DN-ABSH, and (f) DN-Blank, scale bar: 100 μm. The representative images presented are randomly selected from replicate samples (n=3), and data are presented as mean ± standard deviation (n=3).

In the fracture process of SN hydrogels, only the breaking of chains in the plastic zone at the crack tip is required for the crack to continue extending until macroscopic fracture occurs. However, in the fracture process of DN-ABSH hydrogel, in addition to rupturing the plastic zone of the SA network, the detachment of the fragmented SA network from the entangled HA network is necessary. This detachment process is accompanied by dynamic adjustment in chains length and stress state between the "slip-network," ultimately achieving simultaneous stiffening and fracture of the maximum biopolymer chains at macroscopic failure. This dynamic adjustment process imparts DN-ABSH hydrogel with significantly improved compressive strength. Additionally, the movement of HA chains within the "slip-network" also involves mechanical dissipation. Nevertheless, the inherent inhomogeneity of the second SA network unavoidably results in structural defects, compromising the mechanical performance of DN hydrogels.

Repetitive compression tests were conducted on DN-ABSH and DN-Blank hydrogels at their respective 80% compression strain to evaluate their fatigue resistance. As shown in **Figure 4.5c**, when analysing the changes in the toughness of DN hydrogels after the

first and second compressions, DN-Blank hydrogel exhibited a 52.18% decrease in toughness, while DN-ABSH showed a more modest decrease of only 38.63%. Even after undergoing 20 compression cycles, the toughness of DN-ABSH hydrogel (65.5 kJ/m^3) still remained competitive with the first compressive toughness of DN-Blank hydrogel (65.6 kJ/m^3). Furthermore, SEM images of SN-ABSH, DN-ABSH, and DN-Blank hydrogels all revealed dense porous structures. Notably, SN-ABSH hydrogel exhibited relatively larger pore sizes due to the substantial presence of uncrosslinked SA components (**Figure 4.5e**). Conversely, DN-ABSH hydrogel displayed a more consistent and densely distributed pore size, owing to its homogeneous DN structure (**Figure 4.5f**). In contrast, DN-Blank hydrogel exhibited an inhomogeneous pore distribution and a considerable presence of collapsed lamellar structures (**Figure 4.5g**). This was primarily a consequence of the rapid crosslinking of G units within DN-Blank induced by the high concentration of $CaCl_2$, which then resulting in an inhomogeneous distribution of the second SA network (**Figure 4.5d**). Additionally, the inhomogeneous network fragments in DN-Blank hydrogel also impeded the formation of a consistently distributed "slip-network", thereby compromising the

mechanical performance of DN hydrogels.

4.3.4 Anti-swelling, Anti-degradation, and Gastric acid Resistance Properties of DN-ABSH Hydrogels

The DN-ABSH hydrogel benefits from a second rigid network comprising crosslinked SA, resulting in reduced swelling and improved resistance to degradation. This biostability advantage renders the DN-ABSH hydrogel suitable for long-term *in vivo* applications. As shown in **Figure 4.6a**, all three hydrogel groups reached swelling equilibrium in approximately 6 hours. SN-ABSH hydrogel, without the constraints of a rigid SA network, exhibited the fastest swelling rate, reaching an equilibrium swelling mass ratio of approximately 327%. In contrast, DN-ABSH and DN-Blank hydrogels had equilibrium swelling mass ratios of 129% and 135%, respectively. As a crucial component of ECM, HA can be degraded and absorbed by the human body. In an environment with a high concentration of hyaluronidase (100 U/mL), SN-ABSH hydrogel completely degraded after only 14 hours. However, DN-Blank and DN-ABSH, with their interpenetrating DN structures, experienced complete degradation on the 4th and 8th days, respectively (**Figure 4.6b**). It is speculated that the degraded HA fragments are immobilised by the homogeneous SA

network, thereby prolonging the degradation time. Additionally, the hydrogels were exposed to an extremely acidic simulated gastric fluid (SGF, pH≈1.2). SN-AB hydrogel was completely degraded after 21 days, while DN-Blank and DN-ABSH hydrogels only fully degraded on the 46th and 63rd days, respectively (**Figure 4.6c**).

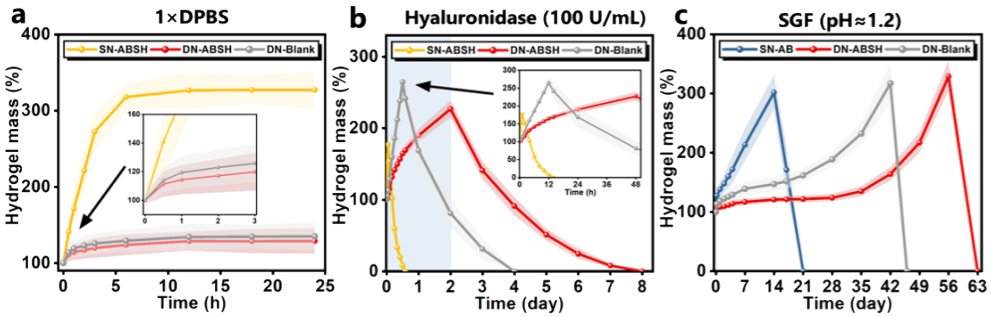


Figure 4.6 Anti-swelling, anti-degradation, and resistance to gastric acid properties of DN-ABSH hydrogel: (a) hydrogel mass in the DPBS swelling process in 24 hours; (b) hydrogel mass in the hyaluronidase with 100 U/mL enzyme activity in 8 days; (c) hydrogel mass in the SGF (pH≈1.2) in 63 days. The data are presented as mean ± standard deviation (n=3).

4.3.5 Customisable Patterning of DN-ABSH Hydrogels

The acid-triggered formation of the second network in DN-ABSH hydrogel can be used to create customised patterns on hydrogels. This technique allows for the efficient development of DN regions on the same hydrogel's surface with the desired high transmittance

and mechanical strength.

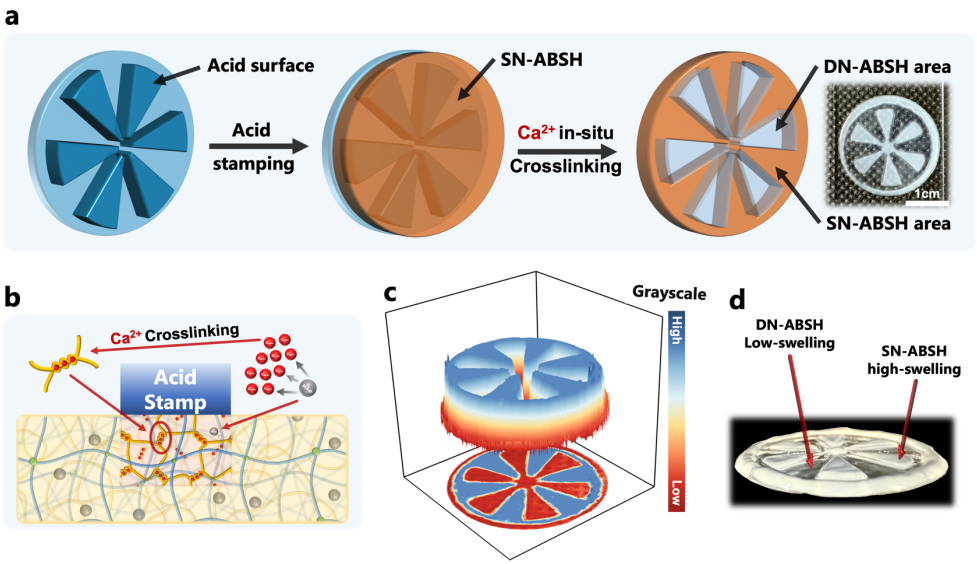


Figure 4.7 Acid-triggered customisable patterning strategy of DN-ABSH hydrogel: (a) Illustration of the patterning process on the DN-ABSH hydrogel system using acid stamping, scale bar: 1 cm; (b) schematic illustration of the moment the acid stamp touches the hydrogel, where the Ca^{2+} released in situ crosslinks the SA in the underlying SN-ABSH hydrogel; (c) a 3D colour mapping of the grayscale analysis of acid stamp treated ABSH hydrogel. The blue part indicates DN-ABSH regions with lower grayscale, while the red part indicates SN-ABSH regions with higher grayscale; (d) swelling behaviour of acid stamp treated ABSH hydrogel system. The DN-ABSH part shows minimal swelling, while the SN-ABSH part exhibits significant swelling.

As depicted in **Figure 4.7a**, a petal-shaped mould, treated with phosphoric acid in advance, was applied to the surface of the SN-ABSH hydrogel for 3 seconds. Subsequently, the hydrogel was

promptly immersed in a large volume of pure water to eliminate excess phosphoric acid. After stamping, the previously cloudy hydrogel became transparent in the contact area, signifying the successful dissolution of HAp. **Figure 4.7b** illustrates the molecular changes involved in the process of patterned DN-ABSH hydrogels. When the acid-treated mould comes into contact with the SN-ABSH hydrogel, phosphoric acid diffuses from the surface of the mould into the interior of the SN-ABSH hydrogel, initiating the dissolution of HAp. The released Ca^{2+} then *in situ* crosslinks the SA chains in that specific region, thus forming the DN structure in that area. By analysis the graysacle of acid stamp treated ABSH hydrogel system, a 3D colour mapping surface was created. As shown in **Figure 4.7c**, the blue region represents the DN structure with a lower grayscale, while the red region represents the SN structure with a higher grayscale. The swelling properties of DN-ABSH hydrogel also exhibited significant disparities compared to SN-ABSH hydrogel. After immersing the patterned DN-ABSH hydrogel in DPBS solution for 6 hours, noticeable volume variations were observed in different regions of the hydrogel. The DN region experienced minimal swelling, while the SN region exhibited significant swelling. This difference

aligns with the results of the swelling test, confirming the successful construction of patterned DN-ABSH hydrogels. This construction method holds potential applications in various fields, including programmable soft materials, hydrogel robotics, and smart materials, among others.

4.3.6 Cytocompatibility of DN-ABSH Hydrogels

Given that DN-ABSH hydrogel consists of pure biopolymers, its excellent cell compatibility is unsurprising. Additionally, the abundance of hydrophilic functional groups and the high G' of DN-ABSH hydrogel surfaces offer advantages for cell adhesion and proliferation. As shown in **Figure 4.8a**, the growth of HaCaT cells on the hydrogel surface was evaluated using live-dead cell staining on the first and third days. In the TC-plate group, cells displayed a robust proliferation trend, and exhibited classical epithelial morphology on TC-plates. In the case of SN-AB and DN-ABSH hydrogels, although cells exhibited different growth patterns compared to TC-plate surfaces, they demonstrated good cell proliferation activity in day 1 and 3. Particularly, cells on the surface of DN-ABSH hydrogel exhibited a significantly higher proliferation rate than the SN-AB group. This is likely due to the higher G' of DN-ABSH hydrogel, which enhances cell adhesion

and, consequently, increases the proliferation rate. The results of the alamarBlue test also confirmed the live-dead staining results. As illustrated in **Figure 4.8b**, on the first day, cells on the DN-ABSH hydrogel surface displayed cell viability exceeding that of the TC-plate group. On the third day, the cell viability of HaCaT cells on the SN-AB hydrogel surface was 98%, whereas on the DN-ABSH hydrogel surface, cell viability reached around 110% on the first day and 115% on the third day. Furthermore, cells on TC-plate surfaces exhibited the typical morphology of epithelial cells, characterised by tightly packed polygonal or spindle shapes (**Figure 4.8c**). However, cells on the surfaces of SN-AB and DN-ABSH hydrogels displayed a pattern of aggregated growth (**Figure 4.8d**). This may be attributed to the 3D-like environment on the hydrogel surface. As cells proliferate on the hydrogel surface, they migrate into the interior of the hydrogel, leading to clustered growth. This pattern simulates cell proliferation behaviour in the *in vivo* environment. These advantages make DN-ABSH hydrogel an ideal biomimetic tissue scaffold, capable of providing a microenvironment similar to the natural ECM. This is significant in various fields such as the study of cell behaviour, drug screening, tissue engineering, and regenerative medicine,

among others.

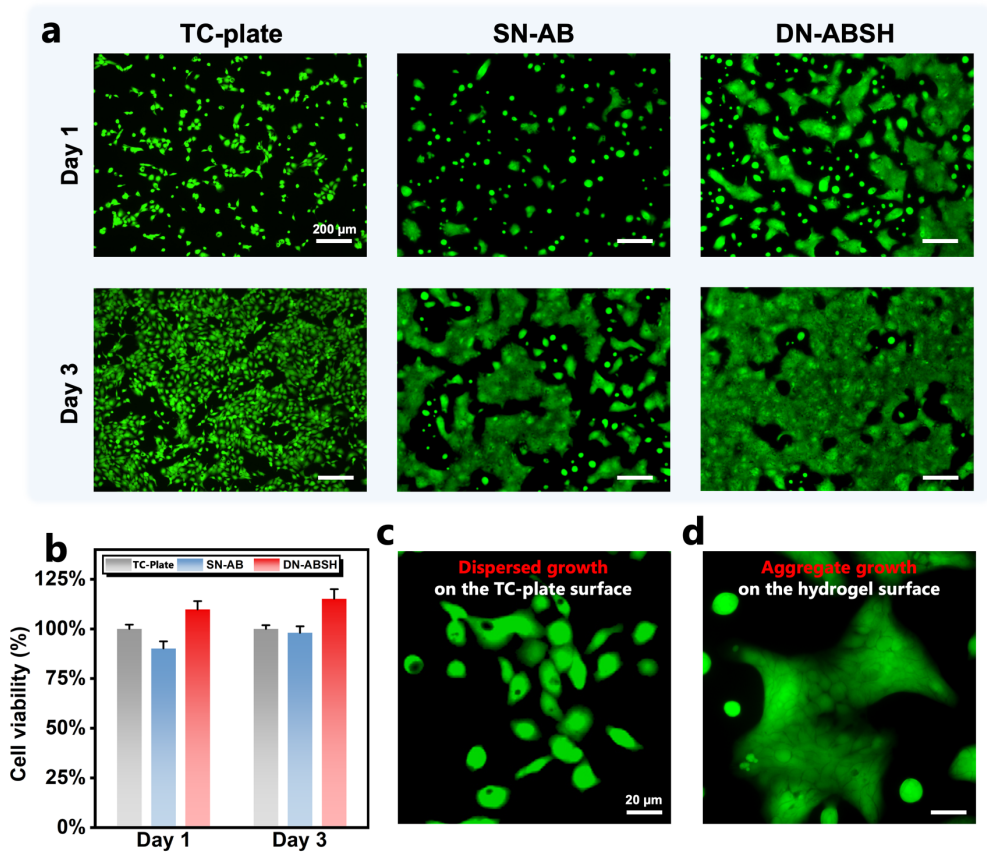


Figure 4.8 Cytocompatibility assessment of DN-ABSH hydrogel system: (a) Live/dead staining images, showing overlay images where green represents live cells and red represents dead cells. Scale bar: 200 μm. (b) alamarBlue cell viability assessment of HaCaT cells cultured on the surface of TC-plate, SN-AB and DN-ABSH at day 1 and 3; (c) cell dispersed growth on the TC-plate surface, and (d) aggregate growth on the hydrogel surface. The representative images presented are randomly selected from replicate samples (n=3), and data are presented as mean ± standard deviation (n=3).

4.4 Conclusion

In this work, a novel strategy for the homogeneous construction of biopolymer-based DN hydrogel with improved toughness was designed and developed. The Thiol-ene Michael addition reaction makes the HA-based first network hydrogel injectable, allowing it to be shaped into a designed form. Additionally, by utilising the property of HAp to dissolve and release Ca^{2+} in an acidic environment, *in situ* and homogeneous crosslinking of the second SA network was achieved. This acid-triggered DN structure construction method has produced DN-ABSH hydrogels with compressive strength and toughness improved 3-fold and 2.5-fold, respectively, compared to their inhomogeneous counterparts obtained through the traditional $CaCl_2$ immersion method. The DN-ABSH hydrogel also demonstrate remarkable resistance to fatigue, swelling, degradation, and excellent cytocompatibility. This acid-triggered DN strategy addresses the challenge of attaining homogeneous DN structures using biopolymers exclusively. The visualised and customised construction strategy for tough DN regions also offers a potential solution for manufacturing high-performance tissue scaffolds and mechanically customisable hydrogel devices.

4.5 References

(1) Zhao, Y.; Song, S.; Ren, X.; Zhang, J.; Lin, Q.; Zhao, Y. Supramolecular Adhesive Hydrogels for Tissue Engineering Applications. *Chemical Reviews*. 2022, 122 (6), 5604–5640.

(2) Liu, X.; Liu, J.; Lin, S.; Zhao, X. Hydrogel Machines. *Materials Today*. 2020, 36, 102–124.

(3) Wu, S. J.; Zhao, X. Bioadhesive Technology Platforms. *Chemical Reviews*. 2023, 123 (24), 14084–14118.

(4) Zhao, X.; Chen, X.; Yuk, H.; Lin, S.; Liu, X.; Parada, G. Soft Materials by Design: Unconventional Polymer Networks Give Extreme Properties. *Chemical Reviews*. 2021, 121 (8), 4309–4372.

(5) Liang, Y.; He, J.; Guo, B. Functional Hydrogels as Wound Dressing to Enhance Wound Healing. *ACS Nano*. 2021, 15 (8), 12687–12722.

(6) Nam, S.; Mooney, D. Polymeric Tissue Adhesives. *Chemical Reviews*. 2021, 121 (18), 11336–11384.

(7) Li, J.; Mooney, D. J. Designing Hydrogels for Controlled Drug Delivery. *Nature Reviews Materials*. 2016, 1 (12), 1–17.

(8) Van Vlierberghe, S.; Dubruel, P.; Schacht, E. Biopolymer-Based Hydrogels As Scaffolds for Tissue Engineering Applications: A Review. *Biomacromolecules*. 2011, 12 (5), 1387–1408.

(9) Nezhad-Mokhtari, P.; Ghorbani, M.; Roshangar, L.; Soleimani Rad, J. A Review on the Construction of Hydrogel Scaffolds by Various Chemically Techniques for Tissue Engineering. *European Polymer Journal*. 2019, 117, 64–76.

(10) Brumberg, V.; Astrelina, T.; Malivanova, T.; Samoilov, A. Modern Wound Dressings: Hydrogel Dressings. *Biomedicines*. 2021, 9 (9), 1235.

(11) Ko, D. Y.; Shinde, U. P.; Yeon, B.; Jeong, B. Recent Progress of *in situ* Formed Gels for Biomedical Applications. *Progress in Polymer Science*. 2013, 38 (3), 672–701.

(12) Bertsch, P.; Diba, M.; Mooney, D. J.; Leeuwenburgh, S. C. G. Self-Healing Injectable Hydrogels for Tissue Regeneration. *Chemical Reviews*. 2023, 123 (2), 834–873.

(13) Fuchs, S.; Shariati, K.; Ma, M. Specialty Tough Hydrogels and Their Biomedical Applications. *Advanced Healthcare Materials*. 2020, 9 (2), 1901396.

(14) Correa, S.; Grosskopf, A. K.; Lopez Hernandez, H.; Chan, D.; Yu, A. C.; Stapleton, L. M.; Appel, E. A. Translational Applications of Hydrogels. *Chemical Reviews*. 2021, 121 (18), 11385–11457.

(15) Zhao, X. Designing Toughness and Strength for Soft Materials. Proceedings of the National Academy of *Sciences*. 2017, 114 (31), 8138–8140.

(16) Zhao, X. Multi-Scale Multi-Mechanism Design of Tough

Hydrogels: Building Dissipation into Stretchy Networks. *Soft Matter*. 2014, 10 (5), 672–687.

(17) Norioka, C.; Inamoto, Y.; Hajime, C.; Kawamura, A.; Miyata, T. A Universal Method to Easily Design Tough and Stretchable Hydrogels. *NPG Asia Mater*. 2021, 13 (1), 1–10.

(18) Sakai, T.; Matsunaga, T.; Yamamoto, Y.; Ito, C.; Yoshida, R.; Suzuki, S.; Sasaki, N.; Shibayama, M.; Chung, U. Design and Fabrication of a High-Strength Hydrogel with Ideally Homogeneous Network Structure from Tetrahedron-like Macromonomers. *Macromolecules*. 2008, 41 (14), 5379–5384.

(19) Liu, C.; Morimoto, N.; Jiang, L.; Kawahara, S.; Noritomi, T.; Yokoyama, H.; Mayumi, K.; Ito, K. Tough Hydrogels with Rapid Self-Reinforcement. *Science*. 2021, 372 (6546), 1078–1081.

(20) Chen, Q.; Chen, H.; Zhu, L.; Zheng, J. Engineering of Tough Double Network Hydrogels. *Macromolecular Chemistry and Physics*. 2016, 217 (9), 1022–1036.

(21) Gong, J. Why Are Double Network Hydrogels so Tough? *Soft Matter*. 2010, 6 (12), 2583–2590.

(22) Gong, J.; Katsuyama, Y.; Kurokawa, T.; Osada, Y. Double-Network Hydrogels with Extremely High Mechanical Strength. *Advanced Materials*. 2003, 15 (14), 1155–1158.

(23) Huang, X.; Li, J.; Luo, J.; Gao, Q.; Mao, A.; Li, J. Research Progress on Double-Network Hydrogels. *Materials Today*

Communications. 2021, 29, 102757.

(24) Nonoyama, T.; Gong, J. Double-Network Hydrogel and Its Potential Biomedical Application: A Review. *Proceedings of the Institution of Mechanical Engineers, Part H: Journal of Engineering in Medicine*. 2015, 229 (12), 853–863.

(25) Nonoyama, T.; Gong, J. Tough Double Network Hydrogel and Its Biomedical Applications. *Annual Review of Chemical and Biomolecular Engineering*. 2021, 12 (1), 393–410.

(26) Matsuda, T.; Nakajima, T.; Fukuda, Y.; Hong, W.; Sakai, T.; Kurokawa, T.; Chung, U.; Gong, J. Yielding Criteria of Double Network Hydrogels. *Macromolecules*. 2016, 49 (5), 1865–1872.

(27) Zhang, X.; Guo, X.; Yang, S.; Tan, S.; Li, X.; Dai, H.; Yu, X.; Zhang, X.; Weng, N.; Jian, B.; Xu, J. Double-Network Hydrogel with High Mechanical Strength Prepared from Two Biocompatible Polymers. *Journal of Applied Polymer Science*. 2009, 112 (5), 3063–3070.

(28) Gu, Z.; Huang, K.; Luo, Y.; Zhang, L.; Kuang, T.; Chen, Z.; Liao, G. Double Network Hydrogel for Tissue Engineering. *WIREs Nanomedicine and Nanobiotechnology*. 2018, 10 (6), e1520.

(29) Aldana, A. A.; Houben, S.; Moroni, L.; Baker, M. B.; Pitet, L. M. Trends in Double Networks as Bioprintable and Injectable Hydrogel Scaffolds for Tissue Regeneration. *ACS Biomaterials Science & Engineering*. 2021, 7 (9),

4077–4101.

(30) Muir, V. G.; Burdick, J. A. Chemically Modified Biopolymers for the Formation of Biomedical Hydrogels. *Chemical Reviews*. 2021, 121 (18), 10908–10949.

(31) Sun, J.-Y.; Zhao, X.; Illeperuma, W. R. K.; Chaudhuri, O.; Oh, K. H.; Mooney, D. J.; Vlassak, J. J.; Suo, Z. Highly Stretchable and Tough Hydrogels. *Nature*. 2012, 489 (7414), 133–136.

(32) Das, A.; Ringu, T.; Ghosh, S.; Pramanik, N. A Comprehensive Review on Recent Advances in Preparation, Physicochemical Characterization, and Bioengineering Applications of Biopolymers. *Polymer Bulletin*. 2023, 80 (7), 7247–7312.

(33) Hernández-González, A. C.; Téllez-Jurado, L.; Rodríguez-Lorenzo, L. M. Alginate Hydrogels for Bone Tissue Engineering, from Injectables to Bioprinting: A Review. *Carbohydrate Polymers*. 2020, 229, 115514.

(34) Lee, K. Y.; Mooney, D. J. Alginate: Properties and Biomedical Applications. *Progress in Polymer Science*. 2012, 37 (1), 106–126.

(35) Song, R.; Wang, X.; Johnson, M.; Milne, C.; Lesniak-Podsiadlo, A.; Li, Y.; Lyu, J.; Li, Z.; Zhao, C.; Yang, L.; Lara-Sáez, I.; A, S.; Wang, W. Enhanced Strength for Double Network Hydrogel Adhesive Through Cohesion-Adhesion Balance. *Advanced Functional Materials*. 2024, 2313322.

(36) Shi, C.; Yang, F.; Hu, L.; Wang, H.; Wang, Y.; Wang, Z.; Pan, S.; Chen, J. Construction of Polysaccharide Based Physically Crosslinked Double-Network Antibacterial Hydrogel. *Materials Letters*. 2022, 316, 132048.

(37) Malektaj, H.; Drozdov, A. D.; deClaville Christiansen, J. Mechanical Properties of Alginate Hydrogels Cross-Linked with Multivalent Cations. *Polymers*. 2023, 15 (14), 3012.

(38) Hamidi, M.; Azadi, A.; Rafiei, P. Hydrogel Nanoparticles in Drug Delivery. *Advanced Drug Delivery Reviews*. 2008, 60 (15), 1638–1649.

(39) Pathak, C.; Vaidya, F. U.; Pandey, S. M. Mechanism for Development of Nanobased Drug Delivery System. *Applications of Targeted Nano Drugs and Delivery Systems*. 2019; 35–67.

(40) You, F.; Chen, X.; Cooper, D. M. L.; Chang, T.; Eames, B. F. Homogeneous Hydroxyapatite/Alginate Composite Hydrogel Promotes Calcified Cartilage Matrix Deposition with Potential for Three-Dimensional Bioprinting. *Biofabrication*. 2018, 11 (1), 015015.

(41) Kiyama, R.; Nonoyama, T.; Wada, S.; Semba, S.; Kitamura, N.; Nakajima, T.; Kurokawa, T.; Yasuda, K.; Tanaka, S.; Gong, J. Micro Patterning of Hydroxyapatite by Soft Lithography on Hydrogels for Selective Osteoconduction. *Acta Biomaterialia*. 2018, 81, 60–69.

Chapter Five

Summary and Future Directions

5.1 Summary

This chapter summarises the objectives, research outcomes, and overall conclusions presented throughout this thesis. ***Chapter Two:*** Tough Injectable Hydrogels via Flexible Chains Liking Rigid Homogeneous Framework. ***Chapter Three:*** Tough Injectable Hydrogel via Thermal Self-entangled Chains Linking Rigid Framework. ***Chapter Four:*** Double Network Injectable Hydrogel with Enhanced Toughness by Acid-Triggered Second Homogeneous Network.

5.1.1 Tough Injectable Hydrogels via Flexible Chains Linking Rigid Homogeneous Framework

The enhancement of toughness in injectable hydrogels depends on the ability to integrate structures that maintain elasticity and dissipate mechanical energy within the same hydrogel.[1–3] Additionally, the hydrogel system should also retain *in situ* forming capabilities while demonstrating excellent biocompatibility.[4–6]

In **Chapter Two**, flexible PEG long chains were used to link to HA-based rigid and homogeneous frameworks within a SN injectable hydrogel. This design integrates structures for

maintaining elasticity and dissipating mechanical energy. The flexible PEG long chains effectively increase the flexibility of the hydrogel structure, thus enhancing its elastic limit. Meanwhile, the rigid and homogeneous HA framework acts as a sacrificial bond, aiding the hydrogel in energy dissipation during deformation. The synergistic interaction between these two structures results in approximately a 7-fold increase in compressive strength and a 4-fold increase in the toughness of the injectable hydrogel.

For both injectable and non-injectable hydrogels, previous studies have often sought to enhance toughness through the introduction of multiple interpenetrating or semi-interpenetrating networks. However, for SN hydrogels, increasing the crosslinking density or polymer concentration can slightly improve mechanical strength but inevitably results in the hydrogel becoming stiff and brittle. This work presents a novel design approach, simultaneously constructing a homogeneous framework and flexible linkage long chains within a SN injectable hydrogel to enhance toughness. This universal toughening design is not only straightforward and easily applicable to various SN injectable hydrogel systems, but it also facilitates clinical application due to its simple implementation steps.

5.1.2 Tough Injectable Hydrogel via Thermal Self-entangled Chains Linking Rigid Framework

Highly entangled structures are ideal for load-bearing designs in SN hydrogels because they resolve the conflict between stiffness and toughness. When these structures are stretched, the knotting and sliding processes prompt a rearrangement of the polymer chains which optimises the stress distribution within the hydrogel network. Before any fracturing occurs, this optimised network causes more polymer chains to stiffen simultaneously, resulting in exceptional limit strength. However, constructing highly entangled polymer networks in injectable hydrogels is currently extremely challenging.

Chapter Three proposes that a self-entangled injectable hydrogel network can be constructed in one step by utilising the self-assembly behaviour of amphiphilic. By incorporating self-entangled polymer chains into a homogeneous, rigid hydrogel framework, the toughness of the *in situ* formed injectable hydrogel is significantly enhanced. This mechanical improvement is attributed to the synergistic effects of the elastic maintenance structure and mechanical energy dissipation structures. The self-entangled polymer chains provide the capacity to maintain high

elasticity through a knotting-sliding mechanism, while the stretching of self-assembled area and the sacrifice of the rigid framework both contribute to high capabilities for mechanical energy dissipation.

Unlike reported highly entangled hydrogels, which mostly rely on polymerising high concentrations of monomers or crosslinking polymer chains at or above the critical entanglement concentration, this study introduces a novel preparation method. It utilises the self-assembly capabilities of amphiphilic polymers to create regions of high entanglement within injectable hydrogels, thereby enhancing their toughness. This work not only bridges the gap between the design of highly entangled structures and injectable hydrogels but also proposes a new universal design strategy for developing the next generation of injectable hydrogels with enhanced mechanical properties.

5.1.3 Double Network Injectable Hydrogel with Enhanced Toughness by Acid-Triggered Second Homogeneous Network

The emergence of double network (DN) structures offers new design for creating tough injectable hydrogels. However, most of

the reported injectable DN hydrogels are predominantly based on synthetic polymers and weak bonding, which raises concerns about their biocompatibility and stability. While crosslinked biopolymers could address these issues, producing a homogeneous, crosslinked, biopolymer-based DN injectable hydrogel remains challenging.

Chapter Four reports that the *in situ* released Ca^{2+} obtained through the acidic dissolution of hydroxyapatite (HAp) nanoparticles can homogeneously crosslink the sodium alginate (SA) network. Utilising this method, this study has developed a biopolymer-based, homogeneous DN injectable hydrogel, comprising a first injectable HA network and a second acid-triggered SA/HAp network. As a result, the compressive strength and toughness of this homogeneous DN hydrogel have increased 3-fold and 2.5-fold, respectively, compared to their inhomogeneous DN counterparts. Moreover, this DN hydrogel also exhibits advanced properties such as fatigue resistance, anti-swelling, and degradation resistance. It is noteworthy that the acid-triggered DN strategy employed in this work can customise zones with different mechanical properties within the same hydrogel, and these variations are visually observable. This strategy offers

an innovative method for manufacturing high performance tissue scaffolds and mechanically customisable hydrogel devices.

5.2 Limitations

In **Chapter Two**, the mechanical performance of the SN injectable hydrogel is effectively enhanced through the structure of flexible long chains linked rigid and homogeneous HA framework. Compared to general SN hydrogel counterparts, this SN injectable hydrogel exhibits a 7-fold increase in compressive strength and a 4-fold increase in compressive toughness. However, due to the inherent conflict between stiffness and toughness, the enhancement in toughness is notably less than the increase in strength. This is because both the flexible PEG chains and the homogeneous HA framework contribute to improve elasticity. However, this more flexible hydrogel network inevitably leads to a significant reduction in the storage modulus (G') and stiffness. Although the relatively rigid HA framework provides stiffness and mechanical energy dissipation capacity, it is still insufficient compared to the enhancement in elasticity. maintenance properties. Therefore, the limited increase in the toughness of this hydrogel relies more on elastic maintenance. Additionally, the Mw of HA has a significant impact on the viscosity of its solutions. When the

concentration of the HA component exceeds 3%, the resulting high viscosity impedes experimental operations and the uniformity of the hydrogel, potentially leading to mechanical structure defects. Therefore, utilising HA materials with a lower Mw facilitates the use of high polymer concentrations, which can further enhance the mechanical properties of injectable hydrogels.

In **Chapter Three**, the self-entangled hydrogel structure alleviates the conflict between stiffness and toughness. This injectable hydrogel system utilised the thermosensitive self-assembly behaviour of amphiphilic polymers to create self-entangled regions within the hydrogel, which then crosslinked *in situ* through a Thiol-ene Michael addition reaction. Compared to general hydrogel with typical network topology, this SN injectable hydrogel maintains a high G' while enhancing compressive strength by 1.7 times and compressive toughness by 2 times. Moreover, compared to the previous chapter, the use of lower Mw HA (110 kDa) allowed for an increased polymer concentration within the hydrogel, resulting in a compressive strength of 9.08 MPa. However, the F127 amphiphilic polymer used in this hydrogel system is not an endogenous material in the human body and therefore lacks biodegradability. This raises significant safety

concerns when used as an implantable hydrogel scaffold.

In **Chapter Four**, the first injectable HA network and the acid-triggered *in situ* formation of the second SA network together create a homogeneous, tough DN hydrogel system. Compared to general inhomogeneous DN hydrogels, this system shows significant increases in both compressive strength and toughness. However, the second SA network in this hydrogel requires additional pH changes for activation. Although this pH-responsive toughness enhancement property is highly practical, the need for pH adjustments post-injection makes this hydrogel less perfect as an implantable material.

5.3 Future Directions

As discussed in the preceding section, constructing tough hydrogels requires an integration between elastic maintenance and mechanical energy dissipation structures. However, for injectable hydrogels, implementation must also be feasible through *in situ* formed methods. This strict requirement limits the use of most toughening strategies. A variety of injectable hydrogels with enhanced mechanical properties has been developed. However, compared to tough non-injectable hydrogels that do not require *in*

situ formation, their mechanical performance still falls significantly short. Although this research project has introduced promising tough injectable hydrogel designs, they still face limitations due to the stiffness-toughness conflict or usability issues. Based on the results achieved, toughening principles, and emerging polymer materials, this section discusses potential future directions that may serve as guidelines for creating robust injectable hydrogels in the near future.

5.3.1 New Combinations of Tough Mechanisms

As discussed in above chapters, the general principle for designing tough injectable hydrogels is to incorporate toughening mechanisms into the hydrogels systems with the *in situ* formed methods. We discussed various mechanisms for elastic maintenance and mechanical energy dissipation in hydrogels. Based on the *in situ* crosslinking methods, the combination of these two sets of mechanisms can provide a table that guides for designing tough injectable hydrogels, as shown in **Table 5.1**. Over the past few decades, scientists have experimented with various combinations of toughening from the design table, and the unexplored combinations serve as promising approaches for constructing tough injectable hydrogels.

As discussed in above chapters, the general principle for designing tough injectable hydrogels is to incorporate toughening mechanisms into the hydrogels systems with the *in situ* formed methods. We discussed various mechanisms for elastic maintenance and mechanical energy dissipation in hydrogels. Based on the *in situ* crosslinking methods, the combination of these two sets of mechanisms can provide a table that guides for designing tough injectable hydrogels, as shown in **Table 5.1**. Over the past few decades, scientists have experimented with various combinations of toughening from the design table, and the unexplored combinations serve as promising approaches for constructing tough injectable hydrogels.

Table 5.1 A matrix provides design guides and publication references of *in situ* formed tough injectable hydrogels by combining mechanisms for elastic maintenance and energy dissipation structure. Notably, it reveals many promising yet unexplored combinations. [Created with BioRender]

Tough injectable hydrogels	Elastic maintenance structure: Homogeneous network	Elastic maintenance structure: Slide ring network	Elastic maintenance structure: Highly entangled network
Energy Dissipation Structure: Sacrificial bonding	Chapter 2	Chapter 4, 7, 8, 9, 10	Chapter 3, 11
Energy Dissipation Structure: Domain transformation	12	13, 14	15, 16
Energy Dissipation Structure: Fibre reinforced network	17		

In addition, multi-functional biological polymers have been developed in recent years. These materials hold the promise of achieving both high elasticity and energy dissipation structures in single polymer, thereby simplifying the preparation steps for tough *in situ* formed injectable hydrogels.[18] Xu et al. prepared a HB-PEG

based tri-functional polymer with terminal acrylate, aldehyde, and diol groups through DE-ATRP.[19] Due to the pre-crosslinking reaction between aldehyde and diol, the polymer could form cotton-like foam with high water absorption capacity. The remaining terminal acrylate groups could be further reacted to produce a dual crosslinked structure, resulting in a mechanically robust hydrogel. This dual-functional polymer containing both aldehyde and acrylate potentially enables crosslinking through both covalent bonds and dynamic bonds. Here, the flexible crosslinked covalent bonds provide high elasticity, while the densely present dynamic bonds enable recoverable mechanical energy dissipation.

5.3.2 New Tough Mechanisms Inspired by Nature

The structure of naturally occurring soft materials with exceptional toughness provides crucial inspiration for enhancing the mechanical properties of hydrogels. Take knee cartilage as an example; the cartilage matrix is a tough hydrogel composed of Type II collagen fibres, proteoglycans (including HA and chondroitin sulfate), and a high-water content. The network of Type II collagen fibres acts as the framework of the cartilage, supporting its shape and structure, and providing necessary

toughness and strength under tensile forces.[20] Proteoglycans are "bottlebrush" large molecular structures formed by core proteins covalently bonded to multiple glycosaminoglycan (GAG) chains (**Figure 5.1a**).

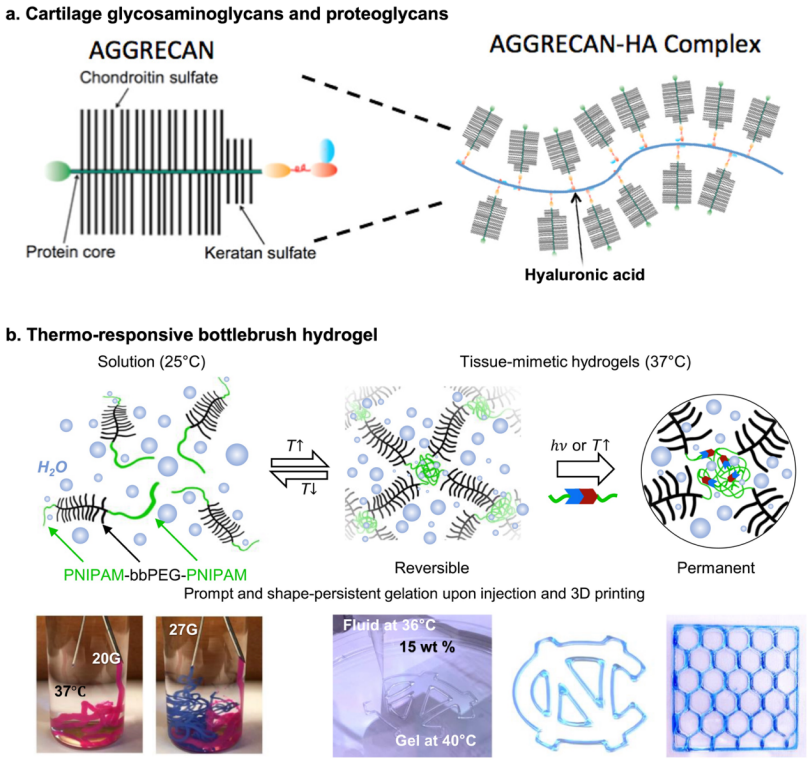


Figure 5.1 Biomimetic *in situ* formed hydrogel mimicking the cartilage matrix: (a) structure of cartilage glycosaminoglycans and proteoglycans;[20] [Cropped image. Copyright© 2021 American Chemical Society] (b) illustration of thermo-responsive bottlebrush *in situ* formed hydrogel.[21] [Cropped and reorganised image. Open Access]

The bottlebrush molecular structure can effectively disperse loads, absorb shocks, and protect joints. Vashiahi et al. developed an

injectable bottlebrush hydrogel platform with tissue-mimetic mechanical properties (**Figure 5.1b**).[21] This hydrogel platform is based on a hydrophilic thermo-responsive linear-bottlebrush-linear (LBL) triblock copolymer, which can self-assemble into a hydrogel at body temperature. Without covalent crosslinking, the LBL hydrogel can withstand deformation up to four times its original size. After covalent crosslinking, the compressive strength of the LBL hydrogel was further enhanced. Nevertheless, these mechanical properties still cannot match those of human knee cartilage, which typically needs to withstand 4-9 MPa of compressive stress over a million cycles annually. Incorporating a robust fibre network structure biomimetically into the existing injectable bottlebrush hydrogel has the potential to produce a tough, *in situ* formable, injectable hydrogel similar to cartilage.

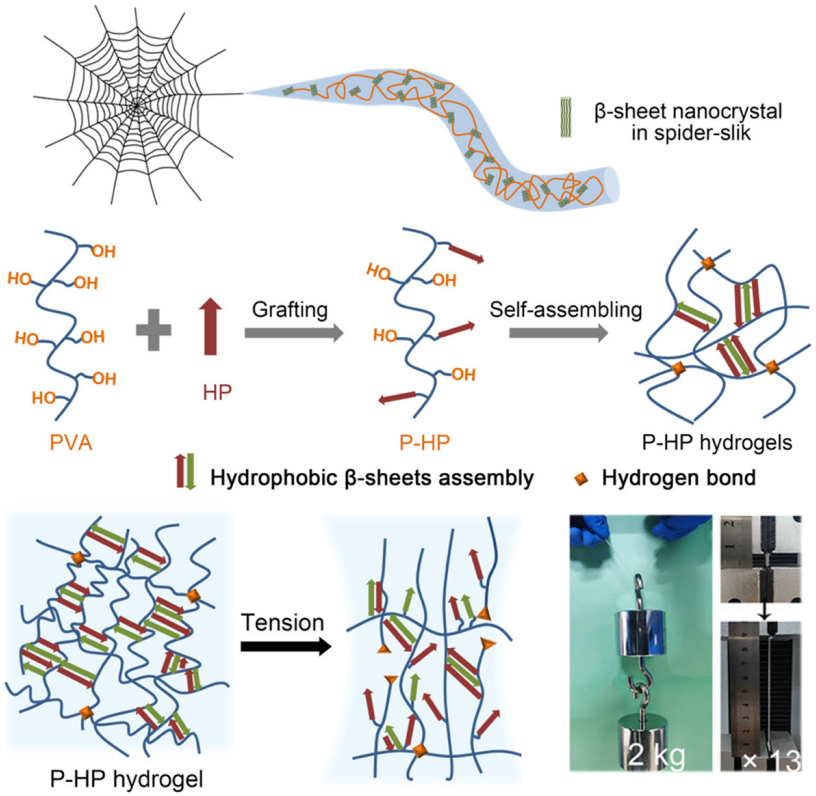


Figure 5.2 Structure of spider silk-like hydrogel and illustration of their tension process.[22] [Cropped and reorganised image. Copyright© 2021 American Chemical Society]

Spider silk is one of the most elastic protein fibres in nature. The toughness of spider silk originates from the combination of its internal β-sheet structure domains (providing energy dissipation) and amorphous coil structure domains (providing elastic). As shown in **Figure 5.2**, Xiang et al. inspired by the structure of spider silk, designed a biomimetic β-sheet structure domain to enhance the mechanical properties of hydrogels through synergistic physical interactions between molecules.[22] This

localised β-sheet structure domain was achieved by grafting the hydrophobic peptide (HP) onto PVA. The hydrophilic PVA can form a second physical crosslinking network through intermolecular hydrogen bonding to mimic the amorphous matrix of spider silk. The assembly of HP peptide β-sheets provides energy dissipation to increase the mechanical strength of the hydrogel. Combining *in situ* crosslinking methods with self-folding domains and amorphous coil domains offers a highly promising strategy for the design of future tough injectable hydrogels.

5.3.3 Multi-scale Combination Design

The toughening mechanisms of the hydrogels we have discussed span from the molecular scale to the millimetre scale. For some traditional tough hydrogels that are not prepared by *in situ* formed methods, the integration of multi-scale toughening mechanisms can be observed. A notable example is the work of Hua et al., which constructed toughening structures across multi-scales through the synergistic effects of freeze casting and salting out.[23] Directional freezing of the PVA solution formed micrometre scale honeycomb structures with aligned pore walls. The salting out process caused local intense self-association and phase separation

of PVA chains, forming localised nanometre scale crystallinity, while the PVA chains exhibited strong molecular scale hydrogen bonding interactions. As the result, the mechanical property of this hydrogel is superior compared to other tough hydrogels and even natural tendons. Although this freeze casting and salting out preparation method cannot be achieved through *in situ* formed method, its multi-scale toughening approach is highly meaningful for constructing tough *in situ* formed injectable hydrogels. From the perspective of *in situ* crosslinking methods, most reactions occur at the molecular scale, such as covalent bonds, dynamic bonds, coordination bonds, and hydrogen bonds, etc. Self-assembly behaviours occur on a relatively larger scale, mostly at the nanometre scale. Fibre reinforcement can even function at the micrometre to millimetre scale (**Figure 5.3**). Therefore, a promising strategy for designing the next generation of tough injectable hydrogels is to integrate multi-scale toughening mechanisms into the single hydrogel through *in situ* formed methods. Thus, should some toughening mechanisms fail, the toughness of hydrogels can still be preserved through alternative structures.

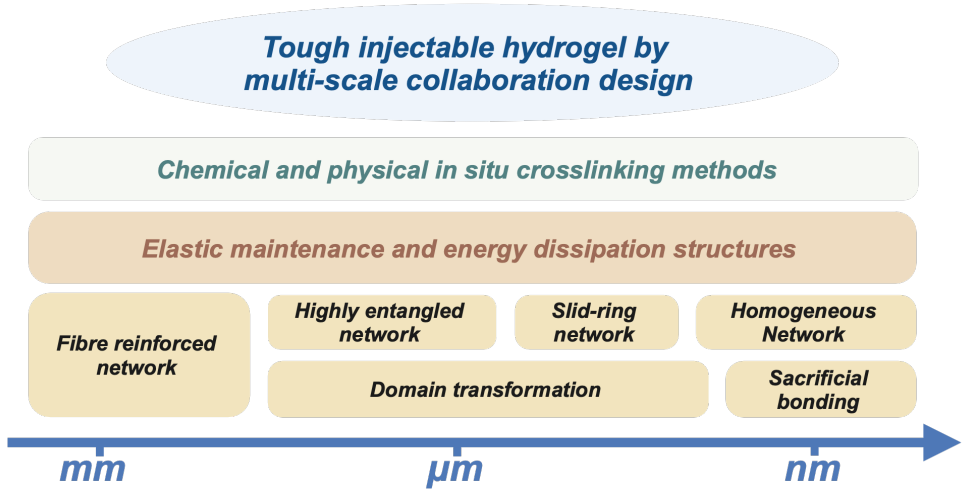


Figure 5.3 A promising strategy to design tough injectable hydrogels by collaborating multi-scale mechanisms. [Created with BioRender]

5.4 Conclusion

In conclusion, this thesis explored the development of tough injectable hydrogel systems through innovative design strategies. By incorporating elastic maintenance and energy dissipation mechanisms, the hydrogels demonstrated significant improvements in mechanical properties while maintaining biocompatibility. The single network hydrogel, formed from a HA framework linked by flexible PEG chains, achieved a 7-fold increase in compressive strength and a 4-fold increase in compressive toughness. The self-entangled hydrogel, utilising self-assembly of F127-DA and crosslinked with HA framework,

exhibited a compressive strength of 9.08 MPa and a toughness of 753 kJ/m³. Additionally, the acid-triggered homogeneous DN hydrogel showed a 3-fold increase in compressive strength and a 2.5-fold increase in toughness compared to conventional DN hydrogels, with enhanced resistance to fatigue, swelling, and degradation. These advancements provide a strong foundation for the mechanical load-bearing required application of injectable hydrogels in various biomedical fields. Future research should focus on optimising these hydrogel systems for specific clinical applications and further exploring the potential of combining multiple toughening strategies to develop next-generation tough injectable hydrogels.

5.5 References

(1) Zhao, X. Designing Toughness and Strength for Soft Materials. Proceedings of the National Academy of *Sciences*. 2017, 114 (31), 8138–8140.

(2) Zhao, X.; Chen, X.; Yuk, H.; Lin, S.; Liu, X.; Parada, G. Soft Materials by Design: Unconventional Polymer Networks Give Extreme Properties. *Chemical Reviews*. 2021, 121 (8), 4309–4372.

(3) Zhao, X. Multi-Scale Multi-Mechanism Design of Tough Hydrogels: Building Dissipation into Stretchy Networks.

Soft Matter. 2014, 10 (5), 672–687.

(4) Correa, S.; Grosskopf, A. K.; Lopez Hernandez, H.; Chan, D.; Yu, A. C.; Stapleton, L. M.; Appel, E. A. Translational Applications of Hydrogels. *Chemical Reviews*. 2021, 121 (18), 11385–11457.

(5) Yang, J.-A.; Yeom, J.; Hwang, B. W.; Hoffman, A. S.; Hahn, S. K. *In situ*-Forming Injectable Hydrogels for Regenerative Medicine. *Progress in Polymer Science*. 2014, 39 (12), 1973–1986.

(6) Ko, D. Y.; Shinde, U. P.; Yeon, B.; Jeong, B. Recent Progress of *in situ* Formed Gels for Biomedical Applications. *Progress in Polymer Science*. 2013, 38 (3), 672–701.

(7) Xu, Z.; Zhang, H.; Huang, Y.; Zhong, H.; Qin, P.; Cheng, S.; Wang, Y.; Yang, C. Tough and Biocompatible Hydrogel Tissue Adhesives Entirely Based on Naturally Derived Ingredients. *ACS Applied Polymer Materials*. 2024, 6 (2), 1141–1151.

(8) Zhao, Y.; Cui, Z.; Liu, B.; Xiang, J.; Qiu, D.; Tian, Y.; Qu, X.; Yang, Z. An Injectable Strong Hydrogel for Bone Reconstruction. *Advanced Healthcare Materials*. 2019, 8 (17), 1900709.

(9) Rodell, C. B.; Dusaj, N. N.; Highley, C. B.; Burdick, J. A. Injectable and Cytocompatible Tough Double-Network Hydrogels through Tandem Supramolecular and Covalent Crosslinking. *Advanced Materials*. 2016, 28 (38), 8419–

8424.

(10) Chen, B.; Zhu, D.; Li, Q.; Wang, C.; Cui, J.; Zheng, Z.; Wang, X. Mechanically Reinforced and Injectable Universal Adhesive Based on a PEI–PAA/Alg Dual-Network Hydrogel Designed by Topological Entanglement and Catechol Chemistry. ACS Applied Materials & Interfaces. 2023, 15 (51), 59826–59837.

(11) Wang, K.; Zhang, Y.; Chen, T.; Bai, L.; Li, H.; Tan, H.; Liu, C.; Qu, X. Chain Entanglement-Driven Tough, Fatigue-Resistant PEG-Based Injectable Hydrogel Adhesive for Joint Skin Wound Healing. *Composites Part B: Engineering*. 2023, 266, 110991.

(12) Qin, Z.; Yu, X.; Wu, H.; Yang, L.; Lv, H.; Yang, X. Injectable and Cytocompatible Dual Cross-Linking Hydrogels with Enhanced Mechanical Strength and Stability. *ACS Biomaterials Science & Engineering*. 2020, 6 (6), 3529–3538.

(13) Mu, Z.; Chen, K.; Yuan, S.; Li, Y.; Huang, Y.; Wang, C.; Zhang, Y.; Liu, W.; Luo, W.; Liang, P.; Li, X.; Song, J.; Ji, P.; Cheng, F.; Wang, H.; Chen, T. Gelatin Nanoparticle-Injectable Platelet-Rich Fibrin Double Network Hydrogels with Local Adaptability and Bioactivity for Enhanced Osteogenesis. *Advanced Healthcare Materials*. 2020, 9 (5), 1901469.

(14) Zhang, Y.; Cao, Y.; Zhang, L.; Zhao, H.; Ni, T.; Liu, Y.; An, Z.; Liu, M.; Pei, R. Fabrication of an Injectable BMSC-

Laden Double Network Hydrogel Based on Silk Fibroin/PEG for Cartilage Repair. *Journal of Materials Chemistry B*. 2020, 8 (27), 5845–5848.

(15) Chen, Y.; Chen, B.; Dong, J.; Yang, D.; Tang, H.; Wen, L.; Li, J.; Huang, L.; Zhou, J. A Tough and Bioadhesive Injectable Hydrogel Formed with Maleimidyl Alginate and Pristine Gelatin. *Carbohydrate Polymers*. 2024, 334, 122011.

(16) Bao, B.; Zeng, Q.; Li, K.; Wen, J.; Zhang, Y.; Zheng, Y.; Zhou, R.; Shi, C.; Chen, T.; Xiao, C.; Chen, B.; Wang, T.; Yu, K.; Sun, Y.; Lin, Q.; He, Y.; Tu, S.; Zhu, L. Rapid Fabrication of Physically Robust Hydrogels. *Nature Materials*. 2023, 22 (10), 1253–1260.

(17) Nishiguchi, A.; Taguchi, T. Engineering an Injectable Tough Tissue Adhesive through Nanocellulose Reinforcement. *ACS Applied Bio Materials*. 2020, 3 (12), 9093–9100.

(18) Muir, V. G.; Burdick, J. A. Chemically Modified Biopolymers for the Formation of Biomedical Hydrogels. *Chemical Reviews*. 2021, 121 (18), 10908–10949.

(19) Xu, Q.; A, S.; McMichael, P.; Creagh-Flynn, J.; Zhou, D.; Gao, Y.; Li, X.; Wang, X.; Wang, W. Double-Cross-Linked Hydrogel Strengthened by UV Irradiation from a Hyperbranched PEG-Based Trifunctional Polymer. *ACS Macro Letters*. 2018, 7 (5), 509–513.

(20) Horkay, F.; Douglas, J. F.; Raghavan, S. R. Rheological

Properties of Cartilage Glycosaminoglycans and Proteoglycans. *Macromolecules*. 2021, 54 (5), 2316–2324.

(21) Vashahi, F.; Martinez, M. R.; Dashtimoghadam, E.; Fahimipour, F.; Keith, A. N.; Bersenev, E. A.; Ivanov, D. A.; Zhulina, E. B.; Popryadukhin, P.; Matyjaszewski, K.; Vatankhah-Varnosfaderani, M.; Sheiko, S. S. Injectable Bottlebrush Hydrogels with Tissue-Mimetic Mechanical Properties. *Science Advances*. 2022, 8 (3), eabm2469.

(22) Xiang, Y.; Zhang, J.; Mao, H.; Yan, Z.; Wang, X.; Bao, C.; Zhu, L. Highly Tough, Stretchable, and Enzymatically Degradable Hydrogels Modulated by Bioinspired Hydrophobic β-Sheet Peptides. *Biomacromolecules*. 2021, 22 (11), 4846–4856.

(23) Hua, M.; Wu, S.; Ma, Y.; Zhao, Y.; Chen, Z.; Frenkel, I.; Strzalka, J.; Zhou, H.; Zhu, X.; He, X. Strong Tough Hydrogels via the Synergy of Freeze-Casting and Salting Out. *Nature*. 2021, 590 (7847), 594–599.

Appendices

Work Output During PhD

Articles to be Published

(1) **Song, R.**, Demircan, A., Milne, C., Guan, T., Zhao, C., Wang, X., Johnson, M., Li, Y., Lyu, J., Zhang, N., A, S.*, Wang, W.* 'Double Network Injectable Hydrogel with Enhanced Toughness by Acid-Triggered Second Homogeneous Network', submitted.

(2) **Song, R.**, Milne, C., Zhao, C., Li, Y., Johnson, M., Geng, Q., Li, Z., Lyu, J., A, S.*, Wang, W.* 'Tough Injectable Hydrogel via Thermal Self-entangled Chains Linking Rigid Framework', submitted.

(3) **Song, R.**, Milne, C., Johnson, M., Li, Y., Zhao, C., Geng, Q., A, S.*, Wang, W.* 'Tough Injectable Hydrogels via Flexible Chains Linking Rigid Homogeneous Framework', Submitted.

(4) **Song, R.**, Milne, C., Johnson, M., Zhao, C., A, S.*, Wang, W.* 'Advances in Toughness for *in situ* Formed Hydrogels'. In preparation.

Published Peer-Reviewed Articles

(1) **Song, R.**; Wang, X.; Johnson, M.; Milne, C.; Lesniak-Podsiadlo, A.; Li, Y.; Lyu, J.; Li, Z.; Zhao, C.; Yang, L.; Lara-Sáez, I.; A, S.*; Wang, W.* Enhanced Strength for Double Network Hydrogel Adhesive Through Cohesion-Adhesion Balance. *Advanced Functional Materials*. 2024, 2313322.

(2) Milne, C.; **Song, R.***; Johnson, M.; Zhao, C.; Santoro Ferrer, F.; A, S.; Lyu, J.; Wang, W.* Dual-Modified Hyaluronic Acid for Tunable Double Cross-Linked Hydrogel Adhesives. *Biomacromolecules*. 2024, 25 (4), 2645-2655.

(3) Li, Z.; Lyu, J.*; Qiu, B.; Johnson, M.; Zhao, C.; Li, Y.; Geng, Q.; **Song, R.**; Yao, L.; Wang, W.* Well-Defined Poly(N,N-Dimethylacrylamide) from a Fast Cu(0)-Mediated Reversible-Deactivation Radical Polymerization in Water. *Journal of Polymer Science*. 2024, 62 (6), 1193–1200.

(4) Li, Z.; Lyu, J.*; Qiu, B.; Li, Y.; Foley, R.; **Song, R.**; Johnson, M.; Geng, Q.; Wang, W.*, One-Pot and One-Step Cu(0)-mediated Reversible-Deactivation Radical Polymerization of N-Isopropylacrylamide in Water. *Chinese Journal of Polymer Science*. 2024, 42 (1), 1-6.

(5) Li, Y.; Qiu, B.; Li, Z.; Wang, X.; He, Z.; Sandoval, D. M.; **Song, R.**; Sigen, A.; Zhao, C.; Johnson, M.; Lyu, J.*; Lara-Sáez, I.; Wang, W.*, Backbone Cationized Highly Branched Poly(β-Amino Ester)s as Enhanced Delivery Vectors in Non-Viral Gene Therapy. *Journal of Controlled Release*. 2024, 367, 327–338.

(6) Zhang, J.; He, Z.; Li, Y.; Shen, Y.; Wu, G.; Power, L.; **Song, R.**; Zeng, M.; Wang, X.; Sáez, I. L.; A, S.; Xu, Q.; Curtin, J. F.; Yu, Z.*; Wang, W.*, Enhanced Gene Transfection Efficacy and Safety through Granular Hydrogel Mediated

Gene Delivery Process. *Acta Biomaterialia*. 2023, 166, 85-94.

(7) Wang, X.; **Song, R.**; Johnson, M.; A, S.; Shen, P.; Zhang, N.; Lara-Sáez, I.; Xu, Q.*; Wang, W.*, Chitosan-Based Hydrogels for Infected Wound Treatment. *Macromolecular Bioscience*. 2023, 23 (9), 2300094.

(8) Wang, X.; Johnson, M.; Zhang, N.; Shen, P.; Yang, L.; Milne, C.; Lara-Sáez, I.; **Song, R.***; A, S.*; Wang, W.*, Stimuli-Responsive Chitosan-Based Injectable Hydrogel for "on-Demand" Drug Release. *Materials Advances*. 2023, 4 (23), 6439–6448.

(9) Liu, J. *; Garcia, J.; Leahy, L. M.; **Song, R.**; Mullarkey, D.; Fei, B.; Dervan, A.; Shvets, I. V.; Stamenov, P.; Wang, W.; O'Brien, F. J.; Coleman, J. N.; Nicolosi, V.*, 3D Printing of Multifunctional Conductive Polymer Composite Hydrogels. *Advanced Functional Materials*. 2023, 33 (37), 2214196.

(10) Li, Y.; Wang, X.; He, Z.; Li, Z.; Johnson, M.; Qiu, B.; **Song, R.**; A, S.; Lara-Sáez, I.; Lyu, J.*; Wang, W.*, A New Optimization Strategy of Highly Branched Poly(β-Amino Ester) for Enhanced Gene Delivery: Removal of Small Molecular Weight Components. *Polymers*. 2023, 15 (6), 1518.

(11) Wang, X.; **Song, R.**; Johnson, M.; A, S.; He, Z.; Milne, C.; Wang, X.; Lara-Sáez, I.; Xu, Q.*; Wang, W.*, An Injectable Chitosan-Based Self-Healable Hydrogel System as an

Antibacterial Wound Dressing. *Materials*. 2021, 14 (20), 5956.

Conference Proceedings

(1) **Song, R.**, A, S. *, Wang, W.*, 'Design and One-Step Fabrication of an *in situ* Formed Hyaluronic Acid-Based Tough Hydrogel with a Long and Short Chain Network Structure'. Oral Presentation at the *Materials Research Society*, November 2022, Boston, USA

(2) **Song, R.**, A, S. *, Wang, W.*, '*In situ* Formed Hyaluronic Acid Based Tough Hydrogels and Its Biomedical Applications' Poster at the *UCD Conway Festival*, October 2022, Dublin, Ireland

(3) **Song, R.**, A, S. *, Wang, W.*, 'Biopolymer-based Tough Hydrogels for Additive Manufacture' Oral Presentation at the *Polymer Replication on Nanoscale*, May 2022, Dublin, Ireland

Accepted Representative Publication

Check for updates

RESEARCH ARTICLE

ADVANCED FUNCTIONAL MATERIALS
www.afm-journal.de

Enhanced Strength for Double Network Hydrogel Adhesive Through Cohesion-Adhesion Balance

Rijian Song, Xiaoyu Wang, Melissa Johnson, Cameron Milne, Anna Lesniak-Podsiadlo, Yinghao Li, Jing Lyu, Zishan Li, Chunyu Zhao, Lizhu Yang, Irene Lara-Sáez, Sigen A, and Wenxin Wang**

Hydrogel adhesives exhibit great potential in various biomedical fields such as tissue sealing and soft robotics. However, the high-water content and defective network structures of these hydrogel adhesives result in low intrinsic mechanical strength, severely impeding their application. In this study, it is reported that the strong hydrogel adhesive strength can be achieved when a balance is established between adhesive forces and cohesive forces. Based on this principle, a new double network (DN) design is created to combine an adhesive polyvinyl alcohol (PVA) as the first network with a flexible sodium alginate (SA) as the second network. A delicate balance is achieved between cohesion and adhesion by adjusting the ratio between the first rigid adhesive network and the second flexible network. As a result, this balanced DN hydrogel adhesive exhibits a strong tissue adhesion strength, approximately three times higher than that in the non-balance situation.

1. Introduction

Hydrogel, with its dual solid and liquid characteristics resembling those of the extracellular matrix (ECM), tissues, and organs, has been utilized for a variety of applications in the biomedical field.[1–3] In recent years, hydrogel-based adhesives have garnered significant attention due to their excellent adhesion, tissue-like viscoelasticity, remarkable biocompatibility, etc.[4–7] The flexible network structure of hydrogel adhesives is conducive to its exchange of substances with organisms, and it provides a range of capabilities for loading, releasing, and adsorption.[8,9] These hydrogel adhesives can not only seal wounds but also create a favorable moist microenvironment for injured tissue, thereby promoting wound healing.[10,11] Additionally, customized functionalities such as conductivity or responsiveness to stimulations like temperature, pH, pressure, etc., can be further endowed through the specialized formulation design of the hydrogel, making it an ideal material to be utilized in soft robotics.[12–14] However, the hydrogel adhesives' inherent high water content and defective network structures normally lead to low intrinsic mechanical strength. As a result, their ability to effectively seal larger tissue defect areas or maintain strong adhesion in load-bearing regions is severely limited.[15,16]

It is widely accepted that the adhesive strength of adhesives is influenced by two distinct factors: cohesive force and adhesive force.[17,18] Cohesive force refers to the internal force that holds the hydrogel network together, while adhesive force refers to the bonding strength between the hydrogel adhesive and the surface of the adhered tissue.[18] The adhesive failure of hydrogel can

R. Song, W. Wang
Institute of Precision Medicine
Anhui University of Science and Technology
Huainan 232001, China
E-mail: wenxin.wang@ucd.ie
R. Song, W. Wang
Research and Clinical Translation Center of Gene Medicine and Tissue Engineering, School of Public Health
Anhui University of Science and Technology
Huainan 232001, China

The ORCID identification number(s) for the author(s) of this article can be found under https://doi.org/10.1002/adfm.202313322

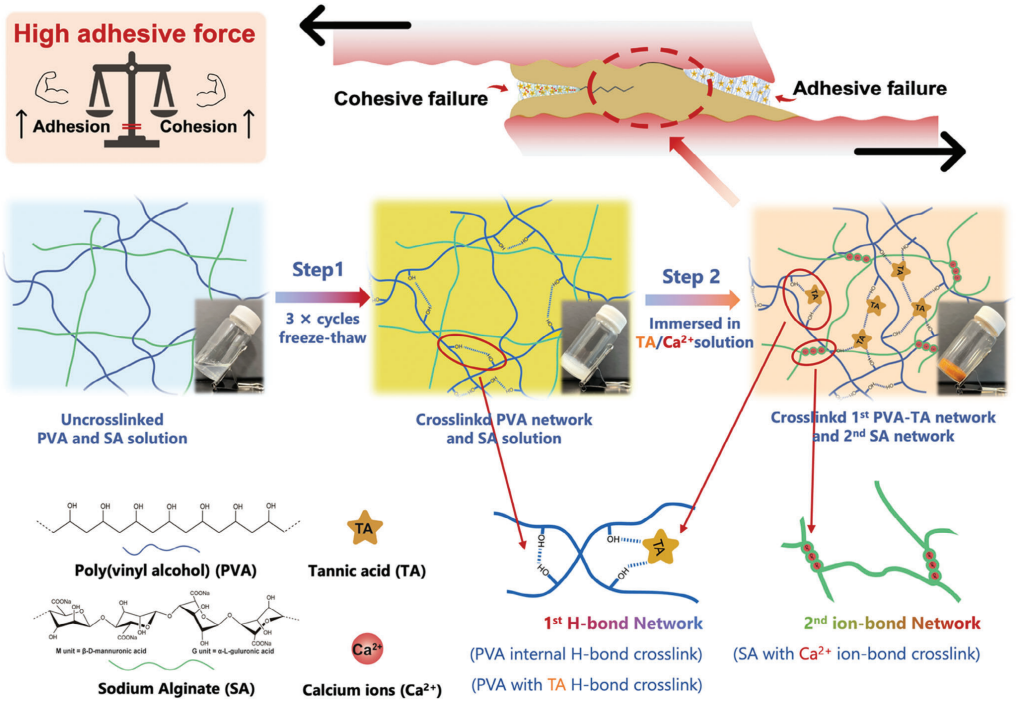
© 2024 The Authors. Advanced Functional Materials published by Wiley-VCH GmbH. This is an open access article under the terms of the Creative Commons Attribution License, which permits use, distribution and reproduction in any medium, provided the original work is properly cited.

DOI: 10.1002/adfm.202313322

R. Song, X. Wang, M. Johnson, C. Milne, Y. Li, J. Lyu, Z. Li, C. Zhao, L. Yang, I. Lara-Sáez, S. A, W. Wang
Charles Institute of Dermatology
School of Medicine
University College Dublin
Dublin 4 D04 V1W8, Ireland
E-mail: sigen.a@aust.edu.cn
A. Lesniak-Podsiadlo
School of Biosystems and Food Engineering
Agriculture and Food Science Centre
University College Dublin
Dublin 4 D04 V1W8, Ireland
L. Yang
School of Pharmaceutical Sciences
Wenzhou Medical University
Wenzhou 325035, China
S. A
School of Medicine
Anhui University of Science and Technology
Huainan 232001, China

ADVANCED SCIENCE NEWS
www.advancedsciencenews.com

ADVANCED FUNCTIONAL MATERIALS
www.afm-journal.de



Scheme 1. Illustration of the preparation of PSTC adhesive DN hydrogels.

sometimes be attributed to either the rupture of interfacial adhesion or cohesive failure caused by poor mechanical stability.[19] In previous studies, many efforts have been devoted to unilaterally either enhancing the intrinsic mechanical performance or improving the surface adhesive strength of hydrogels.[20–24] Nonetheless, such endeavors of solely improving either of these aspects while neglecting the other have been shown to result in limited improvements in hydrogel adhesive performance.[19,25,26] Hence, we are speculating whether the optimal adhesive strength could be achieved when simultaneously considering and balancing both the cohesive force within the hydrogel adhesive and its surface adhesive force.

To achieve the simultaneous regulation of the cohesive and the adhesive force, the double network (DN) hydrogel design would be a desired candidate.[27,28] Previous research on DN hydrogels has mainly focused on how to adjust the proportion and crosslinking density between the two networks to control mechanical properties.[29] However, we believe that the inherent flexibility in the composition of DN hydrogels allows us to selectively match the two networks with distinct properties. This, in turn, enables us to strike a balance between cohesion and adhesion, leading to optimized adhesive strength. Following this design principle, we have fabricated a novel DN hydrogel adhesive by a two-step technique (**Scheme 1**). In the first step, a hydrogen bond crosslinked polyvinyl alcohol (PVA) rigid network hydrogel was formed through three freeze-thaw cycles. In the second step, natural polyphenolic tannic acid (TA) was introduced to confer excellent adhesive properties onto the 1st PVA network. Simultaneously, the 2nd flexible sodium alginate (SA) network was crosslinked by calcium ions (Ca^{2+}), which imparts excellent cohesion properties to the DN hydrogel adhesives. By adjusting the PVA and SA ratio, a cohesion-adhesion balance of DN hydrogel adhesive was achieved, resulting in much enhanced hydrogel adhesive strength. The adhesion strength of this newly constructed DN hydrogel achieved a threefold enhancement despite the reduced content of the PVA adhesion network. Moreover, the presence of TA bestows antibacterial properties with this novel hydrogel adhesive, a feature of paramount importance in clinical applications.

2. Results and Discussion

2.1. Preparation of PSTC Hydrogels

As illustrated in **Figure 1a**, the cohesion-adhesion balanced DN hydrogel adhesives based on PVA/SA/TA/Ca^{2+} (PSTC) system were fabricated through a two-step technique, encompassing two heterogeneous networks formed by hydrogen and ion bonding, respectively. In the first step, the mixture solution of PVA and SA undergoes three repeated cycles of freezing and thawing,

© 2024 The Authors. Advanced Functional Materials published by Wiley-VCH GmbH

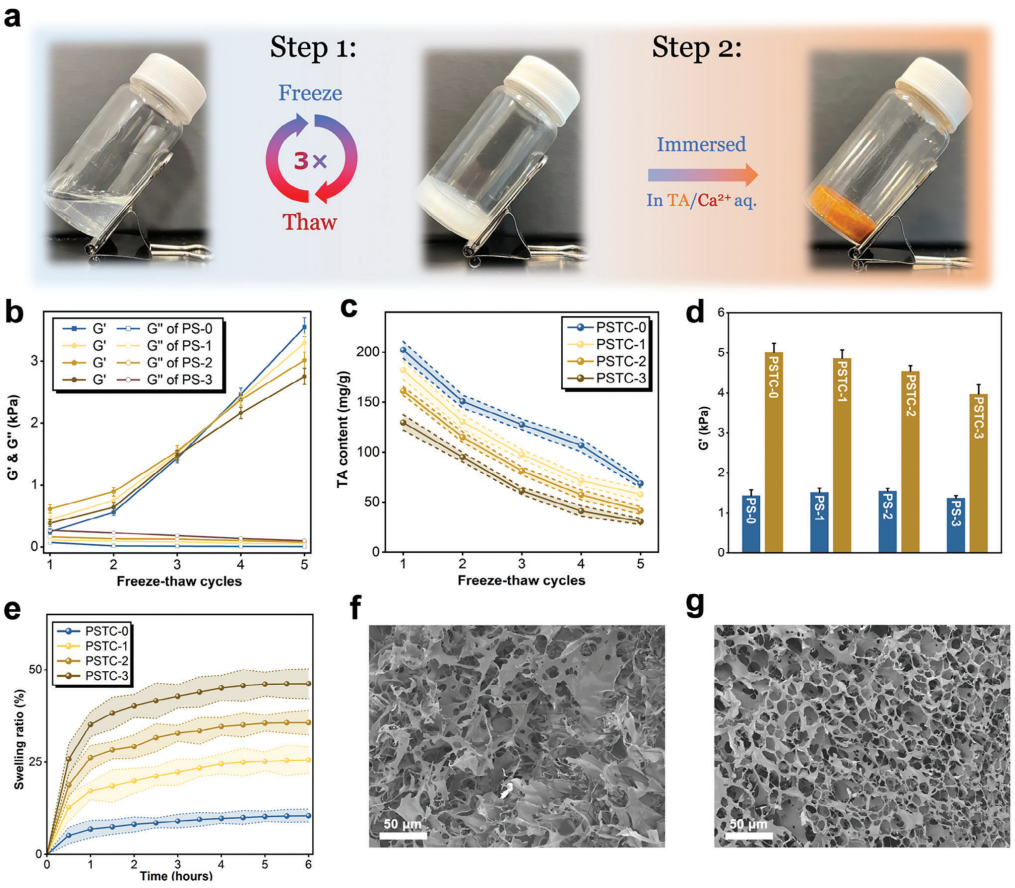


Figure 1. Characterization of PSTC hydrogel preparation process. a) general observation of PS pre-solution, PS SN hydrogel, and PSTC DN hydrogel; b) the G′ and G″ of PS hydrogels with different freeze/thaw cycles; c) TA content of PSTC hydrogels immobilized under different freeze-thaw cycles; d) the G′ of PS and PSTC hydrogels; e) swelling ratio of PSTC hydrogels; SEM images of f) PS-1 and g) PSTC-1. Scale bar: 50 μm.

resulting in the formation of a rigid single network (SN) hydrogel crosslinked by dense hydrogen bonds. The PVA chains tend to aggregate during temperature variations due to their high molecular weight and densely ordered hydroxyl structure.[30] During the freezing process, the crystallization of water induces a phase separation between the polymer and the solvent.[31] In addition, the expansion caused by the formation of ice crystals further compresses the PVA molecular chains, bringing them closer together, and facilitating hydrogen bonding.[32] During the thawing process, the molecular movement of the PVA chains accelerates in accordance with the laws of thermodynamics.[33] This molecular movement causes the previously compressed and aggregated PVA chains to re-expand, ultimately creating a network structure dominated by hydrogen bonding.[34] In the second step, hydrogels were immersed in a treatment solution containing TA and Ca^{2+}. Here, a single Ca^{2+} ion can crosslink four L-guluronic (G) units from the SA chains, forming an "egg-box" ion-binding structure, which produces the second interpenetrated hydrogel network.[35] Simultaneously, TA acts as a crosslinking agent and fosters additional bonding, leading to the development of a denser network structure.[36]

The abbreviation PS is employed to denote the PVA/SA SN hydrogel, while PSTC signifies the hydrogel formed post-immersion in the second step. The mass content of PVA and SA in all hydrogels was maintained at 10%. Specifically, PS-0/PSTC-0, PS-1/PSTC-1, PS-2/PSTC-2, and PS-3/PSTC-3 correspond to compositions comprising PVA (10%) + SA (0%), PVA (9%) + SA (1%), PVA (8.5%) + SA (1.5%), and PVA (8%) + SA (2%) respectively. In addition, the PST and PSC represent PS hydrogels that were post-immersed in TA or Ca^{2+} treatment solution

© 2024 The Authors. Advanced Functional Materials published by Wiley-VCH GmbH

only. As shown in Figure 1b, with the increase in freeze-thaw cycles of PS hydrogels, storage modulus (G′) gradually rises, while loss mudulus (G″) decreases which indicates that more freeze-thaw cycles create denser hydrogen bonding among the hydroxyl groups of the PVA side chains.[37] For PS-0 hydrogel, which has the highest PVA content, it leads to the formation of the most hydrogen bonds. However, during the initial three freeze-thaw cycles, physical entanglement between SA polysaccharide chains with the PVA framework and the high viscosity of SA itself contribute more to the increase in the G' of PS-1, PS-2, and PS-3. Therefore, after the first and second freeze-thaw cycles, the G′ of PS-0 hydrogel is lower than that of the other PS groups. However, when the number of freeze-thaw cycles exceeds three, the hydrogen bonds crosslinked by the higher quantity of PVA in PS-0 contribute more to the increase in G′ compared to the uncrosslinked SA in other groups. Consequently, after the 4th and 5th freeze-thaw cycles, the PS-0 hydrogel exhibits a higher G′. However, this implies that more hydroxyl groups are employed for internal crosslinking rather than binding with TA. As shown in Figure 1c, with the increase in freeze-thaw cycles or SA content, the amount of TA that can be immobilized by PSTC hydrogels diminishes progressively. This change potentially impairs the adhesive strength at the interface. To immobilize as much TA as possible while ensuring the complete molding and demolding of the hydrogel, a three-cycle freeze-thaw process was chosen as the standardized procedure for the preparation of PS and PSTC hydrogels. As shown in Figure 1d, the G′ gradually decreased from 1572 Pa in PS-0 to 927 Pa in PS-3 with the increase in SA content of PS hydrogels. After the second immersion step, the G′ of all PSTC hydrogel groups increased to different degrees. This is due to the additional crosslinking density provided by TA and the formation of the second network through Ca^{2+} crosslinking. As shown in Figure 1e, the equilibrium swelling ratio of PSTC-0 to PSTC-3 hydrogels increased with the SA content. This is because the total crosslinking density in the interpenetrating polymer network is lower if the PVA content is lower. Although PSTC hydrogels act as a DN system, this slightly flexible network allows the polymer chains to be freer, which reduces the elastic restraint. As a result, the hydrogel can swell further and absorb more water, leading to a higher swelling capacity. Scanning electron microscope (SEM) images show that the freeze-dried PS-1 and PSTC-1 hydrogels have a comparatively uniform and dense porous structure (Figure 1f,g). The PS-1 hydrogel exhibits a microporous structure (Figure 1f). However, the PSTC-1 DN hydrogel has a considerably denser porous structure, attributed to the second network, and higher crosslinking density resulting from the second immersion step (Figure 1g).

2.2. Mechanical Properties of PS and PSTC Hydrogels

The inherent mechanical properties of hydrogel adhesives play a crucial role in determining their sealing performance.[20,38] Variations in mechanical properties have a significant impact on the balance between cohesion and adhesion, further determining the strength and durability of the adhesive bond.[18,19] Specifically, maximizing the ability of hydrogel adhesives to withstand mechanical stresses before adhesive failure is a key principle in the design of effective wound tissue sealing materials.[5,39] Moreover, hydrogels with higher compression and tensile strength are better equipped to withstand shear and peel forces, enabling them to maintain their adhesive properties, and provide durable and effective sealing.[15,21] In the PSTC DN hydrogel system, the excellent mechanical properties are attributed to the interpenetrated physical and ionic bonding DN structure formed by the two-step technique. First, the DN structure of PSTC hydrogels provides them with excellent energy dissipation and shape maintaining capabilities under large deformation conditions. Second, the cohesion of the interpenetrating DN can be further tuned by adjusting the ratio of PVA/SA to achieve a balance with the adhesion force. Currently, there is no readily available instrument to measure cohesion for hydrogel adhesives. Normally, cohesion is considered as the internal strength of the hydrogel for holding the network together.[19] The tensile test applies axial tension to a sample body until it fractures, and cohesion is evaluated based on its tensile strength and toughness. Therefore, we have chosen Tensile strength as the indicator for cohesion assessment.

As shown in **Figure 2**a,d, the tensile stress, strain, and toughness of the PSTC hydrogel were significantly improved by increasing the percentage of SA components. The tensile strength of PSTC-1 increased almost threefold from 73.79 to 210.61 kPa compared to PSTC-0. As the proportion of SA components increased from PSTC-1 to PSTC-3, the tensile limit stress, strain, and toughness of the PSTC DN hydrogels were further enhanced. The tensile toughness increased progressively from 39.86 kJ m^{-3} in PSTC-0 to 435.97 kJ m^{-3} in PSTC-1, 527.22 kJ m^{-3} in PSTC-2, and 665.46 kJ m^{-3} in PSTC-3, respectively. This mechanical enhancement of PSTC hydrogel can be attributed to the formation of an interpenetrating DN structure. In this case, a dense network predominantly composed of PVA/TA provides the hydrogel with an effective energy-dissipating structure. This structure provides sacrificial bonds during deformation, thereby increasing the energy required for crack extension. Meanwhile, the flexible network primarily composed of SA/Ca^{2+} helps alleviate stress concentration while preserving the hydrogels' integrity. This, in turn, raises the threshold for crack extension. The synergistic interaction between these two networks provides both an energy-dissipating and shape-maintaining structure, enhancing the mechanical properties of the PSTC DN hydrogels. Figure 2b,e demonstrates that the alteration in hydrogel mechanical properties with the inclusion of SA components in the compression test follows a similar trend to that observed in the tensile test. The compression strength increased from 6.18 MPa in PSTC−0 to 19.01 MPa in PSTC-1, 22.42 MPa in PSTC-2, and 2.43 MPa in PSTC-3, respectively. In addition, the compressive toughness increased from 0.49 MJ m^{-3} in PSTC-0 to 1.77 MJ m^{-3} in PSTC-3. At the same time, the compressive strain increased gradually from 73.63% in PSTC-0 to 93.60% in PSTC-3. It is evident that the flexible and interpenetrating SA network significantly contributes to the deformation capacity of the PSTC hydrogel. This DN structure enhances the mechanical properties with less chain breakage. Furthermore, this advantage also proves beneficial for the anti-fatigue performance of the hydrogel. To assess the anti-fatigue properties of PSTC hydrogels, a compression limit of 80% of the limiting strain was applied to both the PSTC-0 and PSTC-1 groups respectively. Following 20 compression cycles, the compression stress of PSTC-0 decreased from 0.97 to 0.62 MPa

© 2024 The Authors. Advanced Functional Materials published by Wiley-VCH GmbH

ADVANCED SCIENCE NEWS
www.advancedsciencenews.com

ADVANCED FUNCTIONAL MATERIALS
www.afm-journal.de

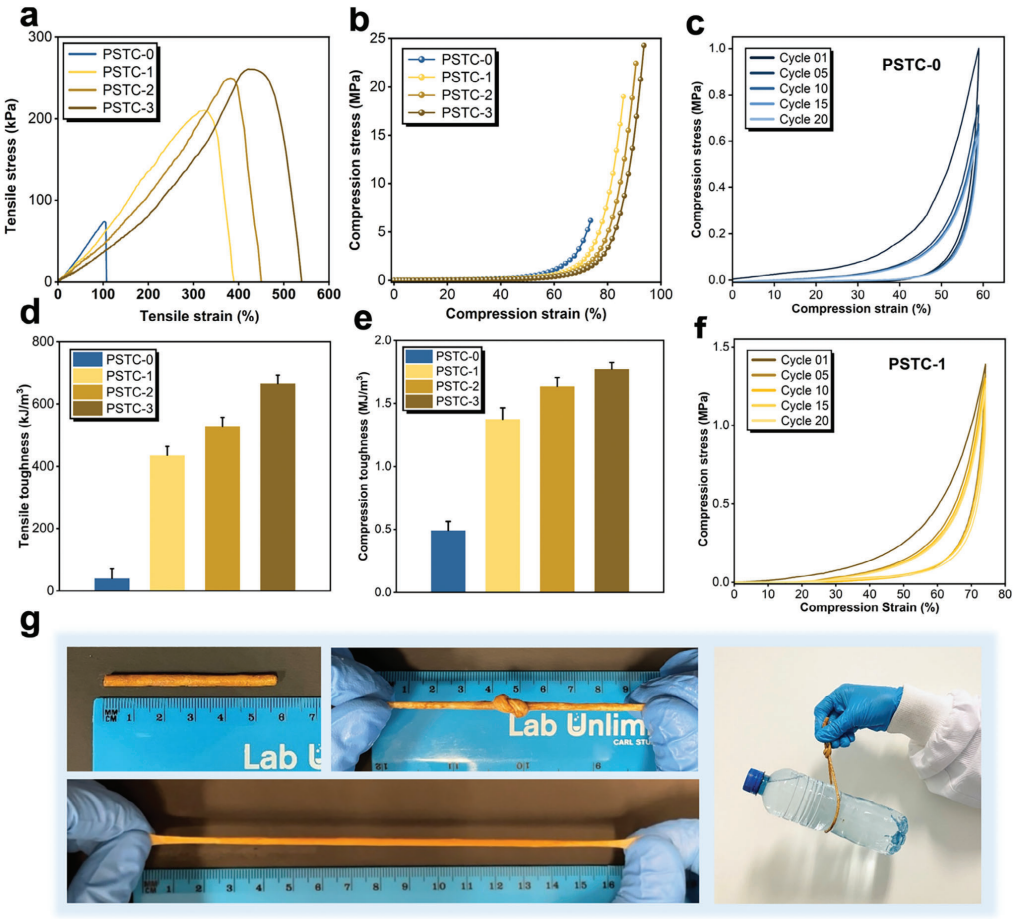


Figure 2. Mechanical properties of PS and PSTC hydrogels. a) tensile stress-strain curves of PSTC hydrogels; b) compression strain-stress curves of PSTC hydrogels; c) repeated compression strain-stress curve of PSTC-0 hydrogel; d) tensile toughness of PSTC hydrogels; e) compression toughness of PSTC hydrogels; f) repeat compression chart of PSTC-1 DN hydrogel; g) general observation of stretching and hanging of 0.5 kg water by PSTC-1 DN hydrogel.

(a reduction of 36%) (Figure 2c). Conversely, as shown in Figure 2h, the compression stress for PSTC-1 only slightly decreased from 1.36 to 1.22 MPa (a reduction of 10%). This substantial disparity highlights the exceptional fatigue resistance of the PSTC DN hydrogel. Figure 2g showcases the impressive mechanical properties of the PSTC-1 DN hydrogel. A strip-shaped hydrogel sample, with dimensions of 6 cm in length and 2 mm in diameter, exhibited a stretch of over 18 cm in length. Even after being knotted, it retained the ability to be stretched to nearly three times its original length without fracturing. Furthermore, the knotted hydrogel exhibited exceptional strength, capable of lifting 0.5 kg water without breaking. Through the construction of a DN structure, the PSTC hydrogels are able to achieve a significant enhancement in toughness and anti-fatigue strength, leading to an improvement in cohesion.

2.3. Adhesive Properties of PSTC Hydrogels

Optimal adhesion strength is achieved when the hydrogel adhesive reaches a balance between cohesion and adhesion near the interface. Moreover, the rheological properties of hydrogels do influence their adhesive capabilities. Typically, hydrogels with higher G′ tend to display weaker adhesion. This occurs because high elasticity restricts the flexibility of polymer chains, leading to adhesive functional groups on polymer chains having fewer

© 2024 The Authors. Advanced Functional Materials published by Wiley-VCH GmbH

ADVANCED SCIENCE NEWS
www.advancedsciencenews.com

ADVANCED FUNCTIONAL MATERIALS
www.afm-journal.de

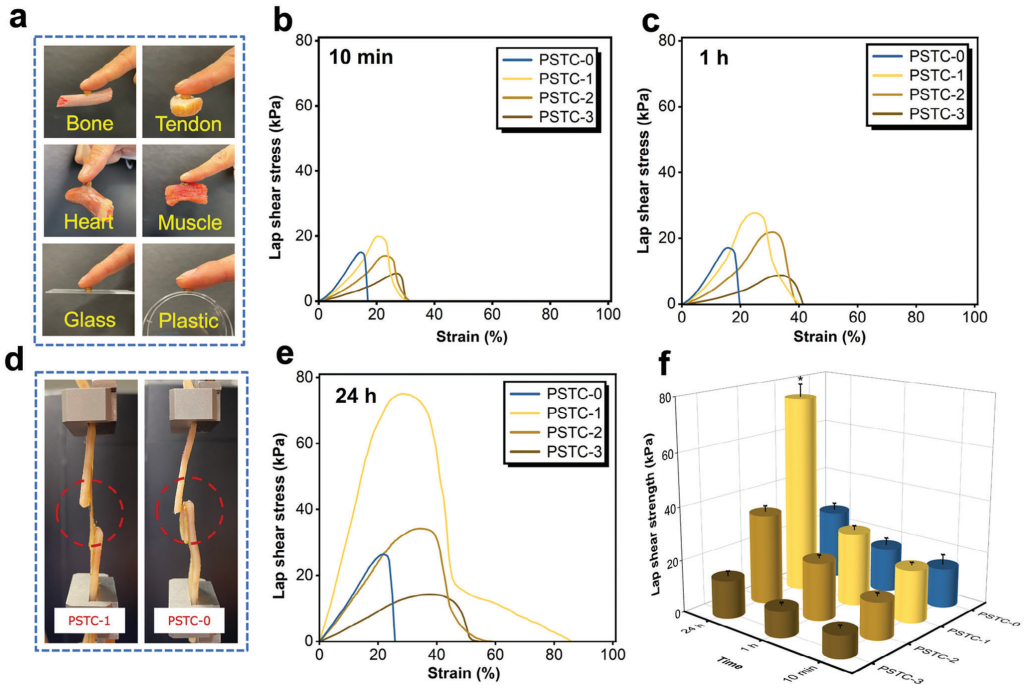


Figure 3. Adhesive properties of PSTC hydrogels. a) PSTC hydrogel adhesion to a variety of objects including tissue, glass, and plastic; b) lap shear stress-strain curve of PSTC hydrogels by porcine skin adhesive test with 10 min contact time; c) lap shear stress-strain curve of PSTC hydrogels with 1 h contact time; d) representative images of lap shear test of PSTC-1 and PSTC-0 hydrogel adhesives; e) lap shear stress-strain curve of PSTC hydrogels with 24 h contact time; f) summary image of lap shear strength of the porcine skin adhesive tests with a minimum of three samples per group. *, $p < 0.05$.

opportunities to connect with the substrate. However, in this study, the G′ for PSTC exhibited only minor variations among the groups, suggesting that they do not play a dominant role in adhesive performance changing (Figure 1d). Much like dopamine-adhesives inspired by mussels, the adhesive capability of this PSTC hydrogel primarily stems from the inherent polyphenolic structure of TA. This structure facilitates the formation of strong hydrogen bonds with the tissue surface. Moreover, the quinone-like structure that emerges from the oxidation of TA forms covalent bonds with nucleophilic groups, such as -NH_2 or -SH, found on the tissue surface.[36,40] As evident from Figure 1c, the adjustment of the PVA/SA ratio alone effectively regulates the amount of immobilized TA, subsequently allowing for the tuning of adhesion strength in the PSTC DN hydrogel. As shown in **Figure** 3a, the PSTC hydrogels exhibit robust adhesion to a variety of tissues and materials, including bone, tendon, heart, muscle, glass, and plastic. Particularly noteworthy is their potent adhesive bond to skin, rendering them exceptionally suitable for application as tissue adhesives. To evaluate the adhesive performance of the PSTC hydrogels, lap shear tests were performed using porcine skin as the adherents. This method has been widely adopted in the literature to assess the adhesion properties of biomaterials and is particularly suitable for soft tissue adhesives. The use of porcine skin as a model substrate also provides a relevant and realistic simulation of in vivo conditions, as it closely mimics the mechanical and biochemical properties of human skin. The hydrogel samples were prepared in a square shape with a side length of 1.2 cm and were placed between two porcine skin tissues. As shown in Figure 3b, the lap shear strength of the PSTC-0, 1, 2, and 3 hydrogels was measured as 14.963, 16.916, 3.627, and 2.292 kPa, respectively, following 10 min of contact time. Furthermore, compared to PSTC-1, 2, and 3 hydrogels, the lap shear stress of PSTC-0 hydrogel reaches its limit earlier and subsequently drops rapidly. This is due to the higher TA content imparts a good tissue adhesion ability to PSTC-0. However, the excessive stiffness of the pure PVA hydrogel network leads to inferior mechanical properties, particularly a lower limit strain (Figure 2b,c). In the Lap shear test, the excessively high adhesion at the rigid interface of PSTC-0 cannot match the brittle cohesion, inevitably leading to adhesive failure at low strains. Moreover, this result also can be attributed to a greater proportion of SA components facilitating the construction of a more flexible and tough DN structure, consequently improving the limit adhesive strain. In addition, the lap shear strength of all PSTC

© 2024 The Authors. Advanced Functional Materials published by Wiley-VCH GmbH

ADVANCED SCIENCE NEWS
www.advancedsciencenews.com

ADVANCED FUNCTIONAL MATERIALS
www.afm-journal.de

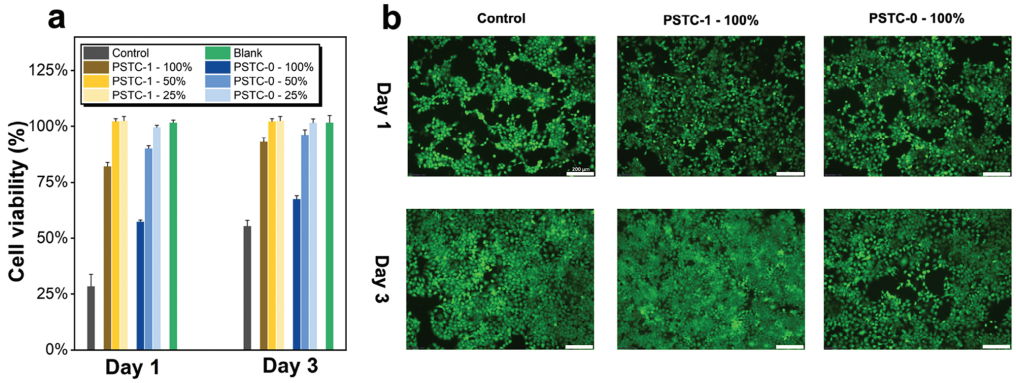


Figure 4. Cytocompatibility of PSTC hydrogels. a) the cell viability of HaCaT cells was assessed after treatment with varying concentrations of the extraction solution from PSTC-0 and PSTC-1 hydrogels; b) live/dead staining of HaCaT cells cultured with the pure extraction solution from PSTC-0 and PSTC-1 hydrogels for 1 and 3 days. Scale bar: 200 μm.

hydrogels increased as the contact time extended from 10 min to 1 h, and then to 24 h (Figure 3b,c,e). Especially, the PSTC-1 DN hydrogel achieved the highest lap shear strength of 75.08 kPa through the balanced cohesion-adhesion structure after 24 h of contact time (Figure 3f). However, for the PSTC-0 hydrogel, the adhesive force on the surface surpasses the cohesive force. As a result, the interior of the adhesive is prone to fracture during the lap shear process, leading to a reduction in overall adhesion strength. For PSTC-2 and PSTC-3 DN hydrogels, too much SA results in excessive cohesive force. At the same time, too little PVA content results in insufficient adhesive force, leading to a significant reduction in macroscopic adhesion strength. Compared to the other PSTC hydrogels, PSTC-3 exhibited the lowest adhesive stress after 24 h of contact, measuring only 14.24 kPa (Figure 3e).

As shown in Figure S1 (Supporting Information), variations in testing methods result in a lack of complete alignment in the measured values of tensile strength and adhesive strength for PSTC hydrogels. However, the changing trend of PSTC, PST, and PSC hydrogels reveal the cohesion-adhesion balance of PSTC-1 hydrogel. Similar to PSC hydrogels, the presence of the DN structure in PSTC hydrogels leads to an increase in tensile strength (Figure S1a,c, Supporting Information). In contrast to PST hydrogels, the lap shear strength of PSTC hydrogels exhibits an initial increase followed by a decrease (Figure S1a,b, Supporting Information). This phenomenon can be attributed to the balance between gradually increasing cohesive forces and decreasing adhesive forces within the PSTC hydrogel. In the PSTC-1 DN hydrogel adhesive, the adhesion network, consisting of PVA, and TA, delivers a robust interfacial adhesive force. At the same time, the DN structure, comprising a flexible crosslinked SA network, and a tightly crosslinked PVA network, significantly enhances the cohesive force of the hydrogel. The synergistic balance between these two forces plays a pivotal role, resulting in an overall enhancement of adhesive strength and the manifestation of a hysteretic adhesive failure behavior. Interestingly, the adhesive of PSTC-1 hydrogel demonstrates a unique "filamentary" phenomenon during the lap shear test, as shown in Figure 3d. This macroscopic observation confirms the cohesion-adhesion balance within PSTC-1 hydrogel.

2.4. Cytocompatibility of PSTC Hydrogels

In addition to its excellent adhesive properties, PSTC DN hydrogel also demonstrates high cytocompatibility, derived from the use of intrinsic biosafe raw materials. To assess the cytotoxicity, AlamarBlue measurements, and Live/Dead staining assays were performed on HaCaT cells. As shown in **Figure 4**a, the PSTC-1 DN hydrogel did not exhibit any toxicity toward the HaCaT cells at 25% and 50% concentrations, and only a slight inhibition of cell proliferation was observed at 100% concentration at day 1. However, the PSTC-0 hydrogel showed slightly poorer cytocompatibility at 50% concentration on days 1 and 3, with a marked restriction of cell proliferation at the 100% concentration. In general, the cytocompatibility analysis revealed that both PSTC-0 and PSTC-1 hydrogels exhibited greater biocompatibility compared to the TA-only control. Fluorescence images of HaCaT cells cultivated with the control, PSTC-1, and PSTC-0 hydrogel extraction solutions were acquired (Figure 4b), and these images were further analyzed to examine the vitality and morphology of the cells. The findings demonstrated that the co-cultured HaCaT cells after 1 and 3 days exhibited desirable cell shape and displayed no signs of cell death. In addition, the rate of cell growth in the control group was significantly slower than the growth rate of cells in the PSTC-0 and PSTC-1 groups, which aligns with the results of the AlamarBlue test. In consideration of practical skin adhesion scenarios extending beyond keratinocytes alone, we conducted an experiment employing NIH-3T3 fibroblast cells to evaluate the cytocompatibility of PSTC hydrogels. As shown in Figure S2a (Supporting Information), the PSTC hydrogel demonstrates a cytocompatibility pattern with NIH-3T3 cells similar to what was observed with HaCaT cells. Despite the slower proliferation rate of NIH-3T3 cells, PSTC-1 hydrogel consistently sustains cell viability above 80% after 1 and 3 days of co-culture. Additionally,

© 2024 The Authors. Advanced Functional Materials published by Wiley-VCH GmbH

ADVANCED SCIENCE NEWS
www.advancedsciencenews.com

ADVANCED FUNCTIONAL MATERIALS
www.afm-journal.de

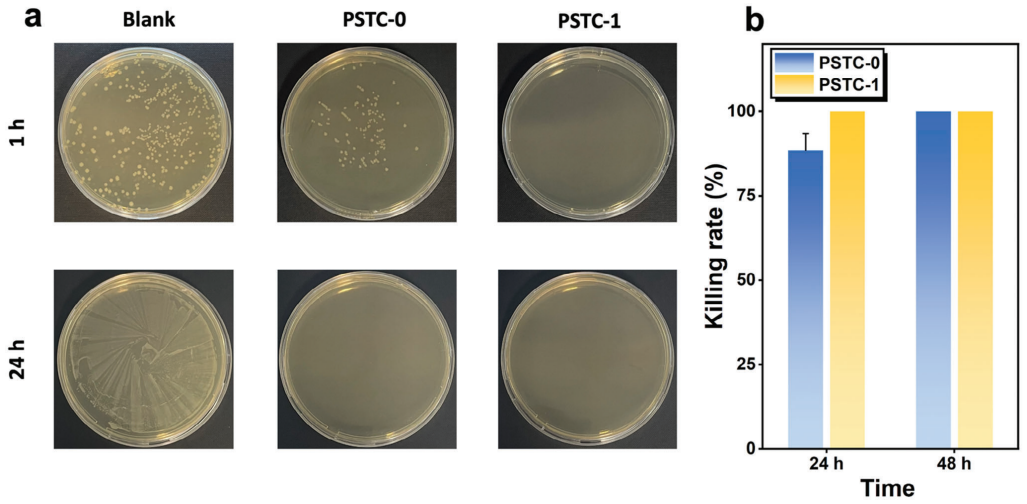


Figure 5. Antibacterial properties of PSTC hydrogels. a) photographs of the growth of bacterial colonies of *E. coli* on agar plates after 1 and 24 h of co-culture with PSTC-0 or PSTC-1 hydrogel; b) killing rate of *E.coli* with treatment of PSTC hydrogels with 24 and 48 h.

NIH-3T3 cells exhibit characteristic spindle or star-shaped flattened structures (Figure S2b, Supporting Information). The results reveal that PSTC hydrogels exhibit strong cytocompatibility with both HaCaT and NIH-3T3 cells, without causing a significant impact on cell viability and proliferation.

2.5. Antibacterial Properties of PSTC Hydrogels

In addition to exhibiting remarkable adhesion, mechanical toughness, and cytocompatibility, PSTC hydrogels also demonstrate excellent antibacterial properties. These inherent properties of PSTC hydrogels enable them to hinder the growth of germs near the wound surface. This, in turn, alleviates the pro-inflammatory state, and renders them valuable in preventing wounds infections.[41] To assess the antibacterial efficacy of the PSTC hydrogels, a spread plate experiment was conducted to evaluate the inhibitory effect of PSTC-0 and PSTC-1 hydrogels on the growth of *Escherichia coli (E. Coli)*, a common gram-negative bacterium. The images presented in **Figure** 5a were obtained by co-culturing PSTC-0 and PSTC-1 with *E. coli* for 1 and 24 h, respectively. After 1 h of incubation, the blank plate showed a significantly higher number of colonies than the PSTC-0 and PSTC-1 groups. However, the PSTC-1 group demonstrated notable acute antibacterial properties, completely eliminating all bacteria on the plate surface after only 1 h of co-culture. In contrast, a small number of colonies remained on the PSTC-0 plate surface. These results were further confirmed by the subsequent colony forming units (CFU) experiment. As shown in Figure 5b, the PSTC-0 hydrogel exhibited notable antibacterial effects after a 24 h co-culture period, resulting in an ≈88.5% reduction in the *E. coli* population. In contrast, the PSTC-1 hydrogel displayed superior efficacy by completely eradicating *E. coli*. When the co-culture period was extended to 48 h, both PSTC-0 and PSTC-1 hydrogels demonstrated highly potent antibacterial activity, resulting in the complete elimination of *E. coli*. These results highlight the potential of PSTC hydrogels as promising antimicrobial bioadhesives.

3. Conclusion

In summary, we have developed a new strategy for constructing a DN hydrogel adhesive. By adjusting the ratio between the first PVA rigid adhesive network and the second SA flexible network, a balance between cohesion and adhesion was achieved. This balance resulted in an approximately threefold enhancement in the adhesive strength of the hydrogel, accompanied by a hysteretic adhesive failure behavior observed during lap shear tests. Moreover, it achieved robust antibacterial performance and excellent biocompatibility, providing a favorable healing environment for sealed wounds. This cohesion-adhesion balance strategy has successfully guided the construction of a new double network hydrogel with high adhesion strength.

Supporting Information

Supporting Information is available from the Wiley Online Library or from the author.

Acknowledgements

The authors acknowledge the financial support from the China Scholarship Council (CSC202108300014), the Science Foundation Ireland (SFI) (Funding Agency Ref No: 19/FFP/6522), and the Enterprise Ireland (EI) (Funding Agency Ref No: DT20180247).

Open access funding provided by IReL.

© 2024 The Authors. Advanced Functional Materials published by Wiley-VCH GmbH

Conflict of Interest

The authors declare no conflict of interest.

Data Availability Statement

The data that support the findings of this study are available from the corresponding author upon reasonable request.

Keywords

adhesion, adhesives, antibacterial, cohesion, double network hydrogel

Received: October 26, 2023
Revised: January 11, 2024
Published online:

[1] H. Geckil, F. Xu, X. Zhang, S. Moon, U. Demirci, *Nanomedicine* **2010**, *5*, 469.
[2] E. González-Díaz, S. Varghese, *Gels* **2016**, *2*, 20.
[3] J. Zhu, R. E. Marchant, *Expert Rev. Med. Devices* **2011**, *8*, 607.
[4] Y. Xiong, X. Zhang, X. Ma, W. Wang, F. Yan, X. Zhao, X. Chu, W. Xu, C. Sun, *Polym. Chem.* **2021**, *12*, 3721.
[5] S. Nam, D. Mooney, *Chem. Rev.* **2021**, *121*, 11336.
[6] J. Yang, S. Wang, *Gels* **2023**, *9*, 138.
[7] S. A., Q. Xu, M. Johnson, J. Creagh-Flynn, M. Venet, D. Zhou, I. Lara-Sáez, H. Tai, W. Wang, *Appl. Mater. Today* **2021**, *22*, 100967.
[8] P. Jiang, Z. Ji, D. Liu, S. Ma, X. Wang, F. Zhou, *Adv. Funct. Mater.* **2022**, *32*, 2108845.
[9] W. H. Kim, Y. Han, I. S. Lee, N.-I. Won, Y. H. Na, *Polymer* **2022**, *255*, 125112.
[10] Z. Fang, T. Lin, S. Fan, X. Qiu, Z. Zhong, G. Yang, J. Yang, G. Zhang, Y. Feng, F. Ai, Q. Shi, W. Wan, *Front. Bioeng. Biotechnol.* **2023**, *11*, 1180073.
[11] T. Hu, G.-P. Wu, H. Bu, H. Zhang, W.-X. Li, K. Song, G.-B. Jiang, *Chem. Eng. J.* **2022**, *450*, 138201.
[12] E. Sachyani Keneth, A. Kamyshny, M. Totaro, L. Beccai, S. Magdassi, *Adv. Mater.* **2021**, *33*, 2003387.
[13] Y. Lee, W. J. Song, J.-Y. Sun, *Mater. Today Phys.* **2020**, *15*, 100258.
[14] Y. Chen, Y. Zhang, H. Li, J. Shen, F. Zhang, J. He, J. Lin, B. Wang, S. Niu, Z. Han, Z. Guo, *Nano Today* **2023**, *49*, 101764.
[15] X. Zhao, X. Chen, H. Yuk, S. Lin, X. Liu, G. Parada, *Chem. Rev.* **2021**, *121*, 4309.
[16] S. Fuchs, K. Shariati, M. Ma, *Adv. Healthcare Mater.* **2020**, *9*, 1901396.
[17] B. J. Kim, D. X. Oh, S. Kim, J. H. Seo, D. S. Hwang, A. Masic, D. K. Han, H. J. Cha, *Biomacromolecules* **2014**, *15*, 1579.
[18] J. A. von Fraunhofer, *Int J Dent* **2012**, *2012*, 1.
[19] Y. Bu, A. Pandit, *Bioact. Mater.* **2022**, *13*, 105.
[20] Y. Zhao, S. Song, X. Ren, J. Zhang, Q. Lin, Y. Zhao, *Chem. Rev.* **2022**, *122*, 5604.
[21] X. Pei, J. Wang, Y. Cong, J. Fu, *J. Polym. Sci.* **2021**, *59*, 1312.
[22] Z. Fu, S. Xiao, P. Wang, J. Zhao, Z. Ling, Z. An, J. Shao, W. Fu, *RSC Adv.* **2023**, *13*, 10903.
[23] B. Sharma, S. Fermanian, M. Gibson, S. Unterman, D. A. Herzka, B. Cascio, J. Coburn, A. Y. Hui, N. Marcus, G. E. Gold, J. H. Elisseeff, *Sci. Transl. Med.* **2013**, *5*, 167ra6.
[24] H. Zhang, T. Zhao, B. Newland, P. Duffy, A. N. Annaidh, E. D. O'Cearbhaill, W. Wang, *J. Mater. Chem. B* **2015**, *3*, 6420.
[25] G. Bovone, O. Y. Dudaryeva, B. Marco-Dufort, M. W. Tibbitt, *ACS Biomater. Sci. Eng.* **2021**, *7*, 4048.
[26] H. Zhang, T. Zhao, P. Duffy, Y. Dong, A. N. Annaidh, E. O'Cearbhaill, W. Wang, *Adv. Healthcare Mater.* **2015**, *4*, 2260.
[27] T. Nonoyama, J. P. Gong, *Annu. Rev. Chem. Biomol. Eng.* **2021**, *12*, 393.
[28] P. Karami, C. S. Wyss, A. Khoushabi, A. Schmocker, M. Broome, C. Moser, P.-E. Bourban, D. P. Pioletti, *ACS Appl. Mater. Interfaces* **2018**, *10*, 38692.
[29] J. P. Gong, *Soft Matter* **2010**, *6*, 2583.
[30] T. Nakano, T. Nakaoki, *Polym. J.* **2011**, *43*, 875.
[31] T. Sakaguchi, S. Nagano, M. Hara, S.-H. Hyon, M. Patel, K. Matsumura, *Polym J* **2017**, *49*, 535.
[32] Y. Chen, J. Li, J. Lu, M. Ding, Y. Chen, *Polym. Test.* **2022**, *108*, 107516.
[33] N. N. Getangama, J. R. de Bruyn, J. L. Hutter, *J. Chem. Phys.* **2020**, *153*, 044901.
[34] L. Xu, S. Gao, Q. Guo, C. Wang, Y. Qiao, D. Qiu, *Adv. Mater.* **2020**, *32*, 2004579.
[35] M. Zhang, X. Zhao, *Int. J. Biol. Macromol.* **2020**, *162*, 1414.
[36] C. Chen, H. Yang, X. Yang, Q. Ma, *RSC Adv.* **2022**, *12*, 7689.
[37] S. R. Stauffer, N. A. Peppast, *Polymer* **1992**, *33*, 3932.
[38] W. Zhang, R. Wang, Z. Sun, X. Zhu, Q. Zhao, T. Zhang, A. Cholewinski, F. (Kuo) Yang, B. Zhao, R. Pinnaratip, P. K. Forooshani, B. P. Lee, *Chem. Soc. Rev.* **2020**, *49*, 433.
[39] Z. Ma, G. Bao, J. Li, *Adv. Mater.* **2021**, *33*, 2007663.
[40] K. Chen, Q. Lin, L. Wang, Z. Zhuang, Y. Zhang, D. Huang, H. Wang, *ACS Appl. Mater. Interfaces* **2021**, *13*, 9748.
[41] Z. Zhou, J. Xiao, S. Guan, Z. Geng, R. Zhao, B. Gao, *Carbohydr. Polym.* **2022**, *285*, 119235.

 © 2024 The Authors. Advanced Functional Materials published by Wiley-VCH GmbH